TRACE ELEMENT ANALYSIS OF KIMBERLITES AND ASSOCIATED ROCKS AND XENOLITHS

by

NICHOLAS WILLIAM ROGERS B.Sc.(Hons.), M.Sc.

A THESIS SUBMITTED IN FULFILMENT OF
THE CONDITIONS FOR THE DEGREE OF
DOCTOR OF PHILOSOPHY
IN THE UNIVERSITY OF LONDON

University of London Reactor Centre
Silwood Park,
Sunninghill
Ascot
Berkshire
SL5 7PY

JANUARY 1980

OUT YONDER THERE WAS THIS HUGE WORLD, WHICH EXISTS INDEPENDENTLY OF US HUMAN BEINGS AND WHICH STANDS BEFORE US LIKE A GREAT, ETERNAL RIDDLE, AT LEAST PARTIALLY ACCESSIBLE TO OUR INSPECTION.

ALBERT EINSTEIN.

A B S T R A C T

The techniques of instrumental thermal and epithermal neutron activation analysis and radiochemical activation analysis as previously used at the University of London Reactor Centre, have been refined and applied to the determination of selected trace elements in samples from kimberlites and similar localities. This thesis describes the techniques as used in geochemical analysis and illustrates their precision and accuracy with determinations of nine rare earth elements (La,Ce,Nd,Sm, Eu,Tb,Ho,Yb and Lu) and six other trace elements (Th,U,Cs,Sc,Co and Cr) in the U.S.G.S. standard rocks BCR.1, AGV.1 and G.2 and in the I.A.E.A. inter-laboratory comparison sample, SL.1 (Lake sediment).

Subsequent analysis of kimberlites and similar volcanic rocks (alnoites and lamprophyres) revealed that, although their trace element abundances showed superficial similarities, those in the kimberlites were systematically different, suggesting differences in kimberlite petrogenesis. The alnoites and lamprophyres were related to a garnet lherzolite source that showed light rare earth element enrichment, tentatively ascribed to a metasomatic event.

In order to compare the trace element composition of the model mantle with that of possible real mantle material, a suite of fertile and sterile garnet lherzolite and harzburgite xenoliths from South African kimberlites were analysed for 13 trace elements. The fertile mantle samples were shown to possess flat rare earth element patterns, with abundances ranging from $\sim$ 1-3x chondrite. No evidence for metasomatic activity was discerned. The analysis of the sterile samples, however, revealed a strong enrichment of the light rare earth elements. This is the opposite of the light rare earth element depletion expected, if the two groups of xenoliths are related by a simple partial melting episode. Trace element abundances were subsequently interpreted in relation to a two component mantle model. This model postulates initial depletion of the mantle in incompatible elements by partial fusion, accompanied, or followed, by metasomatic enrichment of the residue by a fluid with kimberlitic trace element abundances, prior to inclusion of the mantle fragments in the host kimberlite.

Evidence for the higher level effects of any metasomatic activity was sought by the analysis of a suite of lower crustal garnet granulite xenoliths. Once again, different varieties were recognised from whole rock trace element abundances. In this case, however, the abundances were best explained using a conventional model of igneous crystal fractionation.

It was concluded that metasomatic alteration by incompatible element rich fluids is an important process in the sub-continental mantle and plays a significant role in the petrogenesis of some continental magmas. Kimberlites are interpreted as an infrequent surface expression of this widespread mantle phenomenon.

ACKNOWLEDGEMENTS

I should like to express my gratitude to Dr. G.D. Borley and Mr. M. Kerridge for their joint supervision of this project.

My thanks are due to the following people who have generously donated valuable samples for analysis:- Drs. S.W. Bachinski, D.A. Carswell, W.L. Griffin and P.H. Nixon. I am also indebted to Mr. A. Gray (University of Leeds) for his careful X.R.F. analyses of kimberlites and ultrabasic xenoliths.

This work has benefitted greatly from discussions with Dr. P.H. Nixon.

Finally, I should like to thank the staff and students (both past and present) of the University of London Reactor Centre, Silwood Park, for their friendship and hospitality over the past three years. They have tolerated the presence of a geologist in their midst with rare good humour! My thanks, particularly, to Joyce Vine for her typing.

Computer programs for partial melting and least squares mixing models were kindly donated by Drs. I.L. Gibson and R.C.O. Gill respectively.

Financial support was received in the form of a research studentship from the Science Research Council for two years and a grant for one year from the U.L.R.C. Discretionary Fund. My thanks, again, to Mr. M. Kerridge for this extra funding.

CONTENTS

DIAGRAMS

Page

TABLES

CHAPTER 1

INTRODUCTION

1.1 The Use of Trace Elements in Geochemistry

Of the ninety naturally occurring chemical elements, eight constitute 98% by weight of the continental crust. These are oxygen, silicon, aluminium, iron, magnesium, calcium, sodium and potassium and are conventionally described as the major elements. The next three, in order of abundance (the minor elements) are titanium, phosphorus and manganese, while the remaining 79 are known collectively as the trace elements. These definitions also hold for the composition of the mantle except that K, Ti and P are usually regarded as trace elements and Cr and possibly Ni as minors.

During any magmatic or metmorphic process, the mineralogy of the resultant rock is governed by its major element composition and by the externally applied physico-chemical conditions (i.e. pressure, temperature, partial pressure of volatiles etc.). In any such process, however, the trace elements have no controlling effect on the mineralogy, rather the mineralogy controls the distribution of the trace elements. By observing trace element distributions in rocks, it is therefore possible to determine the mineral phases that have played a significant part in the evolution of various igneous and metamorphic suites.

The way in which a trace element is distributed among the various phases in a geological system depends largely upon its crystallo-chemical properties. The work of Goldschmidt (1937, 1954) demonstrated that, for the most part, the main determining properties are ionic charge and radius. These he incorporated into his three empirical rules of trace element substitution. Since his work, however, as more data have become available, a greater number of exceptions to these rules have been discovered. This has led to the consideration of additional properties such as bond strength and electro-negativity (Ringwood, 1955) and crystal field stabilisation (Burns 1970) to explain various phenomena in trace element geochemistry. These properties, however, are only applicable to elements that tend to occur as ionic species in magmatic and metamorphic processes. Consequently, the distributions of elements such as Ge Ga Sn Mo and As that tend to bond co-valently with oxygen are less well understood, their distributions being governed by their ability to substitute for tetrahedrally co-ordinated silicon in liquid as well as in solid phases. More recently, two more factors affecting trace element distributions have been investigated. The first of these involves the rate of diffusion of a trace element through silicate liquids and crystals, a property that, although difficult to measure, is critical in determining the time taken for equilibrium to be attained. Secondly, the presence of a volatile phase can have a marked effect on trace element mobility, probably due to the formation of gaseous complexes (see, e.g. Mysen 1979 and Flynn and Burnham 1978).

From the above brief description, it is clear that the distribution of trace elements in geological systems is a complex process and, as yet, poorly understood from a theoretical stand-point. It has been found useful, however, to express observed distributions in terms of partition coefficients, denoted K_d and defined:-

$$K_d^i = \frac{X_A^i}{X_B^i} \qquad 1.1$$

where X_A^i and X_B^i are the concentrations of element i in phases A and B respectively. In the special case where B is a silicate liquid and A is a co-existing crystalline phase, the K_d value can be used to predict the behaviour of a trace element in such processes as partial melting and fractional crystallisation.

During partial melting, two extreme cases may be considered viz.equilibrium (or batch) melting and ideal fractional melting. In batch melting, in which the whole body of partial melt equilibrates with the residue before extraction, the relative concentration of a trace element in the liquid is given:-

$$\frac{C_L}{C_O} = \frac{1}{K + F(1 - K)} \qquad 1.2$$

where C_L = concentration of the trace element in the melt

C_0 = concentration of the trace element in the original solid

K = partition coefficient

F = degree of partial melt ($0<F<1$).

During ideal fractional melting, the liquid fraction is formed by the accumulation of successive small fractions of partial melt in isolation from the solid residue. In this case the equation becomes:-

$$\frac{\bar{C}_L}{C_0} = \frac{1}{F}\left|1 - (1 - F)^{\frac{1}{K}}\right| \qquad 1.3$$

where $\bar{C}_L$ is the aggregate concentration of the trace element after a fraction, F, of partial melting.

Equations 1.2 and 1.3 refer to the melting of a single phase. If a polyphase aggregate (such as a rack) is melted, a bulk distribution coefficient, D is defined:-

$$D = X^{\alpha} K^{\alpha} + X^{\beta} K^{\beta} + \ldots X^{n} K^{n}$$

Equations 1.2 and 1.3 become:-

$$\frac{C_L}{C_0} = \frac{1}{D + F(1 - D)} \qquad 1.4$$

and $$\frac{\bar{C}_L}{C_0} = \frac{1}{F}\left|1 - (1 - F)^{\frac{1}{D}}\right| \qquad 1.5$$

Furthermore, if the phases are eliminated in non-modal proportions, and the fraction of phase i in the melt is defined p^i, then an additional factor, P is calculated:-

$$P = p^{\alpha} K^{\alpha} + p^{\beta} K^{\beta} + \ldots p^{n} K^{n}$$

and the equations become:-

$$\frac{C_L}{C_0} = \frac{1}{D + F(1 - P)} \qquad 1.6$$

and $$\frac{\bar{C}_L}{C_0} = \frac{1}{F}\left|1 - (1 - \frac{PF}{D})^{\frac{1}{P}}\right| \qquad 1.7$$

For a more complete derivation of these equations see Gast (1968) and Shaw (1970).

Equations can also be used to describe the behaviour of a trace element during fractional crystallisation:-

$$\frac{C_L}{C_0} = F^{K-1} \qquad 1.8$$

C_O = concentration of the element in the original liquid

C_L = concentration of the element in the remaining liquid

F = relative volume of remaining liquid

K = partition coefficient.

Henderson (1975) has incorporated an efficiency factor, E, into equation 1.8, to account for the effects of trapping a fraction of melt. E is defined:-

$$E = (V_R - V_M)/V_R$$

where V_R is the total volume of the rock and V_M the volume of mesostasis. Incorporating this into equation 1.8 gives:-

$$\frac{C_L}{C_O} = F^{(E(K - D)} \qquad 1.9$$

From the above equation, it is clear that if K(or D) is less than 1 for a given element, then that element will tend to be concentrated in the liquid during both melting and crystallisation processes. Alternatively, if K is greater than 1 then the element will be retained in the solid during partial melting, and will be incorporated in the earliest formed cumulates during crystallisation. Such behaviour has led to the development of the terms compatible and incompatible element.

An incompatible element, as defined by Ringwood, is a trace element that is not readily accommodated by a rock forming mineral phase. This is often confused with the term dispersed element (Gast 1968) defined as an element that does not exist as a major (stoichiometric) component of any mineral phase in a given system. As an illustration, the element zirconium, often considered to be an incompatible element, is a stoichiometric componenet of the mineral zircon. It cannot, therefore, be considered as either a dispersed or incompatible element if zircon is present in the magmatic system under study. The rare earth elements, however, are readily but not stoichiometrically accommodated by zircon. In this case, as the K_d values for these elements between liquid and zircon are all greater than one, they cannot be regarded as incompatible in the presence of zircon although they are still dispersed elements. Clearly the terms compatible, incompatible and dispersed elements should be used with care and always with reference to the mineralogy of the magmatic system under consideration.

1.2 The Geochemistry of the Rare Earth Elements

Possibly the most informative data to have been derived from trace element geochemistry are related to the abundances of the rare earth elements, or lanthanides, in various rocks and minerals. The rare earth elements (usually abbreviated to REE) are the fourteen naturally occurring elements of atomic numbers between 57 (La) and

71 (Lu); the fifteenth element (Pm, No. 61), being radioactive, does not occur naturally. As a direct result of their electronic structure, these elements display a remarkable similarity in chemical properties.

The electronic structure of La comprises completely filled orbitals up to 4d, 5s and 5p, (i.e. comparable with the noble gas Xe) with two electrons in the 6s and one in the 5d shells. This is usually denoted $|Xe|5d^16s^2$, and is similar to the other group IIIB elements $Sc|Ar|3d^14s^2$ and $Y|Kr|4d^15s^2$. Energy released during chemical reactions is sufficient to ionise the s and d shell electrons resulting in the very stable noble gas configuration and a common valency of +3 for these elements. In the periodic table, Sc and Y are followed by the first and second row transition elements in which the 3d and 4d orbitals are gradually filled. However, for the elements following La, it becomes energetically favourable to progressively fill the 4f orbital. Hence La is followed by a group of elements with a generalised electronic configuration of either $|Xe|4f^n5d^16s^2$ or $|Xe|4f^{n+1}5d^06s^2$ where n ranges from 1(Ce) to 14(Lu). As with La, energy released during chemical reactions is sufficient to ionise s and d electrons and one f electron, which results in a common valency of +3 for the whole REE series. Anomalous valencies can arise, however, under certain conditions. For example the electronic structure of Ce can be oxidised to the very stable Xe structure by the loss of the 4f 5d and $6s^2$ electrons, giving a valency of +4. Similarly, as half filled

and completely filled electron orbitals are energetically favourable, there is a tendency for Eu to ionise to $Eu^{2+}(|Xe|4f^{7}5d^{0}6s^{0})$ and Yb to $Yb^{2+}(|Xe|4f^{14}5d^{0}6s^{0})$. Under most geological conditions, however, only the Eu anomaly is of particular importance although anomalous Ce abundances can arise under strongly oxidising conditions (e.g. during late stage hydrothermal and other rock-water interactions).

The second, and probably most important consequence of this electronic configuration is a phenomenon known as the lanthanide contraction. The highly directional nature of the individual components of the 4f orbitals in space, leads to the imperfect shielding of 5p and 4f electron by other 4f electrons. Thus, as the atomic number (i.e. nuclear charge) increases so does the effective electrostatic attraction of the nucleus on each of the 4f and 5p electrons. As the 4f orbitals lie within the space occupied by 5d, 5p and 6s shells, this results in a gradual decrease in size of both atomic and ionic radii as the atomic number increases (e.g. the ionic radius of the +3 oxidation state decreases from 1.13$\mathring{A}$(La) to 0.95$\mathring{A}$(Lu)). Furthermore, as the 5p and 6s shells are spherically symmetrical, the ter-positive lanthanide ion is not subject to crystal field stabilisation effects. (It is the spherical asymmetry of the outer d orbitals that leads to crystal field stabilisation effects in the geochemical properties of the transition metals (Burns 1970)). As a result, the geochemical properties of the REE are very similar, the distribution of these elements being controlled by the common +3 oxidation state and the systematic change in ionic radius.

The effects of the lanthanide contraction are particularly well illustrated by the K_d values for the REE between various minerals and basaltic liquids (see fig. 1.1). As the ionic radii decrease, there is a tendency for the heavier REE to become more compatible. This is particularly so for garnet, for which K_d values rise as high as 5(Lu). Also shown in fig. 1.1 are K_d values for plagioclase which illustrate the effects of the divalency of Eu. As Eu^{2+} possesses an ionic radius comparable with that of Ca^{2+} and Sr^{2+}, it substitutes for Ca^{2+} in the plagioclase structure more easily than do the other REE, giving rise to Eu anomalies in rocks affected by plagioclase fractionation.

The REE therefore provide us with useful indications of the possible mineral phases that have played an important role in the evolution of rock suites and, used in conjunction with the equations described in section 1.1, can form the basis of semi-quantitative petrogenetic models. It should be noted that petrogenic models based on K_d values are, at best, only semi-quantitative in that they assume that the value of K_d is a constant. Clearly, from the opening discussion of section 1.1 this is not so. However, until the variables controlling the values of K_d are more clearly defined and quantified more precise models cannot be established.

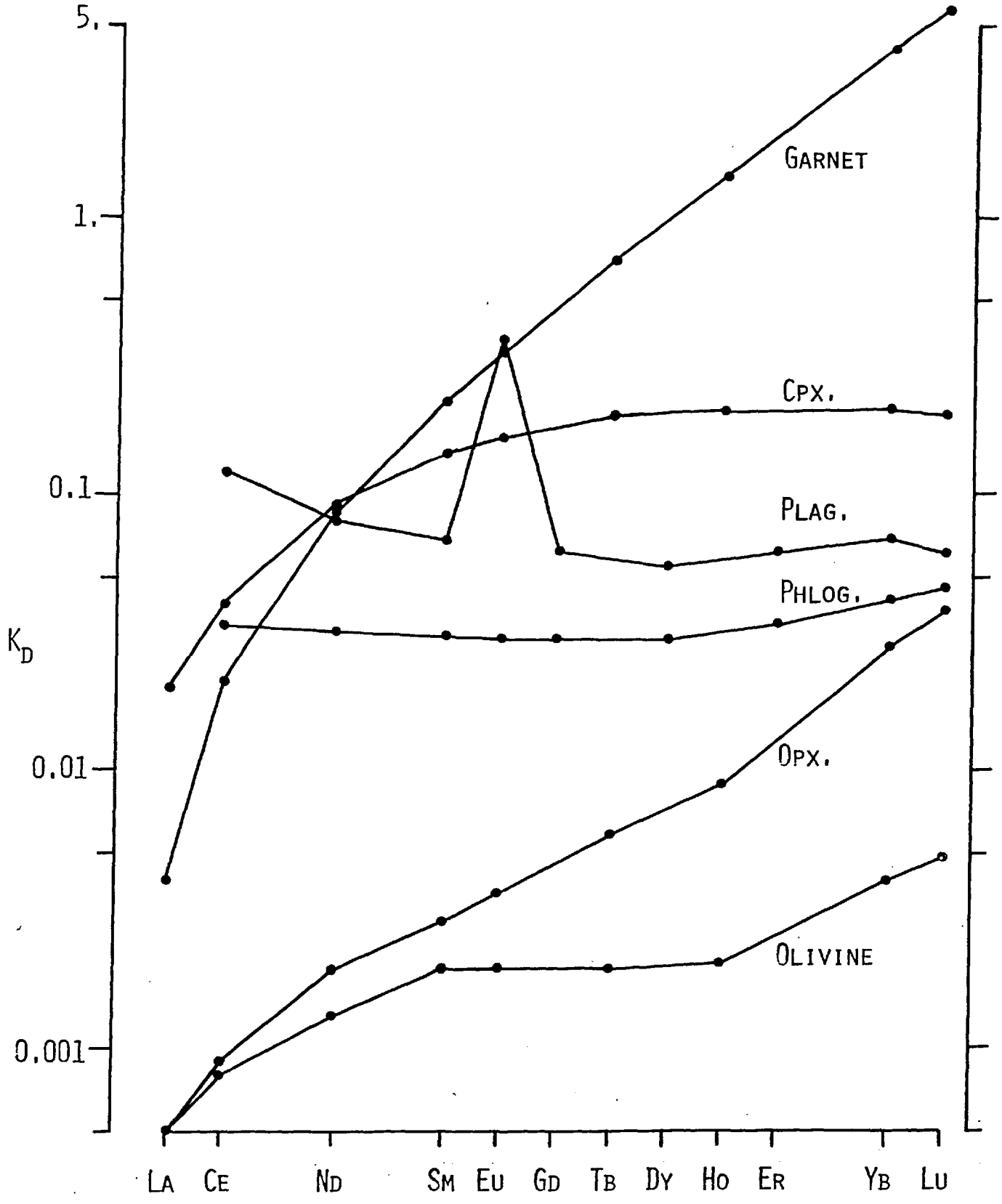

Fig. 1.1 Variation of K_d with REE Atomic No.

Garnet, Opx. (Orthopyroxene), Cpx. (Clinopyroxene) and Olivine data from Frey et. al. (1978). Phlog. (Phlogopite) and Plag. (Plagioclase) data from Arth and Hanson (1975).

1.3 Rare Earth Element Analysis

The similarity in the properties of the REE renders their analysis, by conventional means, a difficult process. The separation of the REE as a group, however, is relatively simple and was first accomplished, as early as 1794, by Gadolin. However, it was not until the early twentieth century that all of the naturally occurring lanthanides had been individually isolated, illustrating the magnitude of the problem when employing classical chemical techniques. Today, the REE are usually separated by ion exchange chromatography after a simple group separation (see Hooker and O'Nions 1975, Brunfelt et al. 1974).

Post separation analysis can be effected using a variety of spectrometric techniques, although only two techniques are of sufficient precision and have low enough detection limits to be of great use in geochemistry. These are isotope dilution mass spectrometry (IDMS) and neutron activation analysis (NAA). Of the two, IDMS is capable of giving the most precise analyses (i.e. better than ±3% at the 95% confidence level) but can only be used for elements with two or more stable isotopes (i.e. La, Ce, Nd, Sm, Eu, Gd, Dy, Er, Yb and Lu). NAA, by comparison, can be used, in conjunction with radiochemical separation procedures, to much lower detection limits, and, in theory, for all fourteen elements. As NAA depends upon the nuclear as opposed to electronic, properties of an element, the problem of mutual inter-

ferences during analysis, although important, is not as prohibitive as in other spectrometric techniques. Thus it is usually possible to analyse a rock for some of the REE using purely instrumental NAA (INAA), without having to resort to even a group separation. Chemical separations for the individual elements, or, at least, separate groups of the REE by ion exchange chromatography are always required in IDMS. Furthermore, during INAA information on other elements can be obtained whereas different chemical separations would be required to gain similar information from IDMS.

Although activation analysis had been used for many years in conjunction with radiochemical separations and NaI(Tl) scintillation detectors, it was only with the development of high resolution semiconductor Ge(Li) detectors during the 1960's that instrumental activation analysis of silicate rocks became possible. (See e.g. Cobb 1967, Gordon et al. 1968 and Denechand et al. 1970.) Further advances occurred with the development of ultra-high resolution low energy photon detectors using small crystals of very pure Ge, allowing more precise analysis of γ-rays in the 60-150 keV energy range (Hertogen and Gijbels 1971). This led, particularly, to an improvement in REE analysis, ten of these elements emitting relatively intense low energy γ-rays after neutron irradiation. The state of the technique is now such that radiochemical separation procedures are only required if the REE are present at levels below about 3 x chondritic meteorites.

The chondrite standard has proven to be particularly useful for graphically displaying geological REE abundances. If an anlysis is plotted on a graph of concentration (ppm) against atomic number, then a characteristic zig-zag abundance pattern is defined, the even atomic number elements being significantly more abundant than their neighborouring odd number elements. This is a result of the Oddo-Harkins rule, reflecting the enhanced nuclear stabilities of the even numbered elements. The zig-zag can be eliminated, however, if the rock abundances are divided by the REE abundances in chondritic meteorites and this normalised value plotted against atomic number. The chondrite values used in this work are from Haskin et al. (1968). Originally the chondrite standard was used in an attempt to relate magma compositions to a possible primitive Earth composition. While the chondritic Earth hypothesis is now subject to considerable debate, this does not invalidate the use of the chondrite standard for the REE for purely comparative purposes, the usefulness of which is manifest.

1.4 The Application of Trace Element Analysis to Kimberlite Geology

The rare volcanic rock, kimberlite, has recently attained a significance to the modern Earth Sciences that is out of all proportion to its limited occurrence at the surface of the Earth. It is the primary surface source of all natural diamonds, thereby suggesting derivation from very great depths within the mantle. In fact it is probable that kimberlites are derived from depths greater than for

any other rock type known to outcrop at the surface. The deep mantle origin is further reflected by the presence of included ultrabasic xenoliths, which result from the violent, gas fluidised mode of eruption. Accidental xenoliths are also derived from the deeper layers of the continental crust. It is these samples from the otherwise inaccessible layers of the Earth that have triggered the recent interest in kimberlite geology.

Kimberlite can be defined as a serpentenised, porphyritic, micaceous peridotite, generally occurring in the form of a pipe (diatreme) or dyke. Although, as suggested above, they are volumetrically insignificant, a single kimberlite province may comprise hundreds of individual pipes, extending over a very large area. They tend to be confined to continental regimes, kimberlites described from oceanic or orogenic environments (e.g. Borneo), being of dubious petrologic affinity. In many respects, kimberlites are compositionally similar to other ultrabasic rocks, possessing low SiO_2 and Na_2O abundances and high MgO and FeO. Other elements, however, are anomalously abundant, e.g. TiO_2, Al_2O_3 and CaO, and K_2O is especially so. This unusual chemical character is further reflected in the abundances of the trace elements. As with all ultrabasic rocks, the abundances of the compatible trace elements, (e.g. Co, Ni, Cr, etc.), are high, but so too are those of the incompatible and volatile elements. In this respect, kimberlites are similar to ultra-potassic volcanic rocks, carbonatites, lamprophyres, nephelinites and other silica undersaturated magmas, character-

istic of continental geological environments. One of the aims of this work has been to discover if these similarities are reflected in the REE and other trace element abundances of these rocks and to elucidate any petrogenetic connections that may exist between them.

Recent research into the petrology and geochemistry of xenoliths from kimberlites has greatly increased our knowledge of the constitution, composition and evolution of the upper mantle. These xenoliths are generally ultrabasic or basic in composition and include such rock types as lherzolites and harzburgites (both often garnet bearing) with subordinate dunites. These rocks are considered to be representative of the greater part of the upper mantle. The less abundant, but still widespread xenoliths of eclogite and pyroxenite are of less certain significance but may have been derived from isolated bodies within the mantle, formed by the solidification and re-equilibration of basic melts trapped at depth. Of increasing significance are xenoliths rich in mica (Dawson and Smith 1977) which demonstrate the importance of volatile elements in mantle processes.

The analyses of ultrabasic xenoliths reported in this work are mainly restricted to garnet lherzolite and harzburgites. These have been shown (e.g. Nixon and Boyd 1973) to possess a variable composition, consistent with their having been depleted, to varying extents, by partial melting. It should be possible, with the semi-quantitative models outlined in section 1.1, to use the trace element abundances to test this hypothesis.

The third group of rocks analysed are a suite of high pressure garnet granulite xenoliths thought to be derived from the lower continental crust. These samples possess a mineralogy of garnet, pyroxene and plagioclase and a basaltic major element composition. Also included in this suite are garnet pyroxenites which are in mineralogical continuity with the granulites. The major element composition of the granulites is again consistent with a depletion hypothesis (Griffin et al. 1979) although it is uncertain whether the depletion is a result of partial melting or crystal cumulate processes. Once again, it is hoped that the application of trace element models will help in defining the probable evolution of these samples and their protoliths.

1.5 Bibliography

Apart from the specific references cited in the text, various other publications were referred to for general background information on the topics discussed. These included:-

Carmichael, I.S.E., Turner, F.J. and Verhoogen, J. 1974 "Igneous Petrology" McGraw-Hill.

Meyer, H.O.A. 1977 Mineralogy of the Upper Mantle- A Review of the minerals in mantle xenoliths from kimberlite. Earth Sci. Rev. 13 251-281.

Nixon, P.H. (Ed.) 1973 "Lesotho Kimberlites" Lesotho Nat. Dev. Corp. Maseru.

Phys. Chem. Earth 9 1975 (Proceedings of the 1st International Kimberlite Conference, Cape Town, 1973).

Comprehensive Inorganic Chemistry 4 Lanthanides and Transition metal compounds Pergamon, Oxford, 1973 .

CHAPTER 2

NEUTRON ACTIVATION ANALYSIS

2.1 Theory

Neutron activation analysis (NAA) involves the irradiation of samples with neutrons followed by the measurement of the radioactivity induced in the sample. During irradiation, a neutron can interact with a target atomic nucleus in any of the following ways:-

1. Excitation. The target nucleus is excited to a higher energy level, from which it decays to the ground state by emitting a γ-ray:-

$$M + n_1 \rightarrow M^* + n_2$$

followed by

$$M^* \rightarrow M + \gamma.$$

2. Neutron Capture. The incident neutron is captured by the target nucleus and a new nucleus of $\sim$1 atomic mass unit greater is formed. As the total mass of the free neutron plus the target nucleus is greater than the mass of the new nucleus, the excess energy is liberated as prompt γ-rays within 10^{-12} sec of the capture occurring. This phenomenon is known as radiative capture and is represented by the (n,γ) symbol.

3. (n,x) reactions. The capture of a neutron by the target nucleus may induce the emission of a second particle, e.g. a proton as in (n,p) reactions, an alpha particle (n,α) etc. These reactions, however, tend to be of importance only in epithermal or fast neutron irradiation, due to the extra energy required to overcome the strong nuclear force before the second particle can be liberated.

4. At very high neutron energies fragmentation of the target nucleus may occur.

5. In a few cases e.g. ^{235}U, thermal neutron irradiation may induce nuclear fission in the target nucleus. Generally, only neutron capture reactions, of either the (n,γ) or (n,x) type are of importance in neutron activation analysis.

During neutron irradiation, the reaction rate is given by the following equation:-

$$R = \frac{m\, f\, N\, \phi\, \sigma}{A} \quad s^{-1} \qquad (2\text{-}1)$$

where m = target mass (g)

f = fractional abundance of the target isotope

N = Avogadro's number

ϕ = irradiating thermal neutron flux (n $cm^{-2}s^{-1}$)

σ = cross section to thermal neutron capture (cm^2)

A = Atomic weight of target element.

If the product nuclide is radioactive with a decay constant $\lambda\,(s^{-1})$ then the amount produced after time t_i (X_i) is given:-

$$X_i = \frac{m\ f\ N\ \phi\ \sigma\ t_i}{A}\ (1 - e^{-\lambda t_i}) \qquad (2\text{-}2)$$

where t_i is the duration of the irradiation.

As the activity is measured a time t_w after irradiation the actual amount of the product isotope, X_t is:-

$$X_t = X_i e^{-\lambda t_w}$$

where t_w is the delay between the end of irradiation and the start of the observation. Furthermore, the activity is decaying while the sample is being counted. Therefore the total number of decays integrated over a count time t_c is given:-

$$D = \int_0^{t_c} X_t e^{-\lambda t} dt = \frac{X_t}{\lambda}(1 - e^{-\lambda t_c}) \qquad (2\text{-}3)$$

If the relative intensity of the γ-ray of interest is given by I and the efficiency of the detector at that energy by ε the observed integrated count is defined as:-

$$C = DI\varepsilon = \frac{\varepsilon\ I\ m\ f\ N\ \phi\ \sigma}{\lambda A}\ e^{-t_w}\ (1 - e^{-\lambda t_i})\ (1 - e^{-\lambda t_i}) \qquad (2\text{-}4)$$

If the only unknown in 2-4 is m, then it should be possible to calculate absolutely, the amount of the element from a knowledge of C. However, in practice, difficulties in measuring some of the parameters, particularly ϕ, σ and ε, lead to considerable errors. Until these parameters are more accurately defined, the most precise method of NAA is to use elemental standards irradiated at the same time as the samples; the technique employed in all the analyses reported here.

For a given element, assuming that sample and standard are irradiated simultaneously and the same detector is used for each analysis, the parameters ε, I, f, N, ϕ, λ, σ, A, t_i and t_c are the same and t_w for both sample and standard are known, then it follows that:-

$$\frac{C_{SAM}}{C_{STD}} = \frac{m_{SAM}}{m_{STD}} \frac{e^{-\lambda t_{w_1}}}{e^{-\lambda t_{w_2}}} \qquad (2\text{-}5)$$

where t_{w_1} and t_{w_2} refer to sample and standard respectively. Therefore m_{SAM} can be easily calculated.

2.2 Modes of Radioactive Decay of use in NAA

Radioactive nuclides produced by (n,γ) and (n,x) reactions decay to stable nuclei usually by β^+ or β^- emission, with or without

accompanying γ-rays. The use of pure β^+ or β^- emitters in NAA is limited by the low penetrating power of the particles. In the case of β^- particles (electrons), this results in much self absorption within the sample and considerable external and internal scattering. Furthermore, the particles are emitted over a band of energies rather than at a discrete energy. Thus energy dispersive spectrometry detects events from all the β^- emitters within a sample. Information regarding a specific isotope can only be obtained by chemically separating it from the sample after irradiation or by analysing the decay of radioactivity within the sample with time, with a knowledge of the half lives of the isotopes involved.

Similarly β^+ particles (positrons) are scattered and come to rest quickly in solid material when they rapidly annihilate with an electron, their anti-particle. They can, therefore be detected indirectly by the 511 keV γ-rays that result from annihilation. However, as all positrons annihilate in the same way, it is again impossible to distinguish two positron emitters without the use of chemical separation or decay analysis.

In many cases, the β particle does not carry the total decay energy and the remainder is liberated in the form of γ-rays. As γ-rays are the result of transitions within the nucleus, they are emitted with

discrete energies, generally within the range from 60 to 4000 keV. Furthermore, γ-rays have great penetrating power and consequently suffer little scattering or absorption. It is through energy dispersive γ-ray spectrometry that much NAA is carried out.

2.3 The Detection of γ-rays

Electro-magnetic radiation can interact with matter in three ways:-

1. The photo-electric effect. All the energy of the incident photon is used to ionise detector atoms.

2. The Compton Effect. This is the result of elastic scattering of photons by electrons in outer orbitals of the target atoms. During a collision part of the γ-ray energy is lost to the electron and the γ-ray is scattered through an angle θ. The energy of the scattered photon is dependent on θ:-

$$E_\gamma = \frac{E_o}{1 + (E_o/m_o c^2)(1-\cos\theta)} \qquad (2\text{-}6)$$

where E_o is the initial γ-ray energy and $m_o c$ the rest mass of the electron (511 keV).

3. Pair production. If a γ-ray is of an energy above 1.022 MeV, it can interact with the electromagnetic field of an atomic nucleus to produce an electron-positron pair.

An efficient γ-ray detector is so designed that as many of the incident photons as possible give rise to the photo-electric effect, and of those that undergo either of the remaining processes, any scattered or secondary γ-rays are absorbed within the detector. An event corresponding to the total energy of the incident photon is recorded if all of its energy is deposited in the detector by any combination of the above three processes. These events correspond to a photopeak in γ-ray spectrometry. However, if after Compton scattering, the scattered photon escapes, only the energy of the scattered electron will be deposited. Since $E_o = E_e + E_\gamma$ and E_γ is a function of cos θ, this produces a broad spectrum of recorded energies with a maximum energy defined:-

$$E_{MAX} = \frac{E_o}{1 + m_o c^2/2E_o} \qquad (2\text{-}7)$$

The sharp drop in the continuum at E_{MAX} caused by this process is known as a Compton edge.

In the case of pair production, should a positron annilate with an electron and one or both of the resulting γ-rays escape, then events at E_o - 511 keV and E_o - 1022 keV are recorded. These are respectively known as single and double escape peaks. All of these features are illustrated in fig. 2.1.

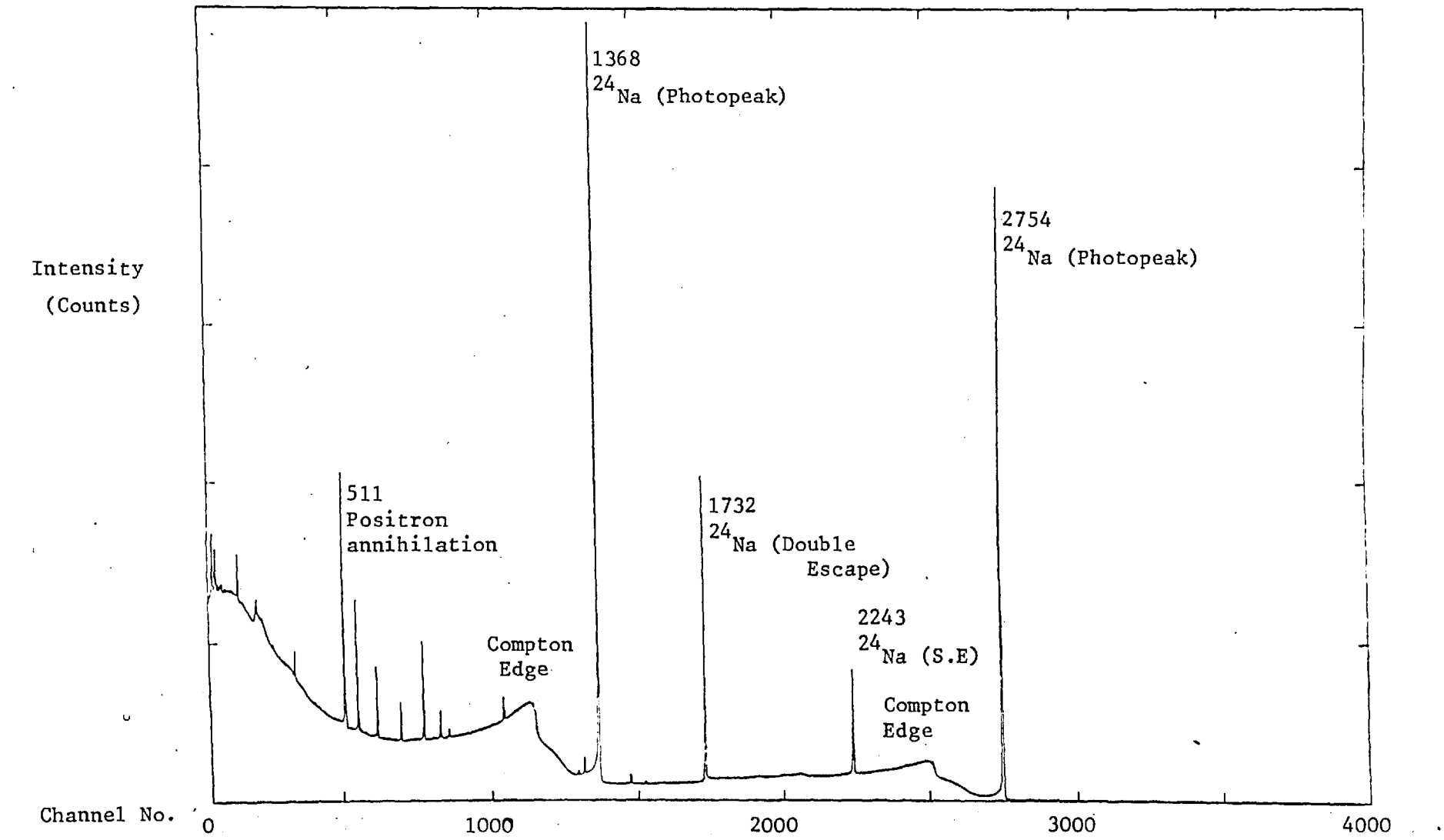

Fig. 2.1 A Typical γ - Ray Spectrum from a Ge(Li) Detector. (^{24}Na Source on filter paper. Unlabeled peaks are due to impurities e.g. ^{82}Br and ^{125}Sb).

The two most widely used types of γ-ray detectors today are scintillation and semi-conductor detectors. The scintillation detectors are usually Thallium-activated Sodium Iodide crystals (NaI(Tl)) which employ, directly, the photoelectric effect. Absorption of a γ-photon excites K-electrons in the crystal, resulting in the production of secondary photons. These are, in turn, detected by the photo-sensitive cathode of a photo-multiplier tube. As the number of secondary photons produced is dependent upon the energy of the initial γ-photon, the amplitude of the pulse from the photo-multiplier tube is proportional to the energy of the γ-ray, thus allowing energy dispersive spectrometry through pulse height analysis.

Semi-conductor γ-ray detectors employ the unusual electrical properties of germanium. When a γ-photon is absorbed by germanium, electrons are excited from the valence band to the conduction band by the photoelectric effect. This produces electron-hole pairs within the detector crystal, the number of electron-hole pairs being proportional to the energy of the incident γ-ray. If an electric field is applied across the detector and the electron-hole pairs collected then the charge pulse so produced is also proportional to the incident γ-ray energy. Defects and impurities within the crystal can slow down the collection process by trapping the charge carriers. In order to optimise the collection process, an electron donor, usually lithium is diffused

into part of the detector and then drifted towards the centre under a strong electric field producing n, i and p layers as shown in fig. 2.2. This configuration is known as a p-i-n junction, only the i (intrinsic) layer acting as the detector, as both p and n layers are conductors. As lithium atoms readily diffuse through germanium at room temperature, lithium drifted germanium detectors (Ge(Li)) must be operated at liquid nitrogen temperatures in order to maintain the p-i-n junction. If, however, the germanium can be made pure enough and a crystal grown such that imperfections and dislocations are kept to a minimum, lithium drifting becomes unnecessary. Thus, hyper-pure germanium detectors, as they are known, can be warmed up to room temperature without permanent damage being done. They are, however, operated at low temperatures to reduce thermal excitation of electrons to the conduction band, which, at room temperature, would result in considerable background noise. Unfortunately, only small crystals of suitably pure germanium can be produced economically (up to $\sim$3 cm^3 volume) so that their use tends to be limited to low energy photon spectrometry in the energy range up to 400 keV, hence their alternative description as low energy photon detectors (LEPD).

Ge and Ge(Li) detectors are now used for γ-ray spectrometry almost to the exclusion of their NaI(Tl) counterparts as they possess a much higher resolution and improved peak to Compton ratios. The improved resolution is a result of the low energy required to excite one

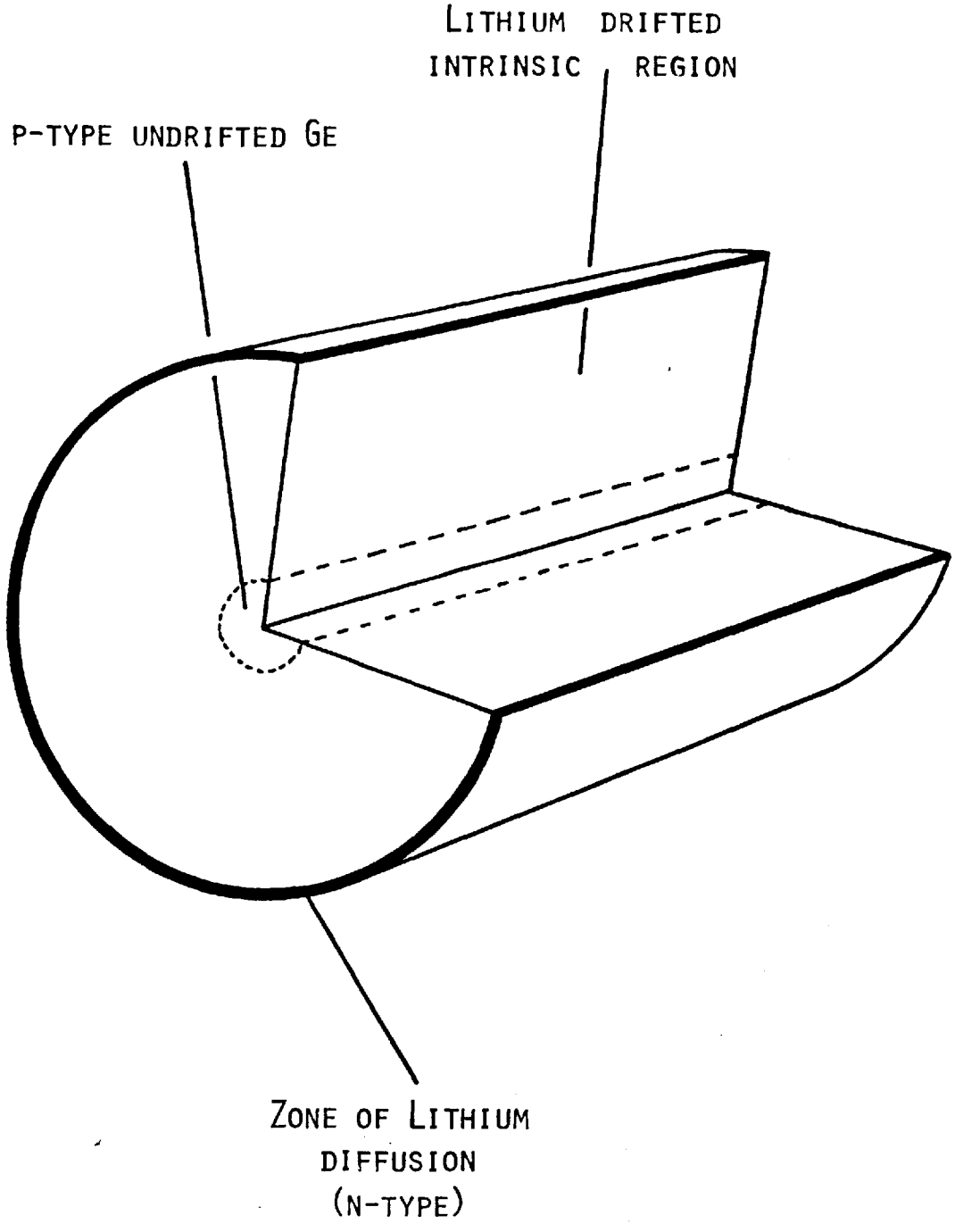

Fig. 2.2 A cut-away diagram of a typical co-axial Ge(Li) γ-ray detector.

electron in Ge (∿2.9 eV) compared with that required to produce one photo electron in NaI (∿300 eV). The improved peak to Compton ratio is achieved by controlling the geometry of the detector, thereby minimising the Compton effect and allowing the absorption of as many scattered electrons and photons as possible, in the intrinsic region of the detector.

As both types of detector produce output signals proportional to the energy of the incident photon, pulse height analysis of the signals allows energy dispersive spectrometry. This is of limited use for NaI(Tl) detectors because their poor resolution and low peak to Compton ratio result in a complex spectrum of overlapping peaks and high continuum counts which is difficult to analyse. This disadvantage is, however, compensated for slightly by their relatively high efficiency, especially in those cases where it is necessary to detect low levels of γ-activity (as in counting natural radioactivity in rocks). In analytical geochemical applications, such situations are rare; therefore the remainder of this chapter specifically refers to the use of Ge and Ge(Li) detectors in NAA.

2.4 Gamma Ray Spectrometry

A block diagram of a typical γ-spectrometer is shown in fig. 2.3 and is briefly described for a Ge or Ge(Li) detector.

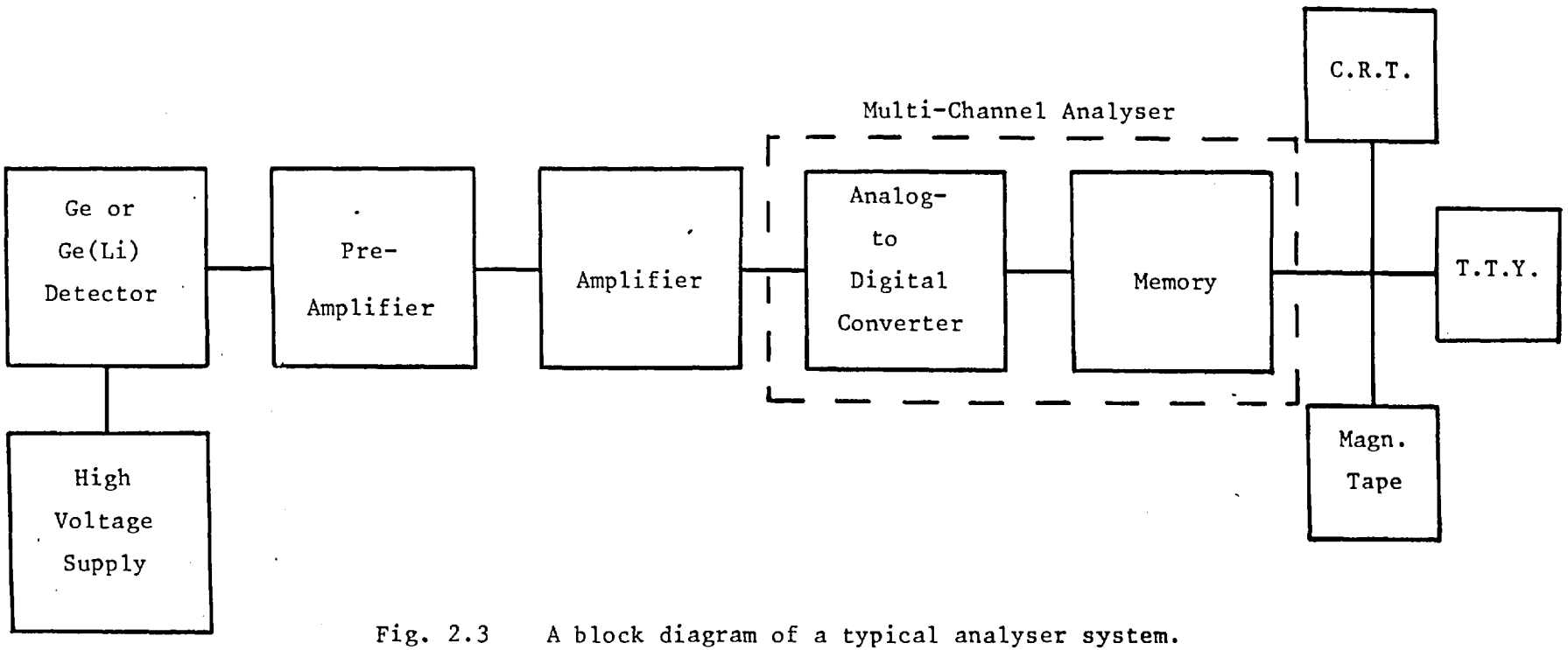

Fig. 2.3 A block diagram of a typical analyser system.

The H.T. unit supplies the high voltage bias, as shown in fig. 2.2., allowing for the rapid sweeping of charge carriers from the intrinsic region. For a typical detector the applied field is approximately 1 kV per cm. The pre-amplifier (or head amplifier) is located physically close to the detector in order to reduce noise which can result from long connecting cables. It is a charge sensitive device with an output voltage proportional to the charge produced by the detector. The main amplifier, as well as providing considerable signal gain, shapes the pulse with respect to time so as to optimise the detector resolution. The signal then passes to the multi-channel analyser which comprises two main parts:- (a) The analog-to-digital converter (A.D.C.) which converts the input pulse height to a digital number. (b) The memory stores the pulse as one event in a channel according to the digital number produced by the A.D.C. The high resolution of semi-conductor detectors necessitates the use of memories with at least 1024 channels and preferably more. Output options from the M.C.A. usually include a visual display unit (such as a CRT or TV screen) as well as the usual computer compatible facilities (e.g. paper tape, magnetic tape, etc.)

The spectrometer used in the work presented here, produced by Link Systems Limited, is based on an 8K Nova mini computer, interfaced, via the necessary electronics, to either a 42 cm^3 Ge(Li) detector or a 5 mm thick planar Ge detector with an active area of 100 mm^2. 5K of

the computer memory is dedicated to recording events in 4096 channels (up to 2^{20} - 1 counts per channel) while the other 3K is programmed for simple data analysis, and the control of sample changers, data output and sample counting times.

2.5 The Analysis of γ-Ray Spectra

The raw data from neutron activation analysis consists of a digital spectrum of counts per channel vs channel number, the latter being linearly related to the energy of the incident photon. From equation 2-5 it is known that for an element x, assuming all counts are corrected for half life decay:-

$$\frac{m_x^{SAM}}{m_x^{STD}} = \frac{C_x^{SAM}}{C_x^{STD}} \qquad (2\text{-}8)$$

Thus C_x values must be determined. For samples with only one radioactive species, C_x may represent the total activity of the sample or standard. In the more usual case, however, the total activity is due to a number of isotopes. Consequently, only those events directly associated with the isotope of interest may be included in equation 2-8. This is accomplished by interpolating the Compton continuum beneath a photopeak of the isotope of interest and calculating the area of the peak above the interpolated line. Such interpolation - correction procedures fall into three main categories of increasing sophistication:-

1. Simple arithmetic correction. A good example of this type of analysis is that described by Covell (1959). It involves the selection of two channels, one either side of the peak centroid (and not necessarily in the Compton continuum), calculating the area of the trapezium so defined and subtracting this area from the total counts in the defined channels. In activation analysis, this type of correction should only be applied when sample and standard peaks are of comparable sizes and is best suited to the determination of intense peaks.

2. Continuum (or background) fitting. Where a computer is available and the spectrum data computer compatible, increased accuracy can be obtained by fitting the continuum on either side of the peak to a low order polynomial which is then interpolated beneath the peak. The peak area is then determined by subtracting the interpolated continuum in each channel from the observed channel counts within the peak region. The two major disadvantages with this method involve the definition of the peak-continuum boundary channels and the resolution of multiple peaks. If multiplets are to be determined mathematically then the third form of spectrum analysis is required.

3. Complete Spectrum fitting. This can only be achieved, with care, using large computer programs based on iterative fitting procedures. As an example, SAMPO (Routti and Prussin 1965) fits each peak to a Gaussian function with exponential tails, superimposed on a linear or binomial continuum. As well as calculating various fitting

parameters, calculating efficiency and energy calibrations and peak areas, it is also capable of resolving multiple peaks. Much of this data is, however, superfluous for routine activation analysis and the program itself uses a large amount of computer time and space. Also it is generally necessary to run each spectrum through the program a number of times, to give the best fit, thereby increasing the analysis time.

As may be appreciated, each method has its own advantages and weaknesses and is suited to different applications. For routine activation analysis, a large number of peaks must be integrated, for which peak areas must be accurately defined and errors calculated. Thus speed and precision are of the utmost importance. It was therefore decided that an interactive graphics computer program should be developed that would allow both rapid inspection and integration of each peak using either a Covell-type or polynomial background fitting correction. As the program displays each peak on a graphics terminal screen, the continuum-peak boundary channels can be chosen individually for each peak encountered. This is a distinct advantage over the preset boundary channels imposed by the calculation procedures on the Link Systems spectrometer and also provides a polynomial correction option which reduces errors due to counting statistics compared with the simple Covell technique.

2.6 SPEC5 - An Interactive Graphics Computer Program for the Rapid Reduction of γ-Ray Spectra

The original aim of this program was to allow a more detailed analysis of γ-ray data from the Link Systems spectrometer using the facilities readily available on a large computer. As the emphasis was on routine use, and so that information from twelve spectra could be stored on the computer, the region of interest output mode was adopted. For every sample, instead of printing out the whole 4096 channel spectrum, which would be very time consuming, only those channels around the peak were recorded. Despite the disadvantage of losing possibly useful data in not printing the whole spectrum, by being selective, total print-out time is much reduced, thereby significantly increasing the available counting time. Furthermore, the amount of data to be sorted is much reduced and therefore more easily analysed.

The program was written to be compatible with the Link System output format. Data is transferred to the computer coded on paper tape. Two simple editing programs need to be run before the data can be read by the program. Once displayed on the Tektronix terminal screen, up to five peaks within the region displayed can be integrated, either by a method similar to Covell's (1959) or by the total peak area (TPA) method using a polynomial fit to the Compton continuum.

The Covell type correction is similar to that described above. The area of the background trapezoid, B, is calculated:-

$$B = \frac{Y(N_1) + Y(N_2)}{2} \quad (N_2 - N_1 + 1) \tag{2-9}$$

where Y(i) refers to the count in channel i (see fig. 2-4). The corrected integral, I, is therefore given:-

$$I = \sum_{i=N1}^{N2} (Y(i) - B \tag{2.10}$$

As the statistics of counting are governed by the Poisson distribution, the standard deviation of a count, N, is defined as its square root. In the case of background correction, only one count, corresponding to I + B, is recorded and to calculate I, B must be estimated as in equation 2-9.

i.e. $I = (I + B) - B$

$\therefore \quad \Delta I = \Delta(I + B) + \Delta B$

$\therefore \quad \sigma(I) = \sqrt{I+B + \sigma^2(B)}$

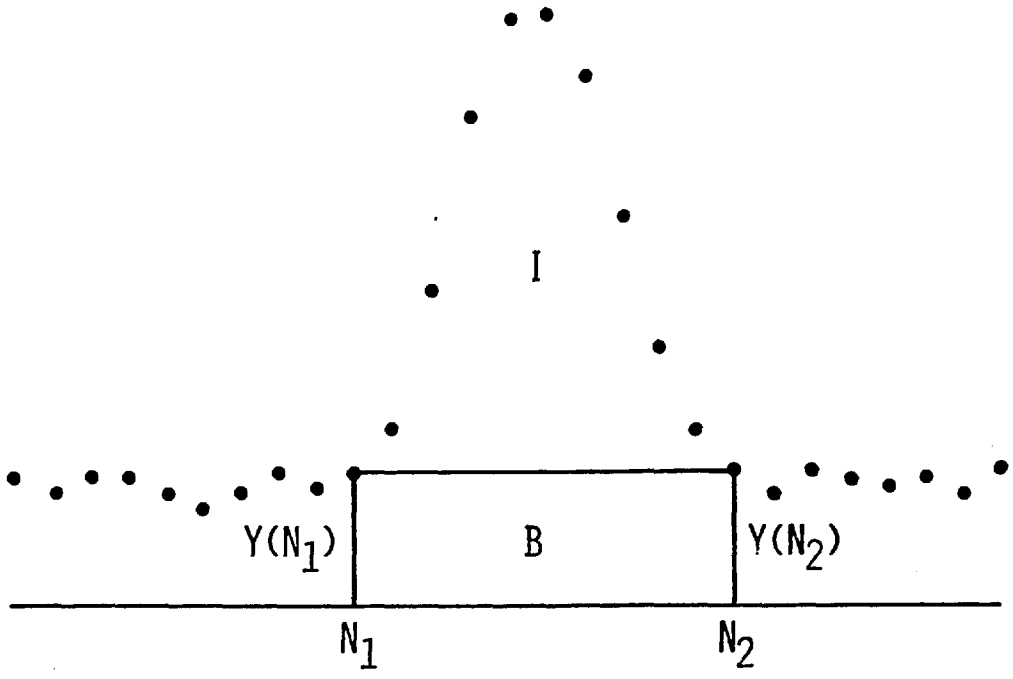

Fig. 2.4 Trapezoid or Covell-type background correction. Note that N_1 and N_2 need <u>not</u> be channels from the continuum region of the spectrum.

Quittner (1972) has demonstrated that $\sigma(B)$ will depend upon the number of channels over which B is calculated. Taking this into account he suggested that $\sigma(I)$ can be approximated:-

$$\sigma(I) = \sqrt{I + (1 + \frac{N2 - N1 - 3}{2})B} \qquad (2\text{-}11)$$

This is the algorithm used in SPEC5 to calculate errors on peak integrals determined by Covell's method.

From a consideration of equation (2-11), it is clear that the wider the peak (i.e. the greater the value of N2 - N1), the greater the value of $\sigma(I)$. This is not too critical for spectra from Ge(Li) detectors where integrals are calculated over a maximum of $\sim$7 channels, resulting in $\sigma(I) < \sqrt{I + 3B}$. However, the broader peaks from Ge LEP detectors, caused by the expanded energy calibration of 0.1 keV/channel, require a more precisely defined continuum in order to reduce the relative size of $\sigma(I)$. In SPEC5 this is achieved by approximating the continuum to a low order polynomial.

When using the polynomial analysis, the channels representing the continuum on either side of the peak are chosen by eye. A pre-written library subroutine then uses these channels and their contents to calculate the polynomial curve which is to be interpolated beneath the peak. The final power of the fitted polynomial is chosen according to the following criterion. If the goodness of fit parameters for the

equation of power n+1 is not 60% better than that for the equation of power n, then the equation of power n is chosen. While the final power chosen depends upon the number of channels to be fitted and the number of peaks within the region of interest, for singlets with ∿15 channels on either side, n is generally 3 or less and only reaches 3 for intense peaks.

Calculation of the integral is illustrated in fig. 2-5. Using the same notation, the integral is given:-

$$I = \sum_{i=L2+1}^{R_1-1} (Y(i) - B(i)) \qquad (2\text{-}12)$$

As before $\sigma(I) = \sqrt{I + B + \sigma^2(B)}$

However, as a larger number of channels have been used in estimating the continuum beneath the peak, a more complicated algorithm is required to account for $\sigma(B)$. In SPEC5, one of the equations from Rogers (1970) has been adopted:-

$$\sigma(I) = \sqrt{I + \tfrac{1}{4}\left|\left(2 + \frac{N-2}{m}\right)(N-2)(\bar{a}_L + \bar{a}_R)\right|} \qquad (2\text{-}12)$$

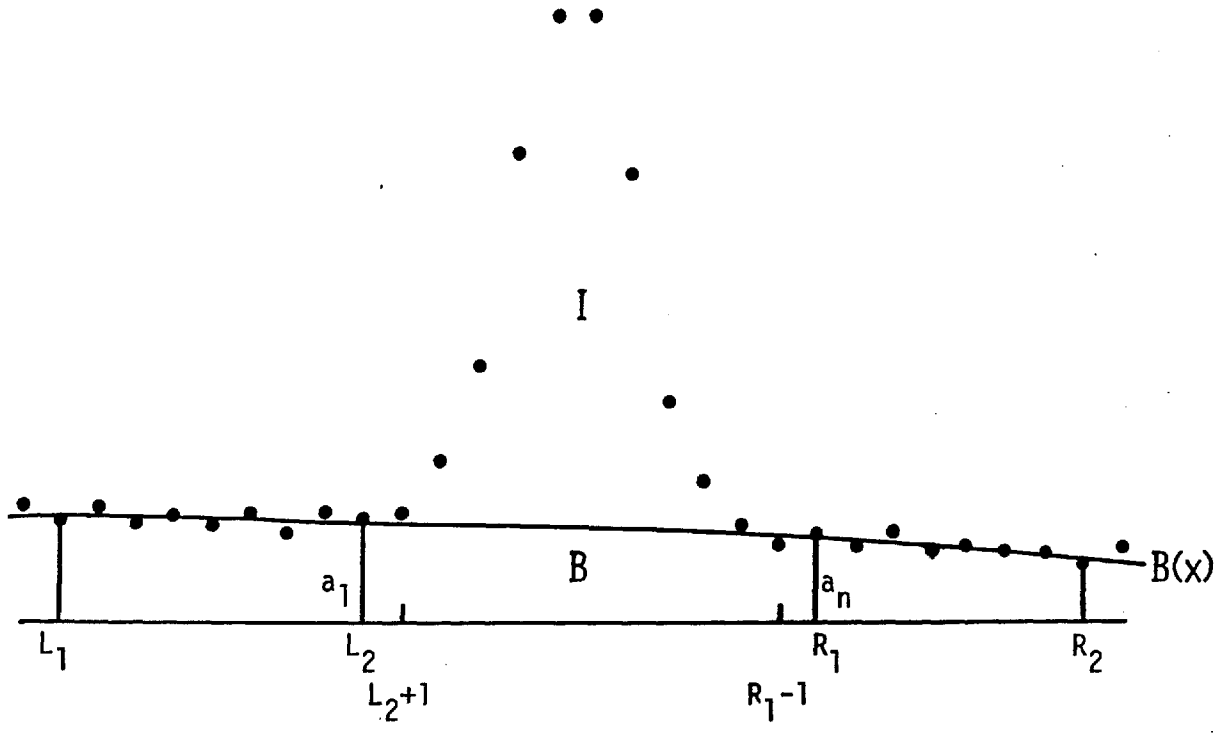

Fig. 2.5 Continuum or background fitting, using a least squares fit on channels L_1- L_2 and R_1-R_2 inclusive, and interpolating the function, B(x), beneath the peak.

where $N = R_1 - L_2\ 1$,

$m = ((L_2 - L_1 + 1) + (R_2 - R_1 + 1))/2$

and $\bar{a}_L$ and $\bar{a}_R$ are the values of B(x) in channels L_2 and R_1 respectively.

If, again, B is the area subtracted, then in a typical example where m=10 and N=15, $\sigma(I)$ is given

$$\sigma(I) \approx \sqrt{I + 1.43B}$$

compared with $\sigma(I) = \sqrt{I + 7B}$ for a simple Covell correction.

Examples of both correction techniques are illustrated in figs. 2-6 and 2-7.

While the program can integrate up to five peaks in any one region of interest, it is not capable of resolving multiplets. In such cases, either the whole area of the multiplet is calculated and then corrected by ratio (see below) or part of the peak relatively unaffected by the interference is calculated using the Covell method. This is illustrated in fig. 2-6.

After the analysis is complete, the area and error are displayed on the screen and there is an option to save the relevant data on a local file for future reference. The program is listed in full in appendix 2-1.

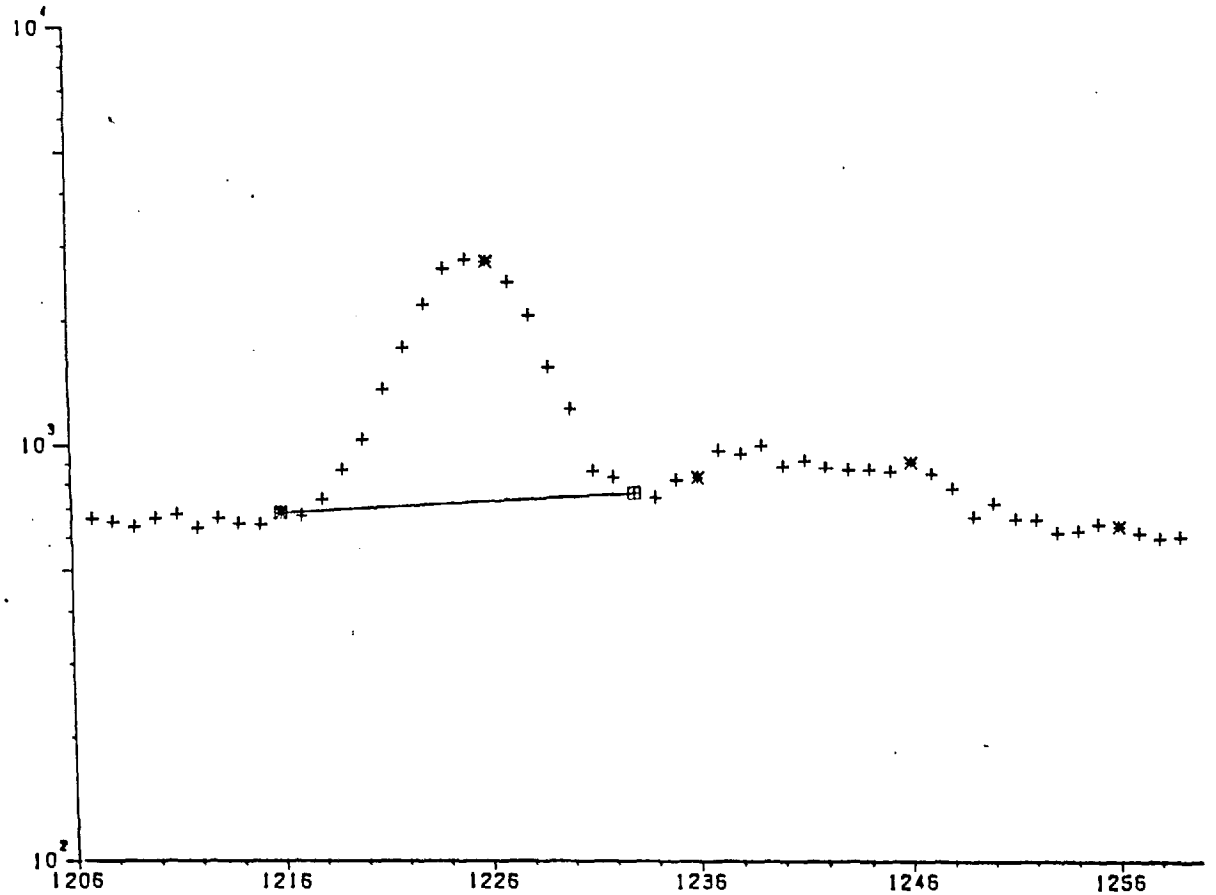

Fig. 2.6 An example of the Graphics terminal screen display of the Covell type correction option of SPEC5 on th 121.4kev photopeak of ^{152}Eu. (taken from a spectrum of BCR-1 after a 35hr irradiation and 3 weeks decay).

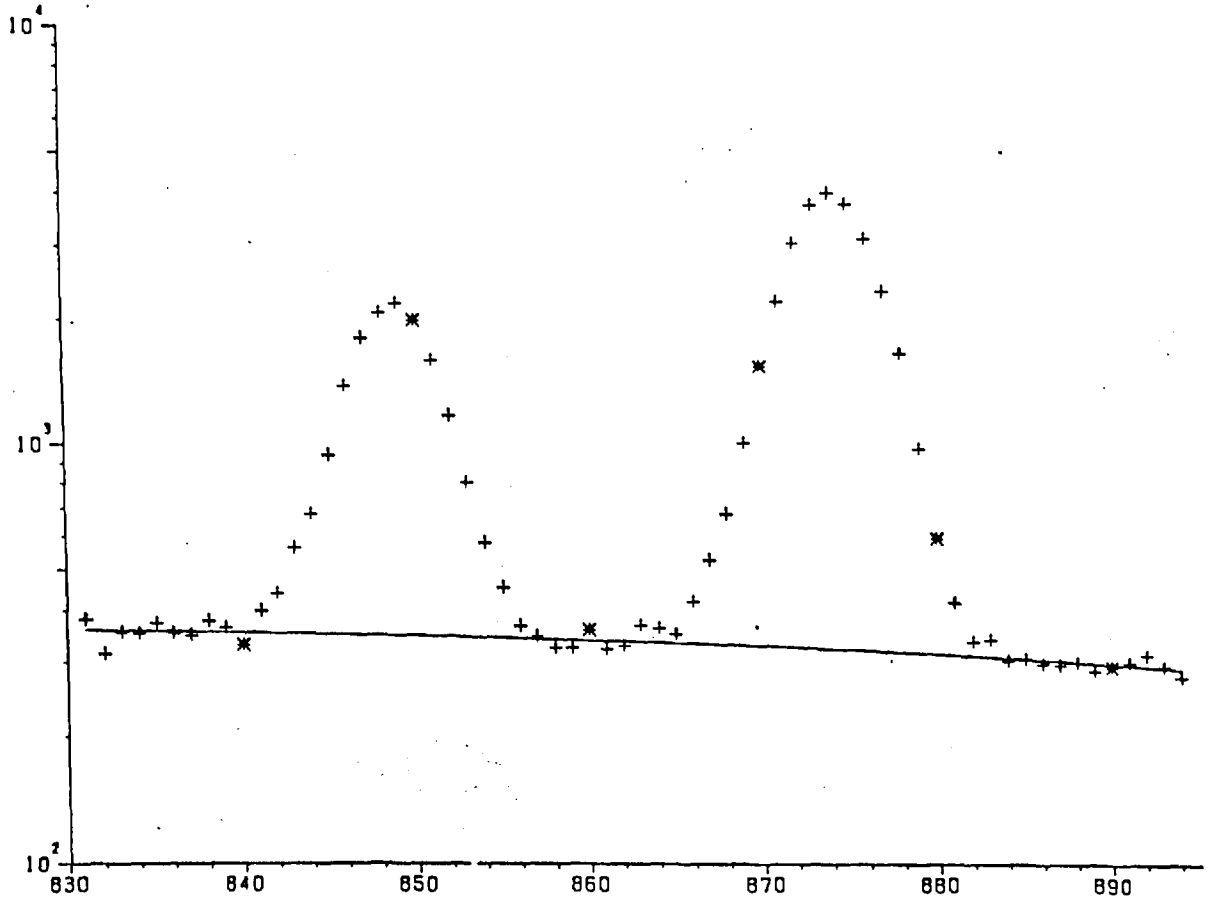

Fig. 2.7 An example of the polynomial background fittingoption of SPEC5 on the 84.4kev peak from ^{170}Tm and the 86.6kev peak from ^{160}Tb. Note that these peaks suffer interferences from Ta and Th, respectively, although both appear as singlets. (Taken from a spectrum of multi-element standard solutions JMES3B and JMES5)

2.7 Analytical Technique

Having described the basis of NAA, it is now possible to synthesise the details into a viable analytical method.

2.7.1 Irradiation

Approximately 100 mg of sample are weighed into a small polythene vial. Nine such vials and three standards are further encapsulated in a large polythene tube which is heat sealed. The standards and samples are stacked in the tube such that there is a standard vial at each end of the tube and one near the middle. This arrangement allows for the correction of systematic variations in the irradiating neutron flux. The tube is then irradiated in a core tube of the ULRC "Consort" Reactor for five working days (∿35 hrs) in a neutron flux of $\sim 10^{12}$n $cm^{-2}s^{-1}$. Samples are unloaded on the morning following the fifth day with the reactor shut down in order to minimise exposure of operating staff to radiation from short lived radionuclides such as ^{26}Al and ^{52}Mn.

2.7.2 Counting and Data Analysis

After irradiation, samples are counted three or four times depending upon equipment availability and the elements to be determined. After 4-6 days, samples and standards are counted sequentially on the Ge and Ge(Li) detectors for ∿3000 secs each, allowing the determination of Ho, Sm, U, La and Lu. The counting procedure is repeated

Table 2.1 Relevant data on the nuclides used for Activation Analysis in this work.

Element	Nuclide	Energy	Half Life	Detector Used	Interferences and energies.
La	^{140}La	328.8 487.1 815.7 1596.5	40.3hrs	Ge(Li)	None
Ce	^{141}Ce	145.4	32.5days	Ge	^{175}Yb 144.7
Nd	^{147}Nd	91.1	11.1days	Ge	None
Sm	^{153}Sm	103.2	46.7hrs	Ge	^{239}Np 103.7 ^{233}Pa 103.9
Eu	^{152}Eu	121.8	12.2yrs	Ge	^{154}Eu 123.1
Tb	^{160}Tb	86.8	72.3days	Ge	^{233}Pa 86.6
Ho	^{166}Ho	80.6	26.8hrs	Ge	None
Yb	^{169}Yb	63.1	30.7days	Ge	Lu X-ray (Standard Only)
Lu	^{177}Lu	208.4	6.75days	Ge(Li)	^{239}Np 209.8
U	^{239}Np	106.1 277.5	2.35days	Ge Ge(Li)	None None
Th	^{233}Pa	94.7 311.8	27.0days	Ge Ge(Li)	^{169}Yb 93.6 None
Cs	^{134}Cs	795.8	2.07yrs	Ge(Li)	None
Sc	^{46}Sc	889.4 1120.3	83.9days	Ge(Li)	None
Co	^{60}Co	1173.1 1332.3	5.23yrs	Ge(Li)	None
Cr	^{51}Cr	320.0	27.8days	Ge(Li)	None

For short irradiations and yield determinations the following nuclides were used:

Eu	^{152m}Eu	121.8 344.2 963.5	9.36hrs	Ge or Ge(Li) Ge(Li) Ge(Li)	None
Dy	^{165}Dy	94.7 361.7 633.4	2.33hrs	Ge Ge(Li) Ge(Li)	None

after a further 2-4 weeks decay for 15-20 000 secs on each detector. From this data the concentrations of Ce, Nd, Eu, Tb, Yb, Sc, Cr, Cs, Th and Co can be calculated. The isotopes used, their most intense γ-photopeaks and other relevant data are listed in table 2-1. Photopeak areas are determined either automatically by the Link System Covell program (Ge(Li) spectra only) or by SPEC5 (data from the LEPD). The areas are then corrected for interferences, the ratios used being listed in table 2-3 together with the energy of a suitable singlet peak of the interfering nuclide. Finally, concentrations are calculated using a second computer program, RIALTO (Carder and Bray 1974).

2.8 Sources of Error and their Evaluation

2.8.1 Sample Preparation

As with all methods of trace element analysis, sample preparation for NAA is most critical especially as it is often necessary to irradiate only small specimens (up to 200 mg). Consequently the sample must be ground finely to ensure homogeneity but in such a way that contamination is kept to a minimum. An additional complication in the analysis of xenolith samples from kimberlites is that the original material may be very limited, most xenoliths being of cm dimensions only and the largest rarely exceeding a few kg in weight. Samples are first broken down into chips of $\sim$.5 cm diameter before being crushed in an agate Tema. An agate barrel is used as this will only add SiO_2 to the sample. A tungsten carbide barrel can add significant amounts of first row transition elements, particularly Co. Unfortunately,

some specimens were supplied that had already been crushed in a tungsten carbide barrel. As well as giving rise to erroneous Co analyses, it was also discovered that X-rays from ^{187}W ($t_{\frac{1}{2}}$ 24 hours) interfered with various low energy γ-rays, notably ^{153}Sm at 69.7 keV. This was overcome by analysing Sm on the 103.2 keV peak. Other samples were prepared by crushing in a cyanide hardened steel hand percussion mortar. No significant contamination of the elements of interest resulted from this method.

2.8.2 Sample Containers

The samples were irradiated in polythene ampoules which were, in turn, sealed in a polythene tube. For instrumental NAA, samples were counted in the ampoules in which they were irradiated. The ampoules were therefore cleaned prior to irradiation by washing in dilute HNO_3 for $\sim$2 hours and rinsed in demineralised water before drying at 110°C. This removes most of the impurities with the exception of Br, Sb and sometimes Au. The standards were prepared by evaporating aliquots of solutions on to filter papers which again contain significant and variable amounts of Br and Sb as well as Na. Consequently, signals from these elements were not used, and any required information on their abundances obtained by alternative means.

2.8.3 Standard Preparation

The multielement standard solutions used in this study were prepared from stock solutions supplied by Johnson Matthey Limited, certified at a concentration of 1g/100ml. Aliquots of these solutions were then mixed in the appropriate proportions and diluted to 500ml with demineralised water. Grade A glassware was used throughout, the standard tolerances being used to calculate the maximum error of the final concentration. Interferences from impurities in the standard solutions were considered negligible from the data given on the certificate accompanying the solutions. The concentrations of the multielement standard solutions are given in table 2-2 a and b.

2.8.4 Neutron Flux Variation

Variations in the observed count rate from a sample due to neutron flux variations during irradiation are of two types:- macroscopic and microscopic. The microscopic variations result from the presence or absence of nuclides with high neutron capture cross sections in the sample, causing local perturbations in the neutron flux gradient and, possibly, self shielding. Fortunately, in most geological samples, these nuclides are present in only trace quantities, far below the minimum level required for self shielding to be of significance.

Table 2.2 Concentrations of elements in artificial multi-element standard solutions used for activation analysis.

1. JMES5 (REE)

Element	Concentration (µg/100µl)	% Error
La	3.0 ± 0.0105	0.35
Ce	6.0 ± 0.0162	0.27
Pr	1.00 ± 0.0037	0.37
Nd	5.0 ± 0.0175	0.35
Sm	0.60 ± 0.0024	0.40
Eu	0.200 ± 0.0008	0.40
Gd	6.0 ± 0.0162	0.27
Tb,Dy,Ho Er & Tm	1.0 ± 0.0037	0.37
Yb	0.50 ± 0.0020	0.40
Lu	1.00 ± 0.0037	0.37

2. JMES3B

Cr	10.0 ± 0.025	0.25
Co	5.0 ± 0.0175	0.35
Cs	2.0 ± 0.0110	0.27
Th	2.0 ± 0.0110	0.27
Sc	1.00 ± 0.0037	0.37
U	1.00 ± 0.0037	0.37

Macroscopic variations are attributable to the geometry of the reactor core. In the case of the Consort reactor, the distribution of the neutron flux along the length of a core tube approximates to a cosine curve. This can result in a significant flux gradient between one end of an irradiating capsule and the other. To correct for this, three standards are included in each capsule, one at each end and the third in a central position. During the data analysis, all samples between two standards are normalised to a straight line defined by those two standards before any concentrations are calculated.

2.8.5 Counting Statistics

As discussed in section 2.4, all counting data is subject to the statistics of the Poisson Distribution. Thus, each calculated peak integral is an estimate of the real peak area and can be assigned a standard deviation dependent upon the method of peak integration used. This error must, therefore, be taken into account when calculating the concentration of an element. From equations 2-11 and 2-12 it can be seen that the ratio $\sigma(I)/I$ is smallest when I is large and B is small. As a result, the multi-element standards have been prepared so that photopeak integrals are large ($>10^4$ counts), giving low relative standard deviations (i.e. <1%). This reduces the statistical error of the analysis to that observed in the gamma spectrum from the sample.

2.8.6 Errors due to Interferences

Sometimes, γ-photopeaks from two different nuclides have energies so close that they cannot be resolved using normal solid state detectors. If this is the case with a peak from one of the isotopes of interest, then either the interference must be resolved using a mathematical fitting routine or a correction factor must be applied from a knowledge of the intensity ratios of the different photopeaks of the interfering isotope. For the reasons given above, the second alternative has been chosen for this work. As an example, in the case of ^{153}Sm, the analysis is usually performed using the 103.2 keV peak. Unfortunately, there are two significant inteferences on this peak, one at 103.7 from ^{239}Np and the second of 103.9 keV from ^{233}Pa. As the half life of ^{153}Sm is 46.7 hrs and those of ^{239}Np and ^{233}Pa 2.35 days and 27 days respectively, it is impossible to allow the interferences to decay before attempting the analysis. From irradiated samples of pure U ($^{238}U(n,\gamma)^{239}U \rightarrow {}^{239}Np + \beta$) it is known that, using the Link System detector, the area of the 103.7 keV peak is 82% of the area of the 106.1 keV peak which is interference free. Hence, after the area of the 103.2 keV peak has been calculated, 82% of the area of the 106.1 keV peak of ^{239}Np must be subtracted before the final concentration is calculated. The ^{233}Pa interference can be treated in the same way by irradiating a sample of pure Th ($^{232}Th(n,\gamma)^{233}Th \rightarrow {}^{233}Pa + \beta$). A list of the relevant correction factors is given in

Table 2.3 Ratio correction factors for photo-peak interferences.

Nuclide	Energy (kev)	Interference	Energy (kev)	Ratio correction factor.
^{144}Ce	145.4	^{175}Yb	144.7	9.25% of 113.8kev peak
^{153}Sm	103.2	^{233}Pa	103.9	8.40% of 94.8Kev peak
		^{239}Np	103.7	82.0% of 106.1kev peak
^{152}Eu	121.8	^{154}Eu	123.1	Use Covell bg. correction only.
^{160}Tb	86.8	^{233}Pa	86.6	25.8% of 94.8kev peak
^{169}Yb	63.1	Lu x-ray		34.2% of 56.1kev x-ray (std. only)*
^{177}Lu	208.4	^{239}Np	209.8	38.8% of 277.5kev peak
^{233}Pa	94.8	^{169}Yb	93.6	3.40% of 63.1kev peak

* This correction need only be applied to the standard JMES5, which possesses a relatively high concentration of Lu.

table 2-3. Note that these factors are relevant only to the Ge and Ge(Li) detectors on the Link System at ULRC, as the measured ratios are related to the detector efficiency characteristics as well as the absolute γ-emission rates of the isotope concerned.

2.8.7 Conclusions and Evaluation of Results

In summary, the only significant errors from the above points discussed are due to counting statistics which are calculated for each peak analysed. To account for possible errors from the way the flux gradient is measured, any errors in standard perparation and errors due to interferences, an arbitrary figure of 2% is added to the 2σ counting statistics figures. Having taken these sources of error into consideration, predicted 2σ values can be calculated during analysis. These are listed in table 2-4a for the USGS standard rock BCR-1 together with results from eight separate analyses of this rock. It is clear that in most cases the predicted 2σ values are in fair agreement with the actual values as are the means of the eight analyses with the various accepted values. Therefore, it is reasonable to suggest that the accuracy and precision of the technique are similar and are best estimated from a consideration of counting statistics. The precision of the technique is further illustrated by the six analyses of the IAEA sample, SL-1 (lake sediment) circulated as an interlaboratory comparison sample in 1977. The results of this international study have only recently been published and the ranges, means and 2σ figures for the various elements are listed in table 2-4b. Again it is clear that good agreement is seen for most elements. The analyses were carried out without prior knowledge of the REE composition of the sample.

Table 2.4a BCR-1 analyses, determined during normal experimental runs

Element	2σ (pred.)	Concentration (ppm)	2σ (actual)	Accepted values 1	2	3
La	5%	25.4 ± 1.1	4.3%	24.2	26.	25.
Ce	8%	56.2 ± 6.7	12%	53.7	53.9	54.
Nd	10%	27.4 ± 3.1	11%	28.6	29.	29.
Sm	3%	6.68 ± 0.426	6.4%	6.70	6.6	6.6
Eu	5%	1.94 ± 0.127	6.5%	1.95	1.94	1.9
Tb	10%	1.09 ± 0.13	12%	1.08	1.0	1.0
Ho	10%	1.29 ± 0.13	10%	1.33	1.2^{m}	-
Yb	5%	3.46 ± 0.34	10%	3.48	3.36	3.8
Lu	10%	0.53 ± 0.05	10%	0.55	0.55	0.6
Sc	5%	31.3 ± 1.8	6%	-	33	34.
Co	5%	36.5 ± 2.4	6%	-	38	37.
Cr	10%	14.0 ± 1.2	9%	-	17.6	16.

2σ (pred.) - 2σ predicted from counting statistics and other sources of error.

2σ (actual) - 2σ values calculated from the 10 analyses

Concentration - Mean values calculated from 10 separate analyses.

Accepted values - 1 Taylor and Gorton (1978)

2 Flanagan (1974)

3 Abbey (1977)

Table 2.4b Results from the analysis of SL-1 (I.A.E.A. inter - laboratory comparison standard, Lake Sediment.)

	This Work			Results from I.A.E.A. comparison			
	μ	2σ	%2σ	Range of values[x]	μ	2σ	%2σ
La	47.2	± 0.7	(2%)	39.7 - 65.6	52.3	7.73	(14.8)
Ce	110.	± 6.8	(6%)	86.8 - 195.	132.5	37.7	(28.5)
Nd	42.6	± 4.2	(10%)	42.6 - 45.7	44.4	1.56	(3.5)
Sm	8.69	± 0.37	(4%)	8.62 - 15.52	10.54	2.36	(22.6)
Eu	1.79	± 0.08	(5%)	1.78 - 2.25	1.90	0.22	(11.6)
Tb	1.13	± 0.13	(12%)	0.93 - 2.20	1.4	0.5	(36%)
Dy*	6.52	± 0.46	(7%)	5.89 - 9.67	7.46	1.71	(22.9)
Ho	1.31	± 0.17	(13%)	n.a.			
Yb	3.28	± 0.12	(4%)	2.90 - 4.27	3.42	0.52	(15.2)
Lu	0.59	± 0.053	(9%)	0.25 - 0.80	0.54	0.18	(33.3)

*Dy was analysed instrumentally after a ten minute irradiation and 30 minutes decay.

n.a. not applicable i.e. no results were reported in the I.A.E.A. document.

x Range of values i.e. those that were not significantly different from the grand mean at the 95% confidence level.

Although this technique is of considerable use for rocks of normal compositions, in the case of ultrabasic samples, where the REE and other trace elements are present in only very low concentrations, the combination of low induced trace element radioactivity with high Compton background from Co, Fe, Cr, Sc etc., necessitates the use of additional analytical techniques involving either chemical separation or epithermal neutron activation. These techniques are now described in greater detail.

2.9 Radiochemical Neutron Activation Analysis

When the signals produced by the isotopes of interest are very small compared with those produced by the major radioactive nuclides in the sample, it is necessary to chemically separate these high activity species before the analysis is undertaken. Such is the case for ultrabasic rocks which possess very variable and usually low concentrations of the REE, but high concentration of Cr, Co and Fe as well as Sc and Na, these five elements accounting for >90% of the induced activity after a 5 day irradiation. After a short irradiation Mn and Na are the main radioactive species. Two radiochemical separation procedures were developed in order to remove these elements before γ-ray spectrometry. The first technique, based largely on that described by Brunfelt et al (1974), involves fusing the rock with a sodium hydroxide/peroxide mixture, followed by dissolusion with dilute acid and separation of sodium in the supernatant liquor. Cr, Co and Fe are then removed by cation exchange

with a column of Dowex 1-X8 resin, pre-equilibrated with 9M HCl. Sc is removed by solvent extraction with tri-n-butyl phosphate and the REE precipitated from the final solutions as fluorides.

Occasionally, the Sc separation step was not particularly successful, only 50% of the Sc being removed. This resulted in a rather higher background than expected and, hence, poorer accuracy in the determination of the very low abundances of Yb and Lu.

The second technique, for isotopes with short half lives (i.e. less than 12 hours), is based on a fluoride precipitation to remove the REE, leaving the main active species (^{56}Mn and ^{24}Na) in solution. A yield determination, based on carrier reactivation, is carried out after the solutions have been counted.

2.9.1 Radiochemical Separation of REE with long half lives

This technique was used in the determination of La, Ce, Nd, Sm, Eu, Yb and Lu and could be extended for Tb and Ho. As with the instrumental technique, samples are irradiated for 5 days in a core tube, four samples and three standards in one capsule. After irradiation and 2-3 days decay, the samples are transferred to Ni crucibles in which a known quantity of REE carrier has been added. The sample ($\sim$200 mg) is then fused with 2g NaOH pellets and $\sim$0.5 g Na_2O_2 for 10 minutes on an electro-thermal bunsen. When the melt has solidified,

the cake is loosened and partly dissolved with a minimum quantity of very dilute HCl. After digestion, the contents of the crucible (which are still alkaline) are transferred to a centrifuge tube, the crucible washed out with dilute HCl and the washings added to the tube. The suspension is then centrifuged at ∿3000 rpm and the sunpernatant liquor discarded. The precipitate is washed with demineralised water, centrifuged again and the washings discarded before the precipitate is dissolved in 5 ml of 9M HCl. If the final fraction of the precipitate does not dissolve, the solution can be heated for ∿5 minutes until it clarifies to a yellow or green colour. When cool, the solution is passed through a column of Dowex 1-X8 resin, pre-equilibrated with 9M HCl, at a rate of 1 drop every 2 seconds, to remove Fe, Co and some Cr. The centrifuge tube is washed out with two further 5 ml quantities of 9M HCl and the washings passed through the column. The eluate from the column (15-20 ml) is then extracted with two 25 ml volumes of tri-n-butyl phosphate to remove Sc and any remaining Fe. The organic phase is discarded. 1 ml of 10% HF is then added to the solution which is carefully neutralised with ammonia solution until a white precipitate of the REE fluorides forms. The suspension is centrifuged, the supernate discarded, the precipitate washed and centrifuged again and the washings discarded. Finally the precipitate is dissolved in a minimum quantity of 6MHNO_3 saturated with H_3BO_3 and the solution made up to 25 ml in a counting vial. A 200 µl aliquot of this final solution is transferred to a 1.3 cm diameter filter paper in an irradiation ampoule and evaporated to dryness ready for the yield determination.

The standards are mounted on aluminium foils and require dissolution in dilute HCl (doped with a known quantity of carrier). The REE are precipitated as hydroxides with NaOH adding the alkali in excess to keep the aluminium in solution as the aluminate ion. The precipitate is centrifuged and washed before being dissolved in a minimum quantity of dilute nitric acid and made up to 25 ml. Again a 200 µl aliquot is taken for the yield determination. This sequence is necessary to remove the aluminium and chlorine from the standard solution, both of which would contribute significant activity to the sample used in the yield determination.

After separation, the REE solutions are counted for 8000-12000 secs each on the Ge(Li) detector and the peak areas determined by the Covell method. Final concentrations are calculated after a correction for relative chemical yield.

2.9.2 Separation of REE with short half lives

This technique is suitable for the determination of Eu and Dy to very low levels with low errors (e.g. 0.1 x chondrite with 2σ <10%).

Two samples of ~0.075 g each together with an aluminium foil mounted standard are irradiated in the In-Core Irradiation System (ICIS) of the Consort Reactor at a neutron flux of 1.1×10^{12}n $cm^{-2}s^{-1}$. After

allowing the induced activity to decay for ∿30 mins (the major activity is due to ^{28}Al ($t_{\frac{1}{2}}$ 2½ mins) from the standard ampoule and must be allowed to decay before handling) the standard is treated as in the above scheme except that the final precipitation of the REE is in the form of fluorides at a pH<7. This prevents the formation of $Mn(OH)_2$, the Mn being derived from impurities in the Al foil.

The samples are fused in Ni crucibles and digested and washed as in the above method. After washing, the precipitate is dissolved in a minimum quantity of HCl; 1 ml of 10% HF is added and the solution diluted. If, on dilution, a white fluoride precipitate does not form, the solution can be partly neutralised with ammonia. If the solution is subsequently over neutralised and a hydroxide precipitate forms, addition of acid will dissolve the hydroxide but leave the fluoride precipitate. This is then centrifuged and washed with dilute HCl before dissolving in the HNO_3/H_3BO_3 mixture. Preparation for counting and yield determinations are as in the first scheme. The solutions are counted for ∿3000 secs each.

2.9.3 Yield Determination

The chemical yields of the separation procedures are determined by re-activation of the .200 µl aliquots taken from the final counting solutions. The aliquots are irradiated simultaneously in ICIS for 10 mins, allowed to decay for up to 3 hours, and then counted using the Ge(Li)

detector for 2-3000 secs. The isotopes used in the yield determination are ^{140}La, ^{147}Sm, ^{152m}Eu, ^{162}Dy and ^{187}Lu. The original carrier solution contains 3 mg of La and Sm and 1 mg each of Eu, Dy and Lu in 100 µl, a 100 µl aliquot being added to each Ni crucible before fusing the sample. The measured integrals are corrected for decay during the counting period and for decay between counting each ampoule. Relative yields are then calculated by dividing the corrected integral for the sample by the corresponding integral from the standard. Assuming the standard to represent 100% yield, each sample integral is then corrected by dividing by the corresponding yield figure before the calculation of the final concentration.

To illustrate the accuracy of the technique and the lowest levels of detection, results from the standard rocks BCR-1, G-2 and PCC-1 are listed in table 2-5.

2.10 The Use of Epithermal Neutrons in Activation Analysis

The previously described techniques have involved irradiation of samples by the total neutron spectrum of the reactor, with neutron energies ranging from virtually zero up to 15 MeV. This reactor neutron spectrum can be divided into three components:-

(1) Fast Neutrons. These are the energetic neutrons, derived directly from nuclear fission, that have suffered little moderation. Their energies typically range up to a maximum of 15 MeV.

Table 2.5 Standard rock analyses by radiochemical NAA

	G-2		BCR-1		PCC-1				
	mean	accepted[a]	mean	accepted[b]	mean	1	2	3	4
La	99.1	96.	23.1	24.2	0.027	0.15	0.147	0.04	-
Ce	169.	150.	50.3	53.7					
Nd	59.3	60.	26.0	28.5					
Sm	7.65	7.3	6.50	6.70	0.0055	0.008	0.0091	0.01	0.0085
Eu	1.47	1.5	1.93	1.95					
Tb	0.52	0.54	0.95	1.08					
Dy	-	-	6.36	6.39	0.022				
Ho	-	-	1.12	1.33					
Yb	0.87	0.88	3.12	3.48	0.024	0.02	0.0149	-	0.031
Lu	0.11	0.11	0.47	0.55	0.005	0.006	0.0037	0.007	0.0085

a - Abbey (1977)
b - Taylor and Gorton (1978)
1 - Flanagan (1974)
2 - Ottonello et. al. (1979)
3 - Garman et. al. (1975)
4 - Frey et. al. (1971)
mean values refer to results from this work.

(2) Epithermal Neutrons may be described as those in the process of being slowed down by the reactor moderator. They possess intermediate energies from ∿1 eV up to 1 MeV.

(3) Thermal Neutrons are in thermal equilibrium with the reactor moderator. Their kinetic energy density function follows the Maxwellian Distribution which shows a maximum at $E = kT/2$ where k is the Boltzmann Constant and T is the absolute temperature of the reactor moderator.

In activation analysis, fast neutron activation has little application as most target nuclides possess small cross sections to fast neutron capture and any radionuclides so produced usually have inconveniently short half lives. In contrast some nuclides possess relatively large cross sections to epithermal neutron capture due to large resonance integrals in the epithermal region.

Many nuclides obey the "1/v - Law", i.e. in the thermal and epithermal energy regions their cross sections to neutron capture are inversely proportional to the velocity of the incident neutrons. This is the case for many nuclides whose (n,γ) products give rise to prominent features in γ-ray spectra from rocks e.g. ^{56}Mn, ^{24}Na, ^{46}Sc, ^{140}La, ^{60}Co. As a consequence of this behaviour, much of the induced activity of these

nuclides is due to thermal neutron activation. In contrast, some nuclides show large departures from this 1/v behaviour in the epithermal region at energies corresponding to favoured nuclear transitions. Such nuclides include U, Th, Cs, W, Ta, Ba, Sb, Rb, etc. Thus much of their induced activity is a result of epithermal neutron activation. It is clear then, that if, during irradiation, the thermal component of the neutron spectrum could be shielded from the sample, the signals derived from these trace elements would be less reduced than those from the other elements. This would result in a relative enhancement of the signal and an increased peak to continuum ratio as some of the continuum is due to the scattering of γ-rays from the 1/v product nuclei. Thermal neutron filtering is achieved by enclosing the sample with a cadmium shield, as cadmium possesses a very high cross section to thermal neutron capture at energies below .55 eV. Above this energy, however, its cross section is virtually zero, thereby allowing almost free passage for the more energetic neutrons.

The epithermal activation properties of a nuclide can be conveniently expressed in terms of the cadmium ratio, R_{Cd}, defined:-

$$R_{Cd} = \frac{\phi_{Th}\,\sigma_0 + \phi_{Epi}(I + 0.44\sigma_0)}{\phi_{Epi}(I + 0.44\sigma_0)}$$

Where ϕ refers to the neutron flux and subscripts Th and Epi to thermal and epithermal neutrons respectively. σ_0 is the cross section to thermal neutron capture and I the total area of resonance integrals in the epithermal region. The factor 0.44 refers to the contribution of the 1/v component to the capture cross section in the epithermal region. For such elements as Na, La, Sc, Co, Fe, etc., the value of I is virtually zero, the epithermal cross section of these elements being defined by the 1/v tail (i.e. $0.44\sigma_0$). Thus, R_{Cd} tends towards high values. Alternatively, when I becomes significantly large, R_{Cd} is reduced. It is, therefore, necessary to know the R_{Cd} values of both the interfering nuclides and the nuclides of interest in order to assess the possible usefulness of an epithermal irradiation. If the R_{Cd} values are comparable, then both activities will be reduced by the same amount if irradiated under cadmium. If, however, R_{Cd} for the nuclide of interest is low compared with the interference, then the activity of the former will be relatively enhanced by epithermal activation. As an aid to this decision Brune and Jirlow (1964) defined an Advantage Factor:-

$$F_a = \frac{(R_{Cd})d}{(R_{Cd})D}$$

where d and D refer to the interfering nuclide and the nuclide of interest, respectively.

Table 2.6 Uranium, thorium and caesium analyses by ENAA.

	BCR-1			AGV-1		
	μ	F	A	μ	F	A
U	1.7	1.74	1.8	1.6	1.88	2.
Th	6.1	6.0	6.0	6.3	6.41	6.4
Cs	1.1	0.95	0.95	1.2	1.4	-

μ - This work
F - Flanagan (1974)
A - Abbey (1977)

It has been subsequently shown that F_a must be >20 for ENAA to be advantageous. Such is the case for U, Th and Cs, and it is by this method that these elements have been determined in the ultrabasic rocks analysed in this study. Although these elements can be determined by INAA in granites and some basaltic rocks, the precision of the analysis is improved with epithermal activation. The method of analysis is similar to that described in section 2.7 except that the ampoules are contained in a cadmium lined aluminium "A-can" during irradiation.

Some results of USGS rocks analysed by ENAA are given in table 2.6. The technique is more fully explained in Steinns (1971).

2.11 Summary

The above described techniques can now be applied to the routine analysis of geological samples. The instrumental technique allows the determination of 9 REE down to a level corresponding to 2-3 x chondrite while the radiochemical procedures can be applied to the analysis of 7 or 8 REE at abundances of 0.1 x chonrite. Under favourable circumstances these numbers can be increased to 11 and 10 elements respectively. U, Th, Cs, Sc and Co can all be determined at sub-ppm levels, instrumentally, using either thermal or epithermal neutron activation, depending upon the elements and samples bein studied. Although Cr has a poorer detection limit of $\sim$10 ppm, it is often more precisely determined by X-ray fluorescence spectrometry. It is possible to determine other elements (e.g. Na, Mn,

Al, Ca, Ni, Ba) by activation analysis, although other techniques, particularly XRF, are quicker and, in many cases, just as precise. As most of the samples in this study have already been analysed for major and trace elements by XRF, it was decided that further analysis for these elements would be an unnecessary duplication.

CHAPTER 3

TRACE ELEMENT ABUNDANCES OF KIMBERLITES AND SIMILAR VOLCANIC ROCKS

3.1 Introduction

The continental crust tends to be dominated by two major suites of igneous rocks related, respectively, to basalts and the granite-granodiorite plutonic association. In addition to these, and sometimes in association, are volumetrically minor volcanic and hypabyssal rocks of much more unusual compositions. These include nephelinites, lamprophyres, alnoites, kimberlites, carbonatites and ultra-potassic rocks. All are characterised by a tendency towards silica undersaturation, volatile element enrichment and high concentrations of incompatible elements. Because of these common chemical features, these rocks have often been considered together in petrogenetic schemes (e.g. Carmichael et al, 1974). In this chapter, the trace element abundances of three different rock types have been determined and compared in an attempt to more closely define any similarities between them. The rocks analysed include lamprophyres (minettes) from the Navajo-Hopi field, Arizona, alnoites from the British Solomon Islands and kimberlites from South African localities. A further common feature of these samples is that they all contain xenoliths of mantle derived garnet lherzolite. The mineralogical and chemical features of these unusual rocks are summarised in table 3.1 a and b.

Table 3.1a. Mineralogy.

Rock	Phenocryst phases	Groundmass phases
Alnoite	phlogopite, olivine	melilite, perovskite, spinel, apatite and feldspathoids.
Lamprophyre* (minette)	diopside, phlogopite, ± olivine	alkali feldspar, diopside, spinel, mica and amphibole.
Kimberlite	olivine (serpentinised) phlogopite	calcite, olivine, mica, diopside, perovskite, spinel + other accessories.

*Lamprophyres also include varieties dominated by biotite, hornblende and plagioclase (kersantites) and others by hb., augite and plagioclase (camptonites).

Table 3.1b Representative Analyses

	1	2	3	4
SiO_2	51.50	48.94	37.36	27.81
TiO_2	1.85	2.03	3.36	2.26
Al_2O_3	11.55	10.11	8.06	5.78
Fe_2O_3	2.38	4.47	5.67	4.48
FeO	4.72	3.60	5.94	4.44
MnO	0.10	0.12	0.18	0.15
MgO	7.90	10.03	18.76	16.71
CaO	9.10	8.98	10.81	16.16
Na_2O	2.55	1.28	3.70	1.11
K_2O	5.67	5.22	2.54	1.15
H_2O^+	1.10	2.92	1.84	6.61
CO_2	n.d.	0.01	0.64	9.37
P_2O_5	0.96	1.08	1.30	1.19

1 - Minette, Ship Rock, Arizona. (Williams, 1936)

2 - Olivine bearing minette, Buell Park, Arizona. (Roden, 1977)

3 - Alnoite intrusive &

4 - Alnoite tuff, both from Malaita, British Solomon Islands (Nixon et. al. in prep.).

It has long been appreciated that kimberlites originate from comparatively great depths within the Earth, probably greater than for any other rock type known to outcrop at the surface. The evidence for this, however, is derived not from the kimberlite matrix itself but from included xenoliths and xenocrysts. Included in this suite is diamond, the high pressure polymorph of carbon which, assuming a continental geothermal gradient, only becomes more stable than graphite at pressures in excess of 45 kb (130-140 km depth). Furthermore, if a diamond contains a silica polymorph, this usually takes the form of coesite, again a high pressure variety suggesting depths of origin comparable with that of diamond.

More recent work on the composition of co-existing minerals in ultrabasic xenoliths from kimberlites has allowed the calculation of 'pyroxene geotherms' (e.g. Boyd, 1973). This work has revealed that some of the samples are derived from depths of up to 200 km + (65 kbar +), thereby suggesting comparable or greater depths of origin for the enclosing kimberlite. Moreover, for the equilibria observed in the xenoliths to be preserved, eruption from these depths must have been very rapid indeed - some estimates range to velocities as high as mach 2 or 3 (McGetchin and Ullrich, 1975), leaving no time for normal magmatic processes, such as fractional crystallisation, en route. Kimberlite is therefore interpreted as being a direct product of the deep mantle and should reflect, in its major and trace element abundances, the processes operative in these deep layers.

Whilst kimberlite alone contains diamond, it is not alone in containing ultrabasic xenoliths. These are found in a variety of volcanic rocks of mantle origin, including lamprophyres, alnoites and other alkalic and silica undersaturated rocks from both continental and oceanic environments (e.g. Jackson and Wright, (1970), Frey and Green, (1974), Frey and Prinz, (1978), Willshire and Shervais, (1975)). The contained xenoliths, however, are usually of the low pressure peridotite facies, with a mineralogy of olivine+orthopyroxene+clinopyroxene+spinel. As this assemblage is unstable towards the assemblage olivine+orthopyroxene+clinopyroxene+garnet at pressures of 20-25 kbar (see, for example fig. 2.10 in Yoder (1976) or fig. 3.10 in Carmichael et al, (1974)) and garnet lherzolites are rare in non-kimberlitic occurrences, most of these host volcanic rocks are inferred to have originated from comparatively shallow depths ($\sim$60 km). Garnet lherzolites are known from some non-kimberlitic localities however, e.g. in minette lamprophyres from the Navajo volcanic field (Ehrenberg, 1977) and in alnoites from the Solomon Islands (Nixon and Boyd, 1977). Derived P-T conditions of equilibration for these xenoliths are in the range of 45-50 kb for the Navajo field and up to 35 kb for the Solomon Islands xenoliths. While these figures correspond to depths greater than those for xenoliths from most basaltic localities, they are still generally less than those derived from most kimberlite nodules.

As well as containing garnet lherzolite xenoliths, alnoites and lamprophyres show other broad similarities with kimberlites. Firstly, they are often closely associated in space and time e.g. alnoites and kimberlites (+ carbonatites) in N.E. Siberia (Nikishov et al, 1972); lamprophyre and kimberlite (+ carbonatite) in Utah, U.S.A. (McGetchin et al, 1973, Roden, 1977) and in Labrador, lamprophyres occur with carbonatite and olivine melilitite and are reported to be chemically similar to kimberlites and alnoites (Dressler, 1975). From the preceeding list of localities, it is clear that this volcanic association is virtually restricted to continental environments. There are no known examples of oceanic kimberlites or lamprophyres and although the Malaita alnoites may be oceanic, the anomalous lithospheric thickening in that region (the Ontong-Java Plateau) suggests that the structure is more complex than is usual for the ocean floor (Nixon and Coleman, 1978). Some lamprophyres are associated with granite intrusions (e.g. Shap, Cumbria) and genetic links have been suggested. However, as has been emphasized by Bachinski and Scott (1979), this is not the case in general, the Navajo field, for example, being free from the granite-granodiorite association.

All three rock types are characterised by relatively high volatile contents and an abundance of volatile-bearing minerals, especially mica. In the case of alnoites and kimberlites, calcite is an essential mineral and the effects of CO_2 rich fluids are manifest.

However, this is not the case with lamprophyres which are relatively CO_2 poor. The importance and primary nature of the volatile constituents is further demonstrated by the mode of occurrence, often in steep sided pipes or diatremes, suggesting gas fluidisation and explosive eruption (Woolsey et al, 1975). Lamprophyres and kimerlites also occur as dykes, especially lamprophyres. Lava flows are seldom seen, although brecciated and tuffaceous varieties of all three rock types are known. All three are basic or ultrabasic in bulk composition but contain high levels of K_2O and TiO_2 and show some enrichment of CaO, FeO and Al_2O_3 over typical ultrabasic rocks. In the case of kimberlites, this is further reflected in the high incompatible trace element concentrations.

The purpose of the work described below is to characterise more fully the trace element geochemistry of these rock types; to compare them with kimberlite and other ultra-potassic rocks, in order to determine whether previously described geochemical similarities are reflected in the trace element abundances; and to investigate the possibility of genetic links existing between these unusual volcanic rocks.

Three suites of rocks have been analysed. The first of these is a collection of minettes (mica lamprophyres) from the Navajo volcanic field, Arizona. There are very few published REE analyses of lamprophyres (e.g. Bachinski and Scott (1979) 3 analyses, Cullers and Medaris (1977) two analyses) but in both cases, a similarity with kimberlite has been

noted. The alnoite suite is from Malaita, British Solomon Islands and these are the first comprehensive alnoite REE analyses. To complete the comparison, fifteen kimberlite samples from Lesotho and South Africa have been analysed and the results compared with those from published work.

3.2 Results

The results of the analysis of the alnoites, kimberlites and lamprophyres, listed in Appendix 3.1, were obtained using the instrumental neutron activation technique outlined in Chapter 2. Representative REE analyses are illustrated in the chondrite normalised diagrams in figs. 3.1 - 3.4 and other trace element data are summarised in table 3.2. It is clear from these data that REE fractionation, as illustrated by the La/Yb ratios, becomes more extreme through the sequence alnoite-lamprophyre-kimberlite. Other features, however, do not vary as systematically e.g. U and Th are most abundant in lamprophyres, less so in kimberlites and poorest in the alnoites, although there is some overlap between the three groups. Co and Cr are least abundant in lamprophyres and most abundant in kimberlites. All the analyses, however, reveal strong light REE enrichment and linear chondrite normalised abundance patterns (except for 5 micaceous kimberlites from the Kimberley region). Also other incompatible elements (e.g. Cs, U, Th) are enriched while the compatible trace elements (Co, Cr, Sc and Ni (from XRF analyses)) are at the usual levels for basic and

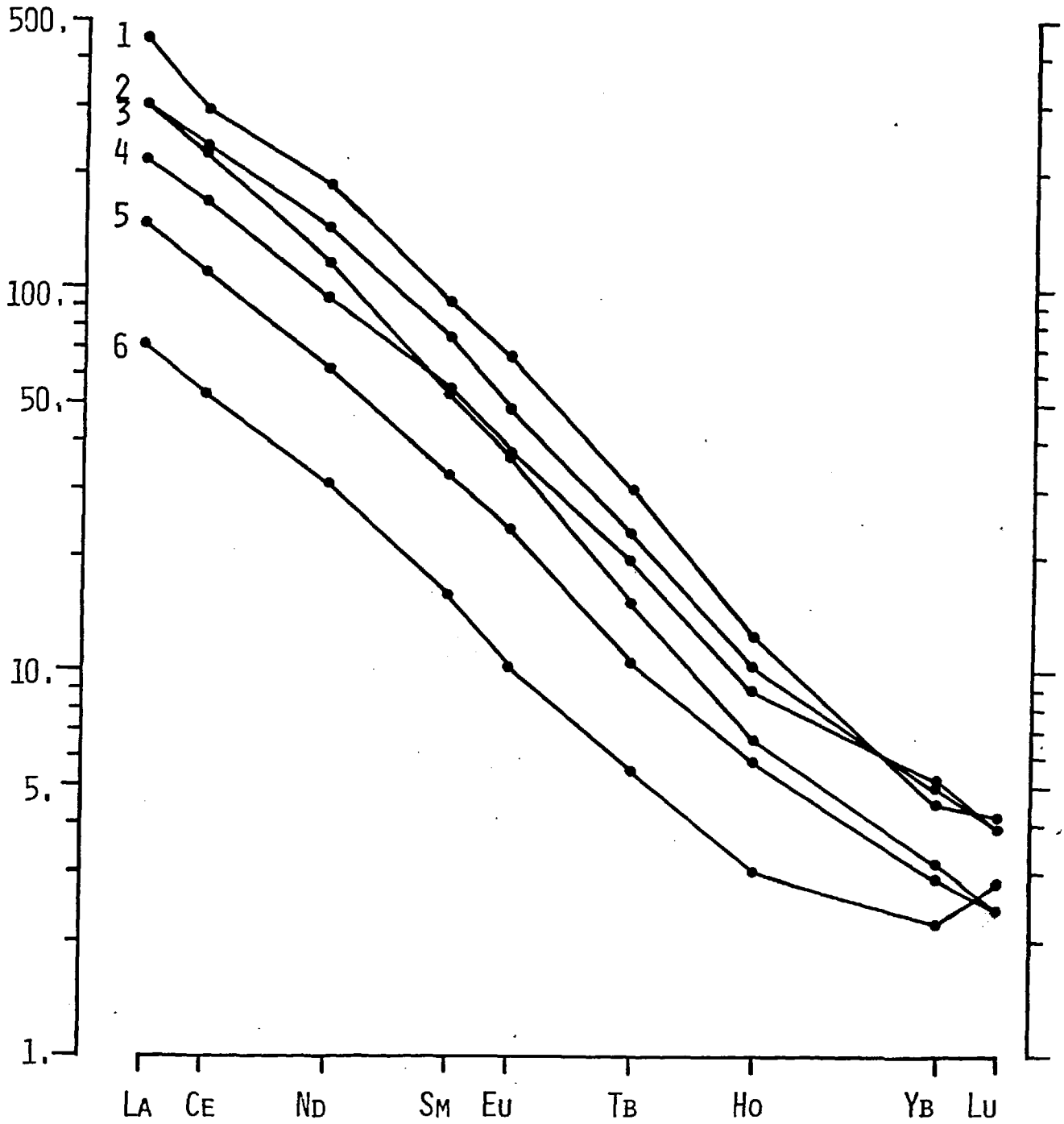

Fig. 3.1 Representative analyses of 6 kimberlites.

Key:- 1 - PHN1867 (Monastery), 2 - PHN2732 (Wesselton),
3 - PHN1334 (Kolo), 4 - PHN3008 (Abbotsford),
5 - PHN1598 (Thaba Putsoa), 6 - PHN2811 (Jagersfontein)

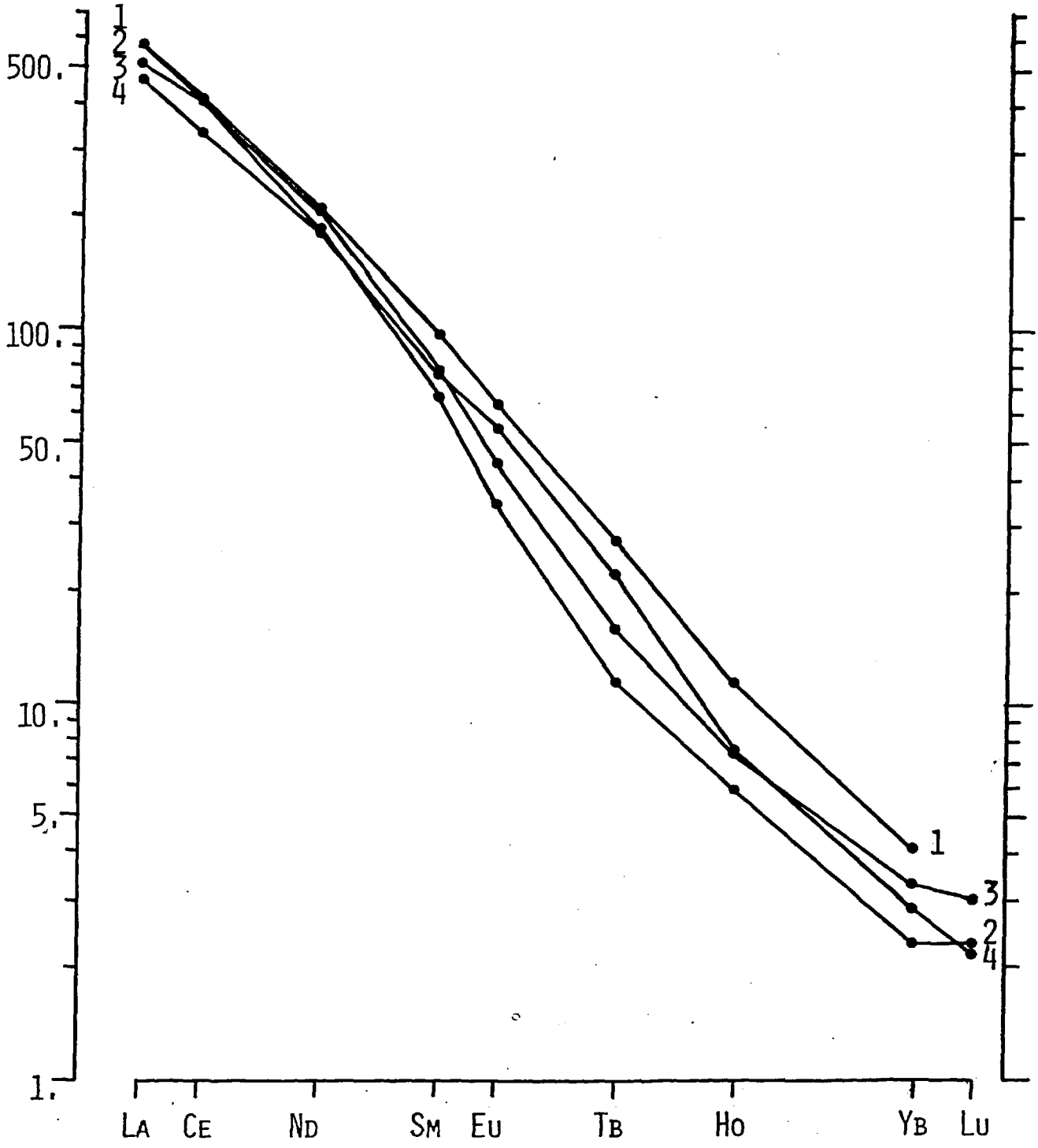

Fig. 3.2 Four kimberlites from Kimberley and The Orange Free State.

Key:- 1 - PHN3249 (Frank Smith) 2 - PHN2796 (Bellsbank)

3 - PHN2201 (Star Mine 4 - PHN2779 (Frank Smith).

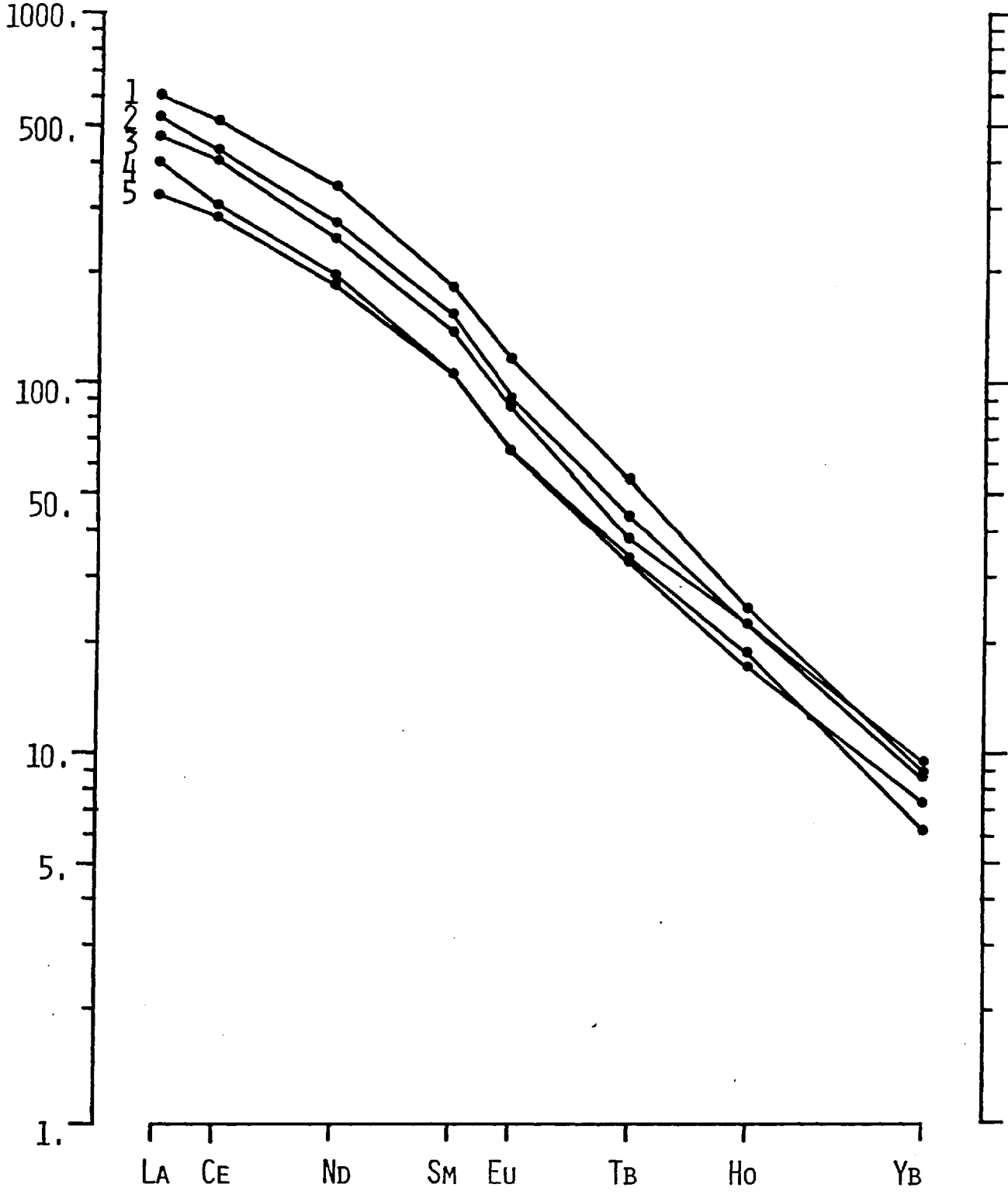

Fig. 3.3 Representative lamprophyre (minette) analyses showing total range of REE abundances.

Key:- 1 - AR8, 2 - AR15, 3 - AR12, 4 - AR1, 5 - AR5.

Fig. 3.4 Analyses of alnoites from Malaita, British Solomon Islands.

Key:- 1 - PHN3552 (Autolith)
2 - PHN3565 3 - PHN3541
4 - PHN3553
Mica - Separated from PHN3553.

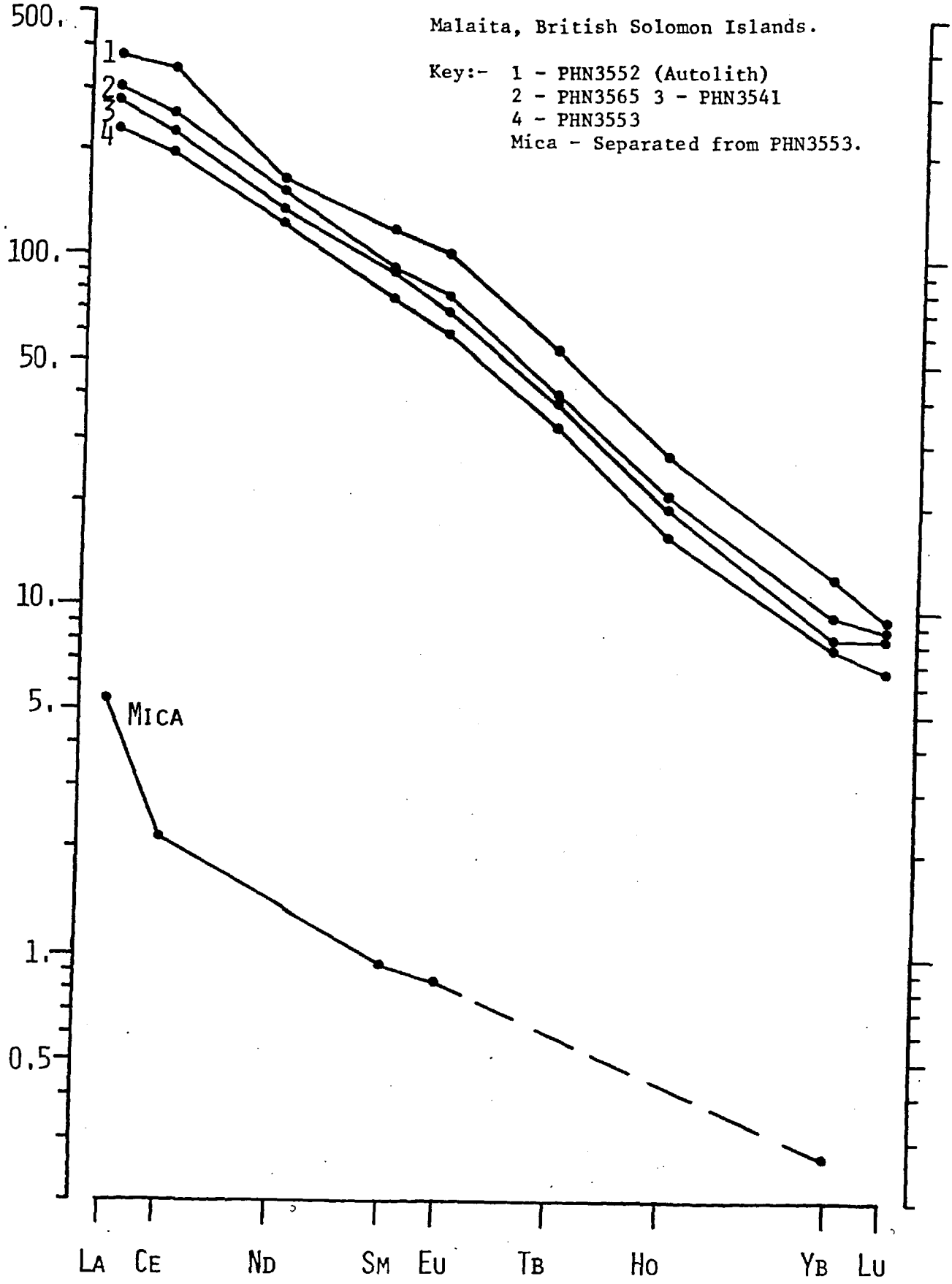

Table 3.2 Trace element data for alnoites, lamprophyres and kimberlites.

	Alnoites		Lamprophyres*		Kimberlites	
	Range	Mean	Range	Mean	Range	Mean
Sc	12.4 - 15.6	14.4	14. - 24.	17.	7.3 - 18.5	14.4
Th	10.7 - 15.0	12.8	24. - 90.	53.	4.2 - 29.5	15.2
U	2.5 - 4.2	3.2	0 - 19.	10.	0.9 - 4.7	2.95
Co	53. - 98.	63.	26. - 47.	42.	67. - 94.	82.
Cr	377 - 681	516	270 - 640	480	850 - 2380	1470
Cs	0.3 - 1.8	1.2	0 - 5.	3.	0.9 - 2.38	1.38
					9. - 11.2	10.4
La/Yb	42 - 49		69 - 112		49 - 240	

* Trace element data for lamprophyres from S.W.Bachinski (pers. comm.). Results obtained using techniques as in this work.

ultrabasic rocks. Although these features are apparently anomalous, they are typical of silica undersaturated basaltic magmas and attain their ultimate expression in the rock types analysed here, particularly in kimberlites. In general, volcanic rocks with these features are thought to have been derived by limited partial fusion of a fertile garnet lherzolite mantle (e.g. Frey et al 1978). However, more informative models require a closer examination of the available data. A useful device for comparing these analyses is a diagram in which the La/Yb ratio is plotted against Sm (ppm), which can be qualitatively interpreted as comparing relative REE fractionation with absolute REE abundance. The analyses from this work are plotted accordingly in fig. 3-5 together with analyses of primitive basalts from S.E. Australia (Frey et al op. cit.). As the alnoites overlap with the most REE enriched samples studied by Frey et al, the petrogenesis of these rocks is considered first.

3.3 Alnoites

Although the alnoite analyses bear a superficial similarity to kimberlites and lamprophyres, it is clear from fig. 3.5 that, when compared with kimberlites with similar Sm abundances, they possess much lower La/Yb ratios and, in this respect, bear a greater similarity to continental alkaline volcanic rocks (e.g. the leucitite and phonolitic tephrite series from the African Rift Valley (Mitchell and

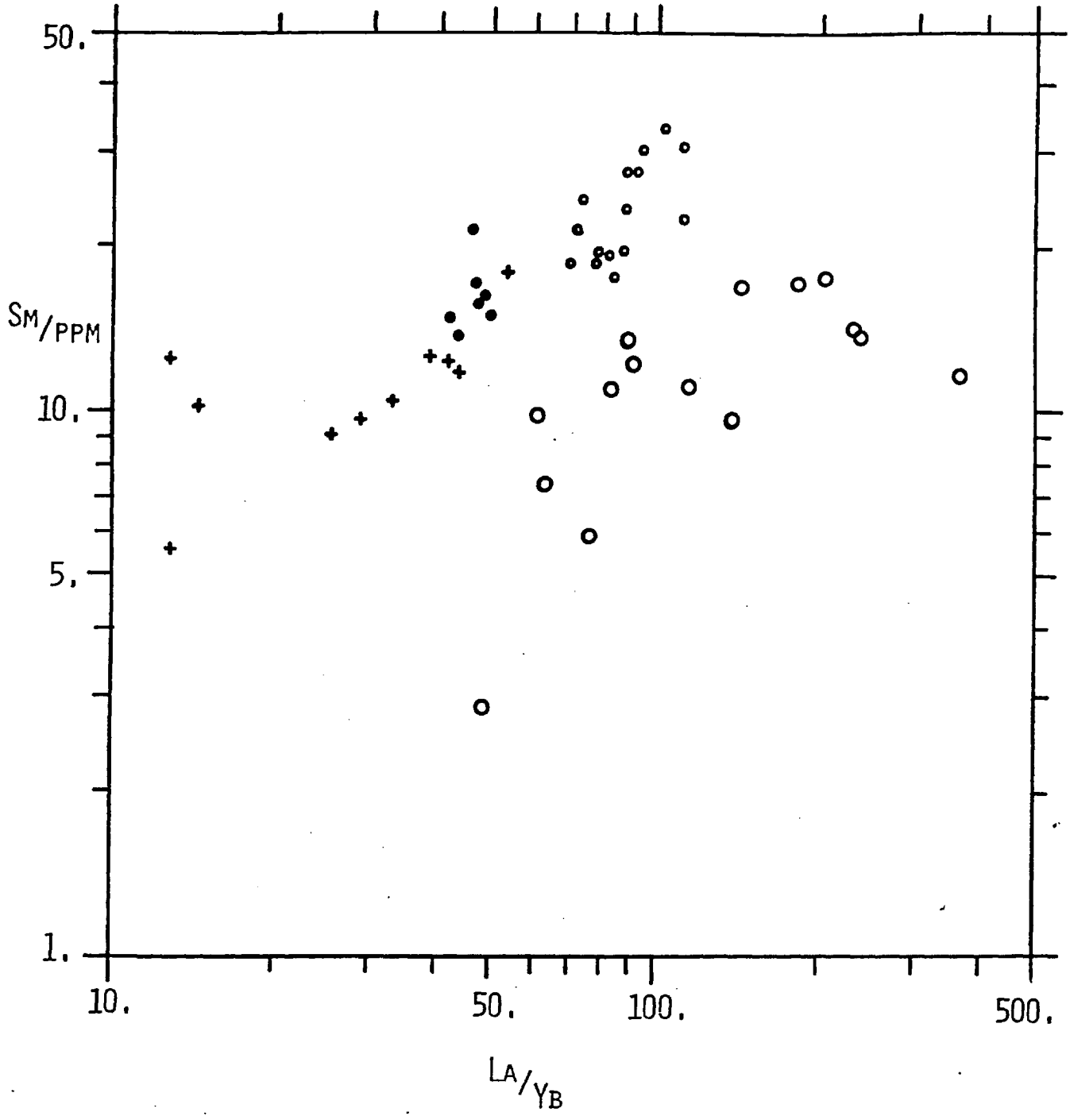

Fig 3.5 A graph of La/Yb vs. Sm for alnoite ● , lamprophyre ⊙ , and ○ kimberlite analyses. Also included for comparison are analyses of primitive basalts from S.E.Australia + , (Frey et. al.1978).

Bell 1977) and the alkaline basalts from S.E. Australia (Frey et al 1978)). It can also be seen from fig. 3-5 that, despite a 25% increase in Sm from the least to the most REE enriched sample (PHN 3553 and 3565 respectively) there is no systematic variation in the La/Yb ratio which remains between the limits of 42-49. This lack of coherent variation is even more pronounced if the autolith analysis is taken into account. The significance of autoliths in kimberlites has been discussed by Danchin et al (1975), who suggested that they probably represent accretions of late stage kimberlitic magma. If they can be similarly interpreted for these alnoites, then the autolith analysis suggests that there was significant enrichment (i.e. $\sim$40%) of the REE and other trace elements in the later stages of alnoite evolution but little REE fractionation. Such a variation could be explained by fractional crystallisation if the crystallising phase contains virtually no REE, as would be the case for olivine. However, despite this mineral occurring as the dominant phenocyst phase, all of the analysed samples possess very high Mg/(Mg+Fe) ratios and high Ni abundances suggesting minimal olivine fractionation. Furthermore fig. 3-6a shows a definite positive correlation between MgO and La for some samples, the opposite of the expected variation. This correlation also rules out perouskite fractionation, another ubiquitous phase in these rocks and the most probable host for the REE. As perovskite is MgO poor ($\sim$ 0.5% R. Mitchell unpublished data) its removal would not give rise to the observed positive trend, but would reduce the REE while allowing MgO to remain virtually

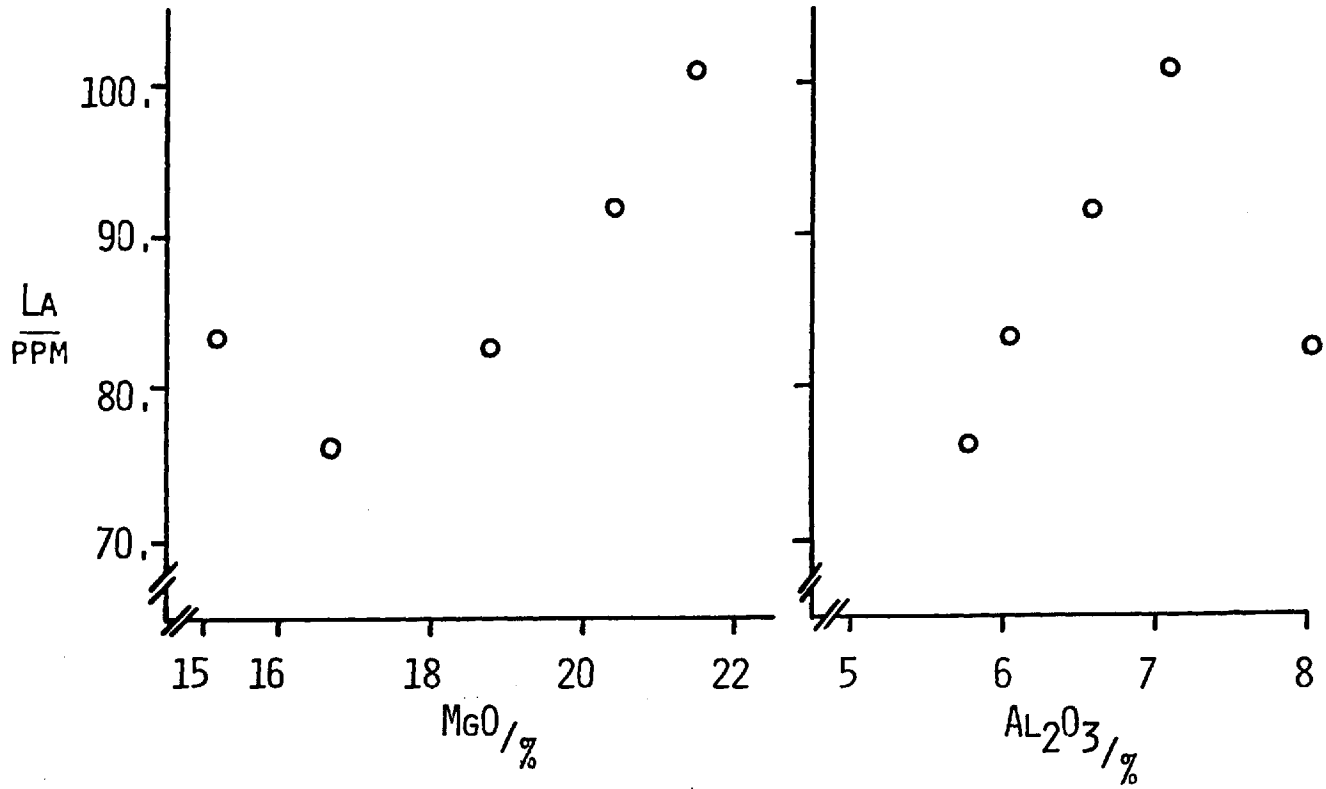

Fig.3.6 Graphs of La against other constituents of the alnoites. Note the positive correlation with MgO, Al_2O_3 and Zr and compare with the scatter in the CaO vs La graph.

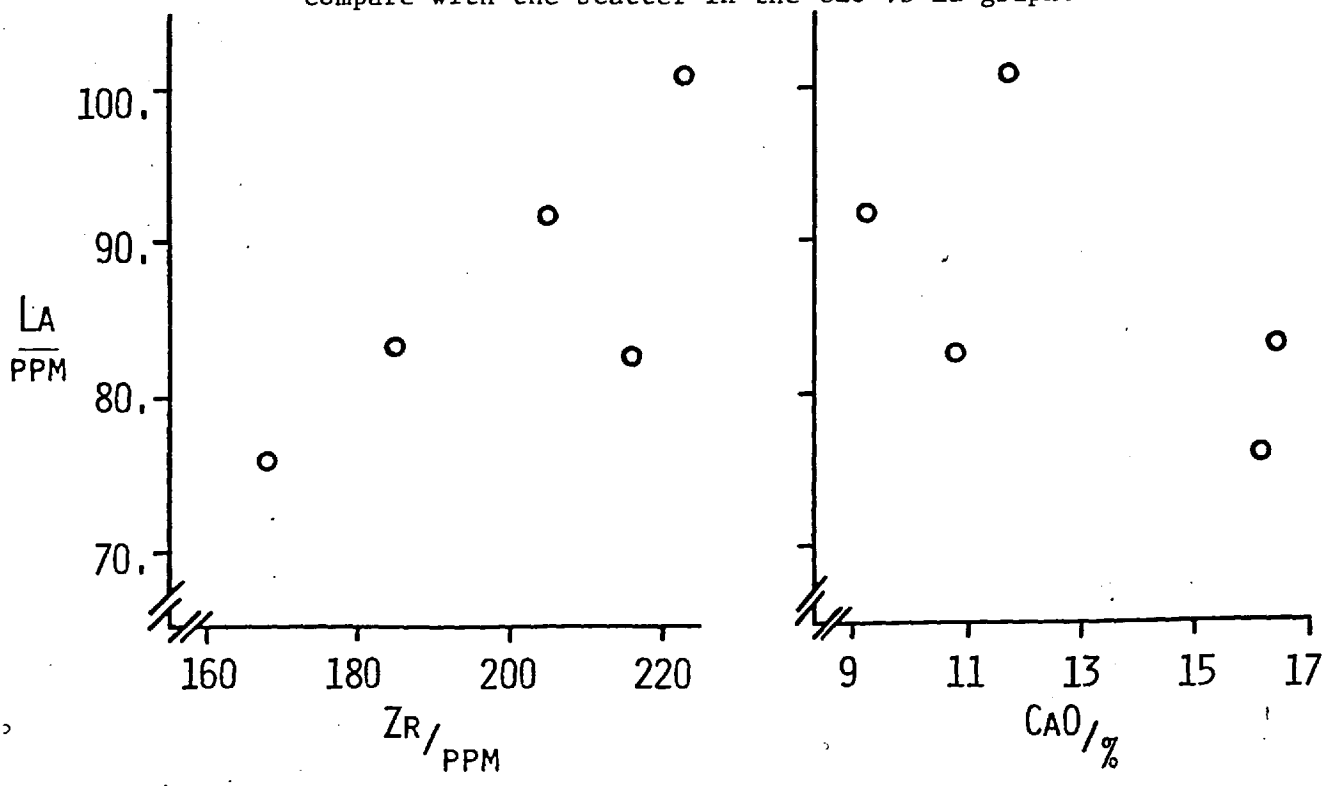

constant. The only other phase that contains both MgO and the REE is mica. Analysis of mica separated from PHN3553, however, reveals that not only are the absolute REE abundances low but the La/Yb ratio is lower than the host rock (29 compared with ∿45). As a result, fractionation of a significant amount of mica, i.e. enough to produce the observed Sm enrichment, would tend to increase La/Yb with Sm, which, as emphasized above, is not observed. Similarly phlogopites from the alnoite contain ∿20% MgO, roughly the same as the alnoite groundmass, and so phlogopite fractionation could not produce the MgO-La correlation.

There are similar correlations between La and other components, La-Zr and La-Al_2O_3 being illustrated in fig. 3-6 b and c as examples. In contrast, a less well defined but negative trend is seen between La and CaO, the latter tending towards higher values in the volatile rich samples. These variations are interpreted as the result of mixing two discrete components, the first similar to the autolith composition and the second mainly calcite, the sole effect of the calcite being to dilute the abundances of the autolith components, and allowing such ratios as La/MgO and La/Yb to remain virtually constant. This is not as might be expected, as igneous calcite (e.g. as in carbonatites and occelli in lamprophyres (Cullers and Medaris 1977)) is often thought of as being REE enriched. To test this interpretation an extra, calcite rich sample, PHN3593c was analysed for the REE in the whole rock. The calcite

fraction was then dissolved out using dilute acetic acid and the REE in the solution determined. From the weight loss during dissolution, the REE concentration of the acetic acid soluble and insoluble fractions were calculated. The results are listed in table 3.2 and illustrated in fig. 3-7a. The same type of experiment was repeated for sample PHN3543, the results of which are similarly illustrated. In both cases the acetic acid soluble fraction is much less REE enriched than the whole rock but possesses a similar La/Yb ratio. This is clearly reflected in the La/Yb vs Sm plot (fig. 3-5). Note also the similarity of the calculated REE abundances of the insoluble fraction and the autolith sample. These results are interpreted as evidence for the purely diluting effect that calcite has on the REE distribution of the alnoites.

The behaviour of the analysed transition elements also conforms to the mixing hypothesis, such ratios as La/Co, La/Sc and Cr/Co showing fairly limited variation. The anomalously low La/Co ratio for PHN3544 is probably due to contamination during crushing as a tungsten carbide tema had to be used. The unusually high Cr/Co ratio of PHN3545 is, however, problematic.

As most of the compositional variation can be attributed to dilution by carbonate, the alnoites are considered to have been derived from mantle depths and to have suffered little subsequent modification.

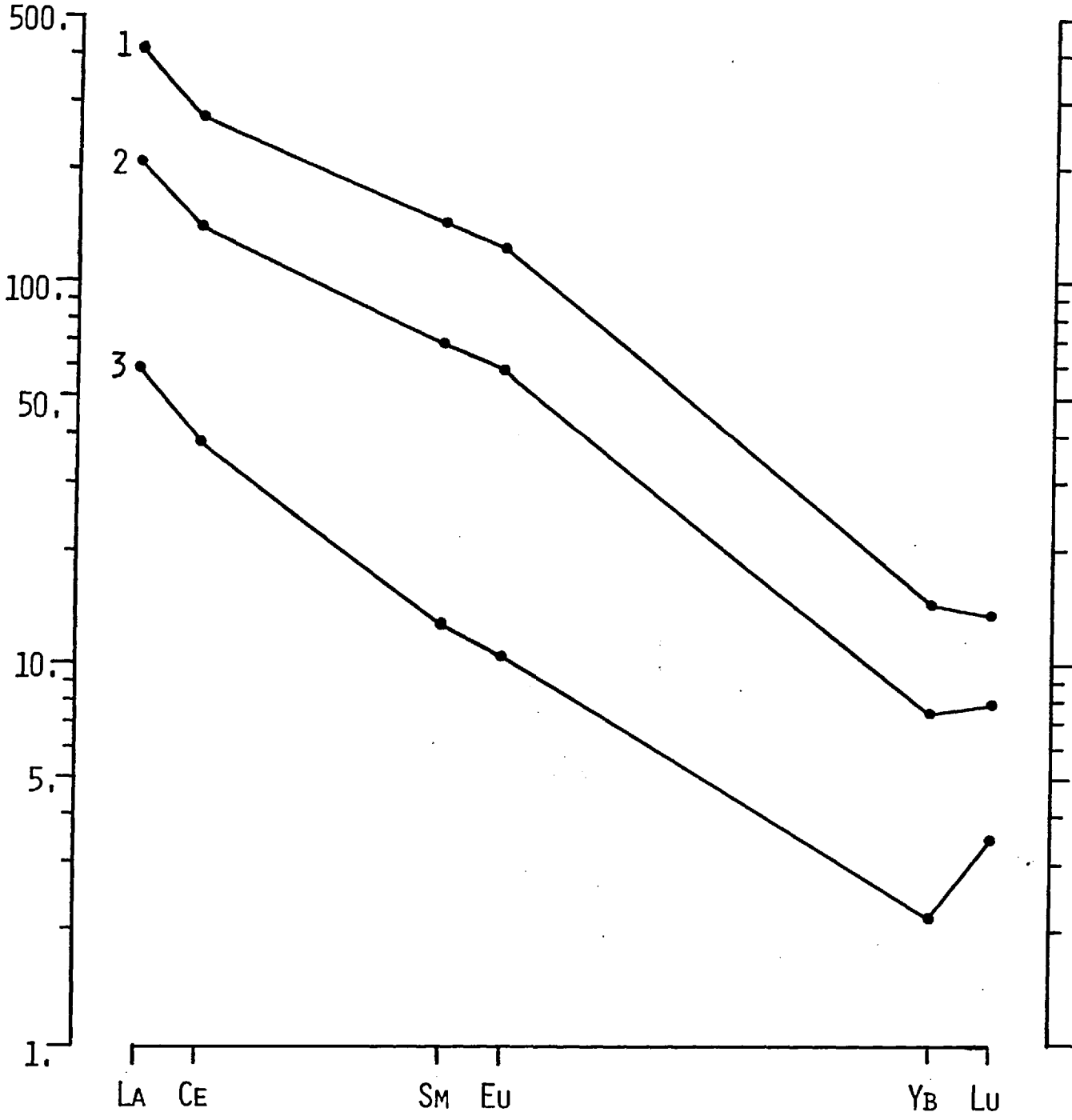

Fig. 3.7a Results from the differential dissolution experiment with dilute acetic acid. Sample PHN3593c.

Key:- 1 - Calculated REE abundances in insoluble fraction.

2 - Whole rock analysis.

3 - REE content of acid soluble fraction (mostly carbonate).

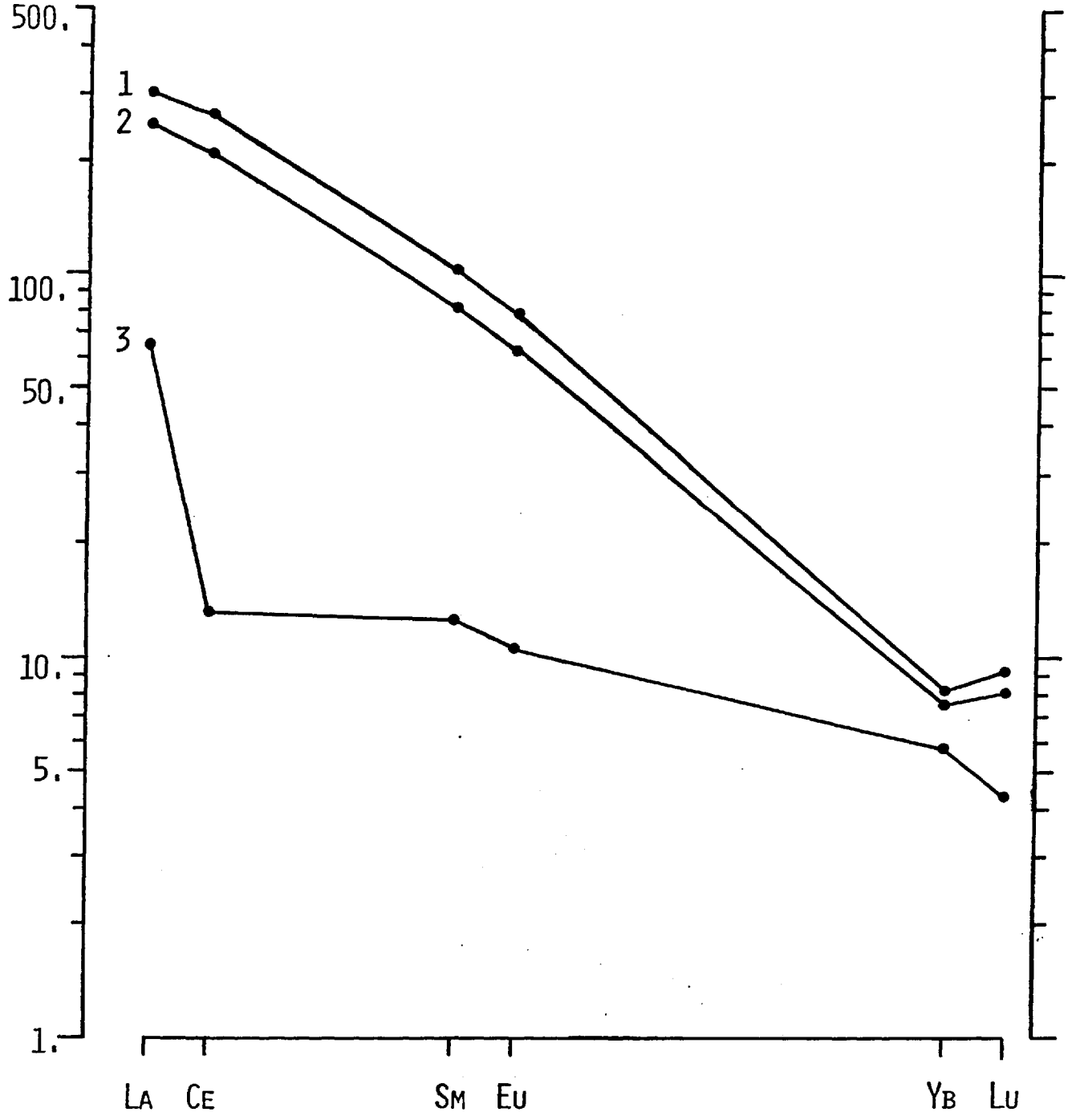

Fig. 3.7b As fig 3.7a. Sample PHN3543. Note the possible negative Ce anomaly in the acid soluble fraction.

This idea is encouraged by the presence of garnet and spinel lherzolite xenoliths and a variety of compositional features. Comparison with the olivine melilite nephelinites from S.E. Australia, considered by Frey et al (op. cit.) to be primary melts, reveals that the alnoites possess similarly high Mg/(Mg+Fe") values and Ni abundances (up to 675 ppm). Such values are acceptable for liquids in equilibrium with an olivine rich mantle. Abundances of Cr and Co are also high, suggesting minimal pyroxene fractionation prior to eruption. Additionally, Sun and Hanson (1975) suggested that primary alkali basalts usually possess P_2O_5/Ce ratios within the range 75 ± 15. The alnoite values lie between 61 and 69, which, although a little low (possibly indicating Ce enrichment), are within the defined range. These features are collectively interpreted as indicating that the alnoites are primary melts and may be used to extend the range of compositions studied by Frey et al. to a greater degree of silica undersaturation.

From fig. 3-5 it is clear that the alnoite REE abundances are comparable with the most REE enriched basalts from S.E. Australia i.e. the nephelinites and melilititites. Comparison of the complete REE patterns, however, suggests a greater enrichment of the light REE in the alnoites, a feature reflected in the slightly low P_2O_5/Ce ratio. Using the criterion of Frey et al. (op. cit.) that the source mantle is pyrolitic and that, on partial fusion, all the P_2O_5 is partitioned into the melt phase, the P_2O_5 abundances of the alnoites indicate

derivation by 4.3 - 5% partial melting. This again compares with the derived figures for the Australian melitites (4.4 - 5.5%). These values can now be used in a similar way to that employed by Frey et al. to derive a possible source REE abundance pattern. Starting with pyrolite, the extraction of a 4.5% melt of alnoite will leave a residue, the composition of which can be calculated by proportion. From this residue composition a modal mineralogy can be calculated by a least squares linear mixing procedure, using probable mineral compositions. The mineral compositions used were taken from the literature; the garnet, clinopyroxene and orthopyroxene are from microprobe analyses of garnet lherzolites from Malaita (Nixon and Boyd 1979) and the olivine was assumed to be similar to those in undepleted ultrabasic nodules from kimberlite, (analysis from Meyer 1978). Having calculated the mode, bulk distribution coefficients for the residue were determined and, hence, from the alnoite REE abundances, the residue abundance pattern was calculated. Finally, by summing the residue and alnoite in the correct proportions, the REE abundances in the undepleted source were determined. The various steps of the calculation are summarised in table 3-3 and the final calculated source illustrated in fig. 3.8 where it is compared with the results of similar calculations from Frey et al on the melilitites. Clearly the three source regions possess very similar REE abundances.

Table 3.3 Least squares mixing model for alnoite petrogenesis.

	1	2	3	4	5	6	7	8
SiO_2	45.79	45.79	-	42.74	53.03	55.96	40.53	0.51
TiO_2	0.58	0.58	-	0.14	0.44	0.16	0.02	50.50
Al_2O_3	3.34	3.16	-.18	22.98	4.22	2.71	0.05	-
Cr_2O_3	0.30	0.38	-.08	1.45	1.05	0.45	0.04	-
FeO*	8.37	7.85	-.52	8.35	2.65	6.22	9.09	46.35
MnO	0.14	0.18	+.04	0.43	0.09	0.14	0.16	1.45
MgO	38.68	38.69	+.01	20.38	15.80	33.38	50.29	0.46
CaO	2.72	2.74	+.02	5.07	20.72	0.53	0.07	0.71
Na_2O	0.42	0.20	-.22	0.02	1.70	0.09	-	-
K_2O	0.01	0.0	-.01	-	-	-	-	-

Calculated "best fit" mode - 8.5% + 10.3% + 28.7% + 51.7% + 0.8%

1 - Calculated residue composition (pyrolite - 4.5% alnoite)

2 - Best fit composition for column 1 using mineral analyses.

3 - Residuals.

4 - Garnet, 5 - Clinopyroxene, 6 - Orthopyroxene, 7 - Olivine

8 - Ilmenite.

Calculation of source REE composition.

	D	C_1	C_{res}	Source ppm	chond
La	0.00255	86.7	0.221	4.11	(12.5x)
Ce	0.00507	197.	1.00	9.82	(11.2)
Nd	0.0121	77.9	0.943	4.41	(7.35)
Sm	0.0232	15.4	0.358	1.04	(5.75)
Eu	0.0298	4.70	0.140	0.345	(5.02)
Tb	0.0441	1.77	0.078	0.154	(3.28)
Ho	0.116	1.25	0.145	0.195	(2.75)
Yb	0.371	1.86	0.69	0.743	(3.37)
Lu	0.517	0.26	0.134	0.140	(4.11)

D - Values calculated from mineral K_d values (set 3 Frey et. al. 1978) and calculated mode (above)).

C_1 - Alnoite REE abundances.

$C_{res} = C_1 \times D$ i.e. calculated residue REE abundances.

Source $= (0.955 \times C_{res}) + (0.045 \times C_1)$

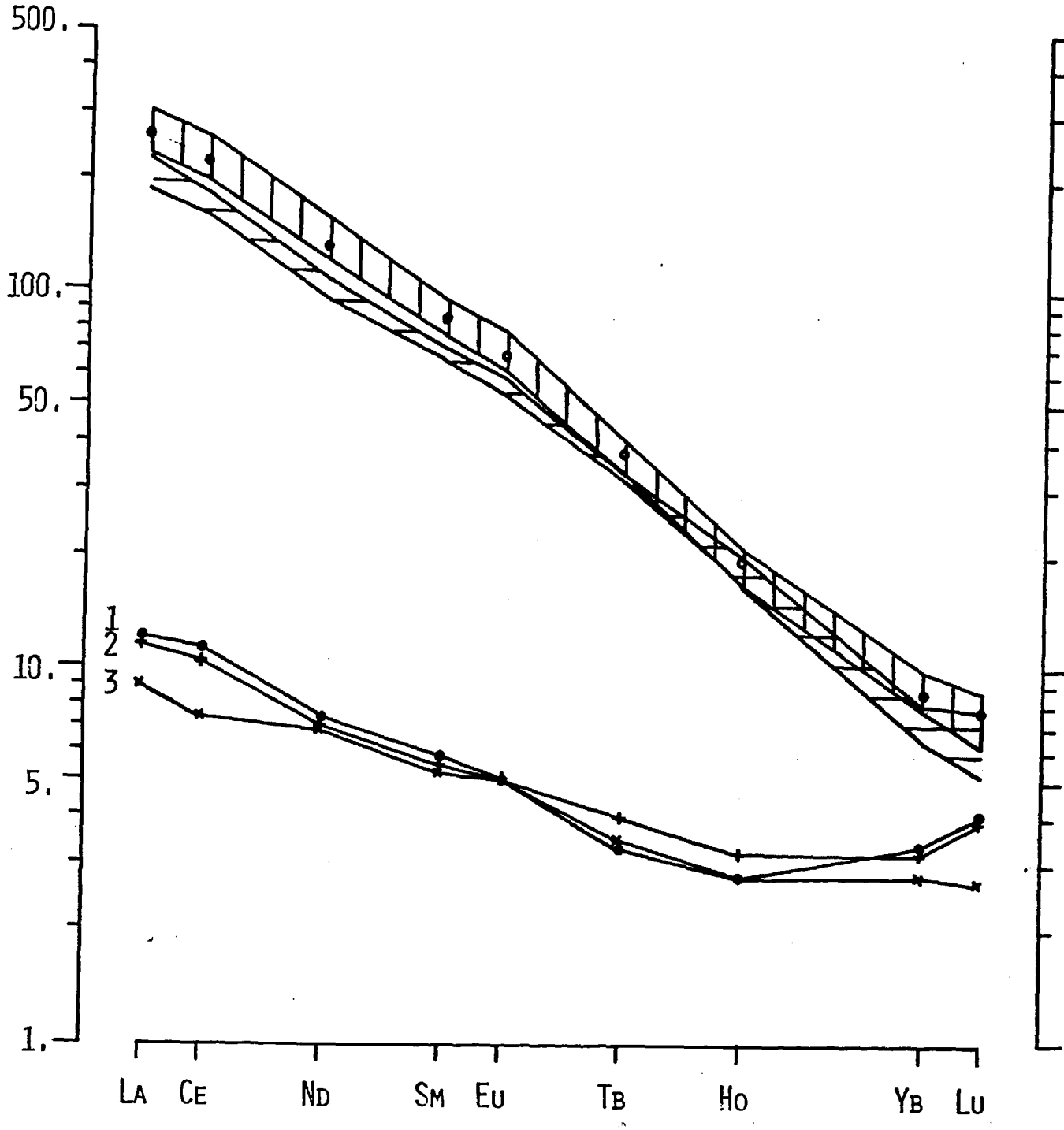

Fig. 3.8 Comparison of petrogenetic models for the Malaita alnoites and the S.Australian basanites, nephelinites and melilititites.
Key:- Vertical shading - alnoites (open circles represent the mean of six analyses used to model the alnoite source)
Horizontal shading - nephelinites and melilititites.
1 - Model source for alnoites.
2 - Model source for melilititites
3 - Model source for nephelinites and basanites (Frey et. al.)

From these results it is clear that the greater degree of silica undersaturation of the alnoites is not explained either by invoking smaller degrees of partial melting or mantle heterogeneity, but must be ascribed to some additional process. Frey et al suggested that, at low degrees of partial melting, the degree of silica undersaturation of a melt may be controlled by $p(CO_2)$ and, particularly, the $CO_2/(CO_2+H_2O)$ ratio of the source material. With respect to the petrogenesis of nephelinites and melilitites they state:- "It is possible that compositional differences in these primary magmas are subtly explained by differences in H_2O/CO_2 proportions in the source region, the olivine nephelinite being a similar melt fraction from a source region with higher H_2O/CO_2 proportions than that for olivine melilitite". From the various lines of evidence, a similar effect is observed in the Malacita alnoites. Petrographic evidence suggests that the calcite causing the previously described dilution originally separated from the alnoite magma as an immiscible liquid. This is particularly clear from the autoliths and lapillae tufts where alnoite is set in a carbonate matrix (P.H. Nixon pers. comm.). Furthermore, in accordance with the proposed effect of increasing $p(CO_2)$ during partial melting (viz. to increase the CaO/Na_2O ratio of the melt) the alnoites show a tendency towards high CaO/Na_2O ratios, values ranging from 2.7 (3544) to 11.4 (3541), calculated after correction of CaO due to the calcite contribution. These values compare with the maximum of 3.75 from the S.E. Australian basalts and are interpreted as a further demonstration of the profound effect of $p(CO_2)$ on the products of partial melting.

The source of the CO_2 in the alnoites is problematic. In some samples there is up to 10% CO_2 while in others less than 1%. If an average content of 5% is assumed and the alnoites are the result of 4.5% partial melting, then the source region must have contained $\sim$ 0.23% CO_2. Available analyses of ultrabasic rocks, however, rarely show such high CO_2 abundances, even if CO_2 analyses are reported at all. It therefore seems possible that CO_2 was introduced into the source region before or during partial melting, where it mixed with or dissolved in the partial melt, resulting in the observed chemical properties of the alnoite magma.

The petrogenesis of the alnoites is, therefore, envisaged in the following manner. A CO_2 rich fluid from deeper within the mantle, equilibrated with the product of 4-5% partial melting and garnet lherzolite at a depth > 130 km. The REE content of the derived magma was governed partly by the CO_2 rich fluid and partly by the partial melting process. Eruption finally occurred directly from $\sim$130 km as a result of the accumulation of volatiles. On eruption, the sudden release of pressure induced the separation of the CO_2 either as a fluid or gas phase, resulting in gas fluidisation of the magma and an explosive mode of eruption. Carbonate or CO_2 separation also concentrated the REE in the silicate fraction, in agreement with recent experimental work on the partitioning of the REE between

silicate and carbonate fluids at low pressures (e.g. Mysen 1979). Physical separation of these two components, probably followed by remixing, resulted in the observed variations in alnoite composition.

The chemical variations seen in the alnoites have implications for carbonatite petrogenesis. It is known that carbonatites are highly enriched in the light REE and other incompatible elements (e.g. Eby 1975). The presence of calcite occelli in lamprophyres (see, e.g. Bachinski and Scott (1979) and Cullers and Medaris (1977)) has often prompted the spculation that carbonatite could be derived from silicate magmas by the exsolution of an immiscible carbonate liquid, depleting the silicate fraction in the light REE and other incompatible elements. The evidence from the alnoites, while supporting the exsolution hypothesis, reveals that the trace elements, under certain conditions, are preferentially accommodated in the silicate fraction. In contrast, the evidence of Cullers and Medaris (1977) suggests that occelli in lamprophyres are relatively enriched in the REE. It is clear, therefore, that physical conditions, especially confining pressure, could play a significant part in determining the distribution of the REE between carbonate and silicate magmas. A similar carbonate-silicate relationship is shown by the Lashaine ankaramite-carbonatite tuff cone, N. Tanzania (Ridley and Dawson 1975). In this locality, both ankaramite and carbonatite are light REE enriched (La/Yb = 58 and 18.4 respectively), but the ankaramite contains much higher absolute abundance of the REE (e.g. Sm = 7.8 and 0.83 ppm

respectively). Although the data does not allow any definite conclusions to be drawn regarding carbonatite evolution, it does suggest that care must be exercised when interpreting trace element abundances of carbonatite with reference to co-existing silicate magmas.

3.4 Lamprophyres

As with alnoites, plotting the REE data on fig. 3.5 reveals that the similarity with kimberlites is purely superficial, the lamprophyres being much more enriched in Sm for a given La/Yb value. However, the lamprophyres are more REE enriched than the alnoites and plot over a greater range of La/Yb and Sm values. Furthermore, there is a tendency for La/Yb to increase with Sm within the lamprophyre group.

Unfortunately, major element and Ni analyses are not available for these samples. Hence, it is not possible to use the compositional criteria to estimate the degree of partial melting and fractional crystallisation involved in the production of the lamprophyres as it was with the alnoites. However, analyses of lamprophyres from Buell Park, Arizona, the same locality as samples AR.1, 2, 3, 5, 6 and 15 give $Mg/(Mg + Fe^{11})$ values of between 80 and 90 (Roden 1978). These rocks also contain high pressure garnet lherzolite xenoliths as does the Thumb, the volcanic plug from which AR.9 was taken. These features are interpreted as suggesting that at least some of the lamprophyres have been derived from considerable depth with only minimal modification by such processes as fractional crystallisation.

Reference to fig. 3.5 shows that the least REE enriched samples continue the same positive trend defined by the alnoites and the S. Australian basalts. As the required degree of partial melting decreases as Sm in the derived liquid increases, it therefore seems possible that the lamprophyre magma could be derived from a similar source to the above mentioned rock types, but by a smaller degree of melting. To test this hypothesis a number of partial melting models involving a parental garnet lherzolite mantle were calculated using the source REE composition proposed by Frey et al (op. cit.) for the S. Australian basalts. The models involved 1-5% partial melting and varying the proportions of garnet and clinopyroxene as in table 3-3. The composition of the melt is based on the work of Davis and Schairer (1965). The results of these models are illustrated in fig. 3-9 and compared with the lamprophyre analyses. It is clear that increasing the gt/cpx ratio of the source tends to increase La/Yb and slightly decrease Sm for a given degree of melting. While significant, this variation does not account for the major internal La/Yb vs Sm correlation within the lamprophyre group. If the whole REE patterns for the three models are compared with the range of REE patterns shown by the most primitive samples, i.e. those lying closest to the calculated curves, (fig. 3.9), it is clear that while they agree qualitatively, the fine detail of the REE pattern cannot be reproduced. As varying the modal proportions of the source mineralogy only serves to produce a shift in the REE pattern and not a change in

Table 3.4 Summary of lamprophyre partial melting models.

Mineral	Garnet	Clino-pyroxene	Ortho-pyroxene	Olivine
Source Modes:-				
Model I	8%	12%	25%	55%
Model II	10%	10%	25%	55%
Model III	12%	8%	25%	55%
Proportions of minerals entering melt :-	47%	47%	3%	3%

Fig. 3.9 Comparison of lamprophyre REE abundance parameters with partial melting models (see text) and theoretical trends from fractional crystalisation.

P - Phlogopite, O - Olivine,
D - Diopside, A - Augite.
Curves marked at 10% intervals.

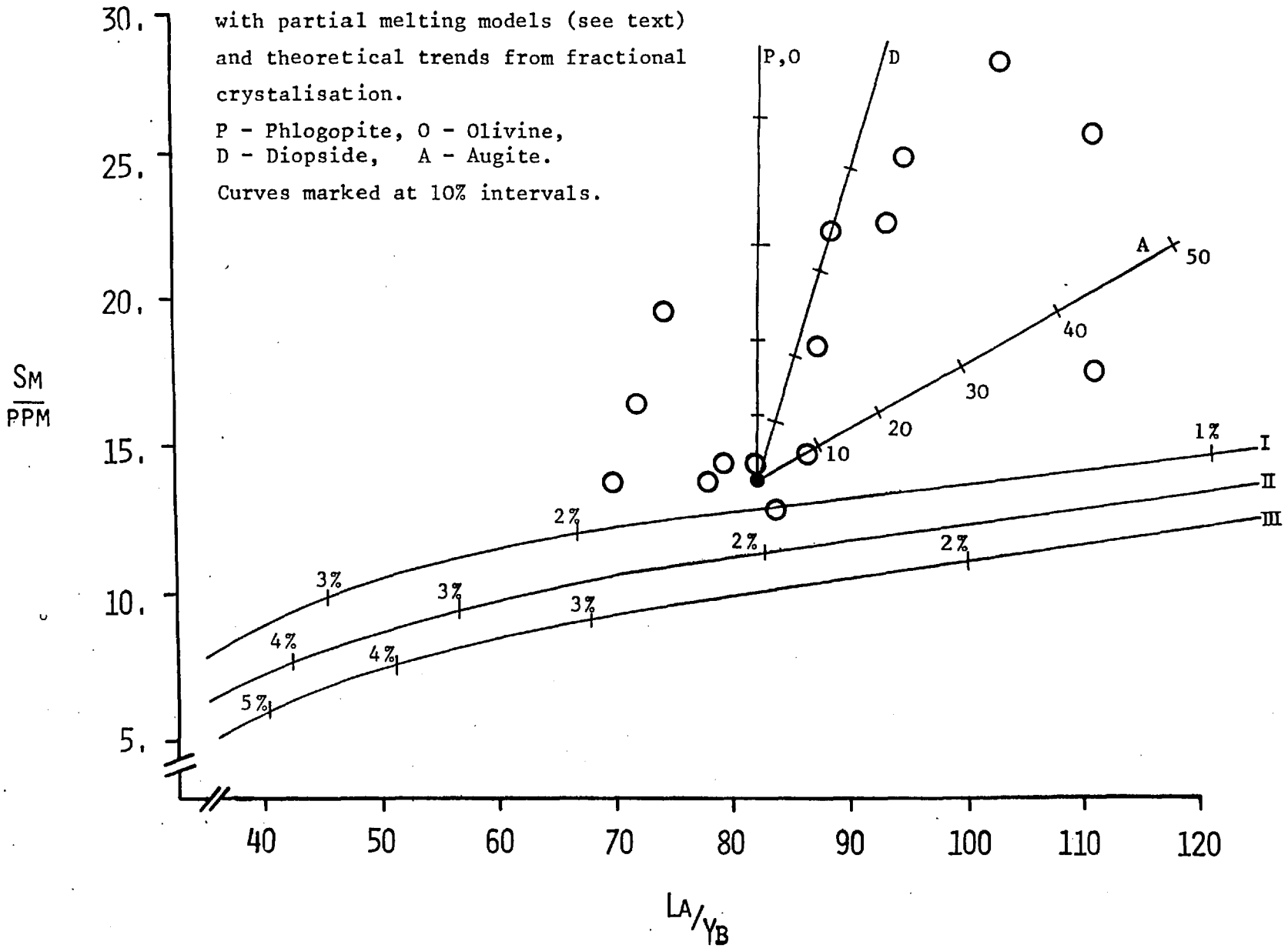

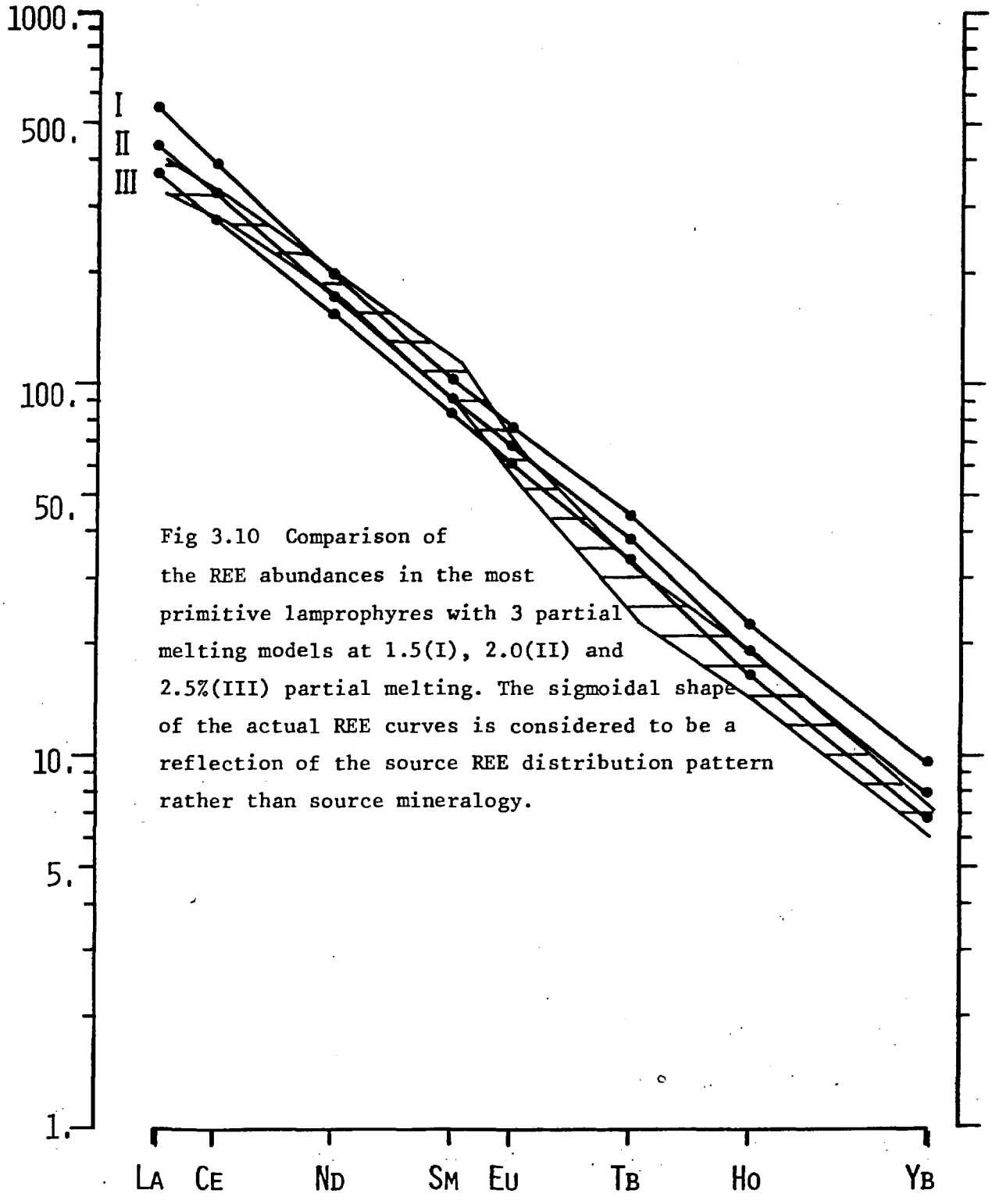

Fig 3.10 Comparison of the REE abundances in the most primitive lamprophyres with 3 partial melting models at 1.5(I), 2.0(II) and 2.5%(III) partial melting. The sigmoidal shape of the actual REE curves is considered to be a reflection of the source REE distribution pattern rather than source mineralogy.

shape, it is inferred that the variation of the light REE reflects differences between the source region of the alnoites and that of the lamprophyres. Note that in both models, the best agreement between the models and the actual analyses is given by the heavy REE. The significance of this variation in light REE abundance patterns will be discussed in a later chapter. The calculations, therefore, suggest that lamprophyre magma is produced by partial melting of garnet lherzolite but that the abundances of the REE in the source are subtly different from the abundance in the alnoite source.

The samples richer in the REE, however, must have evolved by some additional process or processes. Previous workers have shown that fractional crystallisation can produce varying trends on a Ce/Yb vs Sm diagram (e.g. Thorpe 1978). Phenocryst phases in the lamprophyres include olivine, mica and clinopyroxene. Using published K_D values and assuming ideal Rayleigh fractionation, La/Yb vs Sm trends have been calculated for olivine, mica, diopside and augite and are plotted on fig. 3.9. For olivine and mica these calculations reveal a tendency to produce vertical trends. In the case of olivine, this is due to the very low mineral-liquid K_D values, while for mica, although the K_D values are higher there is no tendency to fractionate the light from the heavy REE. Clinopyroxene K_D values, however, give rise to a variety

of trends, depending on the values taken. The two lines in fig. 3.9 correspond to values taken from Frey et al (1978), (curve D, Diopside) and Arth and Hanson (1976) (curve A, Angite). As the two calculated trends encompass that defined by the lamprophyre group, it seems likely that the REE abundances may be controlled by clinopyroxene fractionation, a conclusion supported by the Sm-Co variation (fig. 3-11). From the above calculations, it is known that Sm increases in the liquid during clinopyroxene fractionation. Co, however, with a $K_D > 1$, is easily accommodated by the clinopyroxene and its abundance in the melt should, therefore, be reduced. Fig. 3.11 reveals such a negative correlation, and provides further qualitative evidence for the operation of this process.

In conclusion, the trace element data support the hypothesis that the Arizona lamprophyres have evolved through limited partial melting ($\sim$ 2.5%) of a garnet lherzolite mantle, provided that this source was significantly enriched in the light REE. Source region heavy REE abundances are $\sim$ 3 x chondrite. While some of the magmas were subsequently erupted without further modification, others appear to have undergone varying degrees of clinopyroxene fractionation to account for the absolute REE abundances and the negative Co-Sm correlation.

Apart from the trace element abundances, two other related aspects of lamprophyre chemistry are worth noting. Unlike most proposed products of limited partial melting, lamprophyres tend to be silica

Fig. 3.11 Graph of Sm vs. Co for the Arizona lamprophyres showing the general negative correlation. (An extra point at 72ppm Co and 18ppm Sm plots off of this graph)

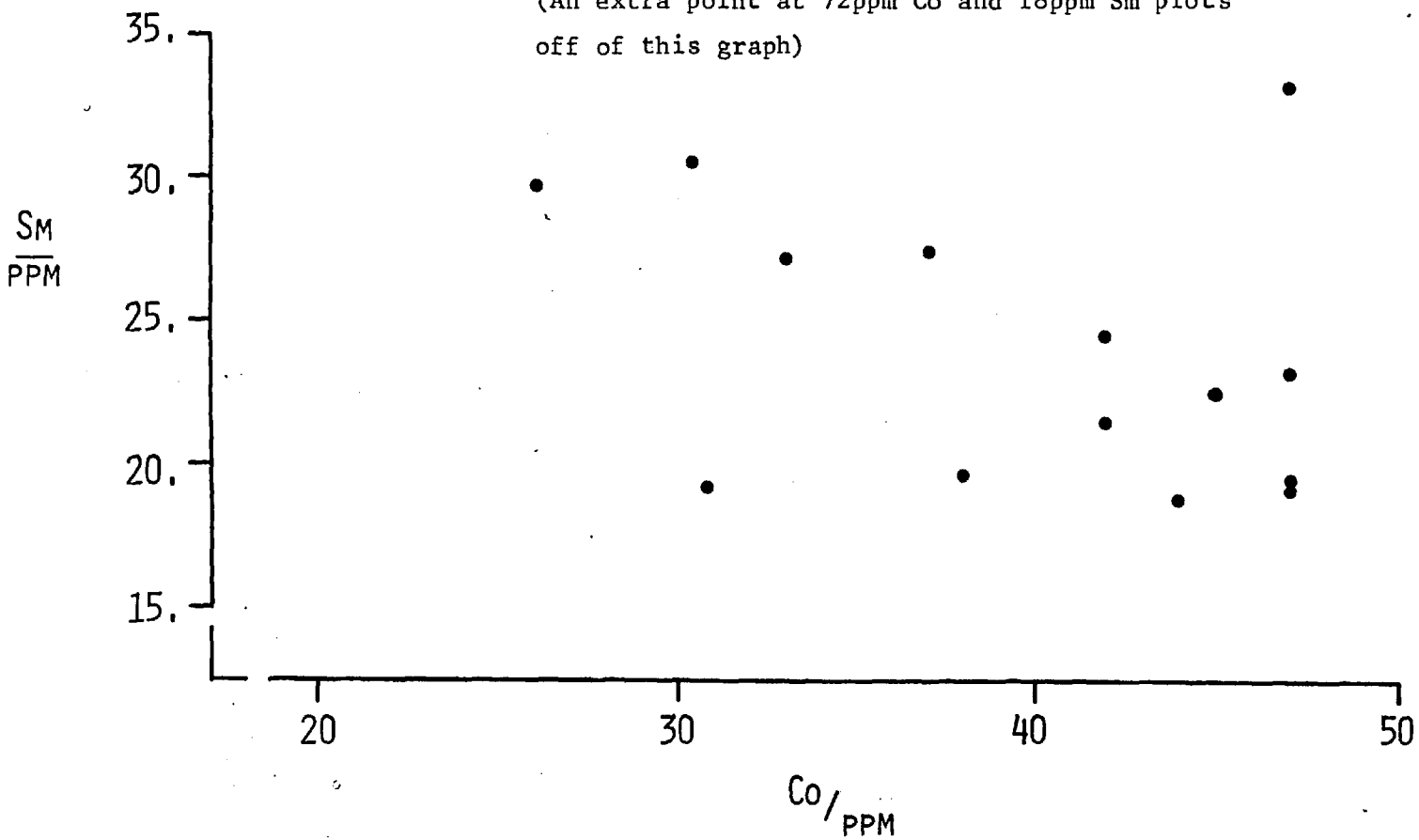

saturated, not undersaturated, and, secondly, the primary volatile constituent is H_2O, not CO_2. It is clear, from the arguments outlined in section 3-3, that this is yet another illustration of the effects of volatile components during partial melting, the high H_2O/CO_2 ratio allowing the higher silica activity in the melt. Note also, that with low partial melt fractions it is not necessary to invoke a source mantle particularly enriched in K_2O. The Buell Park lamprophyres contain 4.8 - 7.2% K_2O (Roden 1977). If, on partial melting, all the K_2O is assumed to enter the melt phase then, at 2.5% partial melting, this is equivalent to .12 - .18% K_2O in the source, a figure that compares well with the pyrolite model of Ringwood (1966) which contains .13% K_2O.

3.5 Kimberlites

The REE analyses of kimberlites presented here, while not being the first, do reveal hitherto unsuspected variations. The first of these concerns the large spread of REE abundances and fractionation of the light elements from the heavy elements. The La/Yb ratios vary from 366 (PHN 2796, Bultfontein) down to 49 (PHN 2811, Jagersfontein). Furthermore the Jagersfontein sample is the most REE depleted kimberlite yet recorded. As the samples were chosen for their freshness, this must be considered a primary feature of this kimberlite occurrence.

The second feature involves only the most REE enriched samples from the Kimberley pipes, in which the heavy REE abundances vary while the light REE remain virtually constant. This variation will be discussed below.

The third and most fundamental feature is seen when the analyses are plotted on a La/Yb vs Sm diagram (see fig. 3.12; this diagram also includes results from previous work e.g. Mitchell and Brunfelt (1975) Fesq et al. (1975) Paul (unpublished results)). All the analyses plot along a broad trend, parallel to that defined by more normal basaltic rocks, but at lower Sm (Σ REE) abundances for a given La/Yb ratio. This clearly has implications for the petrogenetic processes that produce kimberlites and suggests that fundamental differences must exist between the origins of kimberlites and more normal basaltic magmas. Note also the negative slope in fig. 3.12 shown by the most REE enriched samples, a further reflection of the unusual heavy REE depletion mentioned in the above paragraph. However, before the ultimate causes of these variations are discussed, it is important to assess the effects of the known sources of REE variation in kimberlite.

Mineralogically, kimberlites can be classified into two main categories viz micaceous and basaltic (note that the term basaltic refers solely to the texture of the rock and implies no genetic relationship). Analyses of these different types have revealed that the micaceous varieties

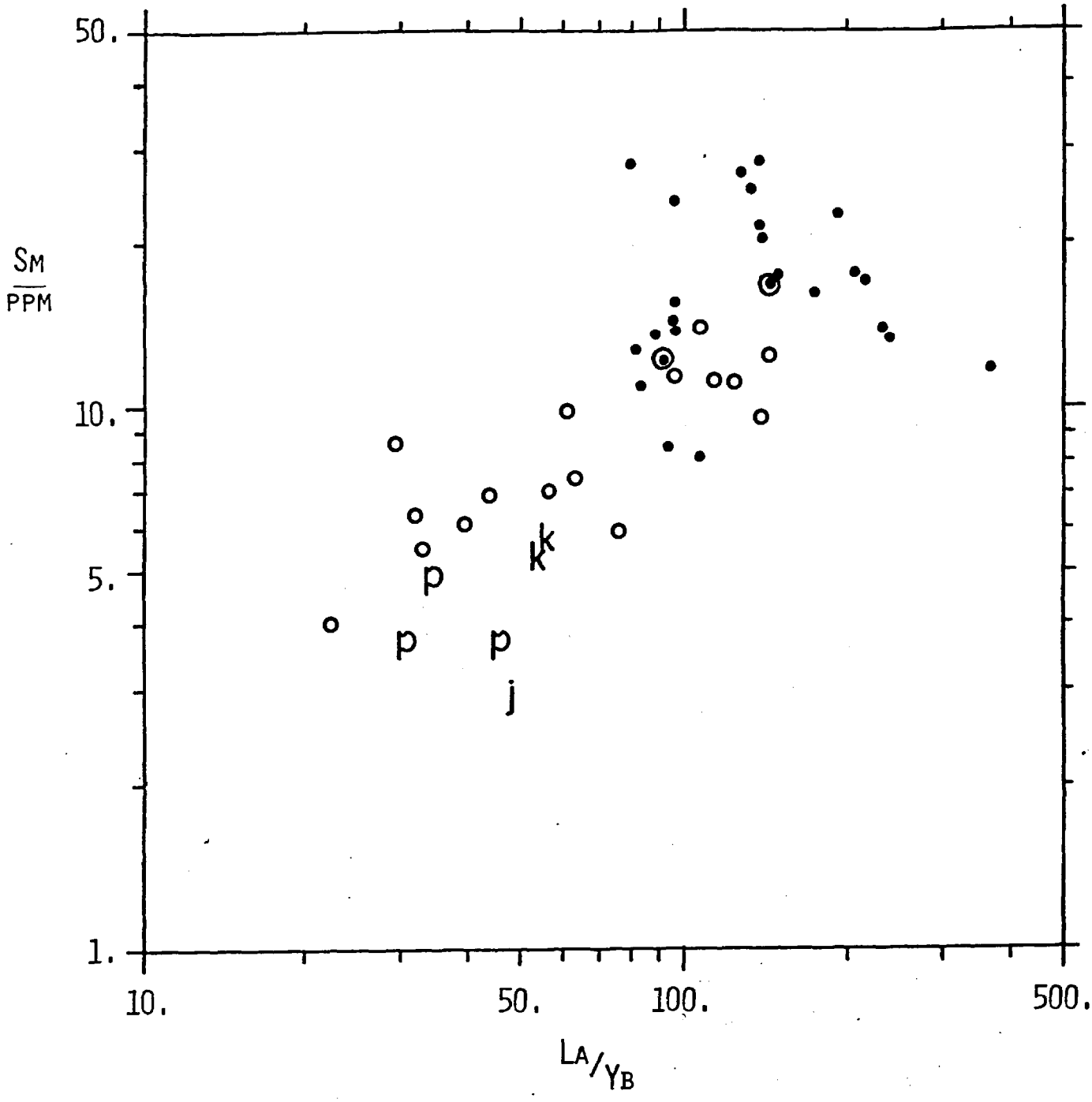

Fig. 3.12 Sm vs. La/Yb plot for kimberlites -
Key - • Kimberley region, o Lesotho,
k - Koffiefontein, j - Jagersfontein, p - Premier Mine,
⊙ Monastery Mine

tend to be more enriched in the REE than basaltic kimberlites (Mitchell and Brunfelt (1975)). Similarly, differences in REE abundances have been observed from kimberlites of different structural types. Paul and Nixon (unpublished results) and Paul and Potts (1977) have shown that there is a tendency for diatreme (pipe) facies kimberlites to be less REE enriched than the hypabyssal (dyke) facies samples. While these relationships hold well within any one kimberlite locality, they can break down when samples from different pipes or dykes are compared, e.g. the Hypabyssal kimberlites from Kao, N. Lesotho (Paul and Nixon op. cit.) are similar with respect to the REE to the diatremic samples from Wesselton (Mitchell and Brunfelt (apcit.)). Other aspects of their chemistry reflect this within locality variation. As emphasized by Paul and Potts (1977), pipe kimberlites are richer in Si, Al and Na compared with their hypabyssal counterparts while the latter seem to have retained a greater proportion of their volatile constituents. Both of these effects may be considered to be a direct consequence of the mode of emplacement, the volatiles being trapped in the kimberlite fluid by the confined environment of the dyke. In the case of the diatreme facies samples, the open system allows the exsolution of dissolved gases, resulting in the gas fluidised mode of eruption, abrading the diatreme walls and adding finely comminuted crustal material (rich in Si, Al and Na) to the kimberlite matrix. The lower REE abundances in the diatreme facies rocks could, therefore, be the result of two effects: (1) Dilution of the kimberlite by the assimilation of crustal material with low La/Yb ratios.

(2) Loss of a volatile rich component which, on analogy with carbonatites, could be light REE enriched. While there can be little doubt of the operation of the first, experimental work on the partitioning of the REE into volatile fluids renders the second process subject to debate (Mysen op. cit.).

The observation that some hypabyssal facies kimberlites compare with diatremic varieties from another locality suggests that important regional differences in kimberlite trace element abundances may exist. This could have implications with regard to heterogeneities within the mantle at the depth of kimberlite genesis, if kimberlite can be regarded as a primary mantle melt. The evidence for this condition is, however, ambiguous. In favour of the primary melt argument are such features as the ultrabasic composition of kimberlites. This, together with the high Co, Ni and Cr abundances, suggests that fractionation of olivine, the predominant phenocrystal phase, has been insignificant in the development of kimberlite. Furthermore, garnet lherzolite and other xenolith samples record P-T conditions of up to 250 km (Boyd 1974, Boyd and Nixon 1975) placing a minimum limit of kimberlite genesis well within the mantle and indicating, solely by their presence, rapid transport from these great depths. Taken together, the above evidence suggests derivation from mantle depths without subsequent fractionation.

In contrast to this, the experimental and trace element models, based on natural garnet lherzolites, have yet to duplicate the features observed in kimberlites. While melts produced experimentally under a range of P, T, a_{H_2O} and a_{CO_2} conditions from garnet lherzolites bear similarities with normal silica saturated or undersaturated melts (e.g. Bravo and O'Hara 1975, Boettcher et al. 1975, Bachinski and Scott 1979), they do not, in any way, resemble kimberlite compositions. (Yoder (1975) however, has shown that melilite bearing undersaturated magmas could be transformed into a kimberlitic assemblage by the addition of volatiles at low pressure. The significance of this effect will be discussed in a later section.) The trace element data, as interpreted in this work also mitigates against an extension of 'normal' partial melting processes. Previous models based on trace element (particularly REE) abundances have invoked limited amounts of partial melting of a garnet lherzolite to account for the observed La/Yb ratios of kimberlites (e.g. Mitchell and Brunfelt 1975). These models, however, do not account for the observed absolute abundances. To overcome this, Paul and Potts (1977) suggested that extensive fractionation of olivine and pyroxene must have occurred to concentrate the incompatible elements and volatiles in the liquid phase. As suggested above, however, the high Co, Ni and Cr abundances of most kimberlites mitigate against the operation of such a process. Furthermore, when the REE data are plotted as in fig. 3.5,kimberlites do not conform to the trend of normal basaltic rock types. If, as has been proposed, kimberlites were formed

by very small degrees of partial melting, then it might be expected that they would continue the trend defined by such samples as the Australian basalts (10 → 4% partial melting) the Malaita alnoites (5-4%) and the Arizona lamprophyres (2.5-1.5%) to higher La/Yb and Sm values. This is clearly not the case. From this it therefore follows that fundamental differences exist between normal basalt and kimberlite petrogenetic processes and that an alternative process must be sought to explain the major features of kimberlite geochemistry.

Much of the available REE data on kimberlites are derived from S. African localities and much of this information refers to two main provinces: Kimberley and N. Lesotho. The remaining information is from analyses of the geographically intermediate occurrences at Jagersfontein and Koffyfontein and also from Monastery Mine. By plotting the available data on fig. 3.12 and distinguishing between the two main provinces, it is clear that, while there is some overlap between the two groups, there is a tendency for the samples from the Kimberley group to plot at higher values than those from N. Lesotho. The Jagersfontein and Koffyfontein samples compare well with those from N. Lesotho (as do the Premier Mine samples) but those from Monastery, geographically close to Lesotho, plot with the Kimberley samples. The overlap between the two groups is probably the result of using both micaceous and basaltic and diatreme and hypabyssal facies samples in the compilation. This is due to the fact that REE analyses are often produced without clear reference to the kimberlite type. If only

dyke kimberlites were compared then the distinction might be even clearer. It has been suggested that kimberlites from the centre of the S. African craton (i.e. Kimberley) might be more REE enriched than those from the periphery. (P.H. Nixon personal communication). While the Kimberley and N. Lesotho samples may be interpreted as substantiating this hypothesis, the more erratic spread of the analyses from the intermediate localities suggests that the implied regional differences are not necessarily related to any structural feature with such a marked surface expression.

The regional differences in REE abundances are also reflected in the absolute abundances of other trace elements such as Zr, Nb, Ta, Hf (Kable et al. (1975)). However, inter-element ratios tend to remain constant as illustrated by the elements La and Th (fig. 3.13). Data used in compiling this diagram were taken from Fesq et al. 1975, Mitchell and Brunfelt (1975, Paul and Potts (1977) as well as this work. Applying a linear regression analysis to this trend, the derived line passes close to the origin with a gradient of between 7 and 8. The fact that the regression line passes virtually through the origin may be interpreted as indicating that the kimberlite is derived directly from its source (with the same La/Th ratio) without significant addition of other components of different La/Th ratios. The same argument can be used in interpreting other element ratios e.g. Zr/Nb, Ta/Hf etc., and suggests that the source region beneath Kimberley and Lesotho are similar with

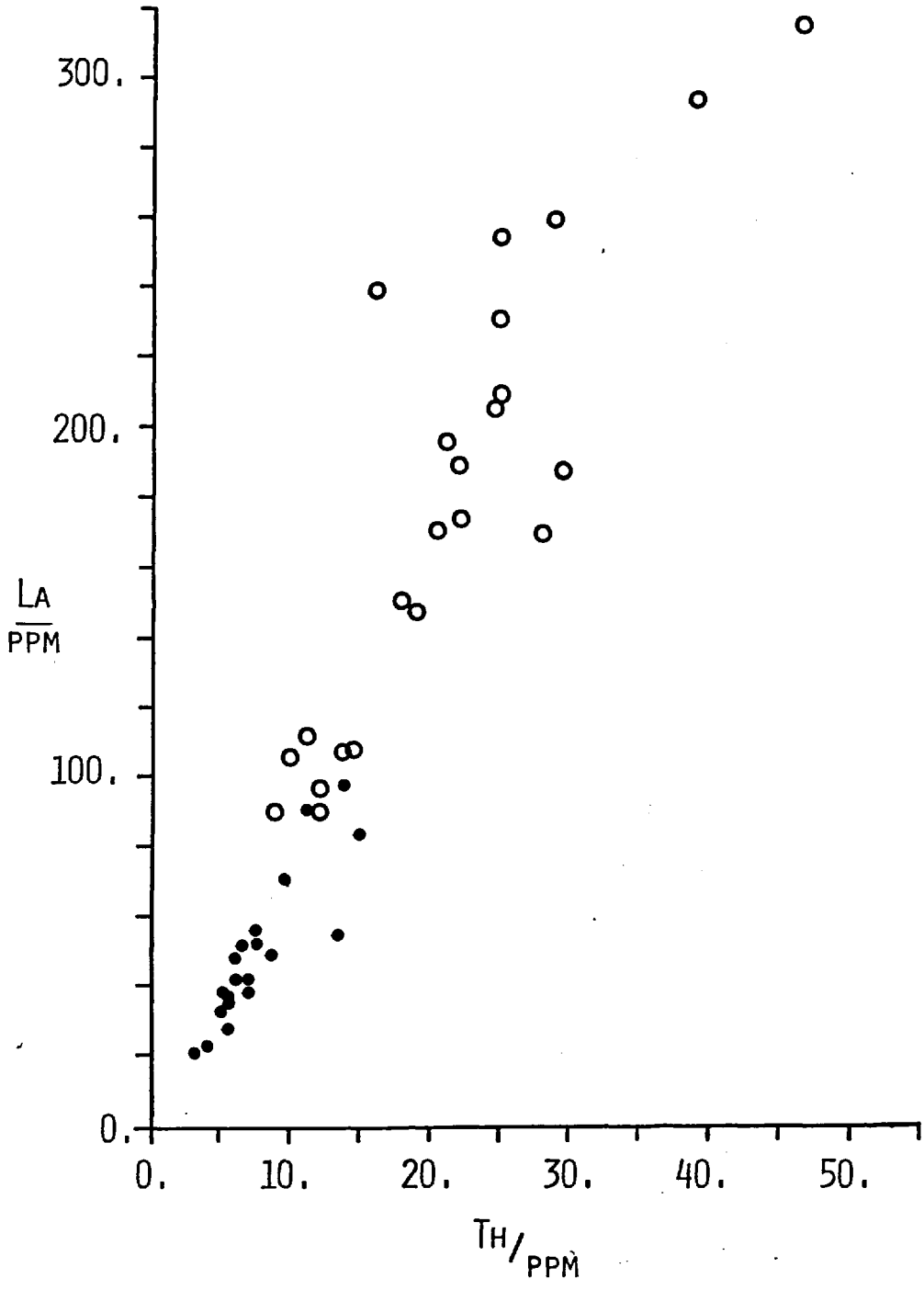

Fig 3.13 Graph of La vs. Th for Kimberley region kimberlites ○ and Lesotho, Koffiefontein and Jagersfontein samples ● . As with fig 3.12, note the tendency for the Lesotho and other samples to plot at lower levels but on a common trend compared with the Kimberley samples.

respect to these inter-element ratios. The differences in abundances, therefore, appear to be the result of individual processes operating in the different regions.

Sr isotope ratios are similarly uniform. Fresh basaltic kimberlites from Kimberley possess ratios of between .7038 and .7046 (Barret and Berg 1975), although micaceous and altered varieties gave initial ratios of up to .716. Those from N. Lesotho give values comparable with the fresh Kimberley samples. Barret and Berg (1975) suggested that the high initial ratios of the micaceous and altered kimberlites may be due to groundwater interaction, although very large quantities of groundwater would be required to produce the observed change in initial $^{87}Sr/^{86}Sr$ ratio. Such a process could also explain the negative trend displayed by the more enriched samples in fig. 3.12. Experimental work (Flynn and Wayne Burnham 1978) indicates that while the distribution coefficient of the REE between an aqueous and a silicate phase is less than one, there is a tendency for this value to increase for the heavy REE. Thus, if groundwater flowed through the kimberlite in the volumes necessary to adjust the initial $^{87}Sr/^{86}Sr$ ratios, then preferential leaching of the heavy REE could occur, thereby increasing the La/Yb ratio while reducing the value of ΣREE (i.e. Sm) in a manner similar to the observed trend. This process is favoured when compared with the alternative of garnet fractionation at depth. As K_D values of Sm between garnet and silicate liquid are <1, fractionation of this

mineral would tend to increase Sm in the resultant liquid while increasing La/Yb. This would produce a secondary trend in fig. 3.12 away from that observed.

Returning to the interpretation of the major trend of kimberlite REE analyses, there are still significant interpretive problems. If, on analogy with normal basalts, the increase from low La/Yb and Sm to high La/Yb and Sm is interpreted as an evolutionary sequence reflecting the variable operation of a process similar to partial fusion, then it should be possible to observe systematic changes in major element compositions. In table 3.4, nine kimberlite analyses are tabulated in ascending order of La/Yb ratio. Although there are considerable variations of some of the major element abundances e.g. TiO_2 varies from 0.35% up to 4.48% there are no systematic variations such as a tendency towards greater degrees of silica undersaturation or even an increase in volatile constituents, as La/Yb increases. Note also that there is only the most general of positive correlations between La and P_2O_5, elements that frequently show a close coherence in their behaviour.

In conclusion, the evidence suggests that partial melting, as envisaged in normal basalt petrogenesis, does not control the trace element abundances of kimberlites. While it is not possible, with the available data, to propose an alternative petrogenetic scheme, certain salient features of kimberlite chemistry and geology are listed below, that must be satisfied in any future hypothesis.

Table 3.5 Representative analyses of kimberlites from southern Africa, illustrating the lack of coherent variation between the REE and other constituents.

	1	2	3	4	5	6	7	8	9
SiO_2	37.57	26.57	31.05	32.70	31.75	31.18	31.77	35.31	35.58
TiO_2	0.35	1.84	4.48	1.82	1.98	3.74	2.72	1.06	0.79
Al_2O_3	2.35	3.22	3.57	4.60	2.40	2.43	3.26	2.74	2.08
Fe_2O_3	4.07	4.86	5.87	5.44	4.92	8.82	6.07	3.59	3.90
FeO	3.26	4.16	5.66	3.30	4.04	3.73	3.33	4.63	3.58
MnO	0.10	0.20	0.16	0.15	0.17	0.20	0.18	0.16	0.13
MgO	33.73	24.15	24.39	26.68	29.50	30.04	30.99	34.88	32.89
CaO	2.12	15.74	7.47	8.40	8.89	6.71	6.81	4.98	4.13
Na_2O	0.03	0.02	0.17	0.60	0.01	0.23	0.27	0.06	0.08
K_2O	0.51	0.82	0.79	2.87	1.11	0.18	1.69	2.49	2.82
H_2O^+	11.63	7.28	8.51	7.82	9.05	10.03	9.32	5.62	7.76
H_2O^-	1.75	0.25	1.63	0.79	0.56	0.19	0.61	0.60	0.45
P_2O_5	0.16	0.56	0.36	0.98	0.69	0.15	1.77	0.64	0.48
CO_2	1.64	10.22	3.76	4.24	5.98	1.99	1.36	3.03	4.97
Total	97.63	99.87	97.87	100.39	101.05	99.62	100.15	99.79	99.64
La/Yb	48.8	62.8	76.0	89.0	139.	146.	180.	232.	367.

1 - PHN2811 Jagersfontein, South Africa.
2 - PHN1725 Ramatseliso, Lesotho.
3 - PHN1598 Thaba Putsoa, "
4 - PHN2732 Wesselton, Kimberley area, South Africa.
5 - PHN1334 Kolo, Lesotho.
6 - PHN1867 Monastery Mine, Orange Free State.
7 - PHN2384 Roberts Victor, South Africa.
8 - PHN2201 Star Mine, South Africa.
9 - PHN2796 Bellsbank, Kimberley area, South Africa.

(1) Kimberlites are distinctly ultrabasic in major element composition, a feature reflected in their content of Co, Ni and Cr.

(2) Volatile elements and compounds, particularly CO_2 and H_2O have played a very important part in the evolution of kimberlites as evidenced by the abundance of calcite, mica and similar phases.

(3) Despite the abundance of phenocrystal olivine, the high transition element abundances suggest a lack of significant fractionation en route to the surface and further indicates that prior to eruption kimberlite may have been in chemical equilibrium with the deeper mantle.

(4) Xenolith and xenocryst evidence indicates a depth of origin well in excess of 150 km.

(5) Significant differences in trace element abundances but not ratios exist between kimberlite localities and provinces.

(6) There appears to be very little coherence between the behaviour of trace and major element abundances except between the trace elements and P_2O_5 and possibly K_2O.

(7) Kimberlites do not plot with normal continental basaltic magmas on a diagram of La/Yb vs Sm.

In addition to these essentially chemical features there are at least two geological features that should be constantly borne in mind viz:

the restriction of kimberlites to continental regimes and, secondly, their spatial relationship to continental tholeiitic magmatism, which they often post-date by a significant length of time. The trace element and experimental data do not indicate that kimberlites are derived by partial melting of a mantle of a normal gt + cpx + opx + ol mineralogy. Unfortunately the available experimental work has been carried out on systems at 30 kb. In the future it will be necessary to increase these pressures to match and exceed those recorded in ultrabasic xenoliths (i.e. 50 kb +) before more definite conclusions can be drawn regarding the constitution of the deeper mantle and the nature of partial melts derived from these great depths.

3.6 The Relationship between Kimberlite and othe Volcanic Rocks

On account of their high potassium and volatile (especially CO_2) abundances, kimberlites are often discussed in relation to the petrogenesis of potassic basalts and carbonatites.

The ultra-potassic volcanic rocks from Toro-Ankole in Uganda have been extensively analysed for trace elements by Mitchell and Bell (1977). From their data, it is clear that the rocks can be subdivided into two main categories on the basis of their La/Yb ratios. The ugandites and mafurites possess La/Yb of 146-312 while those of the leucitite and phonolitic tephrite series lie in the range 30-56. This two-fold division is emphasized when the analyses are plotted on a

La/Yb vs Sm graph (fig. 3.14). The low La/Yb group plot close to the previously defined basalt evolution curve and suggest derivation by 5-10% partial melting. The high La/Yb group, however, overlap the kimberlite field. This similarity with kimberlite is also demonstrated on a La-Th diagram (fig. 3.15). These two features are further evidence for a genetic link between the ugandite/mafurite series and kimberlites, as originally proposed by Yoder (1975) from experimental data. According to Yoder's results, olivine melilite leucitite (ugandite) may be related to olivine kalsilite pyroxenite (mafurite) by the general reaction:-

$$2\,\text{Mel} + 3\text{Lc} + (x+1)\text{Fo} \rightarrow 4\text{Di} + 3\text{Ks} + x\text{Fo}$$

Ugandite (low pressure) Mafurite (high pressure).

Furthermore, addition of volatiles to the mafurite assemblage yields the kimberlite groundmass assemblage:-

$$\underset{\text{Mafurite}}{\text{Di} + 3\text{Ks} + (x+4)\text{Fo} + CO_2 + 3H_2O} \rightarrow \underset{\text{Kimberlite}}{3\text{Phlog.} + \text{Ct} + x\text{Fo}}$$

It seems reasonable to suggest that the reverse may operate in the evolution of these strongly REE fractionated potassic rocks. Kimberlite magma, trapped at depths, undergoes degassing to produce mafurite which is subsequently erupted as mafurite lava or is re-equilabrated at shallower depths to produce ugandite. The degassing of the initial

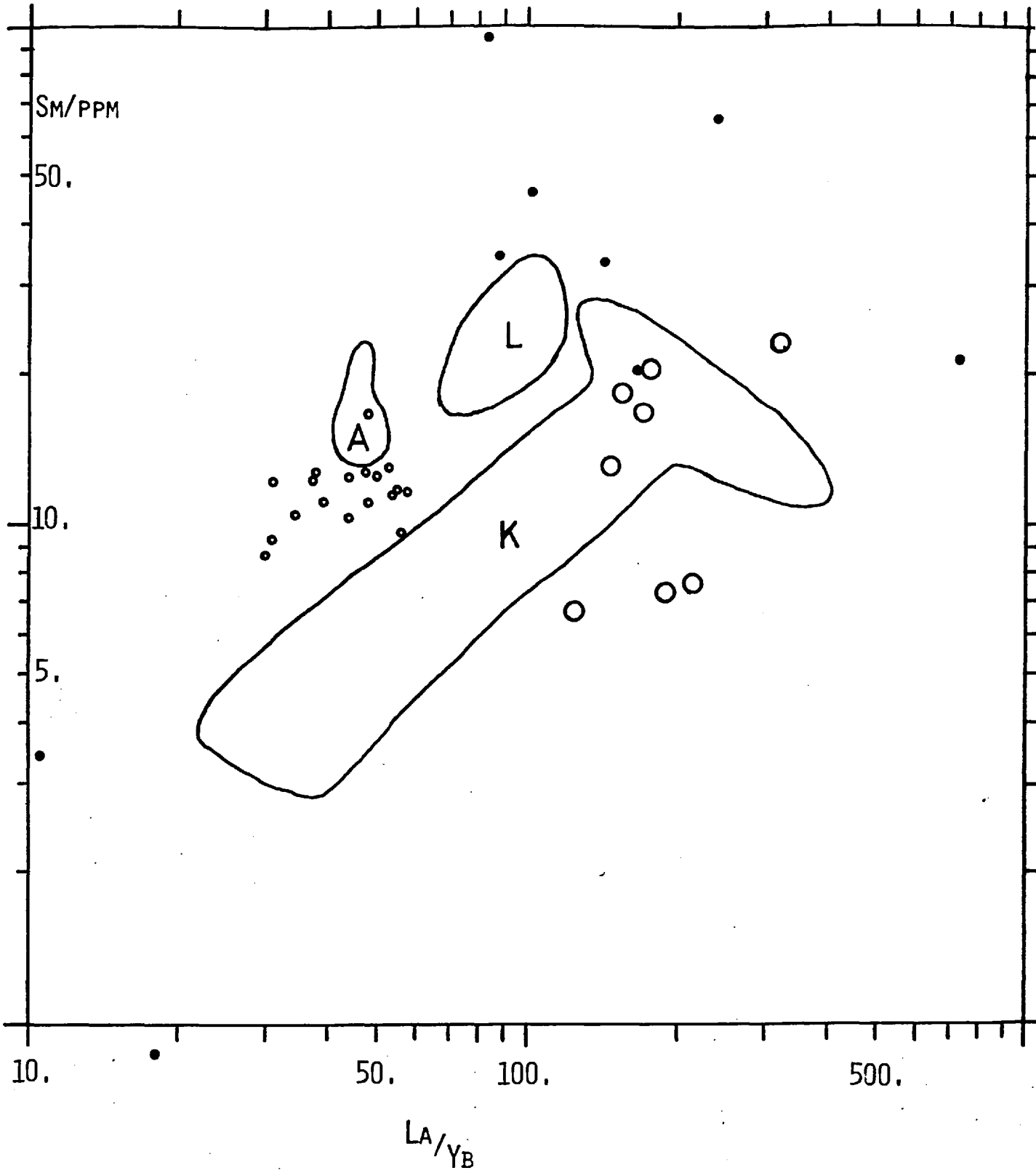

Fig. 3.14 Sm - La/Yb diagram for assorted carbonatites ● , leucitites ⊙ , and the ugandite - mafurite series ○ . A - alnoites, L - lamprophyres, K - kimberlites.

kimberlitic magma may effect the production of the low La/Yb group of volcanic rocks. Their position on fig. 3.14 suggests derivation by the partial melting of a garnet lherzolite assemblage with a light REE enriched pattern (as with the alnoites etc.). However, such a process cannot account for their ultra-potassic composition. If, however, during the initial degassing, the surrounding mantle was altered by the released gases (a process analagous to potassic fenitisation perhaps) then subsequent partial melting could result in the unusual major element composition, as long as the REE abundances were not significantly different from those proposed for the alnoite source.

Such a 'composite' petrogenetic scheme might account for the La-Th variation of this low La/Yb group. From fig. 3.15 it is clear that a regression line through this group does not pass through the origin but cuts the La axis at a positive value. Note, however, that the trend does <u>not</u> transgress the kimberlite line to reach La/Th values greater than $\sim$7. As La and Th are both incompatible elements with $K_D << 1$, on partial melting they would both tend to enter the melt phase almost exclusively, thereby retaining the La/Th ratio of the source. The varying La/Th ratios of this group are, therefore, considered to be reflections of the source heterogeneity, varying from strongly altered mantle (La/Th $\sim$ 7) to weakly or unaltered mantle (La/Th $\sim$ 5).

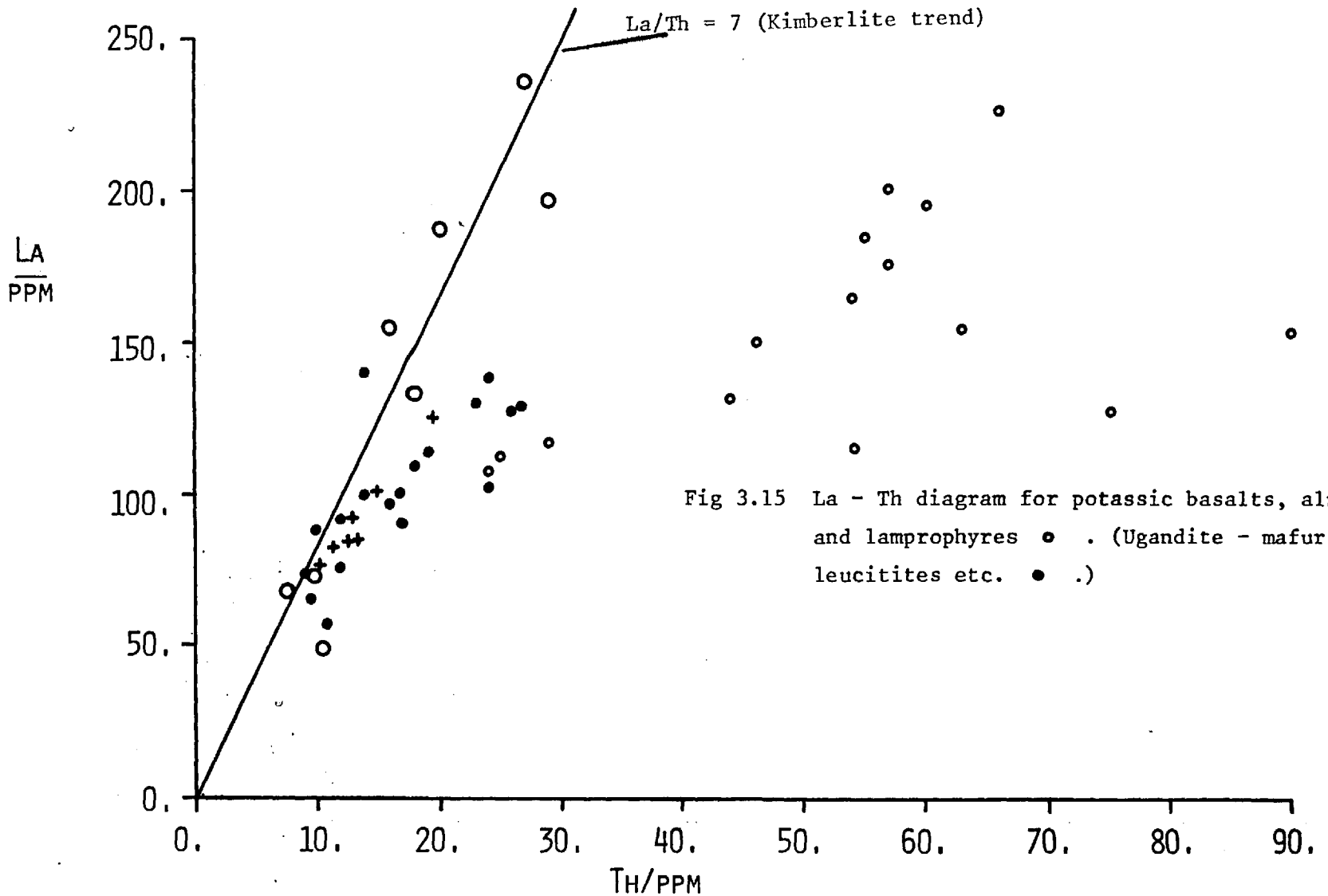

Fig 3.15 La - Th diagram for potassic basalts, alnoites + , and lamprophyres o . (Ugandite - mafurite series O , leucitites etc. ● .)

Note that the bimodal distribution of La/Yb ratios precludes the possibility of magma mixing to produce the observed La-Th trend.

Also plotted on fig. 3.15 are the La-Th analyses for the Arizona lamprophyres. These, too, show a complex variation which may also be interpreted as the result of mantle alteration. A similar interpretation holds for the alnoites that plot with the low La/Yb group of potassic basalts.

The relationship with carbonatites is less clear. Of the published REE data (e.g. Eby 1976, Cullers and Medaris 1977, Ridley and Dawson 1975, Loubet et al. 1972), only 10 analyses give La, Sm and Yb concentrations which can be plotted on fig. 3.14. Like kimberlites, carbonatites are strongly light REE enriched (La up to 10^4 x chondrite) and genetic links have been tentatively suggested (e.g. Loubet et al. 1972). However, the large scatter of the available data in fig. 3.14, with most of the points plotting well away from both kimberlite and basalt fields indicates that more complex processes are involved in carbonatite petrogenesis. This, together with the somewhat conflicting data on carbonate in alnoites (this work) and carbonate ocelli in lamprophyres (Cullers and Medaris 1977) suggests that more work is required on the geochemistry of all types of carbonatite before any definite conclusions can be made.

3.7 Conclusions

1. The alnoites can be considered to represent primary liquids resulting from the partial fusion of a light REE enriched garnet lherzolite under high $p(CO_2)$. The source is very similar to that proposed to account for the composition of Australian nephelinites and melilitites.

2. The poorer chemical constraints on the lamprophyres do not allow the development of such a detailed model. However, their position on a La/Yb vs Sm diagram suggests derivation by limited partial melting ($\sim$2.5%) of garnet lherzolite, indicating kinship with normal continental basaltic volcanism.

3. From a consideration of a great range of kimberlite analyses, it is clear that significantly different processes have operated during kimberlite genesis and that they are not related to normal magmas by any known process.

4. It is suggested that ultrapotassic rocks may be related to kimberlites by degassing and re-equilibration at shallow depths, and by the partial melting of any surrounding mantle so affected during degassing.

5. The present data are inconclusive on the relationship between carbonatites and the above mentioned rock types.

CHAPTER 4

TRACE ELEMENT ABUNDANCES OF ULTRABASIC XENOLITHS

4.1 Introduction

In Chapter 3, the alnoite and lamprophyre magmas were related to a mantle source composition in which the heavy REE were at a concentration of ~3 x chondrite with the lighter REE showing enrichment of up to 12 x chondrite. This model is consistent with others proposed to account for the major chemical features of other continental magmas (e.g. Frey et. al. 1978). The mineralogy of this mantle source was shown to be garnetiferous, in order to account for the fractionated REE patterns of the magmas, thereby conforming to the results of high pressure-temperature experimental results on similar magma types (e.g. nephelinites and basanites, Bultitude and Green, 1971). In order to compare these predicted mantle REE abundances with possible actual abundances, xenoliths of mantle-derived garnet lherzolite and harzburgite from S. African kimberlite pipes have been analysed for 8 REE and 5 other trace elements, using the techniques as described in Chapter 2.

The ultrabasic xenolith suite found in kimberlite shows a great range in mineralogy and composition. The most abundant lithologies are the lherzolites and harzburgites, considered to represent a major part of the upper mantle. Other ultramafic (though not necessarily ultrabasic) types of unknown significance include eclogites and pyroxenites

and occasional mica rich xenoliths known as glimmerites. These are thought to have been derived from isolated bodies formed by the solidification of melts of varying compositions trapped at depth. Occasionally these usually subordinate xenolith types occur in great abundance (e.g. eclogites at Roberts Victor) suggesting considerable lateral mantle heterogeneity.

Although the significance of the peridotite group xenoliths in relation to the upper mantle has been appreciated for 50 years (e.g. Wagner 1928), it is only recently that they have been analysed in any detail in order to elucidate their petrogenesis. From the many studies over the past decade, it has become increasingly clear that the peridotite group xenoliths can be classified into a number of chemical, mineralogical and textural groups. The earliest such comprehensive study, on the xenoliths from Lesotho kimberlites, has been particularly well documented in papers by Boyd and Nixon (1975) and Boyd (1973) and in the Lesotho Kimberlite volume (Nixon, 1973). From their work, three major groups of xenolith could be defined on a textural and mineralogical basis:-

1. Discrete xenoliths, consisting of large single crystals or aggregate crystals of single minerals, especially garnet and pyroxene. Also included in this group are diopside-ilmenite intergrowths.
2. Granular xenoliths. These are polyphase peridotites with a mineralogy of olivine and orthopyroxene $\pm$ garnet $\pm$ clinopyroxene $\pm$

chromite in a coarse granular texture.

3. Sheared Xenoliths are again polyphase peridotites, with a mineralogy comparable with the granular varieties, showing textural evidence of intense deformation and recrystallisation.

In addition to these three groups, a fourth can now be added, following the work of Erlank and Rickard, 1977, on xenoliths from the Kimberley pipes. Members of this fourth group show mineralogical evidence of metasomatism by the presence of phlogopite mica and richterite amphibole in textural equilibrium with the primary ultrabasic mineral assemblage.

In the case of the Lesotho samples, the above mineralogical and textural classification also corresponds to the xenolith's depth of origin and chemical composition. Analysis of co-existing minerals and the application of mineralogical thermo-barometers (e.g. Wood and Banno, 1973) has allowed the construction of a crude mantle stratigraphy from which a mantle geotherm, corresponding to the time of kimberlite eruption, can be calculated (Boyd, 1973, and Boyd and Nixon 1975). The calculations reveal that most garnet lherzolite xenoliths are derived from 100-250km depth and have equilibrated under P-T conditions lying along a shield geotherm (Clark and Ringwood 1964). However, some of the samples derived from greater depths define an inflected geotherm, the P-T gradient increasing below about 175km. There is still consider-

able debate as to whether the inflection is of geological origin or an artefact of the thermo-barometers employed in the geotherm calculation. While recalculation of the P-T values using modified equations (Mercier and Carter, 1975) has removed the inflection, application of new data (based on the Ca content of olivine, Finnerty and Boyd, 1979) has confirmed the original results. The important feature, however, is that the sheared xenoliths are derived from greater depths than the granular varieties, in association with the discrete nodule suite. Originally it was suggested that this could represent a typical section through the continental mantle. The granular lherzolites were thought to represent the lower lithosphere and the sheared varieties the asthenosphere over which the lithospheric plates were moving, with the shearing resulting from the differential motion (Boyd and Nixon, 1975). An alternative suggestion invokes a rising mantle diapir (Green and Gueguen 1974). The sheared lherzolites represent the outer skin of the diapir which rises into the granular lherzolites, kimberlites resulting from partial fusion near the top of the diapir. The role of the discrete nodule association in either hypothesis is not clear but may represent a high pressure phenocryst suite. It must be emphasised that no clear consensus of opinion has yet been reached.

Nixon and Boyd (1973) clearly demonstrated that the granular xenoliths are depleted in such elements as Ca, Fe, Al, Ti and Na (but not K) relative to the sheared varieties. This variation is best

attributed to the effects of partial melting and has led to the adoption of the terms sterile and fertile in describing the theoretical ability of a xenolith to produce a basaltic partial melt (Boyd and McCallister, 1976). This theoretical ability has been demonstrated experimentally by Kushiro (1973). Both types of xenolith, however, show some depletion relative to the pyrolite model (Ringwood, 1966) and only one xenolith so far analysed (PHN1611) closely resembles pyrolite in its major element composition.

It should be emphasised that the above description is somewhat generalised in describing features that may or may not be found in xenolith suites. For example, analysis of ultrabasic xenoliths from Siberian kimberlites suggests a non-inflected geotherm. (Boyd, 1976). Also sheared and granular xenoliths from the Kimberley pipes (Boyd and Nixon, 1978) are derived from the same depth and there is a paucity of fertile varieties.

Until now, little attempt has been made to relate the trace element geochemistry of the peridotite group xenoliths to the above described features. The purpose of the work described in this chapter is to attempt to clarify the processes that have effected the trace elements, particularly the REE, and to see if these abundances conform to such models of petrogenesis as those described in Chapter 3.

4.2 Sample Descriptions

A total of 19 ultrabasic xenoliths have been analysed, radiochemically, for eight REE (La, Ce, Nd, Sm, Eu, Dy, Yb & Lu) using the techniques described in Chapter 2. Sc, Co and Cr have also been determined by INAA and U & Th by ENAA. The samples are essentially garnet lherzolites (ol + opx + cpx + gt) and harzburgites (ol + opx + gt), although a mica rich wehrlite (ol + cpx + phlogopite) and an ilmenite bearing orthopyroxenite were also included for comparison. The salient features of each sample, i.e. mineralogy, texture etc., are listed in table 4.1. Of the samples analysed, four can be described as fertile, but only one of these resembles pyrolite with regards to its major element composition (viz PHN 2838). The rest, excluding PHN 3248 (the orthopyroxenite) and PHN 2771 (the wehrlite), are sterile garnet lherzolites and harzburgites, some of which show evidence of so-called metasomatism in the form of primary phlogopite. The analyses should, therefore, reflect the effects of both partial melting and metasomatism. Although the samples are loosely described as fertile, sterile etc., their major element abundances do show significant variations within each group. The classifications should, therefore, be treated in a purely descriptive way and do not necessarily imply any genetic relationships. Major element analyses are listed in appendix 4.1.

4.3 Results

The results of the 19 analyses are summarised in table 4.2 and

Table 4.1 Xenolith Sample List.

PHN No.	Locality	Texture	Mineralogy	Class
1569	Thaba Putsoa, Les.	C	ol,opx,cpx,gt,chr,phlog.	S/M
2492	Kao, Lesotho.	C	ol,opx,gt,graphite.	S
2713	Monastery, O.F.S.	C	ol,opx,gt,cpx,phlog.	S/M
2759	Bultfontein, S.Af.	C/SD	ol,opx,gt,cpx,phlog.	S/M
2764	" "	P	ol,opx,gt,cpx.	S
2765	" "	M	ol,opx,gt,chr.	S
2766	" "	M(F)	ol,opx,gt,chr.	S
2771	Monastery, O.F.S.	P	cpx,ol,phlog,ilmen.	M?
2780	Frank Smith, S.Af.	P	ol,opx,gt.	F
2782	" " "	P	ol,opx,gt.	S
2814	Jagersfontein,S.Af.	C	ol,opx,cpx,gt.	S
2823	Liqhobong, Les.	C/T	ol,opx,gt,cpx.	S
2838	Thaba Putsoa, Les.	P/M	ol,opx,gt,cpx.	F
2839	" " "	P/M	ol,opx,gt,cpx	F
2848	" " "	C	ol,opx,gt,cpx,spinel.	S
2860	Matsoku, Les.	C	ol,opx,gt,cpx,chr,phlog.	S/M
2862	" "	FL	ol,opx,gt,cpx.	S
3040	Abbotsford, E.Griq.	M	ol,opx,gt,cpx. 60 25 10 5	F
3248	Frank Smith, S.Af.	C	opx(bronzite),ilmen.	-

Abbreviations:- Localities: Les. - Lesotho, O.F.S. - Orange Free State, S.Af. - South Africa.

Textures: C - Coarse, SD - Slightly deformed, P - Porphyroclastic, M - Mosaic, F - Fluidal, T - Tabular, FL - Flaser.

Classes: S - Sterile, M - Metasomatic, F - Fertile.

the REE abundances illustrated graphically in figs 4.1-4.4. From the REE abundances, the xenoliths can be divided into two groups: those with $(La/Lu)_N$ >25, corresponding to the sterile and phlogopite bearing metasomatic xenoliths, and those with $(La/Lu)_N$ < 8, which are the more fertile samples. ($(La/Lu)_N$ values are used, as opposed to La/Yb, as the Lu radiochemical analyses are of a higher precision than Yb). If it is assumed that, to a first approximation, the Earth has a bulk composition similar to chondritic meteorites, then the fertile xenoliths possess REE patterns as expected, showing little deviation from meteoritic abundances. The sterile xenoliths, however, display remarkably fractionated REE patterns with $(La/Lu)_N$ ratios tending to values comparable with the most extreme rock types e.g. kimberlites, carbonatites etc. This light REE enrichment is the opposite of the light REE depletion expected, if these sterile xenoliths are residual after partial fusion. Furthermore, the similarity with the host rock raises the question of contamination on eruption, which must be considered before the analyses can be interpreted in the context of mantle processes. Other incompatible trace elements are also more abundant in the sterile xenoliths, while Co and Cr maintain roughly constant abundances. Sc is more abundant in the fertile samples.

4.4 Comparison with analyses of other ultrabasic rocks.

Despite the obvious importance of garnet peridotite as a source of basaltic magmas and the use of the REE in developing semi-quantita-

Table 4.2 Rare earth and trace element abundances in the analysed xenoliths.

	Fertile samples				Sterile and sterile/metasomatic samples						
	PHN2838	PHN2839	PHN2780	PHN3040	PHN1569	PHN2492	PHN2713	PHN2759	PHN2764	PHN2765	PHN2766
La	0.86	1.81	0.88	1.09	1.05	5.17	3.91	2.90	3.99	2.33	2.18
Ce	2.57	2.02	2.14	2.52	2.18	10.9	9.41	5.87	9.03	4.51	4.45
Nd	1.47	1.41	0.81	1.39	0.93	5.60	3.53	2.69	3.91	1.92	1.70
Sm	0.515	0.316	0.267	0.342	0.219	0.747	0.663	0.571	0.629	0.364	0.344
Eu	0.191	0.086	0.109	0.123	0.074	0.191	0.229	0.147	0.178	0.108	0.101
Dy	0.920	0.263	0.482	0.397	0.107	0.164	0.332	0.199	0.256	0.166	0.120
Yb	0.482	0.150	0.230	0.205	0.024	0.095	0.088	0.061	0.085	0.040	0.020
Lu	0.073	0.024	0.034	0.029	0.004	0.013	0.015	0.009	0.014	0.006	0.006
U	<0.01	<0.01	0.07	0.06	0.02	0.12	-	0.06	0.14	0.10	0.11
Th	0.07	0.07	0.13	0.16	0.09	0.42	-	0.27	0.43	0.32	0.30
Sc	16.3	7.14	9.84	9.75	4.67	7.00	-	6.43	5.00	4.36	4.08
Co	115.	101.	133.	105.	93.	95.	-	89.	103.	94.	87.
Cr	2830.	2570.	1670.	2330.	2430.	2850.	-	2720.	2310.	2410.	2470.
Cs	0.25	0.1	-	0.42	-	-	-	0.14	-	0.92	0.29
$(La/Lu)_n$	1.2	7.8	2.7	3.9	27.	41.	27.	33.	29.	40.	37.

Table 4.2 Contd.

Sterile and sterile/metasomatic samples

	PHN2782	PHN2814	PHN2823	PHN2848	PHN2860	PHN2862	PHN2771*	PHN3248**
La	3.02	4.05	1.57	10.8	2.87	1.35	5.29	6.39
Ce	6.28	7.75	3.28	10.8	5.25	2.70	10.4	9.68
Nd	2.56	2.36	1.28	6.90	2.05	1.33	4.40	4.53
Sm	0.455	0.484	0.245	1.65	0.346	0.198	0.950	0.870
Eu	0.148	0.119	0.074	0.446	0.077	0.051	0.273	0.190
Dy	0.178	0.147	0.076	1.08	0.100	0.064	0.416	0.465
Yb	0.062	0.031	0.026	0.745	0.022	0.018	0.085	0.148
Lu	0.007	0.011	0.006	0.120	0.003	0.003	0.011	0.029
U	0.07	0.12	0.11	-	0.14	0.12	1.12	0.16
Th	0.33	0.47	0.17	-	0.41	0.18	0.19	0.72
Sc	6.89	5.55	4.96	1.00	3.17	2.42	10.8	14.3
Co	102.	81.	96.	6.2	105.	128.	86.	116.
Cr	2660.	1780.	2440.	670.	1910.	1390.	6010.	1740.
Cs	0.39	0.37	0.16	-	0.14	-	1.3	1.3
$(La/Lu)_n$	44.	38.	27.	93.	99.	46.	50.	23.

* Mica wehrlite ** Ilmenite orthopyroxenite

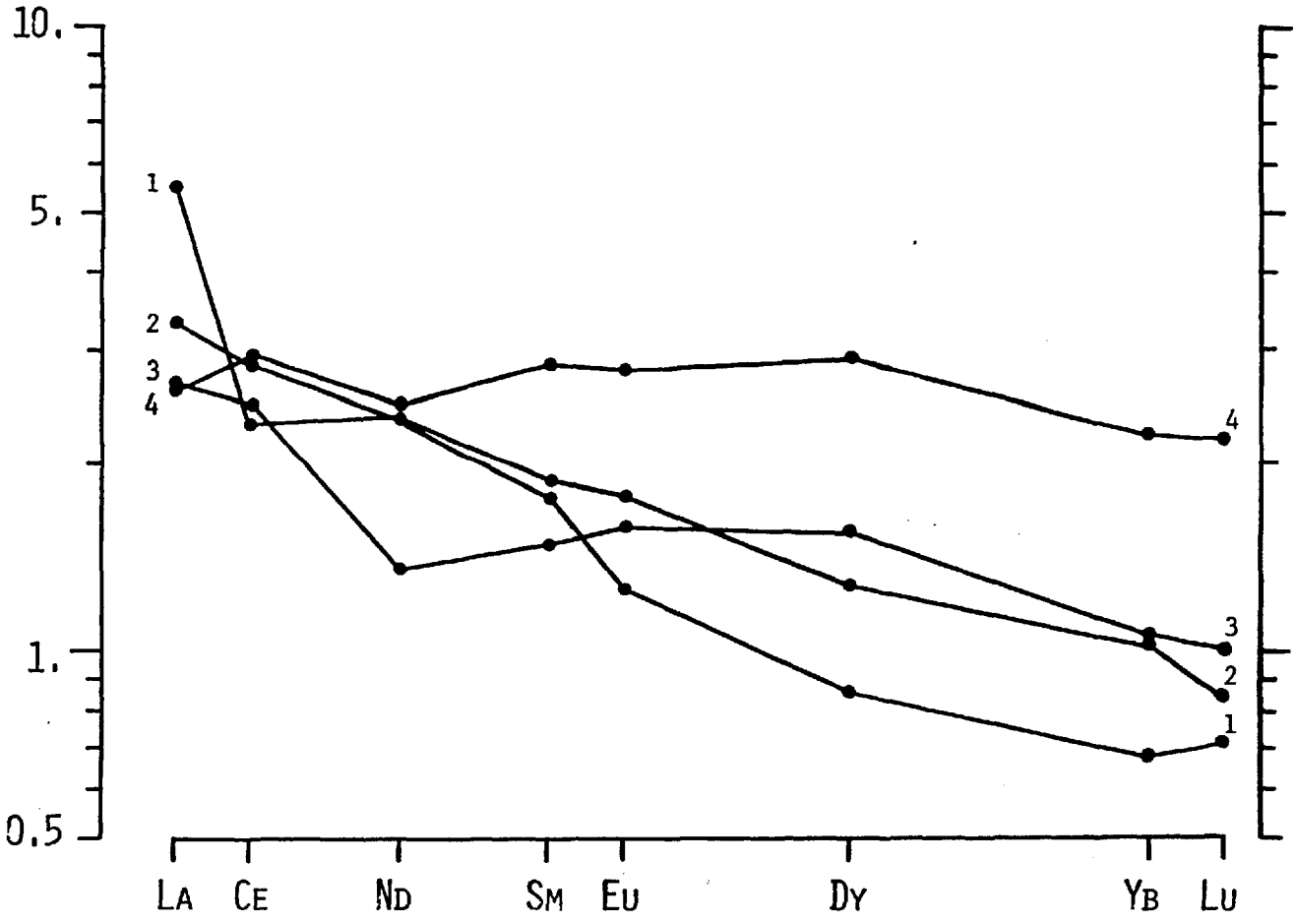

Fig. 4.1 REE abundances for four relatively fertile garnet bearing ultrabasic xenoliths.

1 - PHN2839
2 - PHN3040
3 - PHN2780
4 - PHN2838

Fig. 4.2 REE abundances of 7 sterile ultrabasic xenoliths from N. Lesotho

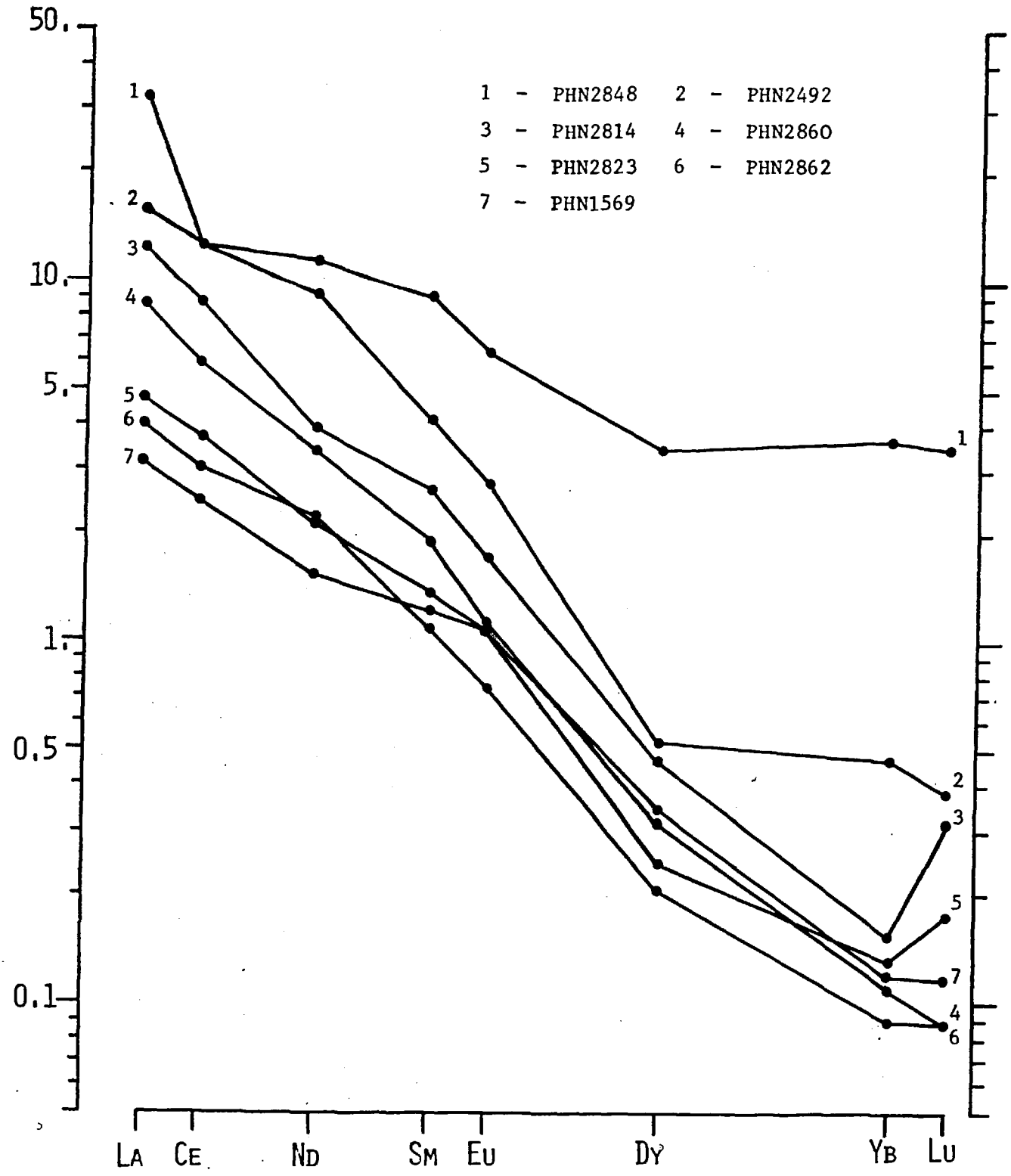

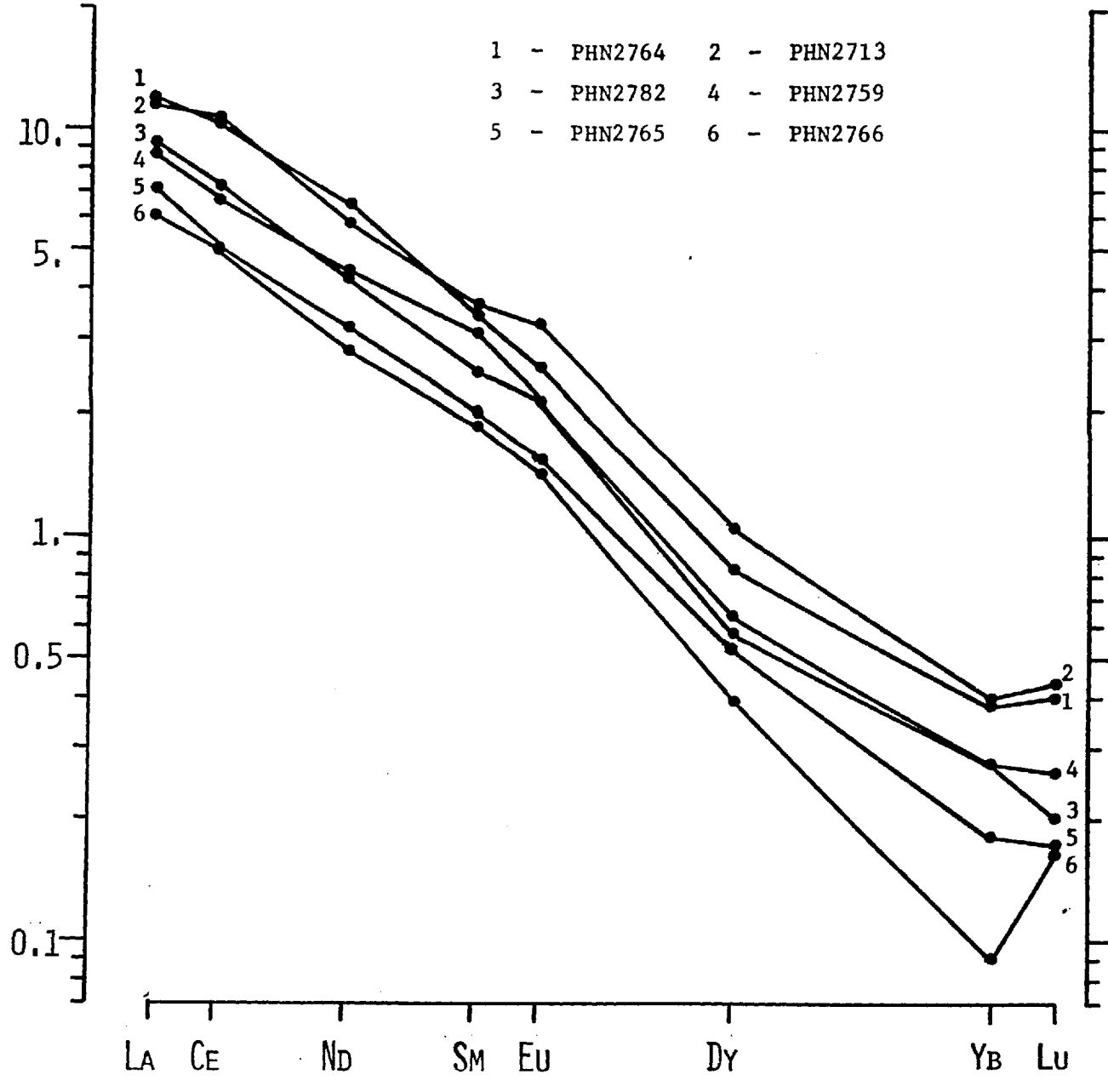

Fig. 4.3 REE abundances of 6 sterile xenoliths from the Kimberley area and Monastery Mine.

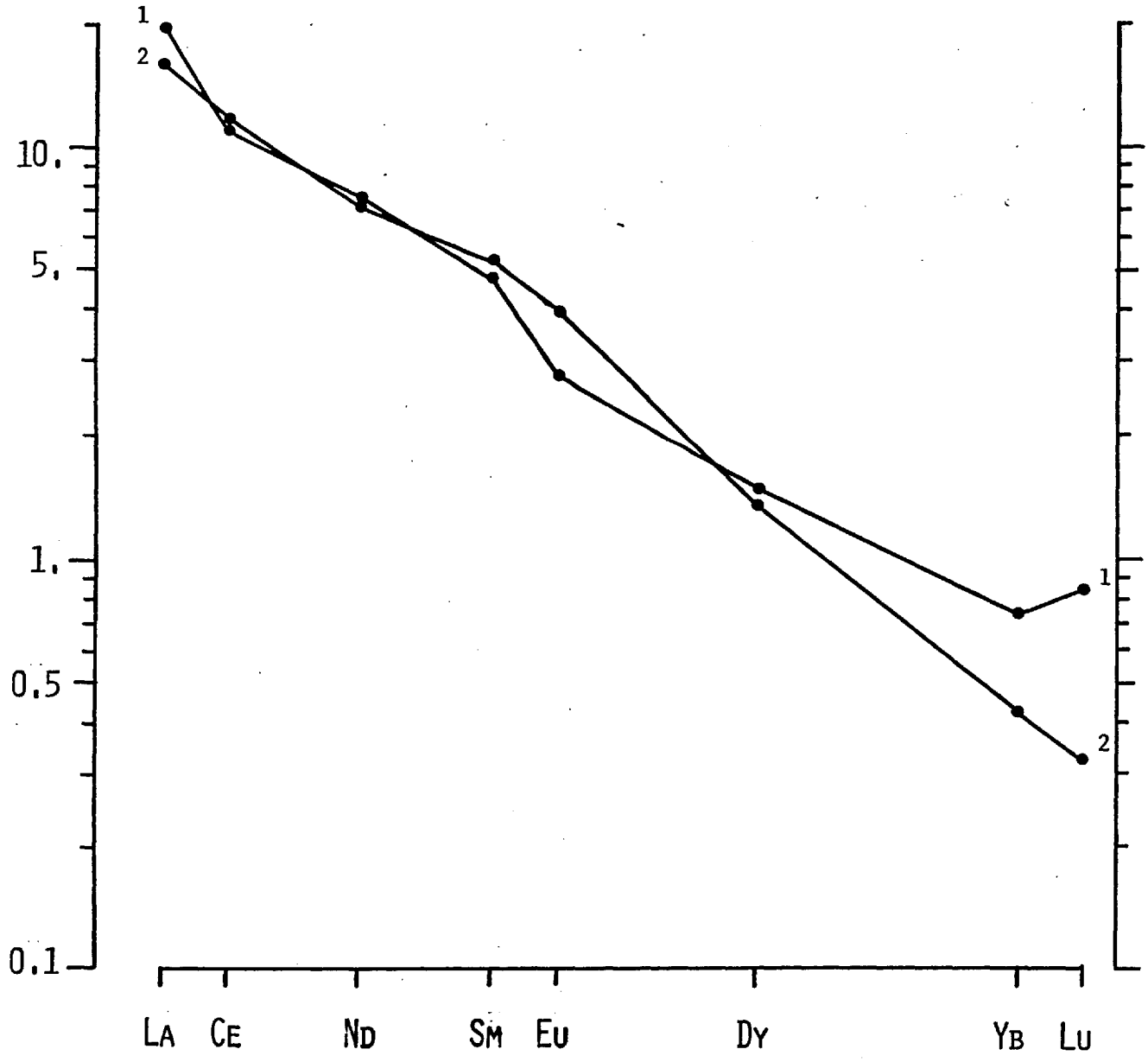

Fig. 4.4 REE abundances of samples:-

1 - PHN3248

2 - PHN2771

tive petrogenetic models, there are relatively few recorded REE analyses of ultrabasic xenoliths from kimberlites. The first reported were by Philpotts et.al. (1972) who analysed two garnet peridotites (from Bultfontein and Roberts Victor) and a lherzolite (from Roberts Victor). Of these, the two Roberts Victor samples showed a strong REE fractionation while the Bultfontein peridotite was much less fractionated. Unfortunately, as complete major element analyses were not presented it is not possible to incorporate these data in the present discussion. However, the analyses do confirm the two fold division of REE abundance patterns. A second study (Shimizu, 1975) involved the analysis of separated garnets and clinopyrocenes from three fertile and three sterile xenoliths from S. African kimberlites. Reconstruction of whole rock patterns, assuming realistic modal abundances of garnet and clinopyroxene, again revealed the two fold division into fractionated (sterile) and unfractionated (fertile) types. A major contribution of this work was to demonstrate the expected distribution of the REE between clinopyroxene and garnet according to K_d values observed in other samples. This important feature is considered to be strong evidence against host rock contamination controlling the REE abundances in the lherzolite nodules. It should be noted that REE K_d (cpx-gt) values from both coarse and porphyroclastic xenoliths are comparable, showing garnets strongly enriched in the heavy REE. These features, together with the fact that the reconstructed patterns compare with the observed whole rock patterns and that the fertile samples show

little sign of light REE enrichment, are interpreted as suggesting minimal contamination; (it is difficult to envisage a process whereby sterile xenoliths only are contaminated on eruption). With regards to contamination, it should be noted that similar conclusions were reached following trace element analysis of granulite xenoliths from kimberlites (Griffin et al, 1979; Rogers, 1977 and this work, Ch. 5).

The paucity of data on garnet lherzolites is partly compensated by analyses of spinel lherzolites from alkali basalt volcanos, many of the results being from the work of F.A. Frey and various co-workers. In general, the results have been similar to those from garnet lherzolites, the relatively fertile xenoliths showing flat chondrite normalised abundances while the sterile varieties posses significant light REE enrichment, although not to the extent observed in the sterile xenoliths in this work. A few of the sterile spinel lherzolite samples from S. Australia (Frey and Green, 1974) and Arizona (Frey and Prinz, 1977), however, revealed light REE depleted abundances, similar to peridotites from the Lizard peninsula (Frey 1969). Such REE abundance patterns are in accordance with partial melting models. (See e.g. fig. 4.9). It was this observation that led Frey and Green (op.cit) to propose their two component mantle model:-

Component A: This represents the bulk of the mantle, its comp-

osition being determined by partial melting depletion processes, which control the abundances of most of the major elements, the compatible trace elements (Co, Ni, Cr, Sc) and the heavy REE.

Component B is derived as a melt from deeper within the mantle and is rich in incompatible elements (viz. the light REE, U, Th, Cs,, Rb, Ba, Zr etc) and probably P_2O_5 and K_2O. It is the result of a limited amount of partial fusion of a garnet bearing source (hence the fractionated REE abundances). The addition of limited amounts of B to A followed by sub-solidus recrystallisation, results in the xenolith mineralogy and composition now observed. The Lizard peridotites and the light REE depleted xenoliths from Australia and Arizona are considered to be pure component A while those with significant light REE enrichment are a mixture of A plus B.

Comparison of the results from this work with the spinel lherzolite analyses suggests that a similar model is applicable for the following reasons. Metasomatic activity has already been suggested as the cause of certain mineralogical and chemical features in some mantle xenoliths (Erlank and Rickard, 1977) while other compositional features are best explained by partial melting depletion processes (Boyd and Nixon, 1975). In addition some of the xenoliths possess patterns inflected at Dy, similar to patterns in spinel lherzolites, where the inflection is interpreted as indicating addition of component B (represented by

Fig. 4.5 Graph of $(La/Lu)_n$ vs. Lu showing the trend towards high $(La/Lu)_n$ at low Lu concentrations.

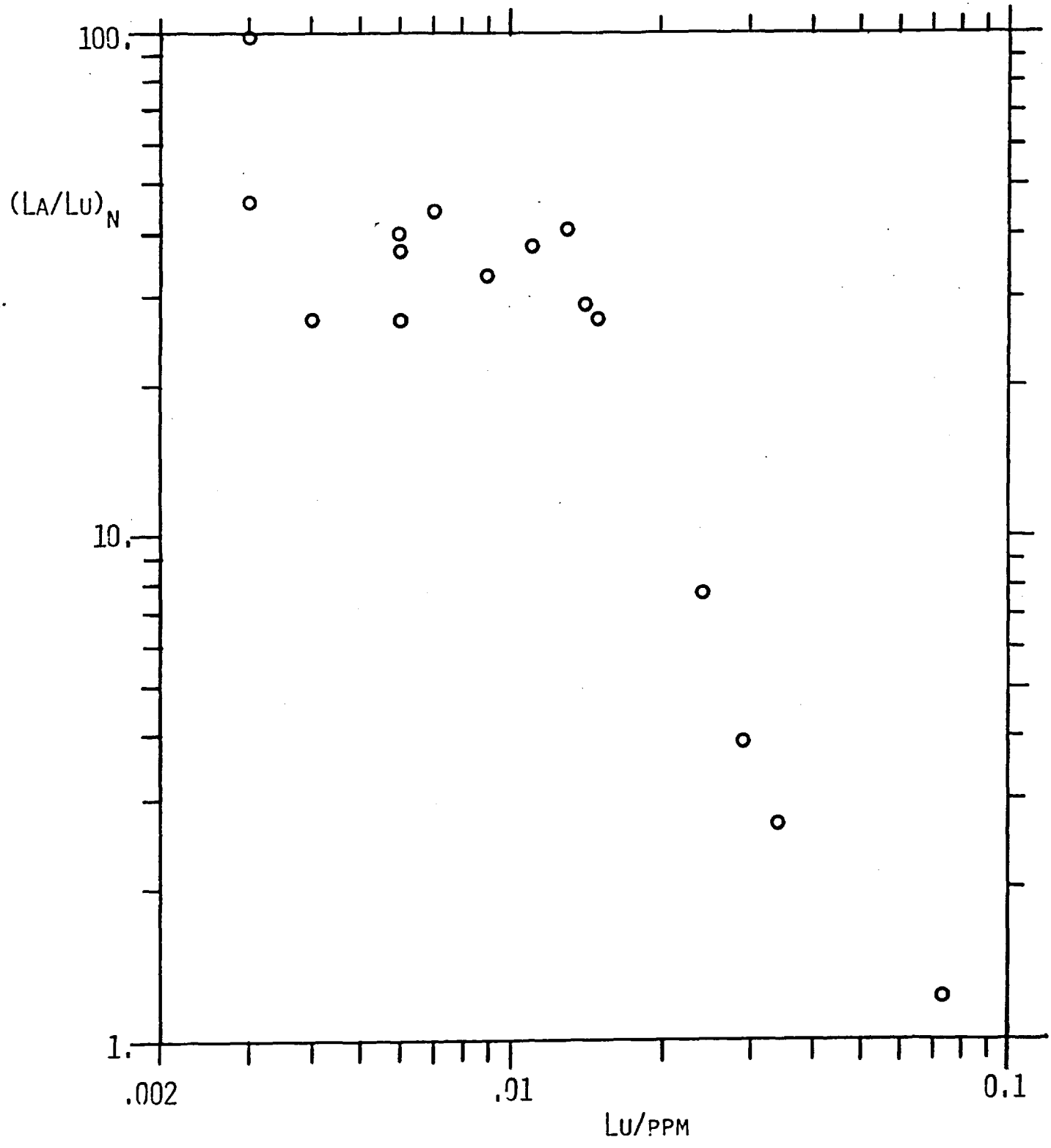

the fractionated light REE) to normally depleted component A with relatively unfractionated heavy REE (Frey and Green op.cit.) While this inflection is clearly shown by only two samples, its presence is demonstrated by a graph of $(La/Lu)_N$ against Lu (fig. 4.5). As Lu increases, so the $(La/Lu)_N$ ratio decreases as would be expected when mixing two components, one of high $(La/Lu)_N$ (Component B) and the other of low $(La/Lu)_N$ (Component A).

4.5 Petrogenesis of the lherzolite and harzburgite xenoliths

Having discounted host rock contamination as a source of the observed trace element abundances, the results can now be interpreted in relation to processes operating within the Earth's upper mantle. As with other xenolith suites, the major element variations follow a typical depletion trend, apparently due to the extraction of a basaltic melt phase. CaO and Al_2O_3 vary coherently, attaining maximum abundances (~3% CaO and ~4% Al_2O_3) in the fertile xenoliths, which also possess the lowest Mg/(Mg + Fe) ratios. The sterile xenoliths show minimum CaO and Al_2O_3 contents (~.3% and .7% respectively) and the highest Mg/(Mg + Fe) ratios. Similar variations are shown by TiO_2 and, to a lesser extent, Na_2O. In previous studies (Frey and Green op.cit. Frey and Prinz op.cit), certain trace elements have been shown to vary with the major elements, notably the heavy REE (exemplified by Lu), Sc, V and Cr (Frey and Green, op. cit). A similar variation is observed in the xenoliths analysed here, the Lu vs CaO and

Fig. 4.6

CaO vs. Lu plot for 17 garnet bearing ultrabasic xenoliths. Note the tendency for Lu to increase with CaO.

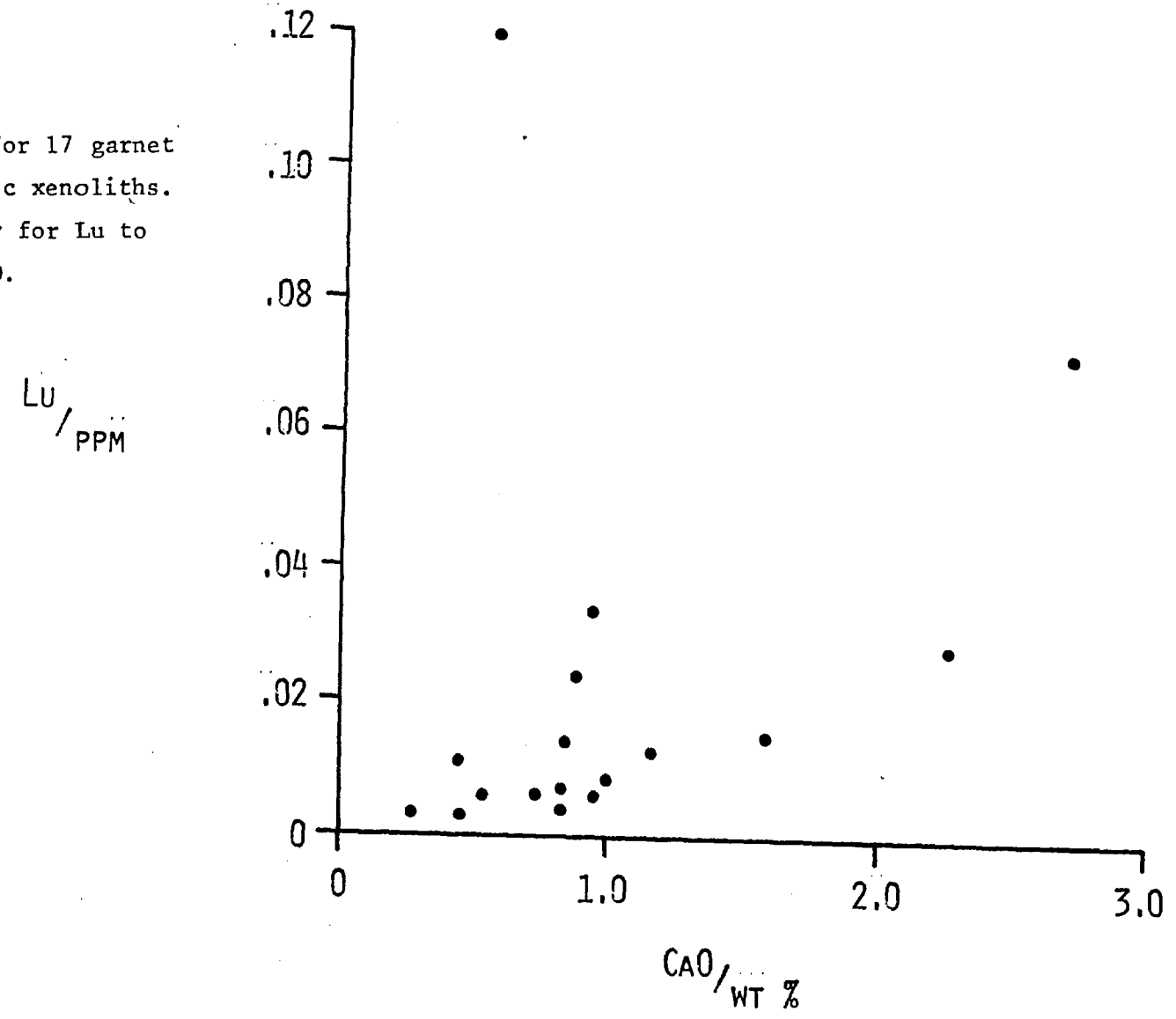

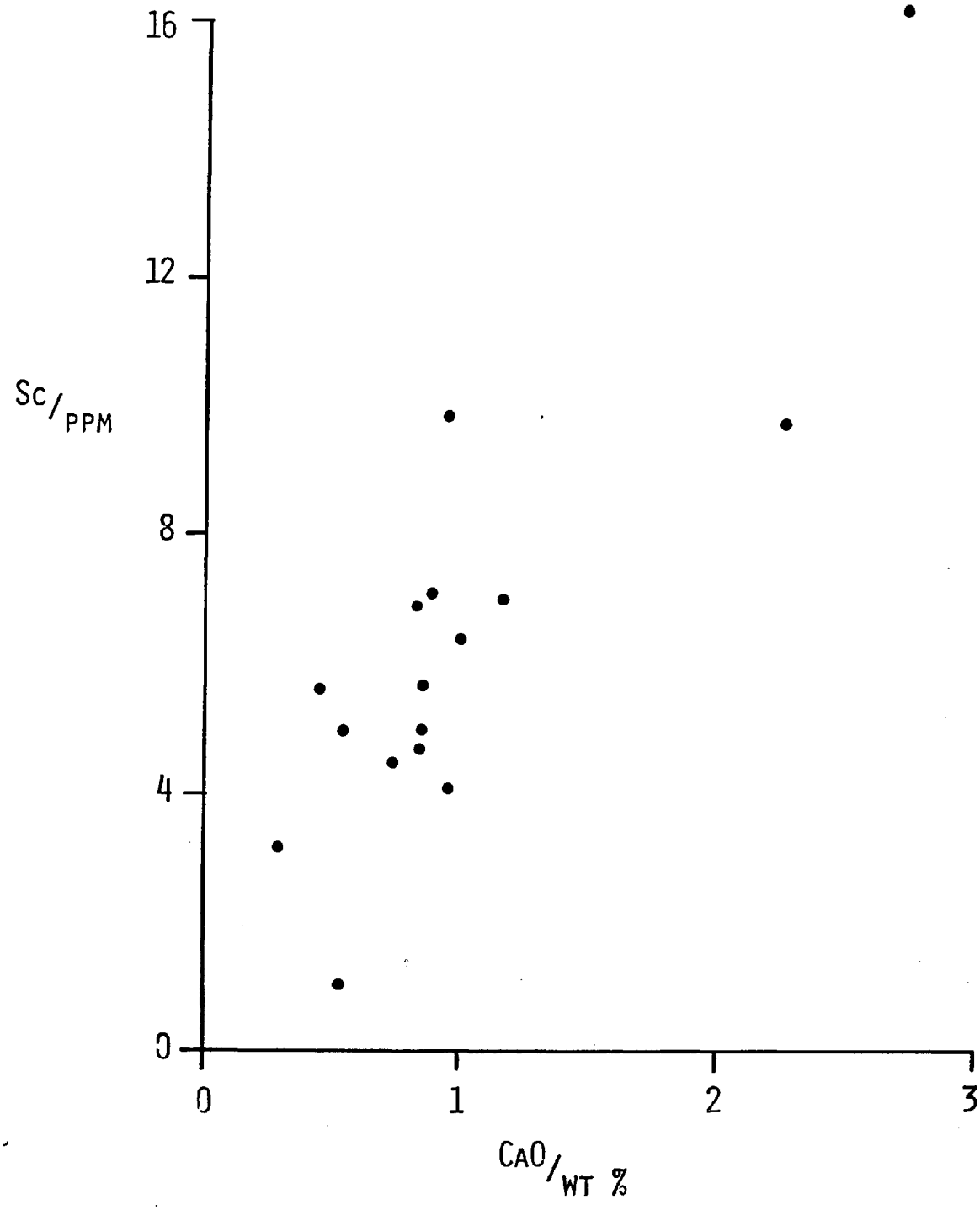

Fig. 4.6b. Plot of Sc vs CaO.

Sc vs CaO diagrams (fig. 4.6a and b) demonstrating this feature particularly clearly. Cr, however, does not show a good correlation with CaO. This is attributed to the stability of chromite spinel, a common accessory mineral of the depleted xenoliths, in the residue during the hypothesised partial melting event. In order to gain a more quantitative impression of this partial melting process, it is possible, using the equations of Shaw (1970) and Gast (1968), to develop partial melting models, based on a knowledge of mineral - liquid partition coefficient data (e.g. Arth and Hanson, 1972, Frey et al 1978) and probable mantle mineralogies.

In general, lherzolites can possess two distinctive mineralogies, depending upon the prevalent pressure and temperature conditions. At low pressures, olivine and two pyroxenes predominate with excess Al_2O_3 being accommodated by aluminous spinel. When the pressure is increased, spinel is replaced by pyrope garnet to give the garnet lherzolite assemblage observed in most kimberlite xenoliths. Both assemblages are considered in the petrogenetic models presented here. In the first model, an initial mantle mineralogy of 18% cpx, 25% opx and 57% ol is used. Spinel is ignored in this assemblage as its ability to accommodate trace elements is poorly understood as is its behaviour during partial melting. It is thought that this approximation should not effect the results of the model too greatly as spinel is never present in more than accessory quantities. The modal mineralogy

is based on data from fertile spinel lherzolite xenoliths (Frey and Green op.cit). Again, following the work of Frey and Green and Frey and Prinz (1978), the melt composition is assumed to correspond to 80% cpx and 10% each of ol and opx until 22.5% partial fusion, at which stage all of the cpx is consumed. After this, the melt is taken to comprise equal amounts of ol and opx.

The second model is based on the higher pressure garnet bearing mineralogy with a mode of 10% cpx 10% gt 25% opx and 55% ol. Again the role of accessory phases, such as ilmenite and chromian spinel, are not taken into account, as their behaviour in such processes cannot be readily assessed. Following the work of Davis and Shairer (1965) melting is considered to be approximately eutectic with the phases melting in the proportions 47% cpx 47% gt 3% opx 3% ol. After ~21% melting, all the garnet and clinopyroxene have been consumed and further melting is assumed to involve orthopyroxene and olivine in equal amounts.

The results of calculations using Shaw's equation for equilibrium partial melting are illustrated in fig. 4.7, plotting calculated C_s/C_o values vs F, the degree of partial melting, for a variety of K_d values corresponding to the elements Ni, Sc and Lu. Because of the large spread in K_d values for Ni between olivine and liquid and orthopyroxene and liquid, two limiting models corresponding to maximum and minimum

Fig. 4.7 See overleaf for caption.

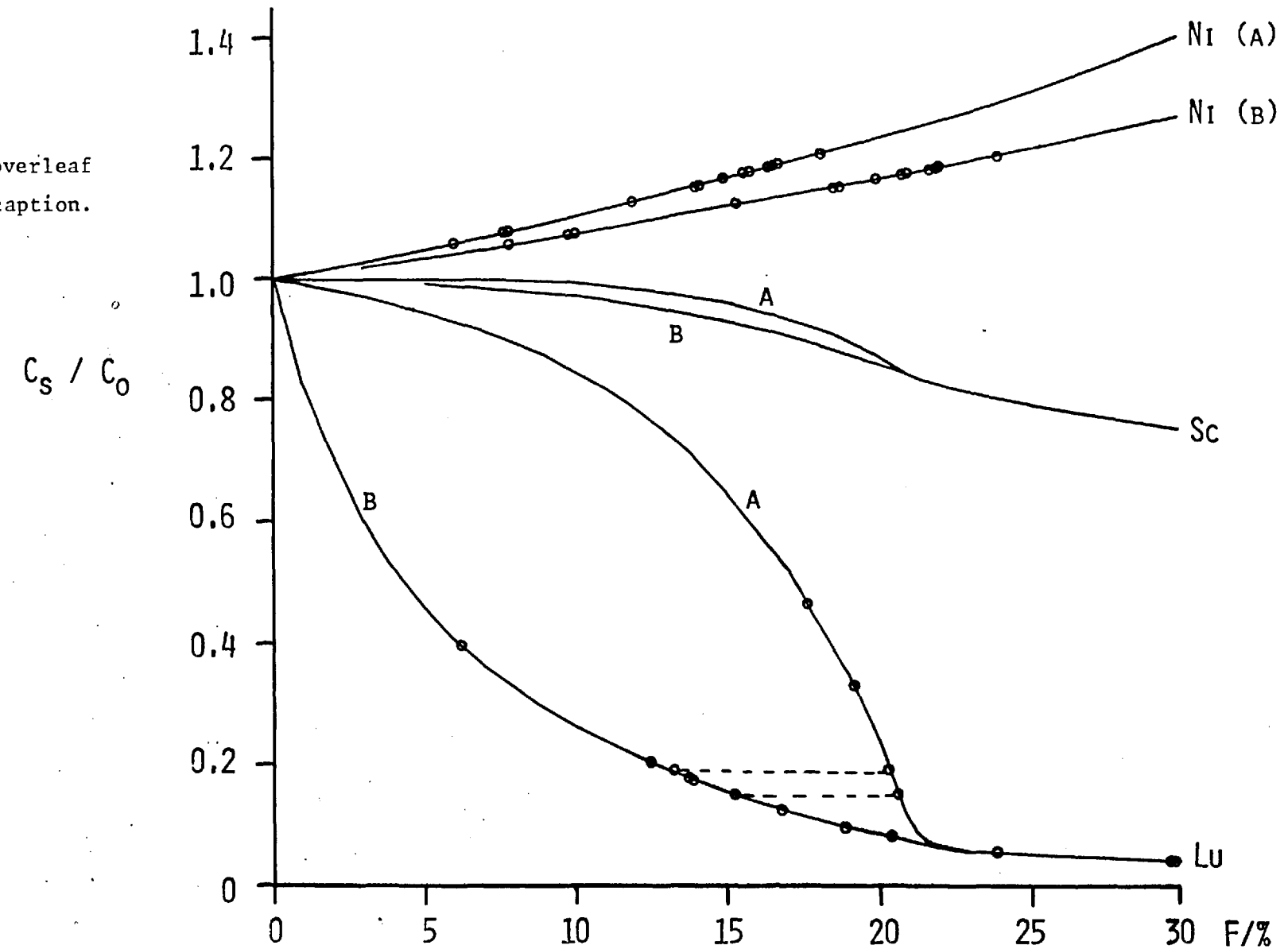

Fig. 4.7 Caption.

C_s = Concentration in residue.

C_o = " " original mantle.

F = Degree of melting.

Ni (a) and (b) are limiting curves for high and low K_d values, respectively.

Sc (a) and (b) and Lu (a) and (b) refer to garnet bearing and garnet free models respectively.

Small open circles locate the positions of calculated C_s/C_o values, where C_s = Concentration of an element in a xenolith and C_o = Concentration of that element in PHN2838, considered to represent undepleted mantle.

Tie lines connect samples whose controlling mineralogy is unclear from fig. 4.8.

K_d values have been calculated. The most realistic model probably lies between these two limiting curves. In the calculation involving Ni and Sc K_d values, there is little difference between the results of the two models (i.e. garnet-bearing and garnet-free sources). In the case of Lu, however, as garnet accommodates the heavy REE with great facility, (K_d (Lu) ≈7), two curves are illustrated, corresponding to the two mineralogies.

These models can now be applied to the analyses by defining suitable values for C_o, the original source concentrations. From the available data, sample 2838 possesses the least fractionated REE pattern and a bulk composition closest to the pyrolite model. For the sake of these calculations it is, therefore, considered to represent pristine fertile mantle. The calculated C_s/C_o values are represented in fig. 4.7 by the small circles. Calculations based on Ni abundances constrain F, the degree of partial fusion, to values <25%, a figure comparable with previous models (Frey and Prinz 1978). Derived values from Sc concentrations, however, agree less well. Using the published K_d values (Frey et al 1978) >30% partial melting must have taken place to account for the presently observed concentrations. There is, however, some uncertainty as to the reliability of these values. The cpx/liquid and gt/liquid K_d values reported by Frey et al. suggest a gt-cpx K_d value of ~2.1. However, analyses of Sc from co-existing gt-cpx pairs in ultrabasic xenoliths (Shimizu and Allegre, 1978) give K_d values of

between 3.1 and 7.4 while mineral pairs from granulites and pyroxenites (ch5, this work) suggest K_d should be about 1.5. In view of this great discrepancy and the experimental observation that the reaction

$$Sc\ (cpx) \rightleftharpoons Sc\ (liq)$$

possesses a very high activation energy (R. Lowry, pers. comm), and therefore attains equilibrium only very slowly, the Sc data cannot be used in this semi-quantitative discussion. The model, however, still serves to illustrate that Sc does preferentially enter the melt phase during partial melting, and that its behaviour in the lherzolite xenoliths is governed by component A in qualitative agreement with the model.

The variation of Lu in these models is a little more complex and must be studied in relation to a major element, such as CaO, before it can be used as a measure of depletion. The models illustrated in fig. 4.7 reveal that Lu variation is so strongly dependent on mineralogy, particularly with respect to the presence or absence of garnet, that these distinctive behaviour patterns should be reflected on a graph of CaO vs Lu. The two models envisaged both involve eutectic melting, i.e. the removal of a liquid of constant composition. It therefore follows that CaO in the residue should be approximately inversely proportional to F, the degree of partial fusion. Experimental studies on the partial melting behaviour of fertile garnet lherzolites further suggest an eutectic-like melting process, the partial melt corresponding

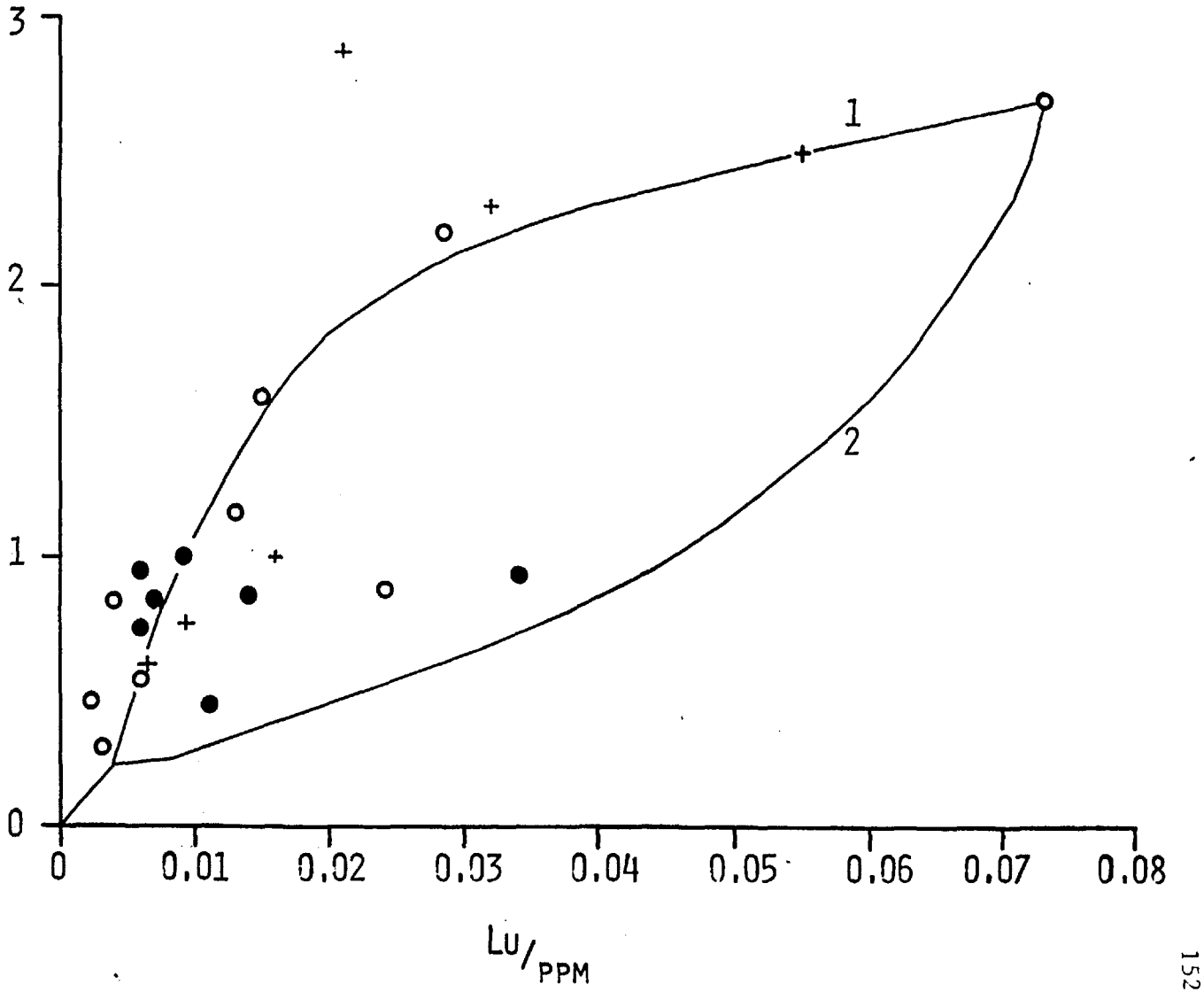

Fig. 4.8 CaO - Lu models.

1 - garnet free

2 - garnet bearing.

O - samples from Lesotho

● - " " S. Africa

+ - spinel lherzolites from S.Australia.

Note that most of the samples lie along a common trend, similar to the garnet free curve, with only a few points suggesting the presence of garnet during partial melting.

to the theoretical eutectic $gt_{47}cpx_{47}opx_{3}ol_{3}$, (Kushiro 1973, Yoder 1976 p35). As this eutectic contains ~12% CaO, it is easy to calculate the amount of CaO left in the residue after F% partial melting, assuming a source composition similar to PHN2838 (2.71% CaO). Such calculations result in two theoretical depletion trends as illustrated in fig. 4.8. The important feature to note is the curvature of the two trends, the garnet free model being convex towards CaO and the garnet bearing model towards Lu. Most of the samples plot along a trend more comparable with curve 1 (the agreement between the curve and data points is probably fortuitous). Only a few samples show any tendency to follow the garnet control curve although some samples plot in that region close to where the two models converge rendering it impossible to say which mineral assemblage controlled the depletion. The conclusion that some of the zenoliths have suffered depletion not controlled by garnet is supported by the similarity of the CaO-Lu data with that from the S. Australian lherzolites (Frey and Green, op.cit).

Returning to fig. 4.7, it is now possible, with a knowledge of the probable controlling mineralogy, to determine F values from the C_s/C_o curves. For samples that have suffered garnet controlled depletion, 17-21% partial fusion is indicated while the remainder have suffered between 13 and 30% melting. Considering the approximations made in the model, however, these figures are in good agreement with the F values from the Ni abundances of between 14 and 25%.

From the above discussion, it is clear that the initial assumption, that 2838 represents relatively 'pristine' mantle, produces a reasonable model, although comparison with pyrolite suggests that even this sample may have suffered some depletion. Using the REE abundances of PHN2838 as representative of the original mantle, it is possible to expand the previously described partial melting models to predict the REE content of liquids produced by batch partial melting. The results for 10, 20 and 30% melting are illustrated in fig. 4.9. The only significant differences between the two models (i.e. gt bearing as opposed to gt free) arise at relatively low degrees of partial melting (<10%) in the abundances of the heavy REE (Dy, Yb and Lu). At higher values of F, when all the clinopyroxene and garnet in the source have been consumed, as olivine and orthopyroxene have such low K_d values for the REE, there is little fractionation of La from Yb, the La/Yb ratio of the liquid being very similar to that of the original source. It is interesting to note that this liquid composition is unlike either the continental crust or continental tholeiitic basalts with respect to the REE, which casts some doubt on the previously accepted and somewhat simplified hypothesis that the depleted mantle is equivalent to undepleted mantle (pyrolitic) minus a partial melt that is now represented as the Karroo basalts (Nixon and Boyd, 1973). The similarity of the model predictions with the komatiite layer, may, however, be significant.

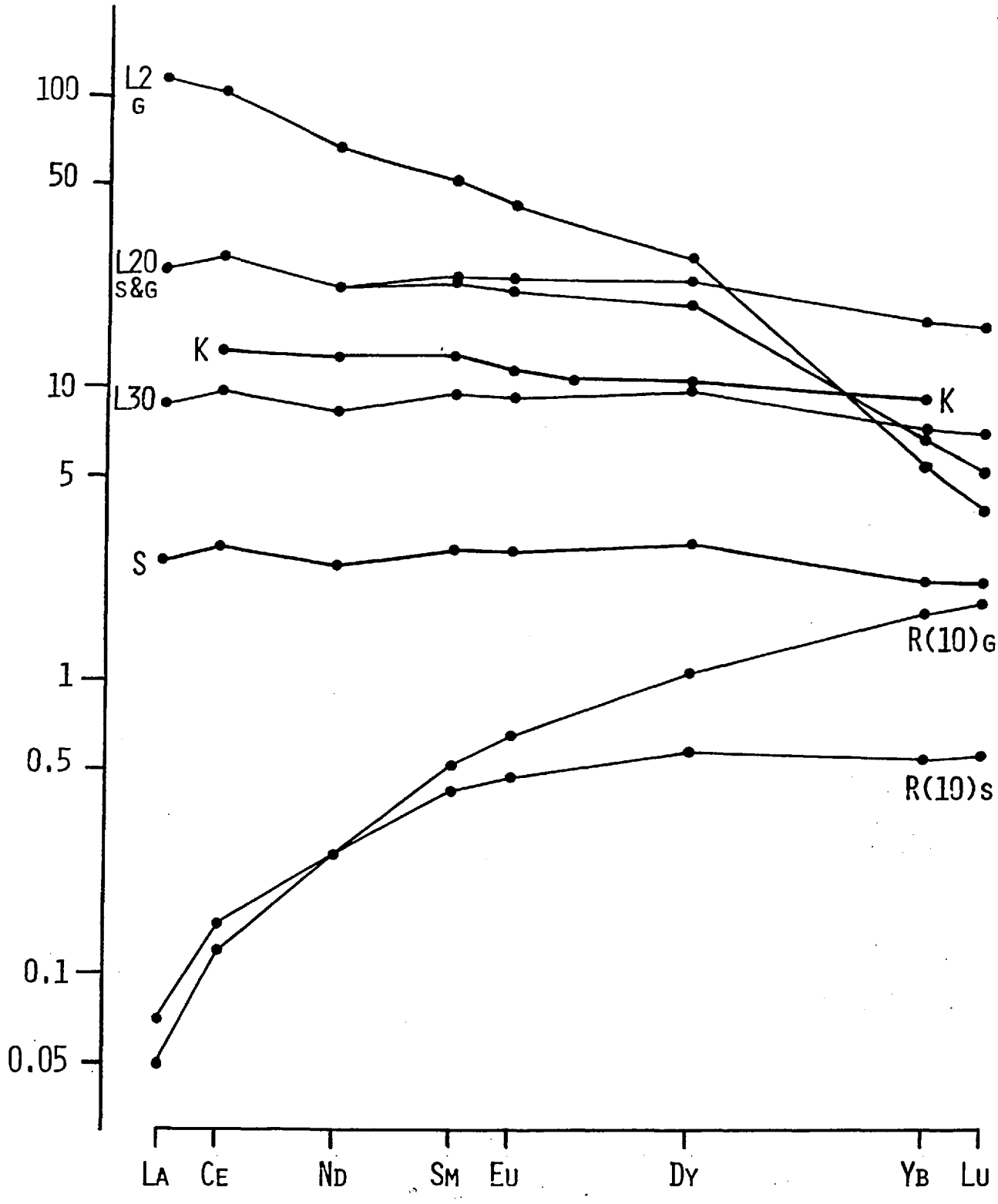

Fig. 4.9 Partial melting models based on PHN2838 - denoted S

Key - G indicates garnet lherzolite while S indicates spinel lherzolite models. Numbers indicate the degreeof partial melting (%) and L & R, liquid and residue, respectively.

Note that liquids such as L2G and L20G bear little resemblance to normal liquid REE patterns observed in basalts and L30 is superficially similar to K, a S.African basaltic komatiite.

The variation of Lu with other major elements may be used to distinguish those constituents relating to component A from those controlled by the addition of component B. Fig. 4.10 shows graphs of TiO_2 and Na_2O plotted against Lu. From a consideration of the concentrations of these elements in basalts relative to ultrabasic rocks and the difficulty with which they substitute into probable residual minerals (olivine and orthopyroxene), they should display a typical "component A' positive correlation with Lu. Examination of the TiO_2-Lu plot suggests that this is so for this element, especially considering the abundances of Ti and the probable precision of the X.R.F. analyses. The significance of the two trends, as marked, is unknown, but could be related to either initial mantle heterogeneity or subtle differences in the accessary mineral phases in the residual assemblage. In contrast Na_2O and K_2O (not illustrated) reveal a greater scatter when plotted against Lu. In mantle systems K can be regarded as an incompatible element; therefore the incoherent behaviour with Lu is considered to be associated with the effects of component B, superimposed upon the depletion effects. This may also be the cause of the scatter in the Na_2O - Lu plot and the poor correlation shown by P_2O_5 (not illustrated).

Previous investigations (Frey and Green 1974, Frey and Prinz 1978) have suggested that the second mantle component is derived from limited partial melting in the deeper mantle (asthenosphere). As this liquid will have been in equilibrium with garnet, it will possess a

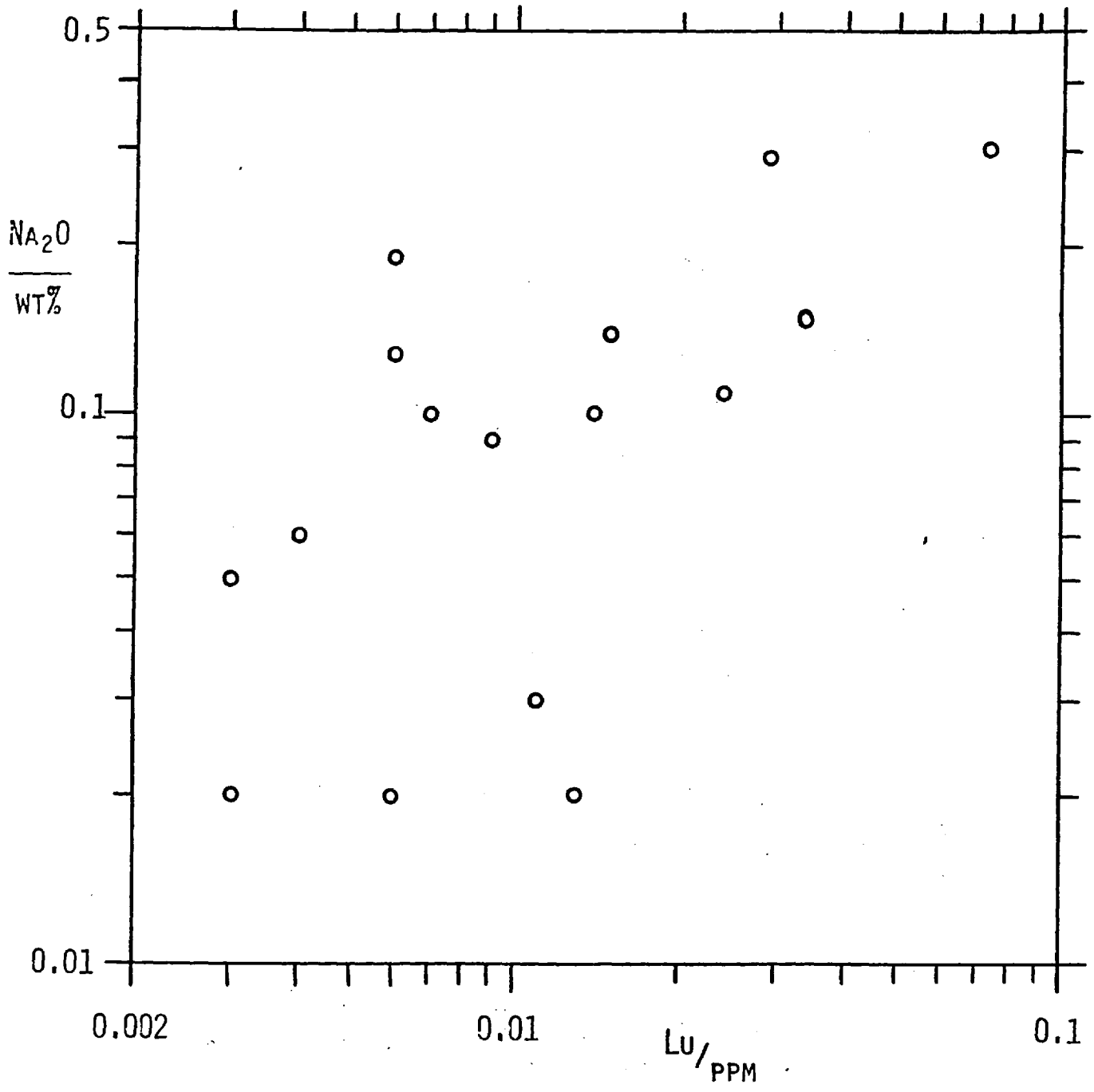

Fig. 4.10a Plot of Lu vs. Na_2O revealing the poor correlation.

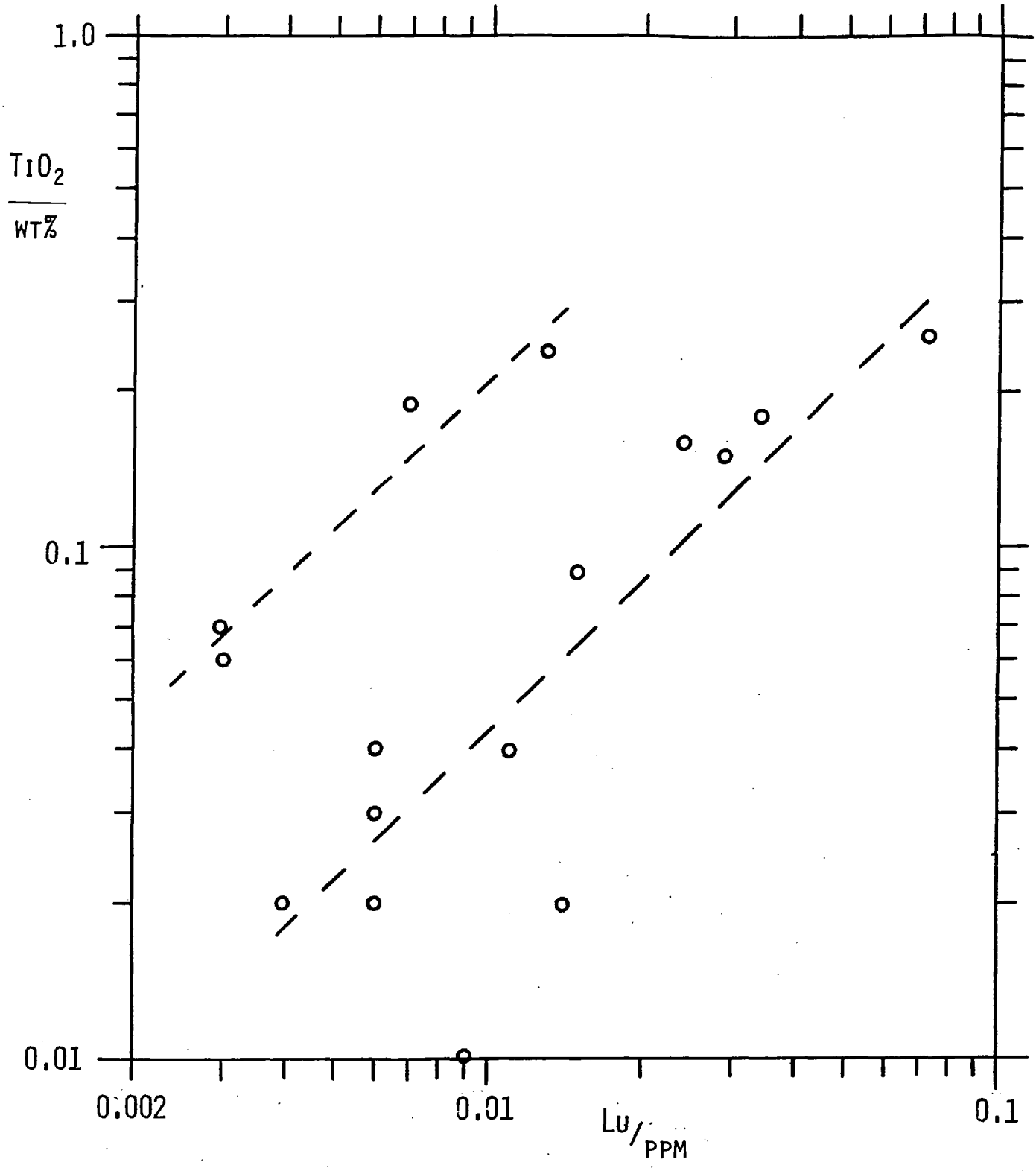

Fig. 4.10b The improved correlation between TiO_2 and Lu. Note also the tendency for the development of two trends.

strongly light REE enriched abundance pattern. According to the hypothesis, this melt then ascends through the mantle and is trapped at shallower depths. Subsequent cooling and subsolidus re-equilibration erases any mineralogical evidence of the event, the only detectable effects being geochemical. The evidence from the present work is in agreement with this general hypothesis, and it is further possible, using the incompatible trace element abundances of the xenoliths, to define more closely the composition of this, now occult, fluid.

From the partial melting models described above, it is clear that the sterile xenoliths have undergone at least 20% partial fusion. During this event, (or events) the concentrations of incompatible elements, such as the light REE, U, and Th would be reduced to negligible amounts in the residue. It therefore seems reasonable to assume that the present incompatible element ratios in the sterile xenoliths reflect those ratios in the metasomatic fluid. Of the trace elements determined only analyses of the light REE (exemplified by La), U and Th are of high enough precision to be of quantitative use. Other incompatible elements such as Rb Sr and Ba have been determined by X.R.F. analysis but as the abundances tend to be close to the lower limit of detection of this technique, the precision and accuracy are poor, and the analyses can only be used qualitatively to indicate the incompatible element enriched nature of component B. Similarly the Cs results are of poor

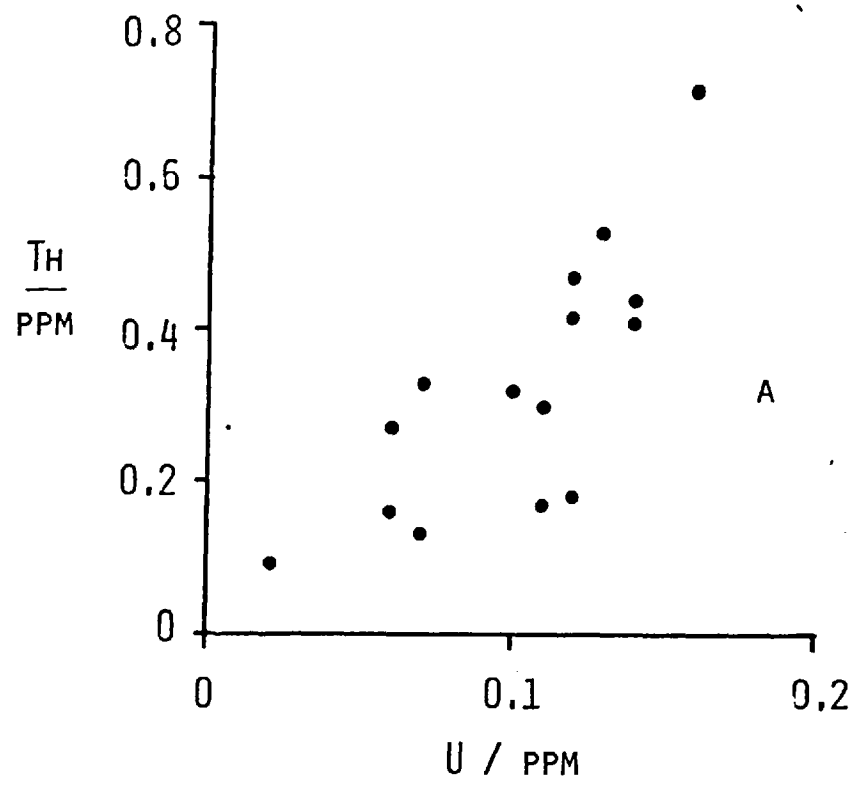

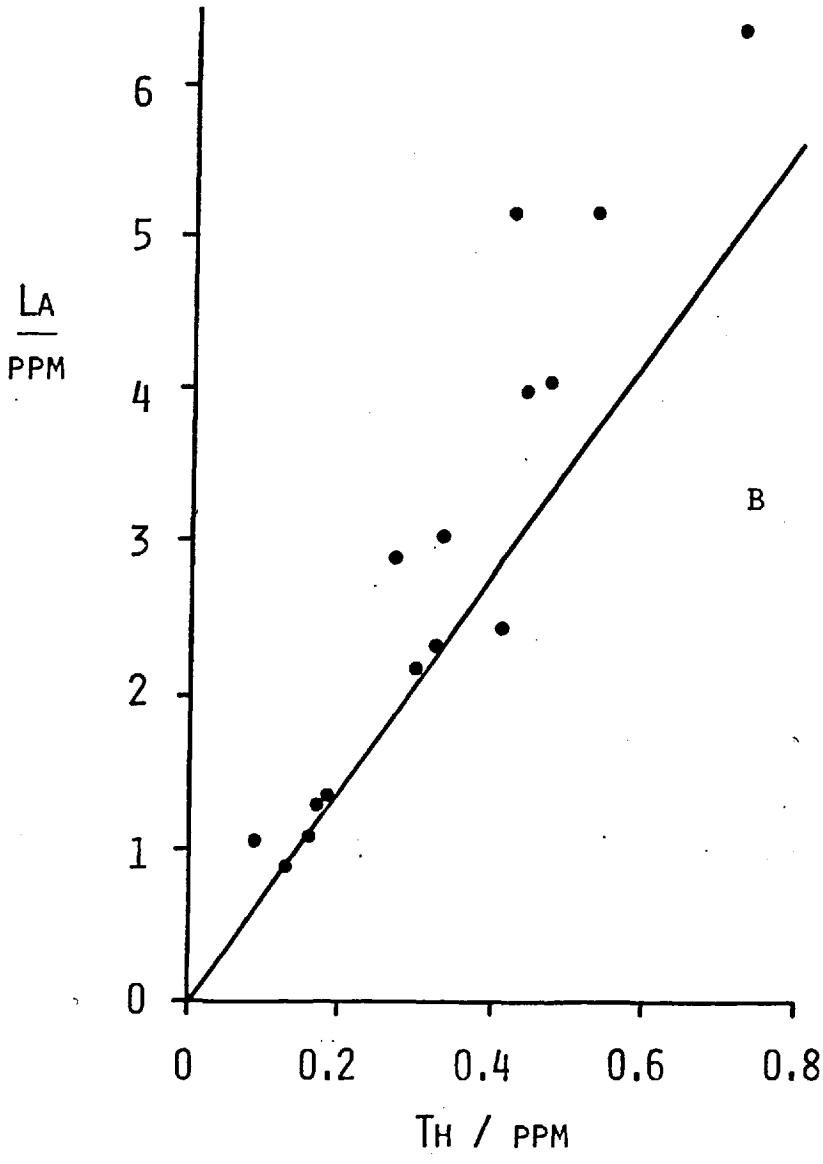

Fig. 4.11a&b. Scatter plots of La vs Th and Th vs U for the analysed ultrabasic xenoliths. Diagonal line in 4.11b represents average kimberlite La/Th ratio of 7.

quality as the analytical technique (ENAA) was being used near the lowest detection limits for this element.

In table 4.3 the correlation coefficients for the elements La, U and Th are listed. All of the values are statistically significant at the 95% confidence limit. The U-Th and La-Th variations are illustrated in fig. 4.11 (a and b) and suggest a Th/U ratio of ~3.5 and a La/Th ratio of ~7, values close to the corresponding ratios in

Table 4.3 U, Th and La correlation coefficients

	La	U
U	0.567	-
Th	0.922	0.775

kimberlites. Similarly, an estimate of the $(La/Lu)_N$ ratio of the fluid can be obtained from fig. 4.5 by taking the $(La/Lu)_N$ value of the most Lu depleted sample. It is clear from fig. 4.5 that this maximum $(La/Lu)_N$ value approaches 100 and again overlaps the range for kimberlites. The inference is, therefore, that the depleted mantle beneath S. Africa has been altered by a kimberlite-like fluid, prior to actual kimberlite eruption. (It is again necessary to emphasise the significance of the work of Shimizu (1975) in demonstrating that the REE are accommodated by garnet and clinopyroxene in these samples and that whole rock abun-

dances are unlikely to have been controlled by kimberlite contamination during eruption).

The coherence observed in the trace element abundances is not apparent when major element abundances are taken into consideration e.g. there is no strong correlation of La with P_2O_5 or K_2O. Again, however, this may be due to the lack of analytical precision, K_2O and P_2O_5 being determined by XRF. Similarly there is no correlation of LREE abundances with xenolith type (i.e. sterile and metasomatic-sterile). Shimizu and Allegre (1978) demonstrated a chemical distinction between these two classes of xenolith on the basis of Sr and Zr contents of their constituent clinopyroxenes. It is of interest to note that one of their metasomatic samples, PHN1569, has been analysed in this work. According to Shimizu and Allegre the mineral chemistry of this sample definately places it in the sterile-metasomatic group. However, its whole rock REE abundance pattern, while showing the characteristic metasomatic overprint, shows the lowest abundances of all the sterile xenoliths, whether they can be classified as metasomatic or not. This lack of coherence is interpreted as demonstrating the highly variable nature of the metasomatising fluid, and its effect on the residual mantle. Assuming the metasomatising fluid is kimberlitic, this is not a particularly surprising result considering the large variations in kimberlite composition (see Ch. 3).

In conclusion, the REE and trace element analyses of the ultrabasic xenoliths conform to the general hypothesis of a two component mantle as proposed by Frey and Green (1974). Component A comprises the greater part of the mantle and its composition, as reflected in most of the major elements, is controlled by the effects of partial fusion and the extraction of the liquid phase. Although the semi-quantitative model presented above only invokes one phase of melting, similar results would occur after more than one melting event. Subtle differences exist between the Australian and African xenoliths, in particular the observation that TiO_2 abundances appear to be controlled by Component A. Furthermore, there is evidence to suggest that garnet controlled as well as 'non-garnet controlled' partial melting has occurred during the evolution of the African samples.

The additive component B is identified as being kimberlitic with respect to U, Th and LREE abundances and must, therefore, only comprise a maximum of 1-2% of any xenolith and, consequently, the mantle. Although K_2O and P_2O_5 abundances do not, as yet, reveal any correlation with the other incompatible elements, this may be an analytical (as opposed to geological) problem. The same is true for Ba, Rb, Sr etc. The observation that there is no difference between the REE abundances of sterile and metasomatic-sterile xenoliths (as defined by Shimizu and Allegre, 1978) suggests that all the sterile

xenoliths are to some extent metasomatic and that the presence or absence of phlogopite is not a clear criterion for classifying these xenoliths. Its abundance, appears to be controlled by sub-solidus re-equilibration after partial melting and metasomatism.

It is clear that sub-solidus re-equilibration has been vitally important in the development of the presently observed mineralogy. Component A, as emphasised above, has, in many cases, been controlled during partial fusion by a garnet-free lherzolite assemblage. As all the xenoliths now contain garnet, this mineral must have appeared after the partial melting event. A potential source of garnet is in solid solution in aluminous orthopyroxene (Wood and Banno, 1973). Similarly, orthopyroxene can accommodate significant quantities of clinopyroxene (Davis and Boyd 1966). As both of these solubilities are temperature dependant (garnet in orthopyroxene is also pressure dependent) subsolidus cooling after partial melting could give rise to significant modal amounts of garnet and clinopyroxene, even though these minerals may have been previously eliminated by partial melting. It is interesting to note that there is textural petrographic evidence to support such an exsolution origin for these minerals in sterile coarse granular xenoliths (Smith, 1979).

In the above discussion, little or no emphasis has been placed on the analyses of the mica wehrlite or the ilmenite orthopyroxenite.

Clearly, these samples are not mineralogically related to the peridotites. Neither do their CaO-Lu values conform to the general pattern revealed by the majority of the peridotites. However, both show strong light REE and incompatible element enrichment, suggesting that the effects of component B are widespread. Beyond this, however, little more can be said of these two samples. Similarly, the analysis of PHN2848, petrographically a normal garnet lherzolite, is difficult to explain in the context of the two component model, with Lu as high as .12ppm and CaO below 1%. Again, without further analyses of similar samples, this result is difficult to interpret.

4.6 Conclusions.

1) Trace element abundances in lherzolite and harzburgite xenoliths are best explained using a two component mantle model, as proposed by Frey and Green (1974). Component A, defined by the abundances of most of the major elements and the compatible trace elements, has evolved through partial melting processes and represents the residue after the melt has been extracted. Component B, defined by K_2O, P_2O_5 and the incompatible trace elements was added to A possibly during partial melting,

2) The partial melting episodes were controlled predominantly by a garnet free mineral assemblage suggesting either a higher temperature or lower pressure for melting than is presently indicated by the garnet

bearing assemblage.

3) Component B is tentatively identified as being kimberlitic in its trace element abundances. Kimberlites are therefore interpreted as an infrequent surface expression of a widespread mantle phenomenon.

4) Subsolidus re-equilibration and exsolution has erased any mineralogical trace of component B, which can now only be recognised by its chemical effects. Exsolution has also given rise to the presently observed garnet and clinopyroxene, which, during partial melting, were hidden in solid solution with calcic and aluminous orthopyroxene.

CHAPTER 5

TRACE ELEMENT ABUNDANCES IN GRANULITE XENOLITHS

5.1 Introduction

Compared with the extensive studies of mantle derived ultramafic xenoliths from kimberlites, there are few published reports of the geochemistry of high grade metamorphic xenoliths, thought to have been derived from the lower continental crust. High grade gneissic nodules have been reported from various basaltic and kimberlitic localities e.g. Scotland (Upton et al.1974), Ireland (Strogen 1974), France (Leyreloup et al.1974), Uganda (von Knorring and Dubois 1961), Australia (Irving 1974), and Lesotho (Rogers 1977). In some cases, the xenoliths belong to the low pressure granulite facies and are similar to rocks found in nearby basement metamorphic complexes, e.g. in Ireland and Scotland, the clasts resemble Lewisian gneisses. In others, however, there is no direct correspondence with any local formation outcropping at the surface. This is the case in Lesotho where the granulites are mainly high pressure facies with a restricted mineralogy of garnet + plagioclase + clinopyroxene ± orthopyroxene with accessory minerals including rutile, mica, sillimanite, potash feldspar and apatite. Also associated with these xenoliths are eclogites and garnet pyroxenites, with which the granulites are in mineralogical continuity.

Preliminary studies of the Lesotho granulites (Rogers op. cit) suggested equilibration under pressures in excess of 9 kbar at temperatures of between 660 and 830°C, indicating a deep crustal origin. A more complete study of a suite of 55 samples (Griffin et al 1979) confirmed these results and allowed the definition of a geothermal gradient which, rather than conforming with a predicted shield geotherm, was more comparable with a predicted oceanic gradient (Clark & Ringwood 1964). Of the xenoliths, twenty were large enough to allow the preparation of samples for major and trace element analysis by X.R.F. All except one were shown to possess a composition similar to olivine basalt with minor ne or hy in the calculated CIPW Norm. The exception, LT-2, is a more leucocratic granulite of intermediate composition (60% SiO_2), with significant modal and normative quartz, and a much lower modal abundance of garnet and pyroxenes. In contrast to this comparatively uniform major element composition, the trace element analyses revealed variations in abundance of over an order of magnitude in the case of some incompatible elements, e.g. Zr varies from <10 ppm to >100 ppm. Similarly, the REE were shown to vary considerably between samples (Rogers 1977).

To account for these geochemical features, Griffin et al (op. cit) proposed that the lower crust had undergone a depletion event, possibly by anatexis. The REE variations were similarly interpreted (Rogers op. cit) although it was suggested that the considerable

variation of the heavy REE meant that garnet could not have been present during the depletion event. However, it was emphasised that the REE distribution patterns were not exclusive in their evidence, as they could equally be the result of fractional crystallisation processes, the positive Eu anomalies observed in some samples being the direct result of either cumulate plagioclase or residual plagioclase after removal of a partial melt phase. The presence of primary mica in the most REE enriched samples was interpreted as indicating the possibility of metasomatic processes in the development of the lower crust. Such a possibility seems more likely now, considering the strong evidence, presented in Chapter 4, for metasomatic activity in the mantle and the probable role of aqueous and CO_2 rich fluids in the development of some granulitic terrain (Janardhan et al 1979).

Despite the presence of significant amounts of sericite and natrolite in some xenoliths, trace element contamination by the host kimberlite was ruled out in most cases. In the preliminary study, the coherent behaviour of the REE with such trace elements as Zr, Nb and Y was interpreted as indicating minimal contamination. However, Ba and Sr varied independently and it was thought that contamination could have effected their abundances. This conclusion was partly borne out by the data from Griffin et al (op. cit) who demonstrated a general correlation between the abundances of these elements and the development of secondary calcite. This relationship does not

hold for all the xenoliths, however, some Ba and Sr residing in small lamellae of potash feldspar within the plagioclase, revealed only after electron microprobe analysis. Similarly K (and presumably Rb) was shown to reside in these lamellae and in mica. As both minerals are in textural equilibrium with the granulite assemblage, it seems most likely that the levels of K, Rb, Sr and Ba in the least altered samples were established before the onset of granulite metamorphism. As rutile and apatite are also in equilibrium, the same is probably true of Ti and P. Thus, it is considered that the observed trace element abundances are a reflection of the composition of the continental lower crust and that, in most cases, they are not an artefact of host rock contamination.

The purpose of the work described in this chapter has been to allow the further investigation of the origin of the granulite xenoliths and to assess the importance of the various processes that may have contributed to their petrogenesis. In order to achieve this, 17 whole rock samples have been analysed for the rare earth and other trace elements and, of these samples, garnet, clinopyroxene and plagioclase have been separated from 7 and similarly analysed. Also analysed were 5 garnet pyroxenites and 1 eclogite and mineral separates from 3 pyroxenites in an attempt to test the validity of the proposal by Griffin et al. that these rocks are co-eval with the granulites.

5.2 Whole rock analyses : Results and Discussion

The results of the analyses are listed in full in appendix 5.1 and the REE abundances illustrated by the chondrite normalised diagrams in figs. 5.1-4. Comparing fig. 5.1 and 5.2, it is clear that the basic granulite xenoliths belong to two separate groups, those showing light REE enrichment and those with either flat or light REE depleted patterns. Similarly, the garnet pyroxenites show a variety of patterns and it is interesting to note that the pyroxenite PHN2495 possesses a similar pattern to PHN1646 but at slightly higher abundances. Three of the xenoliths possess abundances intermediate between the two granulite groups while the fifth (not illustrated) has low abundances with light REE enrichment. The eclogite (PHN2532) shows a flat abundance pattern, with absolute abundances similar to the granulites with flat patterns. Again the considerable variation in absolute abundances is clear, all the REE varying by over an order of magnitude, e.g. La varies from 2.3 x chondrite (L-6) to 54 x chondrite (MAT 12) and Yb from $\sim$ 0.27 to 13 x chondrite in the same two samples. Nine of the eighteen granulites and three of the pyroxenites are from one kimberlite pipe (Matsoku) indicating considerable trace element heterogeneity within small regions of the lower crust, especially as members of both granulite groups are found at Matsoku. The apparent Ce anomalies in some samples e.g. PHN1919 and 2532, L13 and OVKF10303 are thought to be due to hydrothermal effects during the later stages of kimberlite intrusion and related to the production of zeolites and secondary calcite.

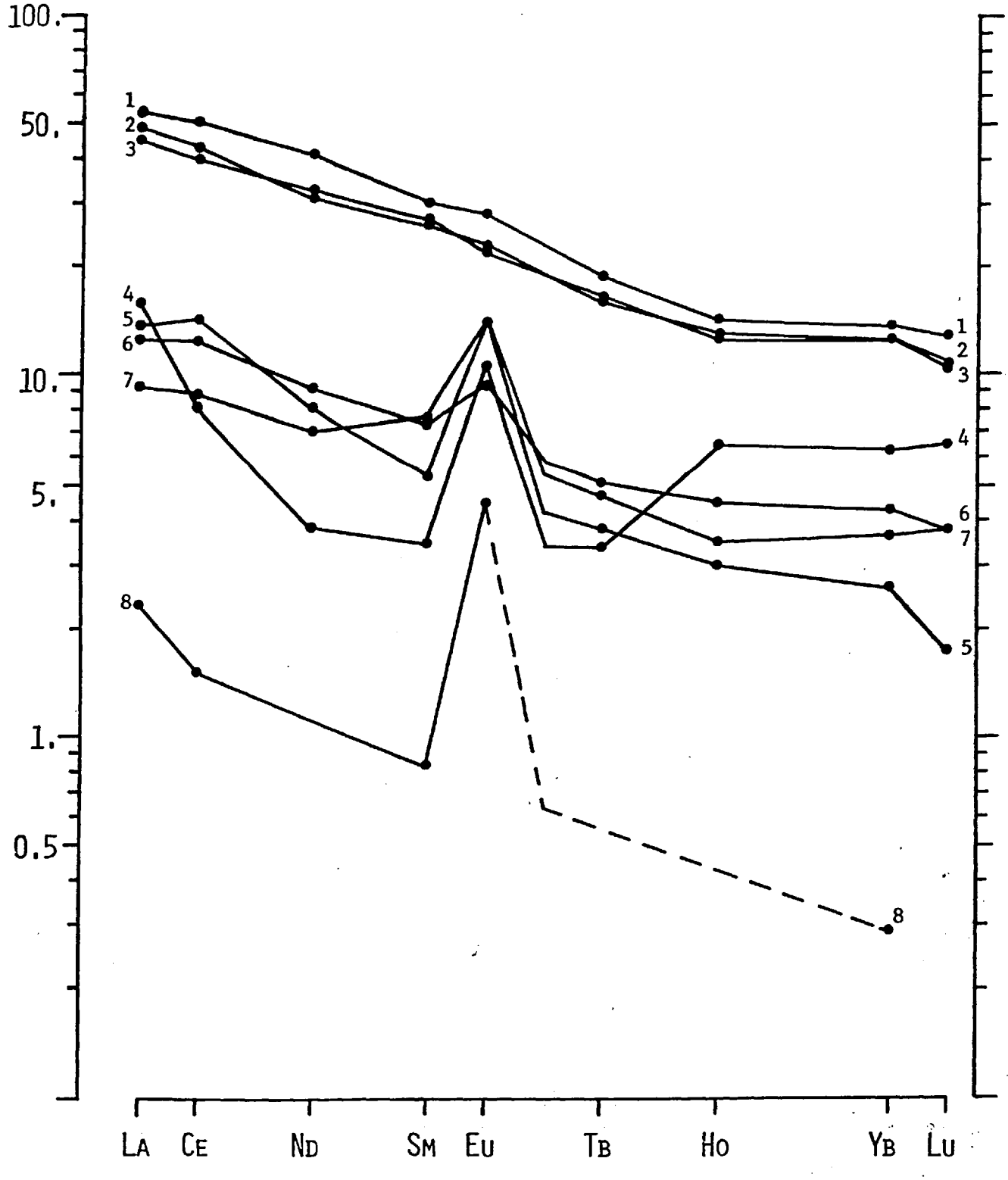

Fig. 5.1 REE abundances in group 1 garnet granulite xenoliths. Key:- 1 - MAT12 (Matsoku), 2 - L20 (Matsoku), 3 - PHN1646 (Matsoku), 4 - PHN2533 (Pipe 200), 5 - PHN1670 (Matsoku), 6 - M1 (Matsoku), 7 - PHN2852 (Matsoku), 8 - L6 (Lipelenang).

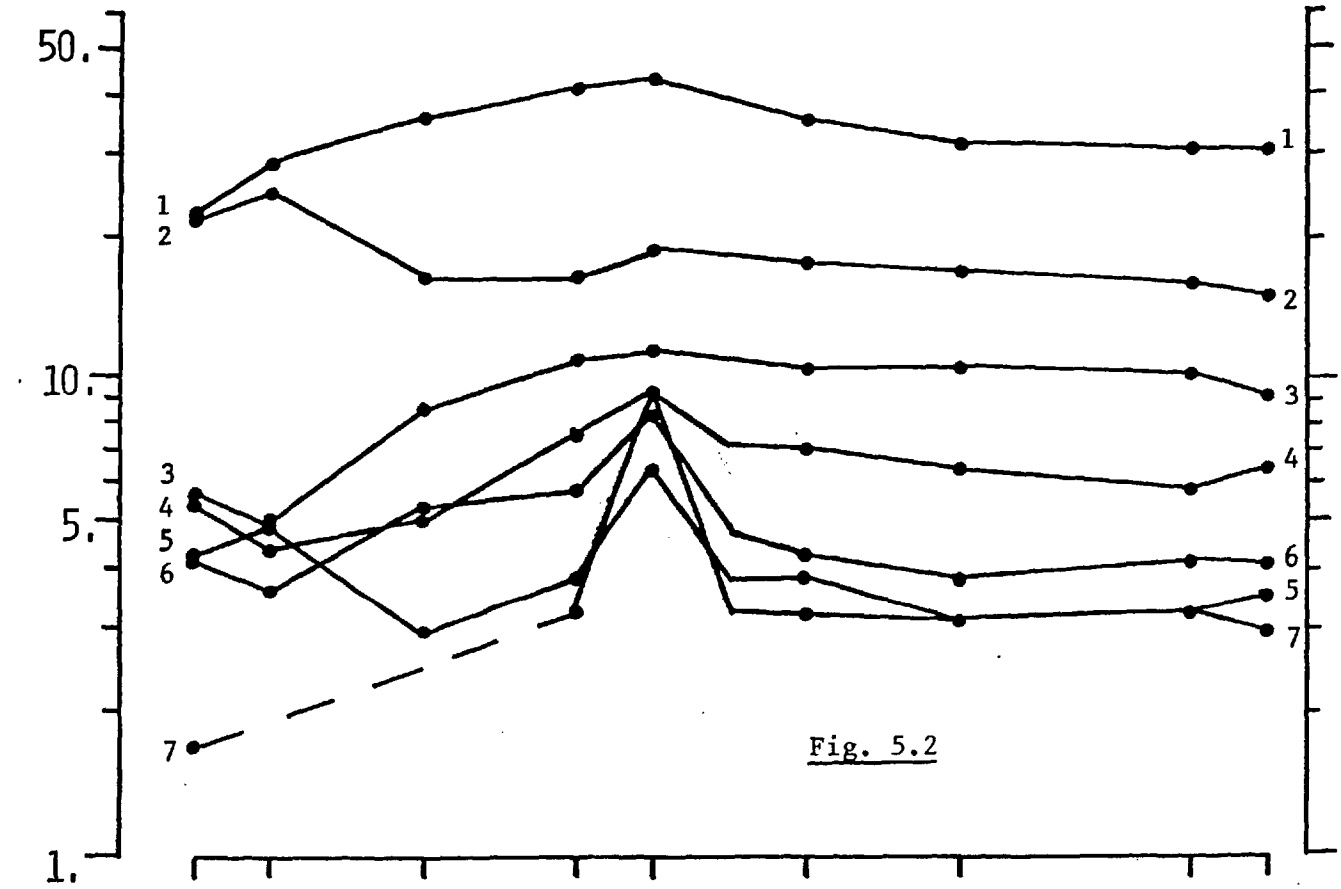

Fig. 5.2

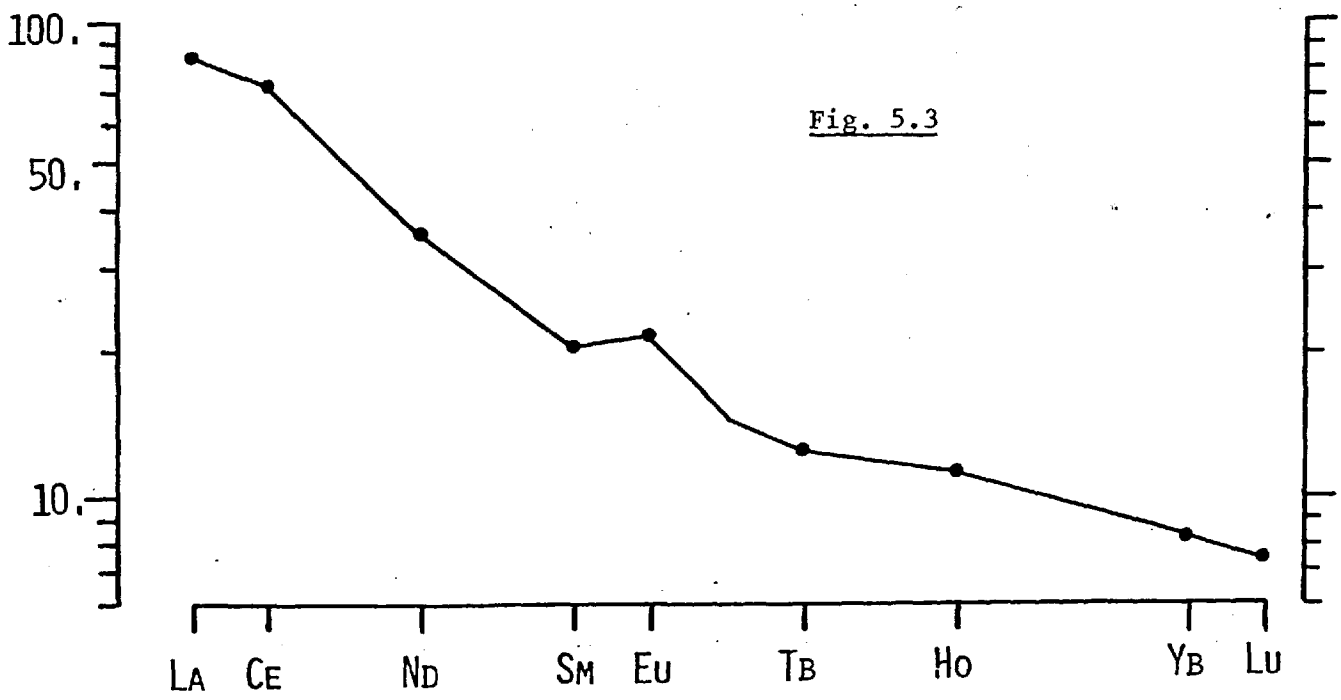

Fig. 5.3

Fig 5.2 Group 2 garnet granulite xenoliths.
Key:- 1 - LQ4 (liqhobong), 2 - PHN2532 eclogite (Pipe 200), 3&4 - L12a & b (Matsoku), 5 - L13 (Matsoku), 6 - OVKF10303 (Matsoku), 7 - PHN2588 (Liqhobong).

Fig 5.3 Felsic garnet granulite LT2 (Letseng-la-Terrae).

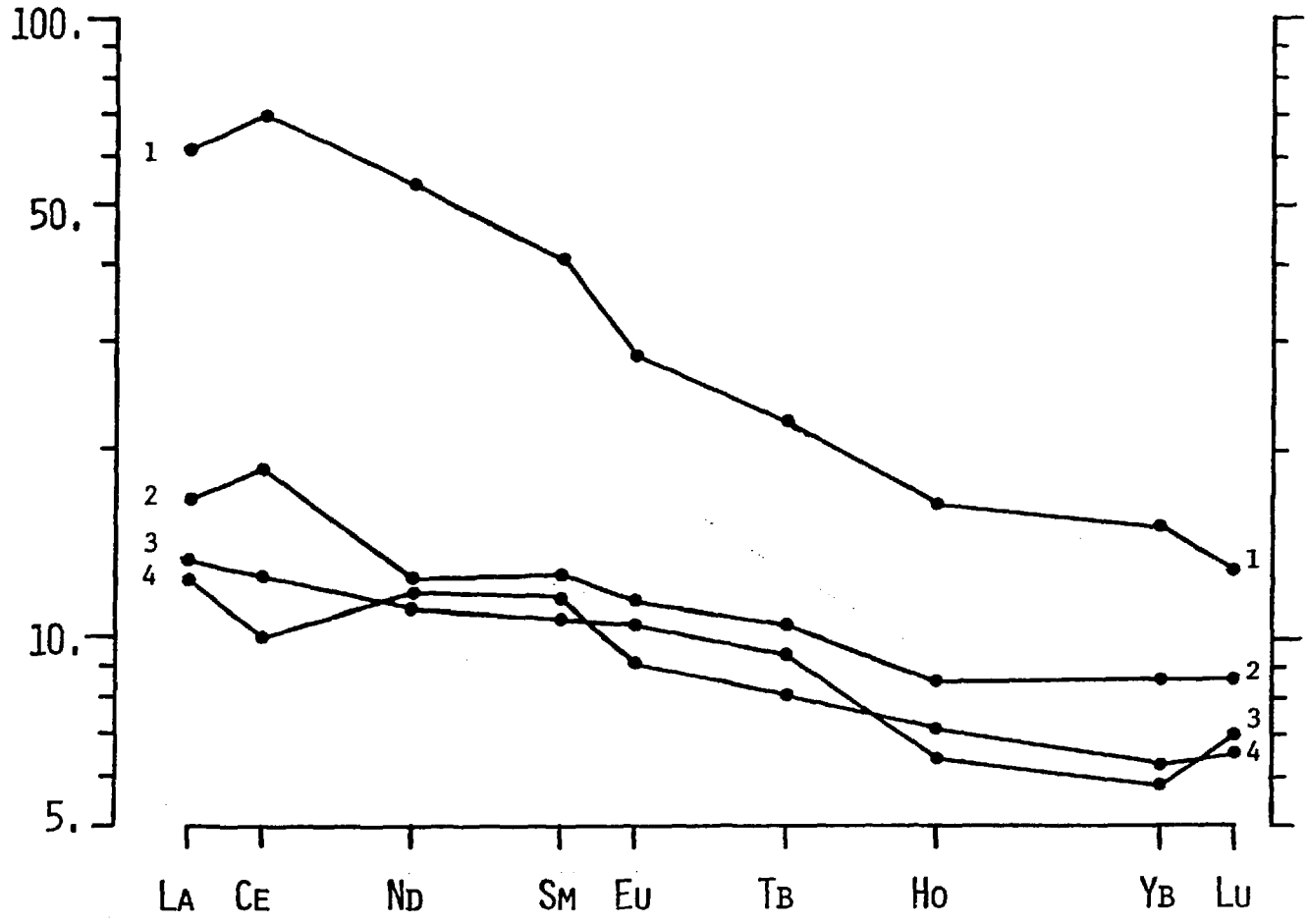

Fig 5.4 REE abundances of 4 garnet pyroxenite xenoliths.
Key:- 1 PHN2495 (Liqhobong), 2 - L9, 3 - L17, 4 - L16, all from Matsoku

From the limited data of the preliminary study (Rogers 1977) it was suggested that those samples with the highest total REE abundances are light REE enriched and the tendency towards lower ΣREE levels is accompanied by a flattening of the pattern. Clearly, from the evidence presented here, this no longer holds, although ΣREE depletion within each group results in the development of more pronounced positive Eu anomalies. This latter feature indicates the importance of residual plagioclase in the depletion process. The large variation shown by the heavy REE, elements easily accommodated by garnet, is sympathetic with that shown by the more incompatible light REE, demonstrating the negligible role played by garnet during depletion. Thus, it appears likely that the whole rock REE patterns have been inherited from a pre-granulite event, in agreement with the hypothesis most favoured by Griffin et al. Their alternative, that the depletion occurred syn- or immediately post- granulite metamorphism, appears unlikely. Such an event would require anatexis and subsequent removal of the partial melt from the garnet containing restite with which, presumably, it had equilibrated. According to this theory the granulite restite (now represented by the granulite xenoliths) would not show the observed heavy REE depletion, due to the high K_d values for the heavy REE between garnet and liquid.

Fig. 5.5 Plot of Sm vs. Zr for granulite (●) and pyroxenite (O) Xenoliths, showing the good positive correlation. (R = 0.968 for the granulites only). Points for L12a & b are joined by a solid line.

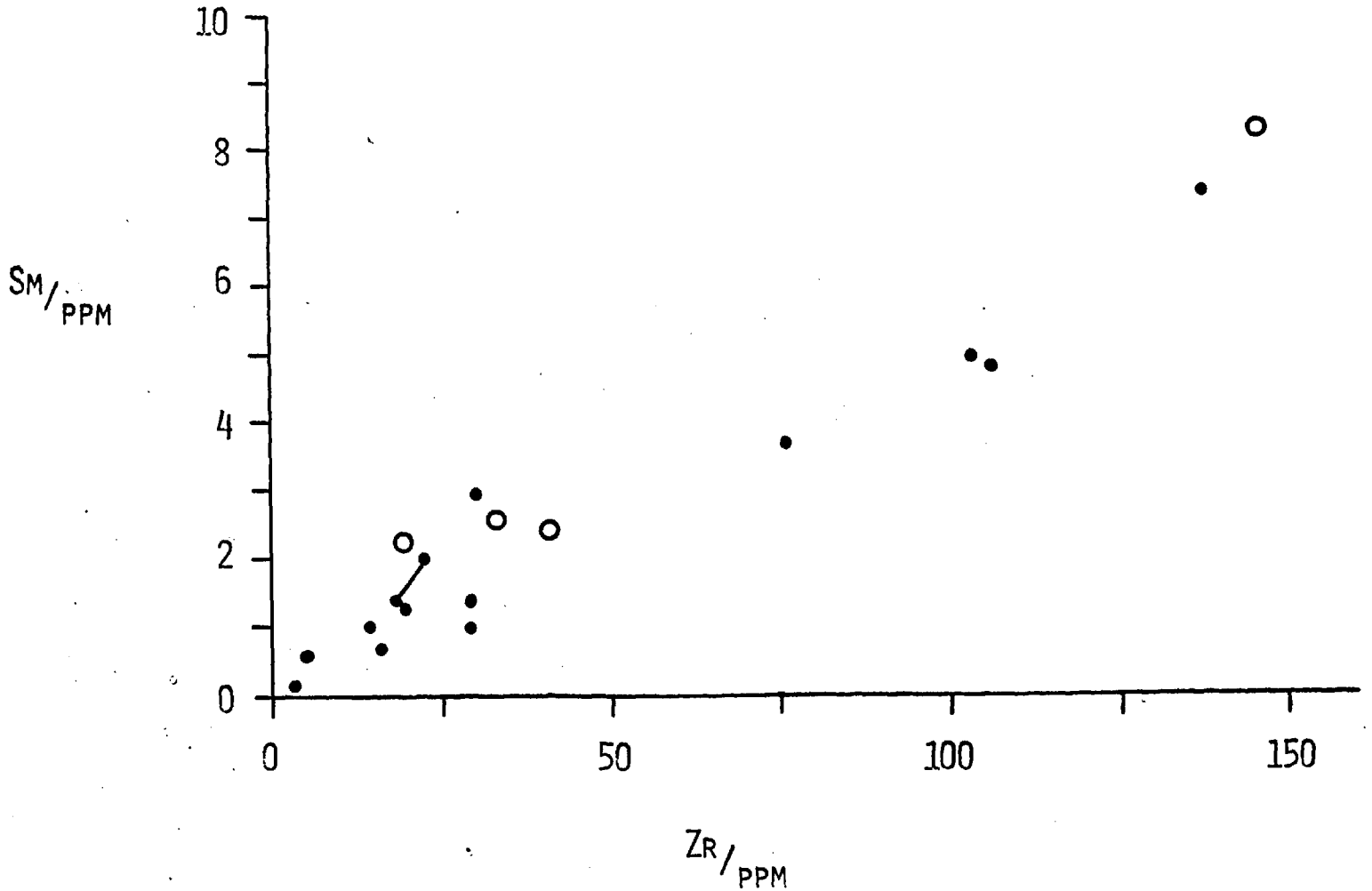

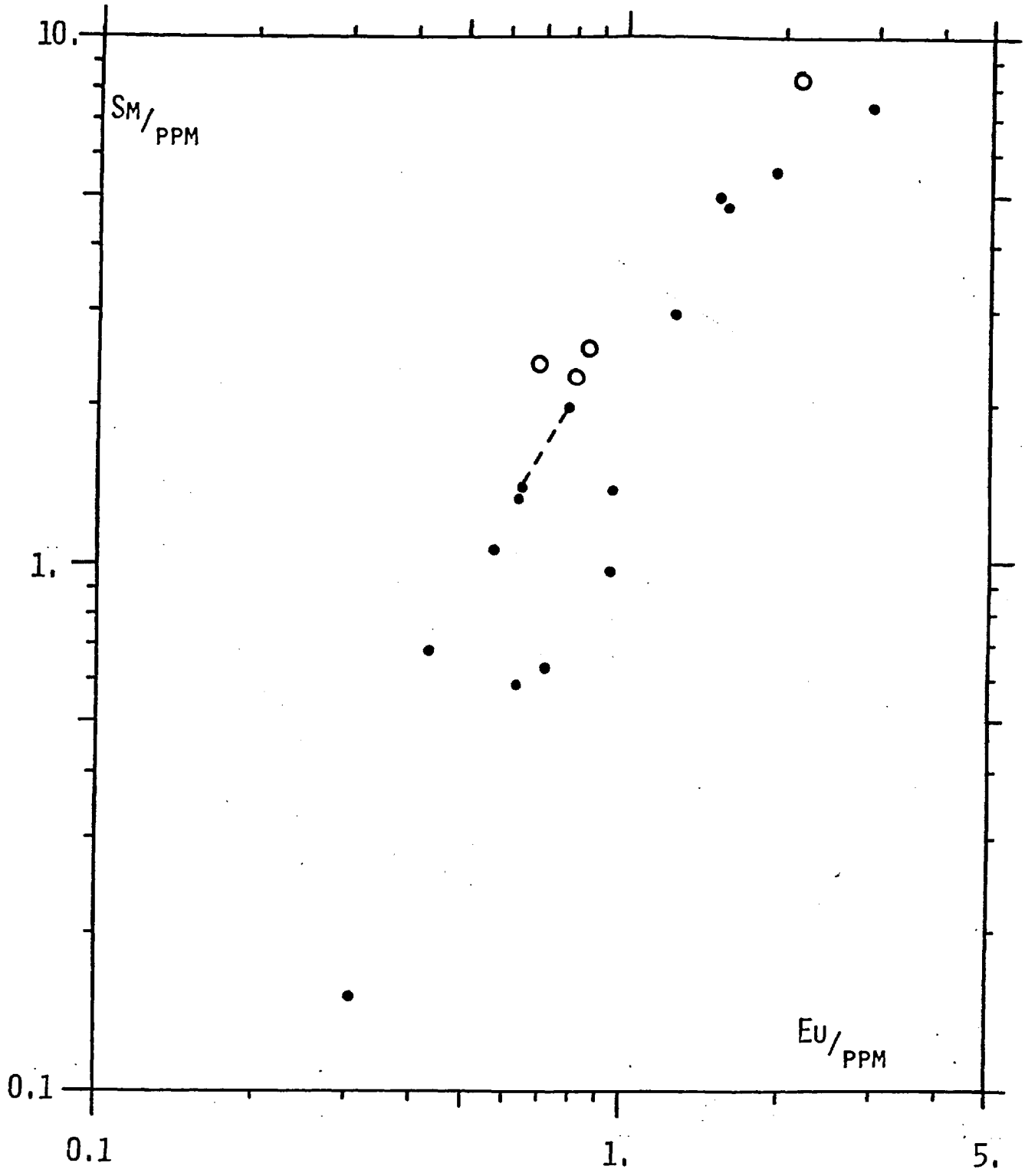

Fig. 5.6 Plot of Sm vs Eu for the granulites and pyroxenites. (Key as for fig. 5.5).

Evidence for the magmatic nature of the depletion process is provided by the very strong positive correlation shown by Sm with Zr (fig. 5.5) Zr being used as a good indicator of variations caused by magmatic processes (see e.g. Pearce and Cann 1973). An interesting feature of fig. 5.5 concerns the relative positions of the two portions of the layered xenoliths L12A and B. The fractionation caused by this layering is in the same general direction as that shown by the whole suite. The same is also true for a graph of Sm vs. Eu (fig. 5.6). As the essential difference between L12A and B is in their modal mineralogy. L12B being an eclogite with no plagioclase and 11% less normative plagioclase than L12A, this difference is probably best attributed to a primary igneous layering. However, before discussing further the ultimate origin of the granulite protoliths and the relative importance of igneous, metamorphic and metasomatic processes, it is important to consider the results of the analyses of the separate minerals.

5.3 Separate mineral analyses : Results and Discussion

The major mineral phases of 7 granulites and 3 garnet pyroxenites have been separated and analysed for the REE, Sc, Co and Cr. Although Cs, U and Th analyses were also attempted, no significant γ-ray peaks corresponding to these elements were found in the spectra from any of the mineral samples. The minerals were separated from the -80 to -120 mesh fraction of the crushed rock, first with heavy liquids (Bromoform and Di-iodomethane) and then by hand. Between 20 and 80 mg of each mineral were separated. As the sample weights were low and the expected

abundances of some of the elements also low, each sample was irradiated for 2 weeks (a total of 60-65 hrs) instead of the normal 1 week, in an attempt to improve the detection limits of some of the elements with long half lives. The results are listed in appendix 5.2 and illustrated in figs. 5.7, 8 and 9.

An idea of the precision of the analyses can be gained by reconstructing the whole rock abundances from the separate mineral analyses and a knowledge of the modal mineralogy. The results of these calculations compared with the actual analyses are listed in table 5.1. As can be seen, most of the calculations agree well, to within ±25%. However, two samples show large residuals viz, the light REE in L20 and the heavy REE in PHN2533. It should be noted, in connection with this, that L20 contains .25% P_2O_5 and could, therefore, possess accessory apatite. As this mineral accommodates the REE, particularly the lighter elements, with great facility, it could easily act as a host for these elements, thereby making up the deficit in the calculated whole rock abundances. Similarly, PHN2533 shows an anomalously high concentration of the heavy REE as evidenced by its 'U-shaped' pattern. The cause of this strange REE pattern is problematic but may be due to a post-metamorphic accummulation of garnet. Indeed, in the hand specimen bands of garnet are visible. Thus, the disagreement between the calculated and actual composition is attributed to mineralogical heterogeneity. Of the other three elements analysed, Sc produces results comparable

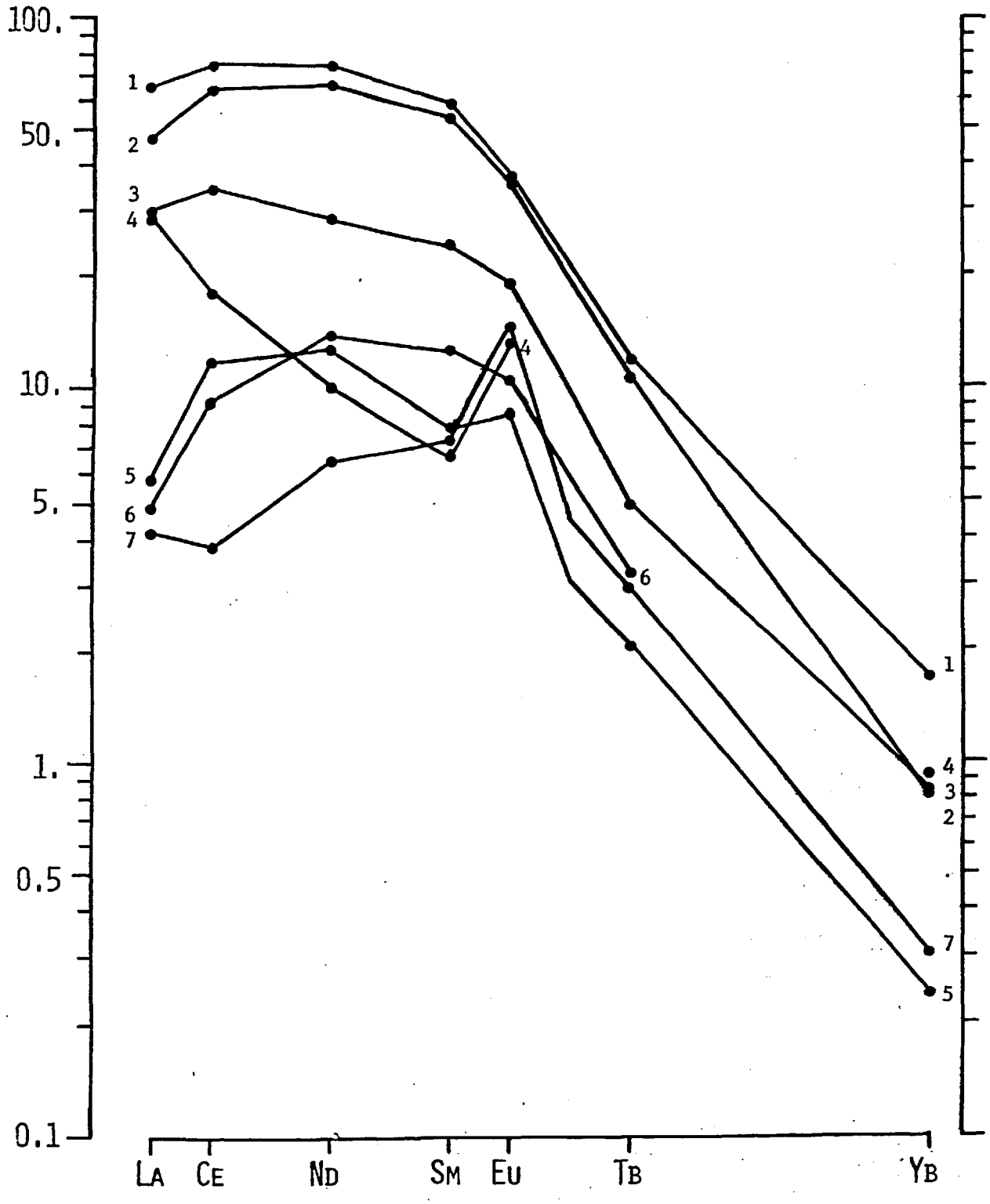

Fig. 5.7 REE abundances of clinopyroxenes from the granulite xenoliths.
1 - PHN1646, 2 - L20, 3 - PHN1919, 4 - PHN2533,
5 - OVKF10303, 6 - L13, 7 - PHN2588.

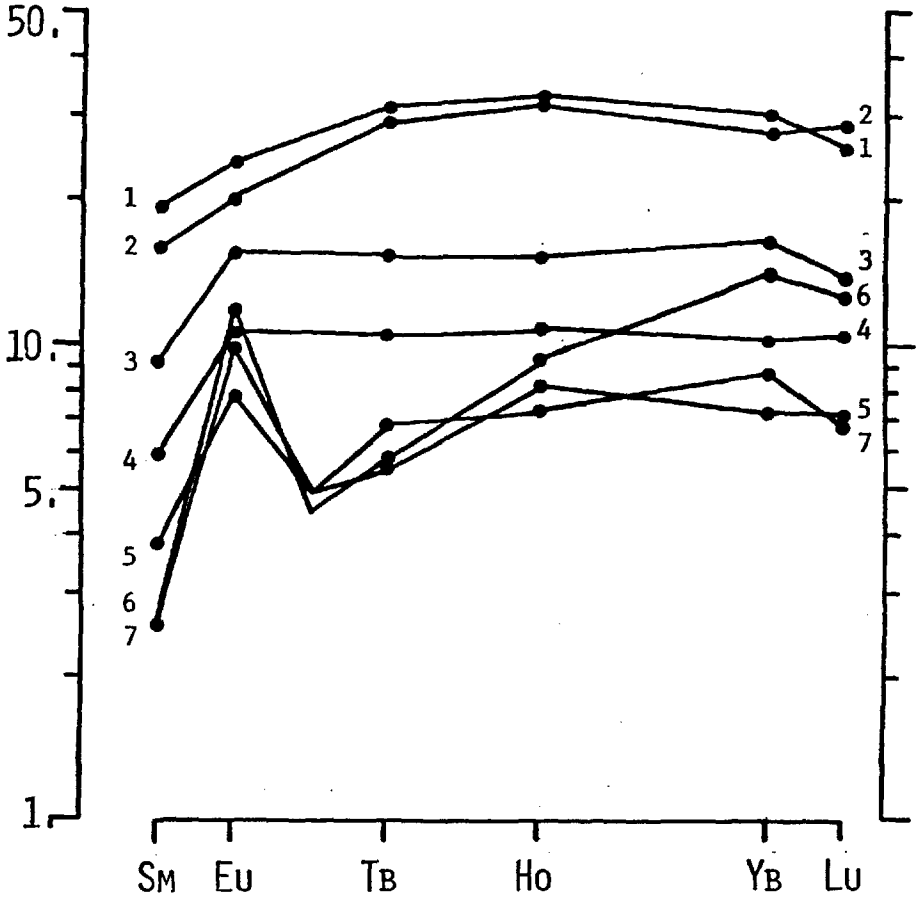

Fig. 5.8 REE abundances of garnets from granulite xenoliths.
1 - PHN1646, 2 - L20, 3 - PHN1919, 4 - L13,
5 - OVKF10303, 6 - PHN2533, 7 - PHN2588.

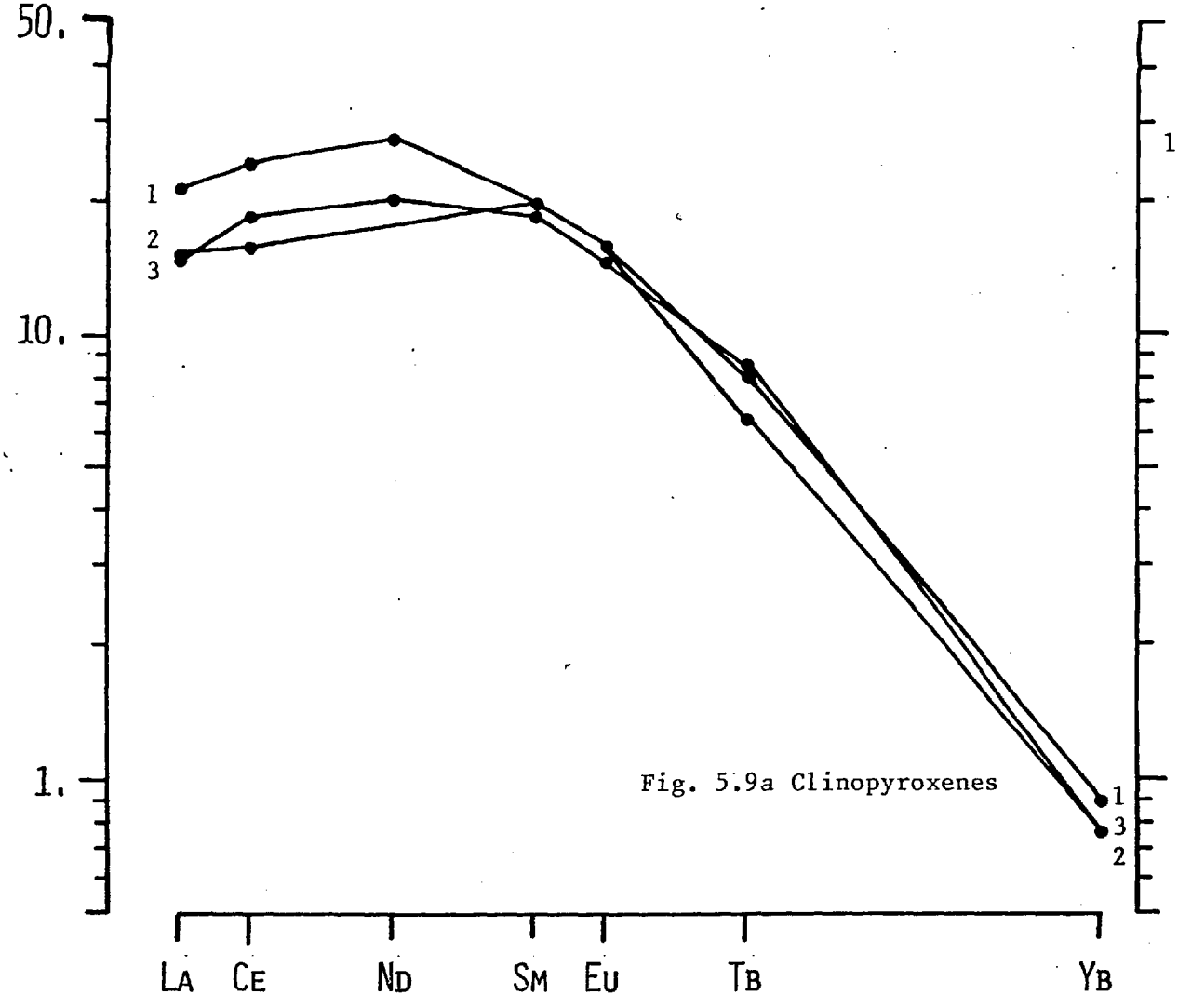

Fig. 5.9a Clinopyroxenes

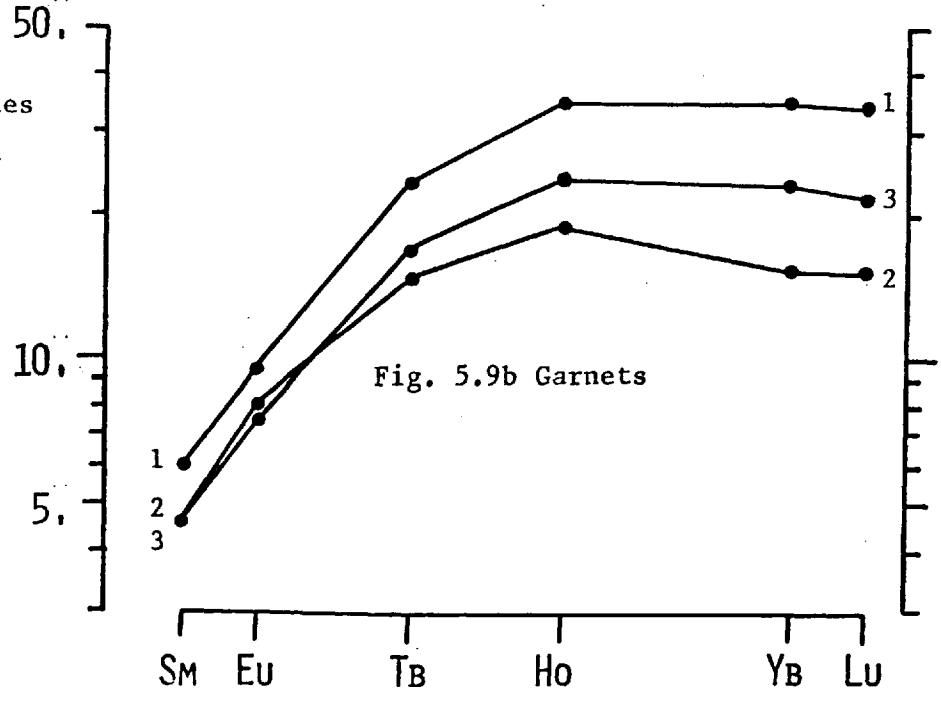

Fig. 5.9b Garnets

Fig. 5.9. REE abundances in minerals from garnet pyroxenites.

1 - L9

2 - L17

3 - L16

with the REE whereas Co and Cr always give low whole rock estimates. This is considered to be due to the incorporation of these transition elements in rutile and other accessory minerals, however, and not due to significant analytical discrepancies. In general, the REE and Sc can be accounted for by the three major mineral phases in any sample and only in the cases of Co, Cr and the light REE in sample L20 are accessory minerals with high concentrations of these elements required to explain the observed discrepancies.

The REE patterns of the minerals are as might be expected from published partition co-efficient data. The garnets show a preferential enrichment of the heavy REE, plagioclase (REE diagrams not illustrated) is enriched in Eu and shows a tendency to light REE enrichment while clinopyroxene accommodates the remainder and is, therefore, similarly light REE enriched. The clinopyroxene patterns show a maximum chondrite normalised abundance at Ce or Nd. This may be due to the ability of plagioclase to accommodate La, producing a lower abundance in the clinopyroxene. However, as a similar feature is displayed by the clinopyroxenes from the plagioclase-free garnet pyroxenites, this is thought to be primarily the result of the crystal chemistry of clinopyroxene, La being slightly too large for the usual REE site in the clinopyroxene structure. Such an explanation has been successfully employed for similar patterns observed in clinopyroxenes from ultra-basic rocks. (Ottonello et al 1978).

Table 5.1 Reconstruction of whole rock trace element abundances from separate mineral analyses and modal mineral proportions

Rock	PHN1646		PHN1919		OVKF10303		PHN2533	
	Calc	Actual	Calc	Actual	Calc	Actual	Calc	Actual
La	14.2	14.9			1.83	1.39	5.51	5.25
Ce	35.4	35.2	12.9	13.8	3.17	4.29	7.71	7.19
Nd	21.9	20.0	6.3	8.1	1.44	1.74	2.73	2.33
Sm	6.34	4.95	2.25	2.3	0.56	0.68	0.67	0.63
Eu	1.89	1.52	0.98	1.2	0.39	0.44	0.70	0.72
Tb	0.70	0.77	0.72	0.4	0.12	0.18	0.07	0.16
Ho	0.67	0.88	0.35	-	0.22	0.22	0.18	0.46
Yb	2.04	2.32	1.21	1.3	0.58	0.75	0.88	1.30
Lu	0.25	0.37	0.15	0.2	0.09	0.14	0.12	0.22
Sc	35.0	31.3	-	-	18.8	22.9	34.6	41.3
Co	44.	60.	-	-	25.0	51.3	29.5	37.6
Cr	135.	189.	-	-	154.	310.	74.	125.
Mode								
Gt	29%		33%		37%		27%	
Cpx	50%		37%		19%		46%	
Plag	21%		30%		44%		27%	

	L20		L13		L17		L16		L9	
	Calc	Actual	Calc	Actual	Calc	Actual	Calc	Actual	Calc	Actual
La	6.07	16.1	1.58	1.33	3.01	4.33	3.11	4.07	5.43	5.73
Ce	17.1	38.3	4.15	3.13	8.0	10.9	9.96	8.62	16.1	15.9
Nd	10.1	18.9	3.10	3.15	-	7.0	7.26	7.49	12.5	7.7
Sm	4.51	4.78	1.22	1.04	2.37	2.22	2.19	2.38	2. 0	2.56
Eu	1.36	1.57	0.47	0.58	0.84	0.82	0.71	0.70	0.96	0.87
Tb	0.75	0.75	0.20	0.20	0.43	0.49	0.41	0.42	0.49	0.54
Ho	1.1	0.90	0.23	0.27	0.50	0.50	0.36	0.55	0.47	0.67
Yb	2.68	2.62	0.61	0.87	1.29	1.30	1.13	1.34	1.52	1.81
Lu	0.45	0.36	0.10	0.08	0.20	0.24	0.20	0.22	0.22	0.29
Sc	33.2	31.0	21.1	22.5	43.3	43.2	46.4	49.3	66.0	61.3
Co	40.	74.	30.	57.	47.	72.	53.	64.	45.	82.
Cr	140.	186.	197.	250.	496.	452.	2263.	3220.	539.	707.
Mode										
Gt	46%		31%		58%		21%		19%	
Cpx	26%		44%		37%		60%		75%	
Plag	28%		25%	Opx	5%		19%		6%	

Mineral modes from Griffin et al. (1979)

Both garnets and clinopyroxenes from samples with whole rock positive Eu anomalies also show +ve Eu anomalies in their individual analyses. As the K_d values for Eu (see below) between these minerals are not anomalous, it can only be inferred that the present mineralogy has had little effect on defining the present whole rock pattern. Therefore, this must have been established before the granulite metamorphic event and consequently requires that the REE have re-equilibrated with the new mineralogy isochemically. This confirms the previously suggested hypothesis that the trace element abundances were acquired before the high pressure granulite mineralogy was established.

Itwas suggested above that there might be some anomalous behaviour of the light REE. This is further indicated by the La abundances in the garnets and is best illustrated by the analysis of garnet from PHN1646. In this sample, La is at $\sim$ 8 x chondrite and Sm at $\sim$ 12 x. However, Ce and Nd were not detected and so can only be present at levels below their lower detection limit (i.e. below $\sim$ 2.5 x chondrite). It therefore appears that La has been enriched in the garnet by some selective process as it is not enriched in other minerals. Contamination by the host kimberlite seems unlikely as this would be expected to effect all the minerals and would also be reflected in the analyses of Ce and Nd which is clearly not the case. The only process known to effect only garnet

is the development of kelyphitic rims and it is therefore suggested that the La enrichment is in some way related to kelyphitisation. The significance of this is, however, problematic as it is still not known whether kelyphitisation pre-dates or is synchronous with inclusion in the host kimberlite.

Of the REE, K_d values between garnet and clinopyroxene can be calculated for five, namely La, Sm, Eu, Tb and Yb. The probable disequilibrium behaviour of La is reflected in the particularly large spread of K_d values, ranging from 2.65 up to 34 ($K_d = X^{La}_{cpx}/X^{La}_{gt}$). However, considering that the mineral pairs are from a suite of very similar rocks derived from a similar P-T-X environment, the K_d values of the other elements also show a considerable spread e.g. K_d^{Sm} varies from 2.07 to 4.28, K_d^{Eu} 0.99 - 1.99, K_d^{Tb} 0.300 - 0.500 and K_d^{Yb} 0.0224-0.0669. In the case of Yb, the large spread may be the result of uncertainty in the analysis of the clinopyroxene, however, for the other elements, analytical errors were no greater than usual (i.e. $2\sigma < 10\%$). Similar studies of garnet-clinopyroxene pairs from lherzolites and eclogites (Philpotts et al 1972, Shimizu 1975) also revealed some variability in K_d values. Using the data presented here and data from the above references, five groups of garnet-clinopyroxene bearing rocks can be discerned - granulite, (7 samples), garnet pyroxenite (3) eclogites (2), granular garnet lherzolite (4) and sheared garnet lherzolites (3). As the data from the literature were obtained by isotope

Table 5.2 Analysis of variance results for Sm, Eu and Yb K_d values.

Element:- Sm

Rock Type		No. of Results	Mean K_d value	Standard Deviation
Granulites	(GR)	7	2.69	0.49
Garnet Pyroxenites	(GP)	3	3.88	0.52
Eclogites	(EC)	2	1.41	0.18
Sheared Garnet Lherzolites	(SGL)	3	1.13	0.47
Granular " "	(GGL)	4	2.21	0.84

ANOVA Results:-

Source of Variation	Degrees of Freedom	Sums of Squares	Mean Squares	F-Ratio	Theoretical F-Ratio
Among Samples	4	14.09	3.522	10.85	2.93
Within Replicates	14	4.55	0.325		
Total Variation	18	18.64			

Element:- Eu

Rock Type	No. of Results	Mean K_d value	Standard Deviation
GR	7	1.33	0.29
GP	3	1.87	0.15
EC	2	0.87	0.15
SGL	3	0.80	0.27
GGL	4	1.25	0.38

ANOVA Results:-

Source of Variation	Degrees of Freedom	Sums of Squares	Mean Squares	F-Ratio	Theoretical F-Ratio
Among Samples	4	2.119	0.530	6.50	2.93
Within Replicates	14	1.140	0.081		
Total Variation	18	3.259			

Table 5.2 Contd.

Element:- Yb

Rock Type	No. of Results	Mean K_d value	Standard Deviation
GR	6	0.0456	0.0147
GP	3	0.0348	0.0136
EC	2	0.0407	0.0087
SGL	3	0.0494	0.0162

ANOVA Results:-

Source of Variation	Degrees of Freedom	Sums of Squares	Mean Squares	F-Ratio	Theoretical F-Ratio
Among Samples	4	0.00303	0.00076	3.88	3.26
Within Replicates	12	0.00234	0.00020		
Total Variation	16	0.00537			

dilution mass spectrometry, only three elements, Sm, Eu and Yb, can be compared. The results of a simple one way analysis of variance test on these five groups are summarised in table 5.2. As is clear from the ANOVA tables, all three elements give calculated F ratios in excess of the theoretical values for the given degrees of freedom, thus indicating statistically significant variation of K_d values between the 5 groups of rocks, i.e. the observed variation between groups is greater than that expected from the variation observed within each group. Comparison of means and standard deviations of K_d values for Sm and Eu suggests that they increase in the following order: Sheared garnet lherzolites ≈ eclogites < granular garnet lherzolite < granulites < pyroxenites. K_d(Yb), on the other hand, does not show so much variation except that it is slightly greater for the sheared garnet lherzolites than the other groups. However, there is no obvious correlation between K_d with either P or T of equilibration. The small number of samples available for each group does not allow the definition of more subtle trends which will only be revealed after further analyses have been presented.

The K_d values for Sc, Co and Cr can be similarly treated, comparing the granulite results with those reported by Shimizu and Allegre (1978) for a suite of 14 garnet lherzolite xenoliths which are divided into three groups: (1) sheared (2) granular and (3) granular-metasomatic. A one way ANOVA test was again applied

Table 5.3 Analysis of variance results for Sc, Cr and Co K_d values

Element:- Sc

Rock Type		No. of Results	Mean K_d value	Standard Deviation
Granulites	(GR)	7	0.676	0.192
Garnet Pyroxenites	(GP)	3	0.810	0.126
Sheared Lherzolites	(SGL)	4	0.201	0.037
Granular "	(GGL)	5	0.162	0.025
Metasomatic "	(MGL)	3	0.211	0.096

ANOVA Results:-

Source of Variation	Degrees of Freedom	Sums of Squares	Mean Squares	F-Ratio	Theoretical F-Ratio
Among Samples	4	1.57	0.393	24.00	3.66
Within Replicates	17	0.278	0.0164		
Total Variation	21	1.85			

Element:- Cr

Rock Type	No. of Results	Mean K_d value	Standard Deviation
GR	7	1.287	0.297
GP	3	0.906	0.076
SGL	4	0.253	0.081
GGL	5	0.290	0.130
MGL	3	0.347	0.084

ANOVA Results:-

Source of Variation	Degrees of Freedom	Sums of Squares	Mean Squares	F-Ratio	Theoretical F-Ratio
Among Samples	4	4.55	1.137	30.1	3.66
Within Replicates	17	0.642	0.038		
Total Variation	21	5.19			

Table 5.3 Contd.

Element:- Co

Rock Type	No. of Results	Mean K_d value	Standard Deviation
GR	7	0.574	0.139
GP	3	0.517	0.051
SGL	4	0.941	0.266
GGL	5	0.639	0.223
MGL	3	0.494	0.070

ANOVA Results:-

Source of Variation	Degrees of Freedom	Sums of Squares	Mean Squares	F-Ratio	Theoretical F-Ratio
Among Samples	4	2.501	0.125	3.93	3.66
Within Replicates	17	0.542	0.032		
Total Variation	21	1.044			

to these five groups, the results of which are summarised in table 5.3. Although Co does not give a very significant F factor, the K_d values from the sheared xenoliths are slightly higher than the rest. Sc and Cr, however, show quite interesting variations. K_d(Cr) varies systematically, decreasing in the order granulites > pyroxenites > garnet lherzolites. This order may be interpreted as being the result of the increased stability of knorringite garnet in solid solution with pyrope-almandine as pressure and temperature increase. The intermediate K_d(Cr) values of the pyroxenites therefore suggest a higher pressure of equilibration than that for the granulutes, in agreement with the P-T estimates obtained from standard mineral thermometers and barometers (Griffin et al (op.cit)). As these derived P-T estimates were indicative of upper mantle conditions, it appears even less likely that the pyroxenites are necessarily consanguinous with the granulites.

The K_d(Sc) values fall into two groups corresponding to ultrabasic xenoliths and the granulite-pyroxenite suite. This also corresponds to an analytical division, the ultrabasic samples being analysed by ion-probe techniques (Shimizu and Allegre 1978). In interpreting their results, these authors defined the Sc distribution coefficient relative to Al:-

$$K_d^{Sc,Al} = (Sc/Al)_{cpx}/Sc/Al)_{gt}$$

and found that its value was constant for all the samples analysed, being $\sim$ 2. The same cannot be said for the granulite pyroxenite nodules, calculated $K_d^{Sc,Al}$ values ranging from a lower limit of 2 up to 10. The significance of this variation is, as yet, unknown and further analyses will be required before any more definite conclusion can be made.

In conclusion, the evidence from the separate mineral analyses clearly demonstrates the pre-granulite character of the whole rock REE patterns and supports the previous suggestions that trace element abundances were established before the development of the garnet bearing assemblage. Furthermore, the reasonable agreement in the mass balance calculations show that the REE and Sc are accounted for by the three major mineral phases and that contamination by the host kimberlite has been minimal. The calculated K_d values for the five REE (La, Sm, Eu, Tb and Yb) are in general agreement with published values, although statistically significant variations are revealed by one way analysis of variance tests when different groups of rocks are compared. Sc also behaves in a more variable way than has been previously observed in ultrabasic xenoliths. The partitioning of Cr between clinopyroxene and garnet appears to be governed by the stability of the knorringite garnet end member, the value of K_d^{Cr} decreasing as pressure and temperature increase. The inference from this is that the pyroxenite protoliths are not associated in depth with the lower crustal granulites but are probably situated within the upper mantle, as indicated by the P-T figures derived from standard pyroxene-garnet thermo-barometers (Griffin et al (op.cit)).

5.4 The origin of the Granulite Xenoliths and their Protolith

Various features of the REE abundances give indications as to the mineralogy controlling the depletion process that has affected these rocks. The large positive Eu anomalies in the more depleted samples show the importance of residual plagioclase while the variation of the heavy REE suggests that garnet was not present in the original residue. From this it is concluded that the present mineralogy has developed since the depletion event and that any models used to explain the present REE and trace element abundances cannot be based on this mineralogy. The strong positive correlation shown by Sm with Zr is interpreted as being indicative of a magmatic solid-liquid depletion event as opposed to the effects of metasomatism. The correlation between Zr and La, while still significant shows more scatter, suggesting that the abundances of the lightest REE may have been adjusted by subsequent events. This is also inferred from the apparently disequilibrium behaviour of La distribution between clinopyroxene and garnet.

Two types of model are, therefore, considered in trying to explain the origin of the granulite protoliths. The first of these involves partial fusion of a more silicic composition to leave a restite comparable with the basic granulites after extraction of a granitic partial melt. The second involves fractional crystallisation, the granulites being metamorphosed cumulates.

The lower crust has often been considered a probable source of granitic and similar melts and many hypotheses have been proposed to explain the development of a chemically zoned continental crust by partial fusion in the lower layers and upward migration of the melt (e.g. Fyfe 1970, Jakes & Taylor 1974). Jakes and Taylor's model further proposed that the lower crust should possess a positive Eu anomaly to complement the negative anomaly observed in silicic calc-alkaline plutonic rocks, typical of the upper crust. Initially the xenoliths might be thought to fit this model, samples PHN1646, L20 etc., representing undepleted lower crust and the residual xenoliths the restite after partial fusion. Such a model is precluded by the major element composition of the xenoliths*, however, samples 1646 and L20 being very similar in composition to the other types, suggesting that any partial melting would be of limited extent and insufficient to give rise to the observed REE depletion. The presence of a partial melt around mica in PHN1646 (Rogers 1977) is attributed to a disequilibrium effect caused by a sudden release of pressure during kimberlite eruption. Similar effects have been observed around hydrous phases in ultrabasic xenoliths (Frey & Green 1974).

A suitable composition for melting is represented in the xenolith suite by LT.2, a silicic granulite with a silica content of $\sim$ 60%, this sample could give rise to $\sim$ 20% of a melt containing 70% SiO_2 leaving a residue with a silica content comparable with

* For major element analyses see Griffin et al (1979).

Table 5.4 Granulite partial melting models

	Source Mineralogy	Melt
Model 1 (Low pressure granulite)	10% Qtz, 10% K-feld, 25% Cpx, 50% Plag, 5% Oxides (K_d=1)	Ab 50%, Or 22% Qtz 28%.
Model 2 (High pressure granulite)	18% Qtz, 23% Gt, 27% Cpx, 28% Plag, 4% Opx.	45% Qtz, 45% Plag, 5% Gt, 5% Cpx.
Model 3 (Amphibolite)	40% Plag, 40% Amph. 20% Qtz.	15% Amph. 25% Plag, 60% Qtz.

K_d data are taken from the compilation of Arth and Hanson (1975)

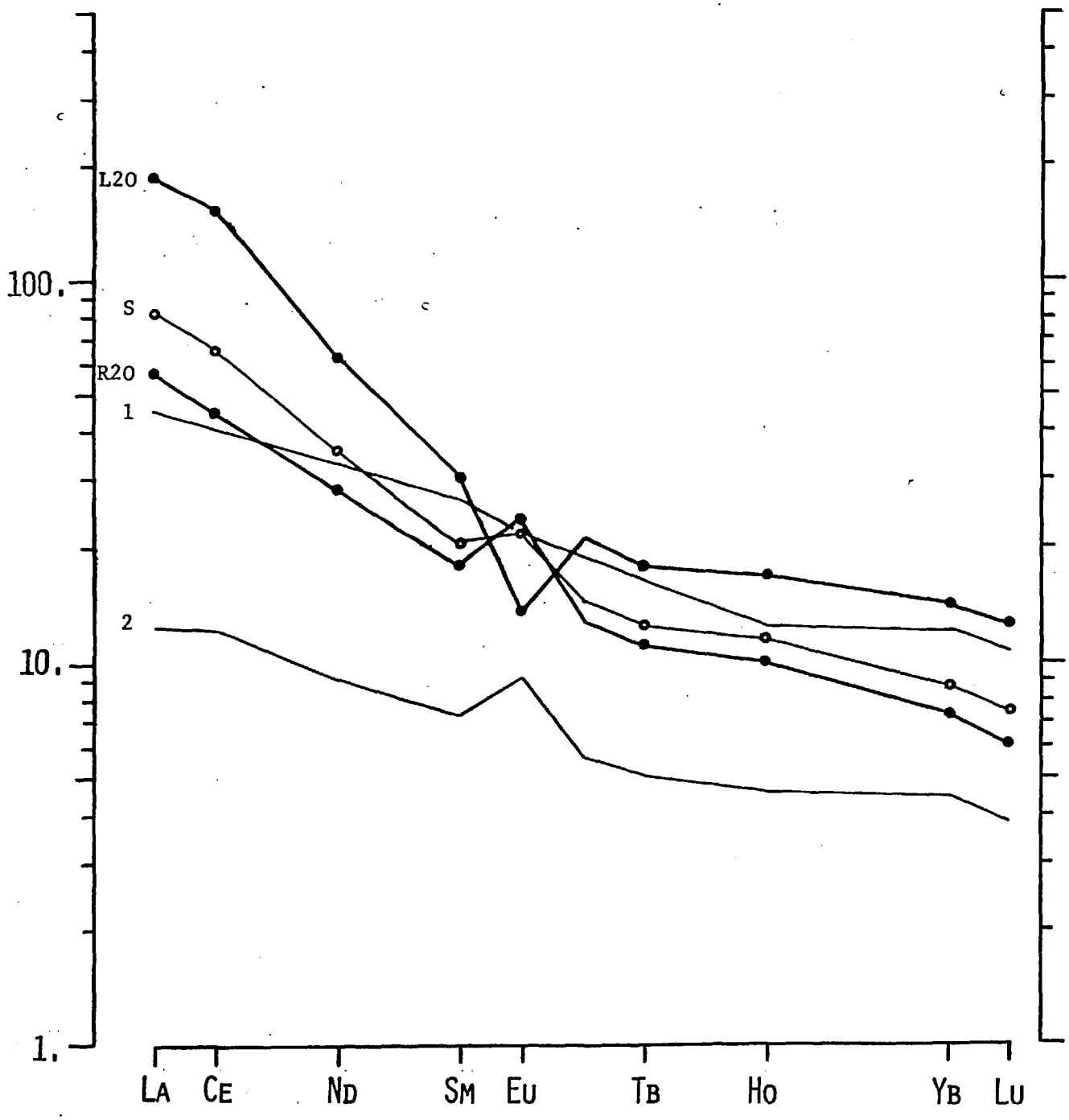

Fig. 5.10a Partial melting model based on pyroxene granulite mineralogy.

Key:- L20 - Liquid from 20% partial melting.

R20 - Residue after 20% partial melting.

S - Source composition (LT-2).

1 & 2 - Examples of basic garnet granulites, (PHN1646 & M1).

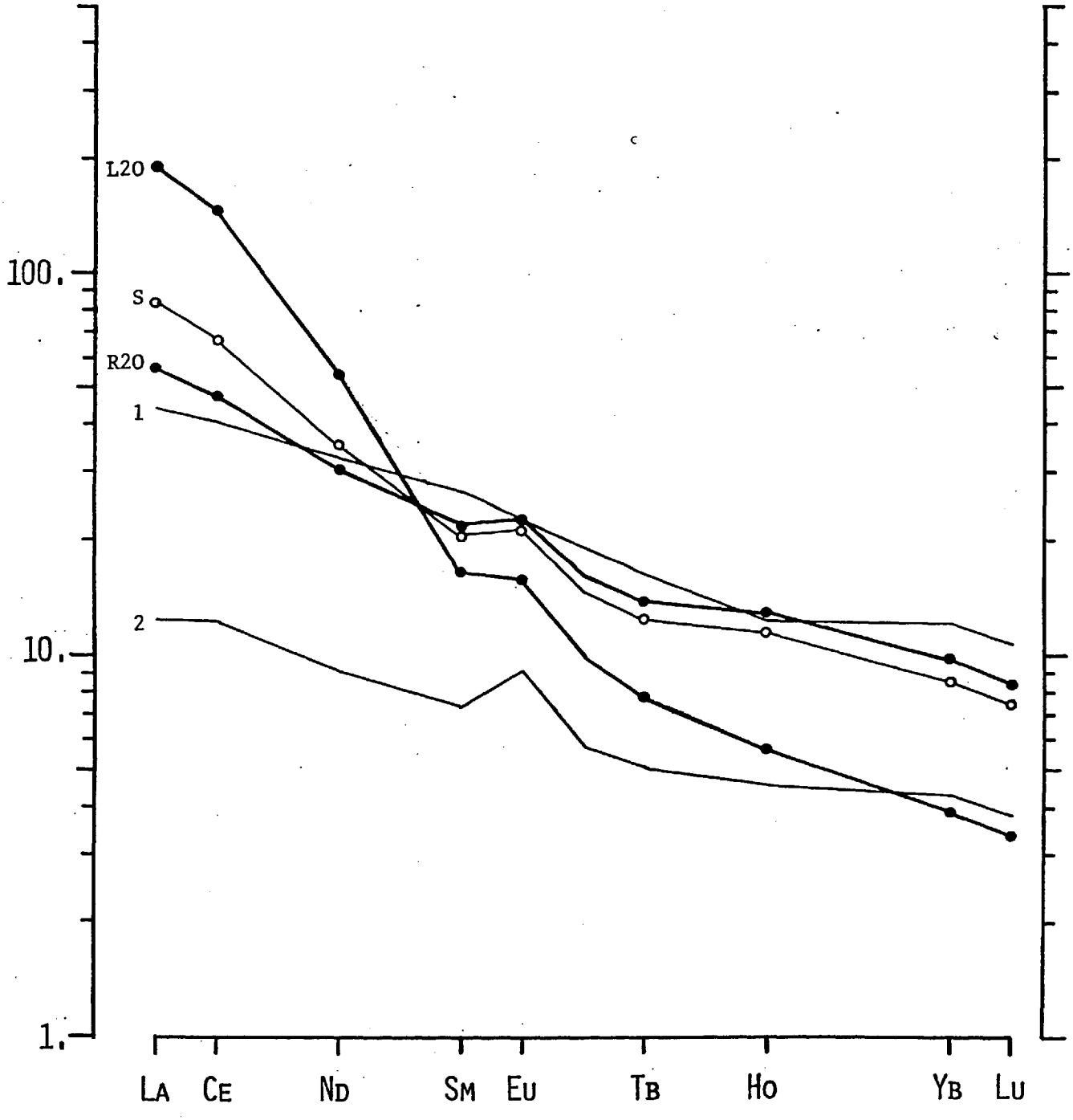

Fig. 5.10b Partial melting model based on garnet granulite mineralogy. Key as in fig. 5.10a.

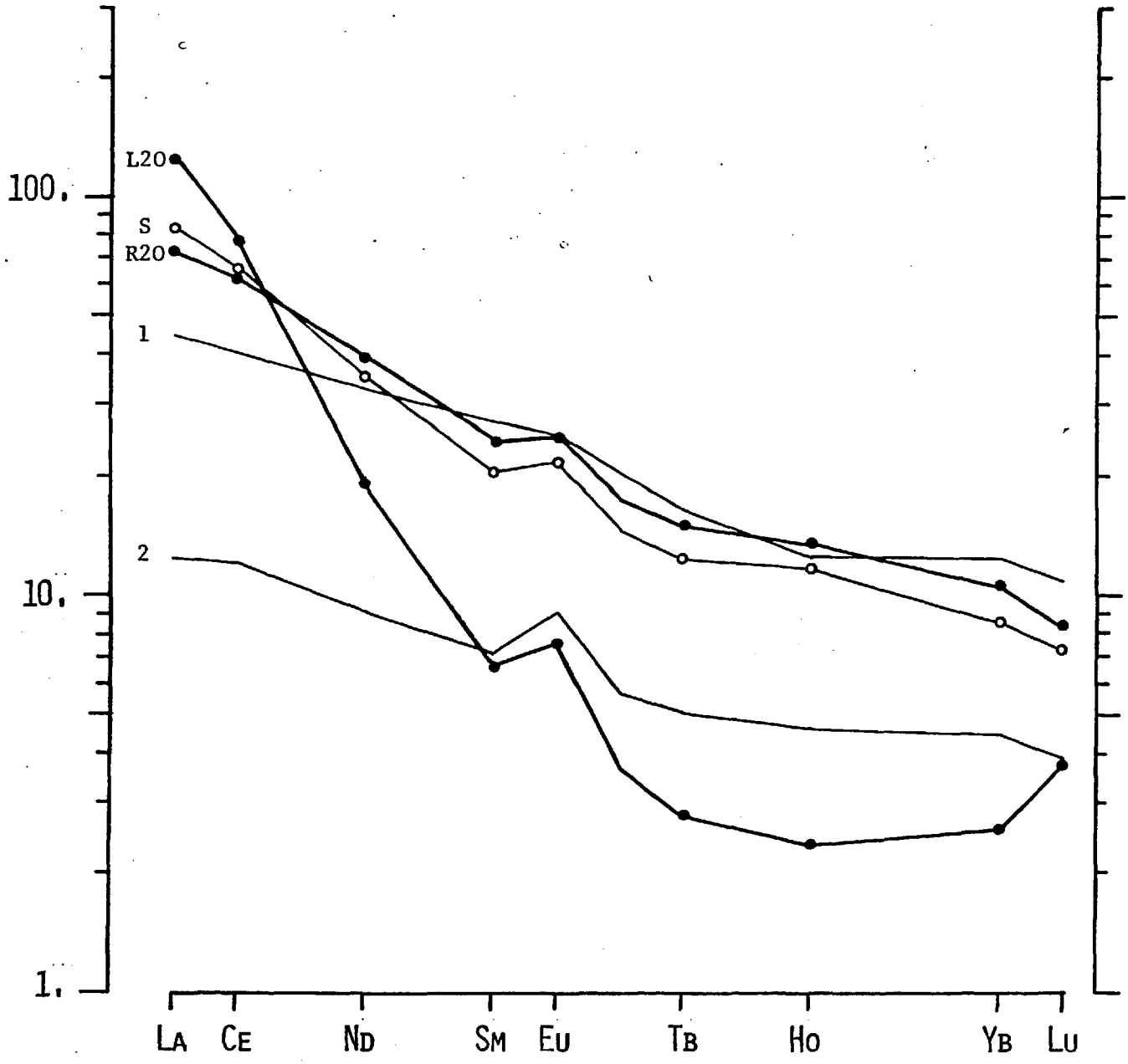

Fig. 5.10c Partial melting model based on amphibolite facies mineralogy. Key as in fig 5.10a.

the basic granulites. Three different partial melting models have been considered and are summarised in table 5.4. Model 1 is based on the normative mineralogy of LT2, model 2 on the modal mineralogy and model 3 on a hypothetical amphibole bearing mineralogy. These models are considered to represent melting under low and high pressure granulite facies and amphibolite facies conditions respectively. The results of the calculations are summarised in fig. 5.10 a, b and c, from which it is clear that none of the models can satisfactorily reproduce the REE abundacnes of the basic granulites. In fact 20% melting appears to have very little theoretical effect on the granulite whole rock REE abundances suggesting that these elements are not particularly suitable indicators of partial melting of granulitic crustal material. The REE abundance pattern of the melt in each of the models is not unlike some natural magmas e.g. model 1 liquids are comparable with some granites, model 2 with anorthosites and model 3 with pre-cambrian dacitic magmas. Thus, while these models fail to reproduce the basic granulite, REE abundance patterns, it seems reasonable to suggest that they may have some application to the production of other magmas.

From the arguments proposed in section 5.3, it appears most unlikely that garnet could have been an active phase during the depletion event. The following fractional crystallisation models are, therefore, based on the CIPW normative mineralogy and should always be considered, realising the assumption made during the norm calculations. The norms have been taken from Griffin et al (1979) and recalculated to give total

olivine, clinopyroxene and plagioclase. Any excess is assumed to represent trapped liquid and is assigned a K_d value of 1 for all elements. The two groups of xenoliths are considered separately:-

(i) The light REE enriched xenoliths are related to a liquid similar to PHN1646 and L20 and their theoretical whole rock abundances calculated from published K_d values (Frey et al 1978, Arth and Hanson 1975) and the re-calculated norms.

(ii) For the flat and light REE depleted xenoliths, a series of possible liquid compositions are calculated from the abundances in the enriched xenoliths using the norms and K_d values.

The relevant data for the first model are summarised in table 5.5 and the group of curves developed from these data illustrated in fig. 5.11. While the agreement between actual and calculated abundances is not particularly good, the model has developed a group of chondrite normalised abundance curves that is qualitatively similar to the analysed group. Note particularly the inflection in both the actual and predicted curves at Ho and their general paralellism. Considering the approximation and assumptions made in this model, the agreement is good and far better than that from any partial melting model. This is interpreted as suggesting that fractional crystalisation is a far more viable process for the development of these rocks.

Table 5.6 contains comparable data for the second group of granulite xenoliths except that, as a probable liquid, (comparable with

Table 5.5 Fractional crystallisation model 1

Normative mineralogies

Rock -	1670	M1	2852	L6
Plag.	64.6%	66.1	55.5	75.9
Cpx.	13.1	14.3	18.1	3.6
Oliv.	16.9	15.9	17.3	18.6
Liquid	5.4	3.2	9.1	1.2

Assuming the above are cumulate assemblages, distribution coefficients for each assemblage can be calculated from K_d data:-

K_d Values

Element	Plag.	Cpx.	Oliv.
Ce	0.12	0.15	0.0069
Nd	0.081	0.31	0.0066
Sm	0.067	0.50	0.0066
Eu	0.34	0.51	0.0068
Tb	0.059	0.65	0.0087
Ho	0.065	0.66	0.0103
Yb	0.067	0.62	0.014
Lu	0.060	0.56	0.016

K_d values from Arth and Hanson (1975)

Finally, the model abundance of the cumulate is calculated from the cumulate D value and the abundance of the element in the parent liquid.

Table 5.5 Contd.

Example M1

	D	Liquid*	Model**	Actual
Ce	0.134	35.2	4.72	10.9
Nd	0.131	20.0	2.62	5.5
Sm	0.149	4.95	0.74	1.32
Eu	0.332	1.52	0.51	0.64
Tb	0.166	0.77	0.13	0.24
Ho	0.171	0.88	0.15	0.32
Yb	0.168	2.46	0.41	0.90
Lu	0.155	0.37	0.06	0.13

* PHN1646 (ppm)

** Calculated from $D = C_c/C_l$ i.e $C_c = D.C_l$

Although the model and actual abundances disagree by 50%, the model calculations are consistently 50% low and the calculated whole rock abundance pattern is very similar to the actual pattern. See fig.5.11 for a comparison of the calculated abundances and the range of abundances shown by the analysed xenoliths

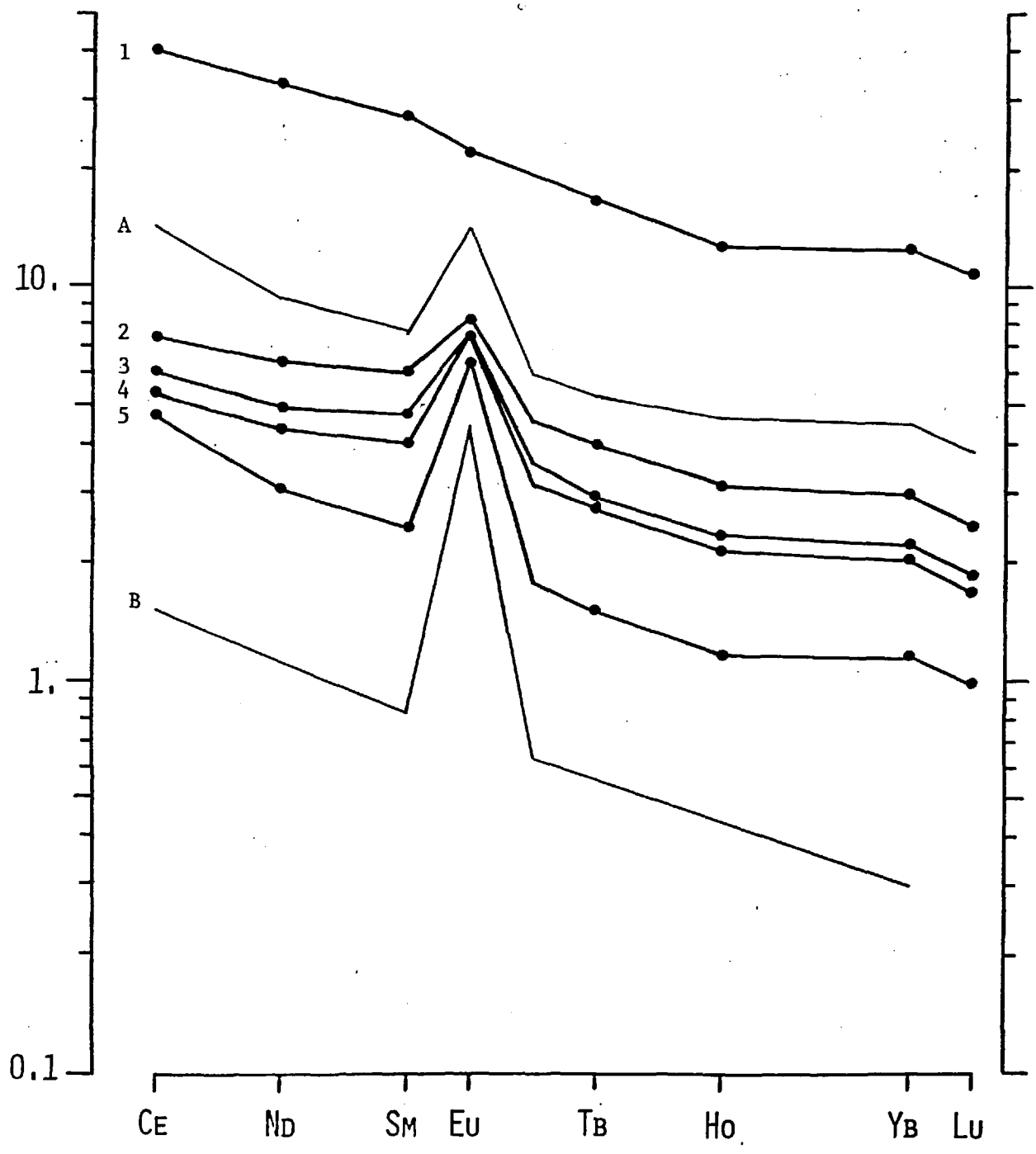

Fig. 5.11 Comparison of model cumulates derived from the normative mineralogy of the residual xenoliths and a parent liquid similar to PHN1646 (1). Xenoliths used to calculate curves 2 - 5 are, in order, PHN2852, PHN1670, M1 and L6. Curves A and B represent the upper and lower limits of the residual xenoliths REE abundances.

Table 5.6

Using the K_d values as listed in table 5.5, hypothetical liquid compositions can be calculated from the analysed xenoliths and their normative mineralogy.

	OVKF 10303	L13	L12A	L12B
Plagioclase	70%	65%	57%	45%
Clinopyroxene	9.5	15	23.5	34
Olivine	15.7	16	15	17
'Liquid'	4.8	4	4.5	4

Example - L12A

	D	Rock REE Abundances*	Calculated Liquid**
Ce	0.15	3.84	11.6
Nd	0.165	2.97	18.0
Sm	0.202	1.38	6.83
Eu	0.360	0.65	1.81
Tb	0.233	0.33	1.42
Ho	0.239	0.45	1.88
Yb	0.231	1.21	5.42
Lu	0.213	0.22	1.03

* As analysed (ppm)

** Calculated knowing $D = C_c/C_l$ i.e. $C_l = C_c/D$, where D is the bulk distribution coefficient, C_c is the cumulate concn and C_l the liquid concn.

The results are illustrated in Fig. 5.12.

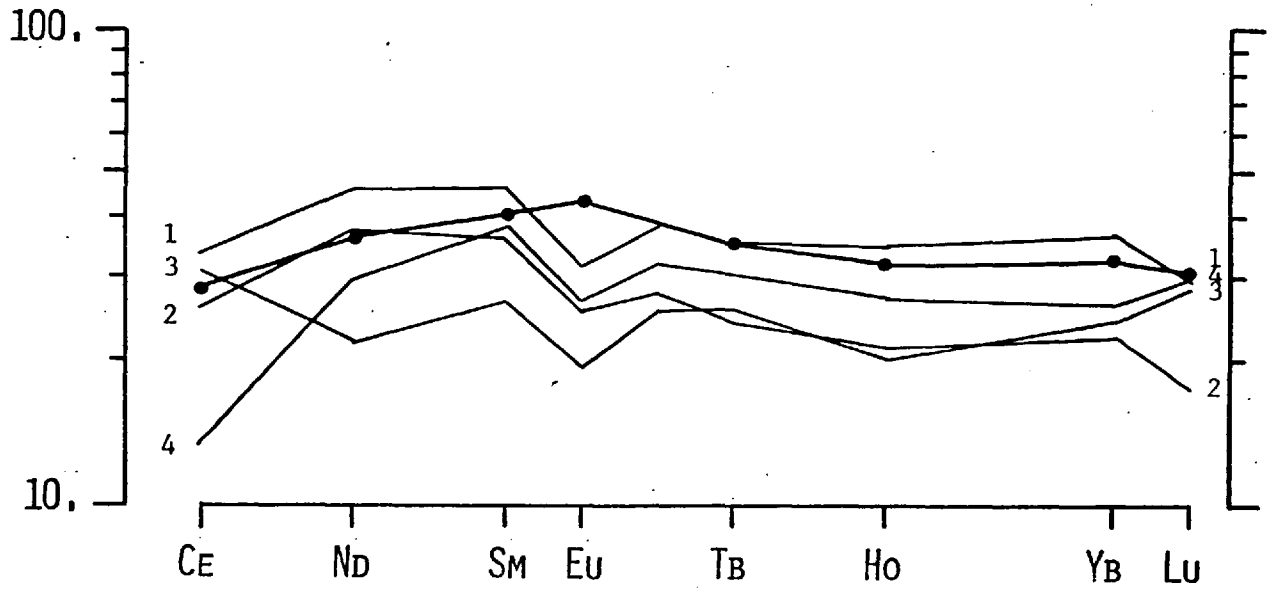

Fig. 5.12 Results of the fractional crystallisation model for the second group of xenoliths. The similarity of the calculated liquid compositions to one another and the xenolith LQ4, suggests initial derivation from a common parent.

Key:- Liquid compositions calculated from 1 - L12b
2 - L12a
3 - OVKF10303
4 - L13

The heavy line represents LQ4.

PHN1646 and L20 for the first group) is not present, the calculations have been carried out in reverse, predicting a probable liquid composition, assuming that the granulites are cumulates. In this context it is important to compare the results from L12A and B. If any samples are related by fractional crystallisation then these two must be as they are the felsic and mafic parts, respectively, of a layered xenolith. Although the two predicted curves differ somewhat in absolute abundances they are parallel, illustrating the qualitative nature of this approach. M13 also produces a liquid REE pattern comparable with those from L12A and B and all three are, in turn, similar to the whole rock pattern from LQ4, except for the lack of a Eu anomaly in the latter. The hypothetical liquids from PHN2532 and OVKF10303 are indeterminate as to which group they belong to.

Using the relevant K_d values (Frey et al 1978), Sc, Co and Ni can be similarly modelled for the xenoliths, the results of the calculations being summarised in table 5.7. For the first group of xenoliths, there is good agreement for Sc and the predicted range of Co abundances includes the actual analyses of the probable liquids. The agreement for Ni is not so good although the very large K_d value for olivine means that its abundance is very susceptible to olivine fractionation. This would have little or no effect on most of the elements but would severely affect the Ni abundance. The agreement of the calculations for the second group of xenoliths is similarly fair, the analysis of LQ4 generally co-inciding with predicted liquid concentrations.

Table 5.7.

1. Calculation of cumulate trace element composition assuming modal mineralogy from norm calculations and a liquid composition similar to PHN1646.

		Cpx.	Oliv.
K_d values*	Sc	3.1	0.25
	Co	1.2	1.3 - 6.5
	Ni	2 - 4	3.8 - 35.

*Taken from Frey et. al. 1978.

Rock -	1670		M1		2852		L6	
	calc	actual	calc	actual	calc	actual	calc	actual
Sc	15.8	14.3	16.2	19	21.7	20.5	5.7	3.15
Co	28 - 93	62.6	28 - 89	62	40 -106	37	23 - 94	57
Ni	110-741	69	171-705	83	128-836	56	92 -825	32

2. Calculation of possible parental liquid from residual xenolith analyses and modal mineralogies.

Rock -	OVKF 10303	L13	L12A	L12B	LQ4 (Possible parent)
Sc	59	41	35	38	39.4
Co	138 - 44	132 - 45	106 - 43	124 - 53	72.
Ni	70 - 10	151 - 24	129 - 24	161 - 33	60.

In summary, while neither partial melting or cumulate models can quantitatively reproduce the trace element abundances of the granulite xenoliths, there is far better qualitative agreement for the cumulate models. The xenoliths are thus best interpreted as fragments of meta-gabbros from the lower crust.

5.5 Discussion

The different groups of magmas reflected in the granulite xenoliths suggest that the lower crust beneath Lesotho has developed through a number of different magmatic and tectonic events, and, in this way, is comparable with the section of the lower crust exposed in the Ivrea Zone of the Alps (Mehnet 1975). The REE abundances of representative rocks from this region have been determined by Dostal and Capedri (1979) and show remarkable similarities with the xenolith analyses presented here except that the Ivrea Zone samples contain twice the concentration of the REE. The similarities are summarised in table 5.8.

Table 5.8

Lesotho Xenoliths	Ivrea Zone	
1. Light REE enriched basic granulites	Basic Granulites)	
2. Light REE depleted basic granulites	Amphibolites)	Meta-igneous
3. Felsic granulites (LT-2)	Biotite gneisses and Stronalites	

The main difference between the basic granulites from the two locations is that cumulate types are not recognised from REE data in the Ivrea Zone samples. The second group of granulites also compare well with REE analyses of eclogites from the Alpine/Apennine Voltric group (Morten et al, 1979) which have been interpreted as metamorphosed oceanic basalts and their associated cumulates. The evidence from the xenoliths is therefore interpreted as suggesting that the lower crust beneath Lesotho has evolved in a very similar way to lower crustal sections as exposed in Phanerozoic mobile belts. The light REE depleted granulite xenoliths could very well represent subducted oceanic basalts and gabbros while the light REE enriched granulites may be related to magmas produced during subduction. The felsic granulite is probably representative of metamorphosed sediments. Although there has been no systematic geochronological study of the granulite xenoliths, the few available dates suggest ages in the order of 1-2 by. (Griffin et al. op.cit., Jackson pers. comm.) This makes the similarity between the xenoliths and more recent (Alpine) granulites even more remarkable and suggests that plate tectonic processes could have operated for at least this length of time. Such a suggestion is compatible with the observation of Griffin et al. that the basic garnet granulites are only found as xenoliths in kimberlite pipes near the edge of the Kapvaal Craton, the latter being composed of Archean metamorphic rocks and bounded by Proterozoic mobile belts.

The results of this work therefore endorse the conclusion of Griffin et al.(1979) that the lower crust beneath Lesotho is heterogeneous and has a complex geological history. Of their three accumulation processes, the first, anatexis, now appears to be unlikely. The evidence is much more strongly in favour of basic granulite development through a combination of their second two processes:-

(a) intrusion of basic rocks into the lower crust during and after orogenic episodes and

(b) lateral emplacement of basic material beneath the craton margin by subduction.

CHAPTER 6

GENERAL DISCUSSION AND CONCLUSIONS

The results discussed in Chapters 3 and 4 amply illustrate the dichotomy that exists between the direct and indirect approaches to the determination of trace element abundances in the mantle. Petrogenetic models relating unfractionated primary magmas to a possible mantle source suggest that, if the undepleted mantle approximates pyrolite in its major element composition, then it must be light REE enriched (La up to 12 x chondrite) with heavy REE abundances at $\sim$ 3 x chondrite. Although one model presented by Frey et al (1978) related magma REE abundances to sources with flat REE abundance patterns, the degree of melting required to produce the liquid REE were so small (in some cases less than 1%) that the model was rejected as being unrealistic. Furthermore, some of the mass balance calculations for the major elements were not satisfied, further reducing the credibility of this alternative model.

In contrast, direct analysis of fertile garnet lherzolites which approach pyrolite with respect to their major element compositions possess flat REE abundances at 1-3 x chondrite (this work PHN2838 and 2839 and reconstruction of 1611 whole rock (Shimizi 1975)). A similar situation exists for the spinel lherzolites from S. Australia (Frey and Green 1974) and Arizona (Frey and Prinz 1978) with the most fertile samples possessing the flattest REE abundances.

Similarly, the partial melting models predict that the mantle residual after parial melting should be light REE depleted with the level of the heavy REE being dependent upon the presence or absence of garnet during melting. As emphasized in Chapter 4, the REE analyses only partly agree with these model predictions. While the heavy REE abundances are indeed controlled by garnet bearing and garnet free mineral assemblages, the light REE show a marked enrichment as opposed to the expected depletion. Similar features are shown by some garnet free lherzolite xenoliths (Frey and Green op. cit., Frey and Prinz op. cit.) although a few obey the model predictions as do spinel lherzolites from peridotite intrusions (Frey 1969).

By studying the associated problems of magma genesis and mantle depletion from opposing aspects, it is, therefore, possible to gain a more complete impression of melting processes. Both sets of evidence indicate that incompatible element enrichment of the upper mantle must have occurred. The data from primary magmas suggest this enrichment occurred either before or during melting, while the xenolith compositions could only result from enrichment either during or after melting. Assuming the two enrichment features are manifestations of the same process then enrichment must have accompanied partial melting, thus adding another variable to the already complex process of magma genesis.

The evidence from the depleted xenoliths indicates that the metasomatic component B possesses kimberlitic trace element abundances, leading to the conclusion that during parial melting, the mantle is infiltrated by a kimberlite-like fluid. On analogy with kimberlites exposed to the Earth's surface, this fluid will greatly affect not only the abundances of incompatible elements, but, also, the partial pressure of various volatiles. In Chapter 3 it was suggested that the Solomon Islands Alnoites, although more silica undersaturated than the S. Australian nephelinites and basanites (Frey et al, op. cit.), were derived by similar amounts of partial melting (4.5-6%) of a source with comparable REE abundances, the silica activity being controlled by the p_{CO_2} of the source and not the degree of melting. This hypothesis can now be modified by suggesting that the source mantle is similar in each case but that the fluids effecting partial melting possessed variable $CO_2/(CO_2 + H_2O)$ ratios, the value of this ratio increasing from basanites through nephelinites to alnoites. In all these cases, however, the fluid resembles kimberlite with respect to the rare earth and incompatible elements.

This scheme inherently accounts for the differences between kimberlites and other magmas as revealed in fig. 3.5 (La/Yb vs. Sm), the trace element abundances of the more usual magmas being the summed effects of partial melting and source enrichment. Kimberlites, on the other hand, are interpreted as being the surface expression of the

enriching fluid only. This hypothesis, however, still begs the question of the ultimate origin of the fluid and, hence, kimberlites. Clearly, this is an important question as kimberlite or kimberlitic fluids appear to play an essential role in the genesis of many mantle derived continental magmas.

Although no viable petrogenetic scheme for kimberlites has yet been presented, the above hypothesis adds two more constraints to the list that must be satisfied in any future hypothesis. Firstly, as kimberlite or a kimberlitic fluid is the cause of mantle enrichment during partial melting, kimberlite itself cannot be derived from incompatible element enriched mantle. To invoke such a tautological argument would not help in our understanding of kimberlite petrogenesis. Secondly, as kimberlite and other forms of continental vulcanicity are widespread phenomena, kimberlite and proto-kimberlite fluids effecting vulcanicity, must be derived from a normal mantle composition, i.e. a peridotite resembling pyrolite and fertile mantle xenoliths. This second point, while constraining the chemical composition, does not necessarily constrain the source mineralogy to that usually seen in ultrabasic xenoliths in kimberlites. These, quite clearly, must be derived from above the highest level at which kimberlite was last in chemical contact with the mantle. As some of the xenoliths from Lesotho kimberlites record depth in excess of 200 km, it is suggested that kimberlite must be derived from even greater depths. Unfortunately,

the mineralogy of the mantle at depths greater than 200 km is poorly known, although ultra-high pressure phase changes have been suggested from both experimental and seismic investigations (see, e.g. Akimoto 1972, Liu 1974).

Although kimberlites do not appear to be the result of partial melting processes, as give rise to the more usual continental magma suite; that they exist as magma is indisputable from field evidence, such as the Benfotein sills (Dawson and Hawthorne 1973). At this locality there is evidence for the fractional crystallisation of REE rich minerals, such as perouskite and niobian rutile (McMahon et al. 1979) suggesting that the observed differences between the REE in kimberlites and other magmas could be the result of such fractional crystallisation. At present, it is not possible to cite direct evidence against the general operation of such a process due to the paucity of data on trace elements in kimberlite perouskites etc. However, if fractional crystallisation was a frequent process in kimberlite petrogenesis, then one would expect a continuum of REE compositions ranging from normal magmas to the most fractionated of kimberlites, and not the hiatus between the two trends as shown on a diagram of La/Yb vs Sm. Furthermore, although the Benfontein Sills provide evidence for fractional crystallisation of kimberlite, they are, as far as is known, a singular occurrence and do not indicate the widespread operation of this process. It is possible that the scatter

shown by the kimberlite data on the La/Yb vs Sm diagram is the result of the separation of a REE rich phase, but it seems most likely that kimberlite could be derived from a parent magma with REE abundances comparable with nephelinite, for example, by fractional crystallisation.

The unusual REE abundances of kimberlites must, therefore, be a reflection of the processes operating in the source mantle. As emphasised in Chapter 3, conventional partial melting models cannot adequately explain the apparently decoupled trace and major element compositions of kimberlite despite the fact that kimberlite is a magma and melting must be involved in its formation. A possible alternative to simple partial melting that has been suggested previously in discussions relating to alkalic and, in particular, potassic magams, is zone melting (Harris 1957). During this process, a body of melt passes upwards through the mantle, melting the roof material and crystallising similar minerals at the base. As with partial melting, incompatible elements are concentrated in the melt phase. With zone melting, however, this effect is even more marked, the relative increase in concentration being a function of both K and L, the number of zone lengths through which the melt has passed. Under ideal circumstances this relative increase is given by the equation:

$$\frac{C_L}{C_O} = \frac{1}{K} - (\frac{1}{K} - 1)e^{-KL} \qquad 6.1$$

where C_L = concentration in the melt

C_0 = concentration in the original solid

K = partition (or bulk distribution) coefficient

L = number of zone lengths through which the melt has passed.

If such a process occurs in nature, however, ideal circumstances are unlikely to be attained. For example, equation 6.1 assumes complete melting of the source material. Clearly, in the mantle, this is highly unlikely, the zone probably consisting of a region of partial melt. Secondly, it assumes that an equal amount of material is crystallised at the base of the zone as is melted at the roof, i.e. the volume of the melt is a constant, and heat loss to the surrounding mantle, zero. Again such an isothermal, dynamic equilibrium appears most unlikely. Furthermore, the model does not take into account the role of a possible volatile phase that could easily form if the natural mantle was zone melted. Despite these limitations, however, equation 6.1 can still be used as a first approximation, particularly for the REE. These elements are accommodated by clinopyroxene and garnet which are, in turn, the first minerals to melt from the garnet lherzolite assemblage. Thus, the greater part of the REE content of the parent rock will enter the melt zone. The effects of a volatile phase on trace element partitioning are only important when it exists as a separate gas phase. In this system, the melted zone is under pressure and volatiles are assumed to remain in solution until the melt becomes saturated with gas

in the latter stages of magma evolution. A volatile phase will, however, have a marked effect on both the majot element composition of the melt and the amount of partial melt formed. It is possible that as zone melting proceeds and the partial pressures of the various gases increase, so the degree of melting may also increase. Finally, although it is not possible to assess how much out of balance the melting and solidification process would be, it is probable that, due to heat loss, more material would crystalise than melt. The effect of this, however, may be countered by the effects of volatiles as discussed above.

In the following model, the mantle being zone melted possesses a flat REE abundance pattern at 3 x chondrite, and is assumed to possess a garnet lherzolite mineralogy (10% Gt, 10% Cpx, 25% Opx, 55% Oliv.). Application of equation 6.1 to such a source produces a series of REE abundance curves, each curve corresponding to a value of L. Although the curves corresponding to values of L between 100 and 200 superficially resemble kimberlite in being steeply inclined and non-inflected, they do not coincide with the kimberlite trend on a diagram of La/Yb vs Sm (see figs. 6.1 and 6.2). Clearly for zone melting to be at all applicable to kimberlite petrogenesis, the crystallising minerals must be able to produce a much greater fractionation of La from Yb. This can be achieved in two ways. Either the K_d value for the heavy REE between garnet and liquid must be much greater than published values or more garnet must crystallise from the melt than is suggested by the model. From the evidence presented in Chapter 5 (Table 5.2) there is not systematic

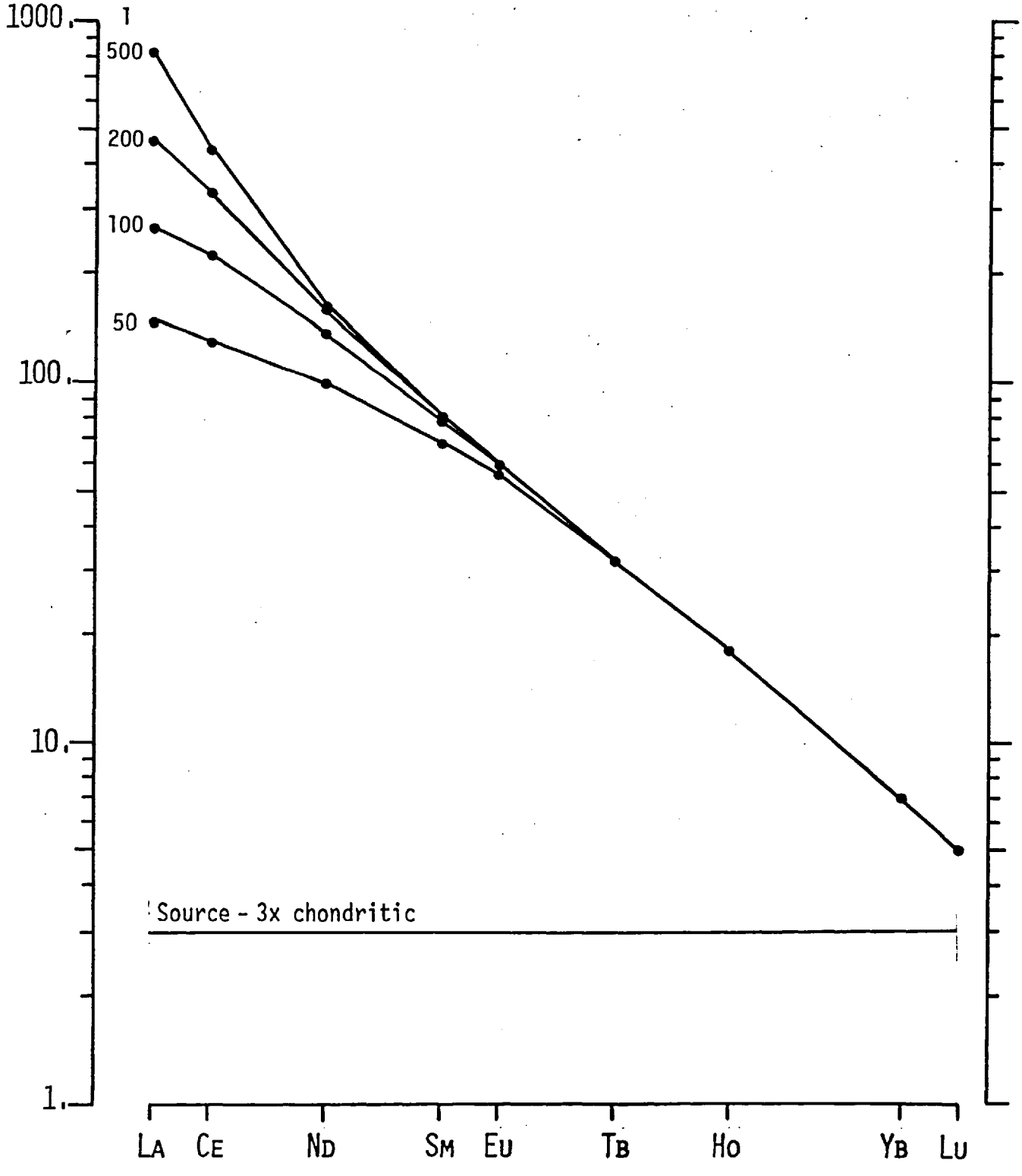

Fig. 6.1. Zone melting model 1. Based on a garnet lherzolite mineralogy.

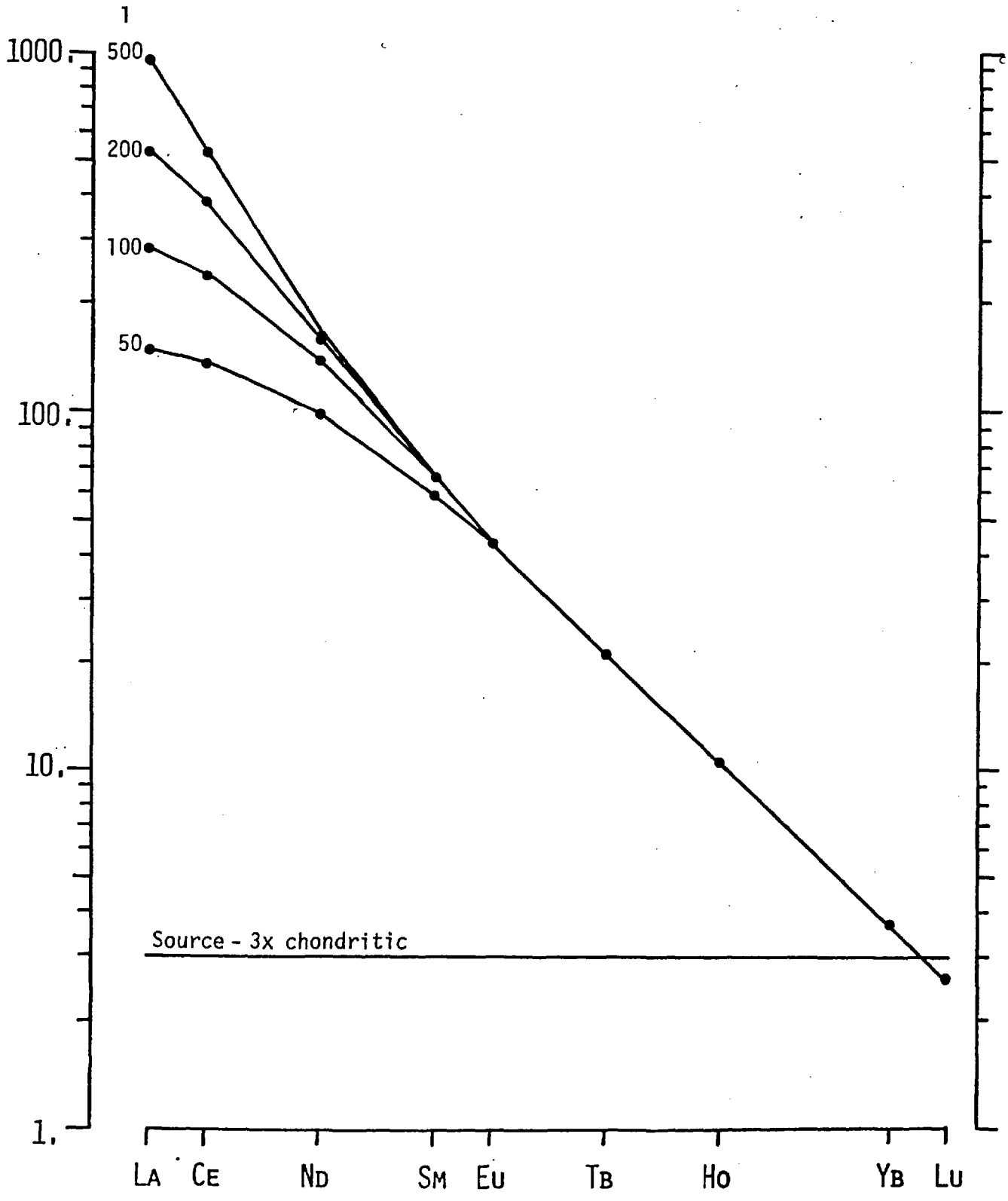

Fig. 6.2. Zone melting model 2. Based on a garnet harzburgite mineralogy.

change in K_d values for Yb between clinopyroxene and garnet with pressure. Therefore, unless K_d values between both clinopyroxene and liquid vary in the same way it seems unlikely that the K_d value for Yb between garnet and liquid is going to vary sufficiently to cause the desired increase in fractionation.

This leaves the second alternative of crystallising more garnet in the residuum than is suggested by the model and the question that must be answered as to whether such a process is possible. Does the mantle become garnet rich as pressure increases? From experimental work (e.g. Ringwood 1966 cited by Yoder 1976), the answer to this question is yes; diopside breaks down to garnet and ilmenite structures. From the extrapolated phase boundaries in Yoder (1976, fig. 4.2), at a temperature of 14-1600°C this phase change takes place at $\sim$ 100 kb corresponding to $\sim$ 300 km depth which is within the range of depth suggested for kimberlite formation. Invoking the possible importance of such a high pressure phase change has a significant effect on trace element models, although our lack of knowledge concerning the nature of this reaction renders these models even less rigorous. If, however, a garnet harzburgite mineralogy of 20% gt, 25% opx and 55% oliv., is assumed and equation 6.1 applied, REE patterns closely resembling those of kimberlite can be derived. Moreover, these results plot closer to kimberlites on a graph of La/Yb vs Sm (figs. 6.2 and 6.3). Again it is emphasised that both of these models are purely qualitative, serving only to demonstrate how kimberlitic fluids might develop if a zone of melt or partial melt moved upwards through fertile mantle.

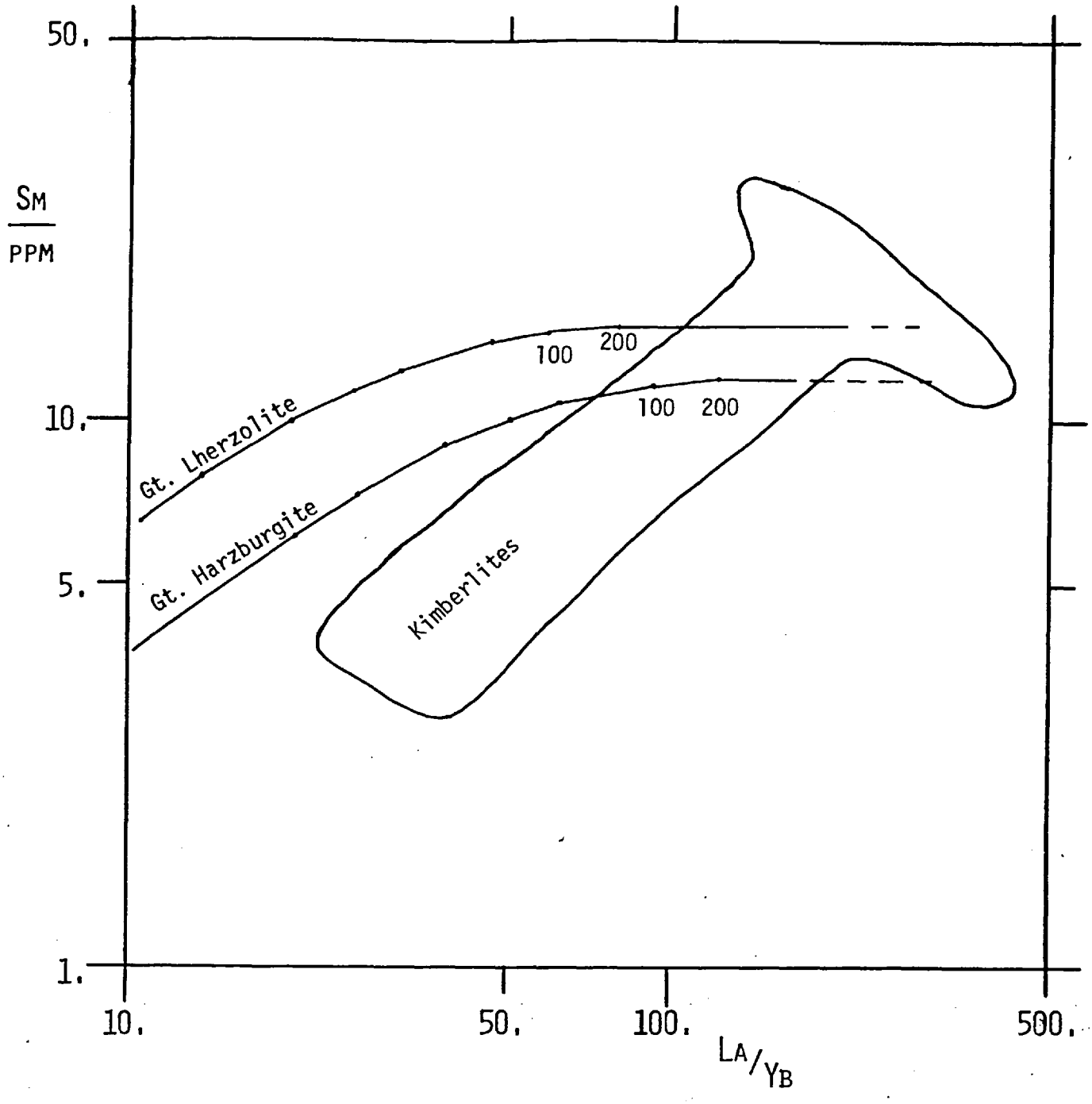

Fig. 6.3. Zone melting models plotted on a diagram of La/Yb vs Sm Showing the general similarities of REE abundances for values of 1 between 1GO and 200 for the garnet harzburgite model.

A question that has caused problems in previous petrogenetic schemes involving zone melting concerns the 'driving-force' behind the upward motion of the melt zone. In this hypothesis, however, such a force can be envisaged, if the high pressure, cpx → garnet + ilmenite phase change is invoked. One of the characteristics of kimberlites, as outlined in Chapter 3, is that they are restricted to the cold centres of continents, usually in cratonic regions. As dP/dT for most anhydrous phase changes in the mantle is positive, in these cold regions, high pressure phase changes will occur at their shallowest depths. The continents, however, show evidence in their geological records for having once been at much higher temperatures. During such thermal events, high pressure phase changes would have occurred at much greater depths. It is suggested that the slow rise of the phase change during cooling could provide the trigger and driving force behind zone melting. During the initial phases of cooling, recrystallisation would release volatiles trapped as fluid inclusions. As the partial pressure of these volatiles (predominantly CO_2) increase so a small amount of melting might be induced in the fertile mantle. From then on the process is self perpetuating, further cooling releasing more volatiles which in turn produce a greater degree of melting. All the time, however, the zone of volatile release and ensuing partial melting is being pushed upwards by the high pressure recrystallisation in a manner analogous to a metamorphic front. Again, this hypothesis explains one of the strange features of kimberlite composition, namely the apparent decoupling of major elements, incompatible elements and

volatile constituents. During normal zone melting volatile and incompatible elements should behave similarly, assuming volatile containing phases, such as amphibole, are not being precipitated from the melt. In the 'metamorphic front' process as hypothesised, the volatile elements accumulate first, before the melt forms, and are, therefore, inherently decoupled from the development of the trace element abundances.

The decoupling of compatible and incompatible elements is a natural feature of zone melting and is well illustrated in fig. 6.4. It can be seen that the value of C_L/C_O tends to a limit of $\frac{1}{D}$ as L increases and that this limit is attained when $1 \approx 10D^{-L}$. Clearly this limit is more rapidly approached the larger the value of D. Therefore, the major and compatible trace elements in the melt will tend to remain at relatively constant concentrations while the incompatible element abundances will show considerable variation. In the system envisaged, in which the kimberlite is considered to be derived from a zone of partial melt (as opposed to total melt), the mixing of melt and crystals will result in a more complex variation in compatible element abundances. The zone will consist of melt plus melted roof material (mainly olivine and orthopyroxene) plus crystallising floor material (i.e. olivine and orthopyroxene, unaltered from the roof and the phases crystalising from the liquid). Kimberlite, as erupted at the surface will, therefore, be a mixture of these three components. The incompatible element abundances of kimberlites will be controlled solely by the fluid fraction, whereas the compatible elements, which

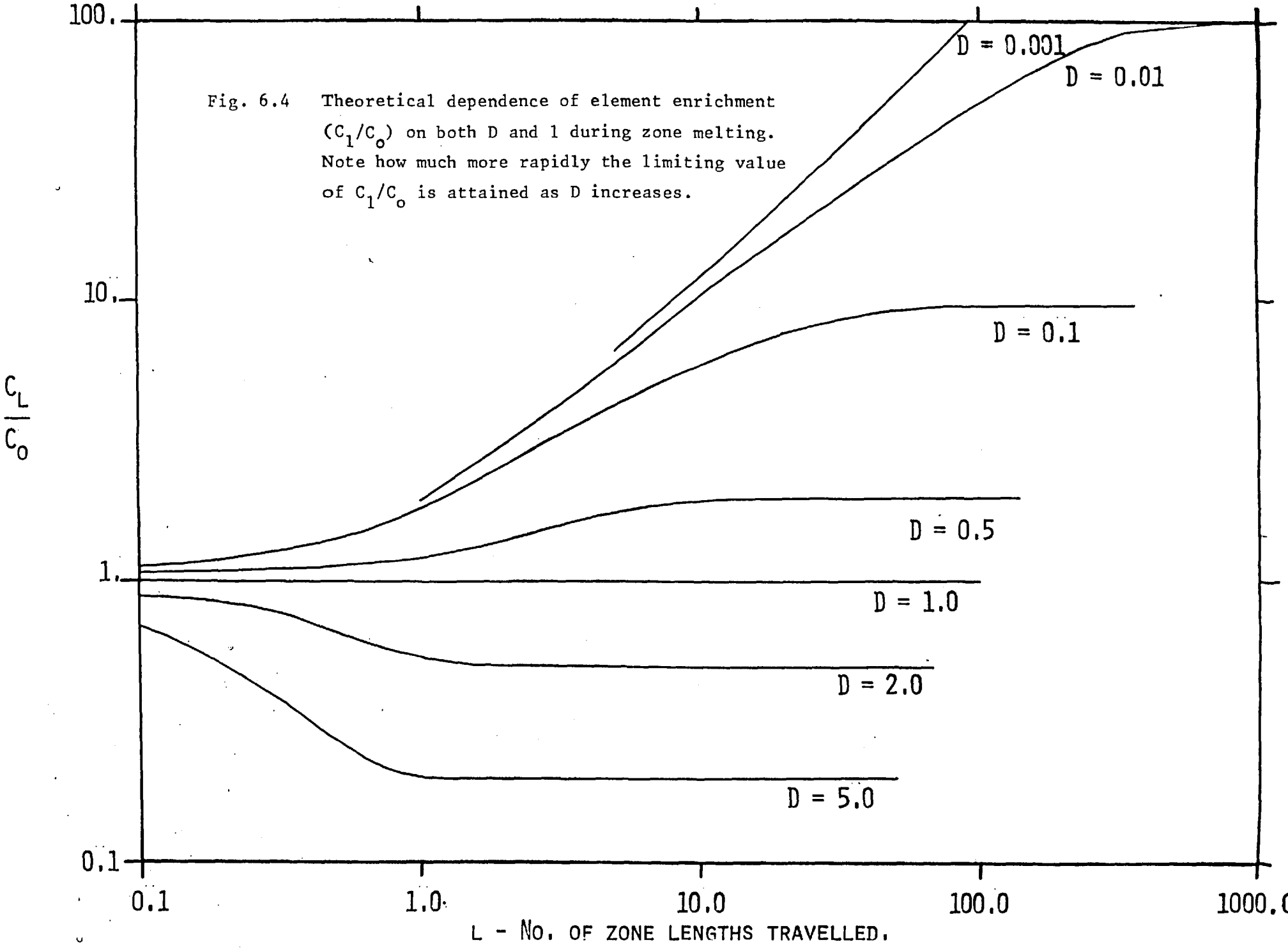

Fig. 6.4 Theoretical dependence of element enrichment (C_1/C_o) on both D and 1 during zone melting. Note how much more rapidly the limiting value of C_1/C_o is attained as D increases.

are present in varying amounts in all three components, will show a range of abundances in the resultant kimberlite. The minimum of this range (if D > 1) will be determined by the fluid while the maximum, probably by the abundance in the original source material.

From the data presented in Chapter 3, it can be seen that the analyses generally conform to this prediction. The greatest variation in compatible element abundances is a factor of 3 shown by Cr. This compares with the order of magnitude variation in the abundances of incompatible elements such as U and Th. Similarly, the model predicts that the heavy REE should not vary greatly when compared with the lighter elements, due to the high K_d values of garnet for the heavy REE. Again the data agrees with this prediction. Reference to figs. 3.1 and 3.2 shows that while Yb varies slightly, from 2-5 x chondrite, La varies through almost an order of magnitude, from 70 to 600 x chondrite.

A further criterion satisfied by this hypothesis is, that kimberlite magma, although widespread, is volumetrically insignificant. Zone melting only requires a small amount of liquid to operate successfully and operates more successfully (for geological purposes) as the volume of liquid in the zone is reduced. Furthermore, for small volumes of melt, the magma body does not have to move very far for L to become large and the steady state concentrations of compatible and major elements to be achieved. Indeed, kimberlite incompatible abundances

are only developed for L > 100. Therefore, unless a large zone can travel a considerable distance, only small magma bodies will ever attain kimberlitic trace element abundances.

To summarise, the petrogenesis of kimberlite is thought to be the direct consequence of mantle cooling and the gradual re-equilibration of the mantle to higher pressure mineral assemblages. As cooling progresses, the isograds representing the re-equilibration rise to shallower mantle depths, taking with them volatiles released by the recrystallisation. These volatiles in turn accumulate and eventually induce a small amount of partial melting. Further cooling induces higher level recrystallisation, increasing the volatile content of the system which in turn produces more melt. Eventually, the volume of melt is such that the partly molten zone could become detached from the rising isograd and rise as a result of its own buoyancy allowing the formation of the often proposed mantle diapir (Green and Gueguen 1974). Zone melting would cease as soon as the rising body of crystal mush encountered a refractory layer, such as the thick zone of mantle beneath the continents. This may explain the relative paucity of fertile mantle xenoliths in kimberlites generally. The proto-kimberlite partial melt is able to rise through fertile mantle through the processes of zone melting, solution stoping and diapirism but must be forcefully intruded into overlying rigid sterile peridotites. After the progress of the zone or diapir has been halted, ensuing fractional crystallisation causes a further increase in the pressure of volatiles, with subsequent doming and fracturing of the roof material, permitting the further ascent of the proto-kimberlite magma.

To return to the problem of the genesis of alkali basaltic and similar continental volcanic magmas, their formation can be regarded in a similar manner to fenitisation around carbonatite intrusions in the crust. Fluids emanating from the zone of partial melt or veins leading from that zone, react with the surrounding mantle. If the fluids interact with fertile mantle, the introduction of volatiles depresses its melting point and partial fusion follows. The composition of the melt is therefore controlled by both normal partial melting processes and the composition of the fluid. It is envisaged that the residue after melting will bear the imprint of the metasomatic/melting event and will be anomalously enriched in incompatible elements. The presence of this enrichment may be revealed by the presence of potassic minerals such as phlogopite and richterite, although sub-soludus re-equibration may erase any such mineralogical evidence. By invoking the operation of an enriching fluid, however, the basis of the previously favoured petrogenetic models (e.g. Frey et al 1978) is seriously questioned. These models use the P_2O_5 content of primary magmas to estimate the degree of partial melting involved in their formation, assuming P_2O_5 to behave as a totally incompatible element (i.e. D=0). It follows, therefore, that P_2O_5 will also be concentrated in the zone melting process producing the proto-kimberlite fluid. Subsequent enrichment of a magma source prior to and during partial melting will also enrich the source in P_2O_5.

Any models using P_2O_5 abundances as a guide to the extent of melting should, therefore be treated with caution and considered as 'minimum' conditions (the more P_2O_5 in the source, the greater the degree of partial melting is allowed to produce the observed magma P_2O_5 abundance).

Alternatively, the fluid may encounter only sterile mantle. In this case, due to the infusible nature of the country rock, only local metasomatic activity can occur and the fluid continues on its route towards the surface. It should be emphasised that this progression towards the surface is envisaged as being a relatively quiescent process. Recent exploration of the root zones of kimberlitic pipes from South Africa suggests that pipe formation is preceded by a relatively long period of magma intrusion by such processes as stoping, hydraulic fracturing and intermittent gas brecciation. Furthermore, the pre-diatreme phase of intrusion appears to be controlled by the structure of the country rock (Clement 1979). These features collectively indicate a comparatively peaceful upward progression of a column of magma, headed by a zone of 'precursor gas'. It is only after the surface has been broken that the violently explosive diatreme mode of eruption occurs i.e. after the release of the load pressure allowing exsolution of the gas phase from the magma and consequent gas fluidisation.

The hypothesis presented here is highly tentative, being based on the analysis of only a few trace elements in magmas and mantle xenoliths. Clearly more analyses are required to test the various predictions, particularly concerning the metasomatic component in sterile mantle xenoliths. Possibly isotopic studies and more information on the trace element abundances of the separate minerals, particularly phlogopite and richterite will help in more closely defining the composition of component B. The role of the MARID suite of xenolith (Dawson & Smith 1977) in metasomatic enrichment is also problematic. These are composed of volatile and incompatible element-rich minerals (particularly K and Ti rich) that could well represent proto-kimberlite fluids that have solidified at depth. Do their mineral compositions compare with those of richterite and phlogopite in the sterile xenoliths? Experimental studies on the phase relations of garnet lherzolite at ultra-high pressures (i.e. 100 kb or more) are also required to discover the dominant minerals that could co-exist with a proto-kimberlite liquid. The hypothesis does not adequately explain the role of the megacrysts found in most kimberlites. Could they represent material that has crystallised from the proto-kimberlite fluid during zone melting or are they another accidental sample of the deep mantle?

The results described have answered some questions, but, in so doing, have posed many more, illustrating our lack of knowledge concerning the constitution of the mantle. The samples from kimberlites provide us with a tantalising glimpse of the complex chemical and geological processes that occur at depth and it can be hoped that their further analysis will greatly aid our understanding of the evolution of the mantle and continents.

Appendix 2.1. Program SPEC5

This computer program allows the rapid reduction of γ-ray spectral data, using interactive graphics routines available on the I.C.C.C. CDC6500 machine. Data from the Link Systems spectrometer (in the form of paper tape) is loaded on to the computer and editted into a file, TAPE9, from which it is read directly by the program. (The two necessary ancilliary editting programs are also listed). Output data, comprising peak centre channels, corrected integrals and percentage errors, are retained on a second file, TAPE11, for future reference. An example of TAPE11 is listed at the end of the section.

N.B. The updated version of the program listed below, SPEC7, was completed in September 1979. Most of the analyses reported in this thesis were obtained using SPEC5, which is slightly less sophisticated.

```
JOB(TOM.N015,J1)
PASSWOK(      )
COPYCK(INPUT,TAPE1)
REWIND(TAPE1)
FTN(SL,L=0)
LGO.
REWIND(TAPE2)
UPDATE(Q,N)
COPYSBF(COMPILE,OUTPUT)
SAVE(NEWPL=NAY)

  7/8/9 - END OF SECTION

  PAPER TAPE IN HERE

  7/8/9 - END OF SECTION

      PROGRAM CHECK(OUTPUT,TAPE6=OUTPUT,TAPE1,TAPE2)
      DIMENSION ALINE(9)
      DATA ABLANK/1H /
   50 READ(1,10) ALINE
      IF(ALINE(1).NE.ABLANK)WRITE(2,10)ALINE
      IF(EOF(1)) 40,50
   10 FORMAT(A5,8A7)
   40 STOP
      END

  7/8/9 - END OF SECTION

*DECK EC
*READ TAPE2

  6/7/8/9 - END OF INFORMATION
```

Program CHECK.

Program CHECK is used to load the paper tape data on to the computer, recording it in a permanent file, in this example NAY. The program also deletes blank lines from the data, reducing the required computer storage space.

```
JOB(TQEN015,J1)
PASSWOR(      )
GET(OLDPL=NAY)
UPDATE(Q,N,C=TAPE9,D,8,L=0)
SAVE(TAPE9)

  7/8/9 - END OF SECTION

*ID MESS
*D EC.1,10
*D EC.94,102
*D EC.186,194          UPDATE editting cards (different for each file)
*D EC.278,286
*D EC.370,378
*C EC

  6/7/8/9 - END OF INFORMATION
```

UPDATE job.

This job is used to edit the file produced by program CHECK (in this case, file NAY), deleting lines with headings and spurious characters. The editted data is then saved on a second permanent file, TAPE9, ready for analysis by SPEC5 or SPEC7.

```
00100 PROGRAM SPEC7(INPUT=131B,OUTPUT=131B,TAPE6=131B,TAPE64=131B,
00110+TAPE61=131B,TAPE66=131B,TAPE5=INPUT,TAPE9=131B,TAPE10=131B,
00120+TAPE11=131B,TAPE12=131B)
00121C
00122C  -  AN INTERACTIVE GRAPHICS COMPUTER PROGRAM FOR THE RAPID
00123C  -  INTEGRATION OF GAMMA-RAY PHOTOPEAKS.
00124C
00130 DIMENSION NN(12,15),MM(12),X(120),ITITLE(3),IX(3),IY(3),A(6)
00140 COMMON NN,MM,X
00150 CALL START(2)
00160 41 READ(12,45)(A(I),I=1,6)
00170 45 FORMAT(6A8)
00180 IF(A(1).EQ.4HSTOP)GO TO 40
00190 WRITE(10,45)(A(I),I=1,6)
00200 GO TO 41
00210 40 CALL BUFFEM(-10)
00220 CALL PROMPT(19HTYPE GO TO CONTINUE,19)
00230 34 READ(5,100)XYZ
00240 IF(XYZ.EQ.2HGO)GO TO 35
00250 GO TO 34
00260 35 CALL PROMPT(19HHARDCOPY, ON OR OFF,19)
00270 READ(5,100)AB
00280 IF(AB.EQ.2HON)CALL SWITCH(9HHARDCPYON)
00290 CALL PROMPT(25HAUTO OR NORMAL DATA ENTRY,25)
00300 READ(5,100)A1
00310 IF(A1.EQ.4HAUTO)CALL AUT(NN,N,MM)
00320 IF(A1.EQ.4HNORM)GO TO 5
00330 CALL PROMPT(37HDO ANY SPECTRA NEED TO BE SKIPPED Y/N,37)
00340 READ(5,100)A2
00350 IF(A2.EQ.1HY)CALL SKIP(NN,MM,I,J)
00360 IF(A2.EQ.1HN)CALL SKIPD(I,J)
00370 WRITE(11,110)I
00380 GO TO 2
00390 1 I=I+1
00400 WRITE(11,110)I
00410 110 FORMAT(/,4X,19HSPECTRUM/SAMPLE NO.,I3,//,
00420+11HPEAK CENTRE,6X8HINTEGRAL,5X,9HPC. ERROR,/)
00430 J=0
00440 2 IF(I.GT.N)STOP
00450 4 AN3=1HN
00460 3 J=J+1
00470 IF(J.GT.MM(I))GO TO 1
00480 K=NN(I,J)
00490 READ(9,100)ICH
00500 READ(9,101)ISTART,(X(KK),KK=1,K)
00510 IF(AN3.EQ.1HS)GO TO 4
00520 GO TO 103
00530 5 CALL PROMPT(35HENTER NO.OF CHANNELS IN PEAK REGION,35)
00540 READ(5,*)K
00550 READ(9,100)ICH
00560 READ(9,101)ISTART,(X(KK),KK=1,K)
00570 103 CALL ANSIS(X,K,ISTART,AN3)
00580 IF(AN3.EQ.1HO)GO TO 103
00590 IF(AN3.EQ.1HN.OR.AN3.EQ.1HS.OR.AN3.EQ.1HZ)GO TO 104
00600 100 FORMAT(1A10)
00610 101 FORMAT(I4,5F9.0,31X,/,(4X,5F9.0,31X))
00620 104 IF(A1.EQ.4HAUTO)GO TO 3
00630 IF(A1.EQ.4HNORM)GO TO 5
00640 STOP
00650 END
```

```
00660 SUBROUTINE ANSIS(Y,N,ISTART,ANS)
00661C
00662C  -  SUBROUTINE FOR DISPLAYING DATA AND CONTROLLING THE
00663C  -  SUBSEQUENT ANALYSIS.
00664C
00670 DIMENSION X(120),Y(120)
00680 IF(ANS.EQ.1HS)RETURN
00690 DO 10 I=1,N
00700 10 X(I)=FLOAT(ISTART+I-1)
00710 CALL NEWPAGE
00720 CALL SCALE2(1.5)
00730 CALL MINMAX(Y,N,XMIN,XMAX)
00740 ALMN=ALOG10(XMIN)
00750 ALMX=ALOG10(XMAX)
00760 DIF=ALMX-ALMN
00770 IF(DIF.GT.0.5)GO TO 30
00780 IF(DIF.LE.0.5)GO TO 31
00790 30 CALL LOGPLOT(XMIN,XMAX,2,14.0,2,2)
00800 GO TO 32
00810 31 CALL LINPLOT(XMIN,XMAX,2,14.0,2,2)
00820 32 ALGNX=185.0/FLOAT(N)
00830 INTX=IFIX(FLOAT(N)/10.0)+1
00840 VINC=10.0
00850 START2=FLOAT(ISTART-1)
00860 CALL LINAX(1.7,0.8,1,ALGNX,INTX,START2,VINC,5,1,1,-1,1)
00870 DO 20 I=1,N
00880 CALL LOCATE(X(I),Y(I),XP,YP,NNN)
00890 XNI=FLOAT(I)/10.0
00900 NI=IFIX(XNI)*10
00910 IF(NI.EQ.I)ISYM=11
00920 IF(NI.NE.I)ISYM=3
00930 CALL SYMBOL(XP,YP,0.2,ISYM,0.0,-1)
00940 20 CONTINUE
00950 21 CALL PROMPT(41HO,N,L,S,C,P,H,SM,TYPE HELP FOR ASSISTANCE,41)
00960 READ(5,97)ANS
00970 97 FORMAT(A7)
00980 RP=1HA
00990 IF(ANS.EQ.1HS)RETURN
01000 IF(ANS.EQ.1HN)RETURN
01010 IF(ANS.EQ.1HL)STOP
01020 IF(ANS.EQ.1HC)CALL SORT(Y,X,RP)
01030 IF(ANS.EQ.1HP)CALL BFIT(X,Y,N,RP)
01040 IF(ANS.EQ.1HH)CALL XTITLE
01050 IF(ANS.EQ.2HSM)CALL SMOTH(N,X,Y)
01060 IF(ANS.EQ.4HHELP)CALL ASSIST(ANS)
01070 IF(ANS.EQ.1HO)RETURN
01080 IF(RP.EQ.1HC)GO TO 35
01090 GO TO 21
01100 35 ANS=1HZ
01110 RETURN
01120 END
```

```
01130 SUBROUTINE SORT(Y,X,RP)
01131C
01132C  -  CONTROL OF COVELL-TYPE BG. CORRECTION.
01133C
01140 DIMENSION NQ(10),Y(120),X(120)
01150 CALL PROMPT(15HNUMBER OF PEAKS,15)
01160 READ(5,*)NP
01170 NP2=NP*2
01180 CALL PROMPT(21HENTER PEAK BOUNDARIES,21)
01190 READ(5,*)(NQ(I),I=1,NP2)
01200 K=0
01210 DO 10 J=1,NP2,2
01220 I1=NQ(J)
01230 JJ=J+1
01240 I2=NQ(JJ)
01250 XMAX=0.0
01260 DO 20 I=I1,I2
01270 20 IF(Y(I).GT.XMAX)XMAX=Y(I)
01280 DO 21 I=I1,I2
01290 21 IF(Y(I).GE.XMAX)CCH=X(I)
01300 CALL LOCATE(X(I1),Y(I1),XA,YA,NN)
01310 CALL LOCATE(X(I2),Y(I2),XB,YB,NM)
01320 CALL SYMBOL(XA,YA,0.2,0,0.0,-1)
01330 CALL SYMBOL(XB,YB,0.2,0,0.0,-2)
01340 K=K+1
01350 CALL CALC(Y,I1,I2,K,CCH,NP,RP)
01360 10 CONTINUE
01370 RETURN
01380 END


01390 SUBROUTINE CALC(Y,I1,I2,K,CCH,NP,ANS)
01391C
01392C  -  SUBROUTINE USED BY SORT TO CALCULATE PEAK AREAS.
01393C
01400 DIMENSION X(120),Y(120),ICH(10),YTY(10),YERR(10)
01410 YSUM=0.0
01420 DO 10 I=I1,I2
01430 10 YSUM=YSUM+Y(I)
01440 BG=(Y(I1)+Y(I2))*FLOAT(I2-I1+1)*0.5
01450 CORINT=YSUM-BG
01460 ERR=(SQRT(CORINT+BG*(1.0+FLOAT((I2-I1-3)/2)))/CORINT)*100.0
01470 IF(K.EQ.1)WRITE(10,99)
01480 99 FORMAT(/,2X,4HPEAK,2X,8HINTEGRAL,3X,8HPC.ERROR,/)
01490 WRITE(10,100)K,CORINT,ERR
01500 ICH(K)=IFIX(CCH)
01510 YTY(K)=CORINT
01520 YERR(K)=ERR
01530 100 FORMAT(4X,I2,3X,F10.2,2X,F5.2)
01540 IF(K.LT.NP)RETURN
01550 CALL BUFFEM(-10)
01560 CALL PROMPT(29HSTORE RESULTS ON TAPE11 Y/N/C,29)
01570 READ(5,101)ANS
01580 IF(ANS.EQ.1HN)GO TO 50
01590 IF(ANS.EQ.1HY)CALL SAVE(ICH,YTY,YERR,K)
01600 IF(ANS.EQ.1HC)CALL SAVE(ICH,YTY,YERR,K)
01610 101 FORMAT(1A1)
01620 50 RETURN
01630 END
```

```
01640 SUBROUTINE BFIT(X,Y,NX,REP)
01641C
01642C  -  CALCULATION OF PEAK AREAS USING POLYNOMIAL
01643C  -  REGRESSION ANALYSIS THROUGH THE CONTINUUM.
01644C
01650 DIMENSION X(120),Y(120),XX(120),YY(120),NP(12),BG(120),W(120),
01660+P(20),SI(20),ICR(10),YTY(10),YERR(10)
01670 COMMON XX,YY,NP,BG,W
01680 LOGICAL LL
01690 CALL PROMPT(21HENTER NUMBER OF PEAKS,21)
01700 READ(5,*)N
01710 CALL PROMPT(34HENTER BG LIMITS AND MAX POLY POWER,34)
01720 NN=2*(N+1)+1
01730 READ(5,*)(NP(I),I=1,NN)
01740 K1=NP(NN)
01750 NN=NN-1
01760 K=0
01770 DO 10 I=1,NN,2
01780 I1=NP(I)
01790 J1=I+1
01800 I2=NP(J1)
01810 DO 10 J=I1,I2
01820 K=K+1
01830 YY(K)=Y(J)
01840 XX(K)=X(J)
01850 10 CONTINUE
01860 YTOT=0.0
01870 DO 11 J=1,K
01880 YTOT=YTOT+YY(J)
01890 11 W(J)=1.0
01900 YMEAN=YTOT/FLOAT(K)
01910 LL=.FALSE.
01920 IFAIL=0
01930 CALL POLY(K,XX,YY,W,K1,NH,SI,P,LL)
01940 NH=NH+1
01950 DO 20 J=1,NX
01960 BG(J)=0.0
01970 DO 20 I=1,NH
01980 BG(J)=BG(J)+(X(J)**(I-1))*P(I)
01990 20 CONTINUE
02000 NF=NH-1
02010 WRITE(10,100)NF
```

```
02020 100 FORMAT(14HBEST FIT POWER,I2)
02030 ST=SI(NH)/YMEAN
02040 WRITE(10,103)ST
02050 WRITE(10,102)
02060 MK=NN-1
02070 DO 41 J=2,NN,2
02080 JJ=J+1
02090 JJ1=J+2
02100 J1=J-1
02110 JK=J/2
02120 JL=J/2
02130 YINT=0.0
02140 ERR=0.0
02150 I1=NP(J)
02160 I2=NP(JJ)
02170 XMAX=0.0
02180 DO 40 I=I1,I2
02190 IF(Y(I).GT.XMAX)XMAX=Y(I)
02200 YINT=YINT+Y(I)-BG(I)
02210 40 ERR=ERR+Y(I)
02220 DO 42 I=I1,I2
02230 42 IF(Y(I).GE.XMAX)CCH=X(I)
02240 ICH(JL)=IFIX(CCH)
02250 YTY(JL)=YINT
02260 XM=FLOAT((NP(J)-NP(J1))+(NP(JJ1)-NP(JJ)))/2.0
02270 XERR=SQRT(YINT+(ERR-YINT)*0.25*(2.0+FLOAT(I2-I1-2)/XM))
02280 ERR=(XERR/YINT)*100.0
02290 YERR(JL)=ERR
02300 41 WRITE(10,101)JK,YINT,ERR
02310 CALL POINTS(X,BG,NX)
02320 CALL BUFFEM(-10)
02330 CALL PROMPT(29HSTORE RESULTS ON TAPE11 Y/N/C,29)
02340 READ(5,105)REP
02350 IF(REP.EQ.1HN)GO TO 60
02360 IF(REP.EQ.1HY)CALL SAVE(ICH,YTY,YERR,JL)
02370 IF(REP.EQ.1HC)CALL SAVE(ICH,YTY,YERR,JL)
02380 105 FORMAT(1A1)
02390 102 FORMAT(26H PEAK  INTEGRAL   PC.ERROR,/)
02400 101 FORMAT(1X,I2,2X,F10.2,3X,F5.2)
02410 103 FORMAT(15HGOODNESS OF FIT,E11.4,/)
02420 60 RETURN
02430 END

02440 SUBROUTINE SAVE(ICH,YTY,ERR,K)
02441C
02442C  -  SAVES DATA ON TAPE11
02443C
02450 DIMENSION ICH(10),YTY(10),ERR(10)
02460 DO 10 J=1,K
02470 10 WRITE(11,100)ICH(J),YTY(J),ERR(J)
02480 100 FORMAT(4X,I4,5X,F12.2,5X,F6.2)
02490 RETURN
02500 END
```

```
02510 SUBROUTINE AUT(NN,N2,MM)
02511C
02512C  -  AUTOMATIC CONTROL OF DATA ENTRY.
02513C
02520 DIMENSION NX(12),NN(12,15),MM(12)
02530 N1=1
02540 I1=1
02550 1 CALL PROMPT(46HENTER NO.OF SPECTRA + NO.OF PEAKS PER SPECTRUM,46
02560 READ(5,*)N,M
02570 N2=N1+N-1
02580 CALL PROMPT(40HENTER NO.OF CHANNELS IN EACH PEAK,REGION,40)
02590 READ(5,*)(NX(I),I=1,M)
02600 DO 10 J=1,M
02610 DO 10 I=N1,N2
02620 MM(I)=M
02630 NN(I,J)=NX(J)
02640 10 CONTINUE
02650 N1=N2+1
02660 CALL PROMPT(20HANY MORE SPECTRA Y/N,20)
02670 READ(5,100)A1
02680 IF(A1.EQ.1HY)GO TO 1
02690 100 FORMAT(1A10)
02700 RETURN
02710 END


02720 SUBROUTINE SKIP(NN,MM,I,J)
02721C
02722C  -  ALLOWS DATA TO BE SKIPPED BEFORE THE
02723C  -  START OF THE ANALYSIS.
02724C
02730 DIMENSION NN(12,15),MM(12),X(120)
02740 CALL PROMPT(33HENTER NO.OF SPECTRA TO BE SKIPPED,33)
02750 READ(5,*)N1
02760 DO 10 I=1,N1
02770 M=MM(I)
02780 DO 11 J=1,M
02790 N=NN(I,J)
02800 READ(9,100)ISTART
02810 11 READ(9,101)(X(K),K=1,N)
02820 10 CONTINUE
02830 CALL PROMPT(31HENTER NO.OF PEAKS TO BE SKIPPED,31)
02840 READ(5,*)NP
02850 I=N1+1
02860 IF(NP.EQ.0)GO TO 30
02870 DO 20 J=1,NP
02880 N=NN(I,J)
02890 READ(9,100)ISTART
02900 READ(9,101)(X(K),K=1,N)
02910 100 FORMAT(1A10)
02920 101 FORMAT(4X,5F9.0)
02930 20 CONTINUE
02940 30 J=NP
02950 RETURN
02960 END
```

```
02970 SUBROUTINE SKIPD(I,J)
02971C
02972C  -  DUMMY ROUTINE IF NO DATA IS TO BE SKIPPED.
02973C
02980 I=1
02990 J=0
03000 RETURN
03010 END


03020 SUBROUTINE MINMAX(X,N,XMIN,XMAX)
03021C
03022C  -  CALCULATION OF MINIMUM AND MAXIMUM VALUES IN A PEAK REGION.
03023C
03030 DIMENSION X(120)
03040 XMAX=X(1)
03050 XMIN=X(1)
03060 DO 10 J=1,N
03070 IF(X(J).GT.XMAX)XMAX=X(J)
03080 IF(X(J).LT.XMIN)XMIN=X(J)
03090 10 CONTINUE
03100 RETURN
03110 END


03120 SUBROUTINE LOGPLOT(XMIN,XMAX,MODE,DISPL,ION,IOP)
03121C
03122C  -  TO PLOT A LOGARITHMIC AXIS
03123C
03130 DIMENSIONX(120)
03140 XMAX=ALOG10(XMAX)
03150 XMIN=ALOG10(XMIN)
03160 INTY=IFIX(XMAX)-IFIX(XMIN)+1
03170 IPSY=IFIX(XMIN)
03180 ALGNY=DISPL/FLOAT(INTY)
03190 CALL LOGAX(1.7,0.8,MODE,ALGNY,INTY,IPSY,ION,IOP,1)
03200 RETURN
03210 END


03220 SUBROUTINE LINPLOT(XMIN,XMAX,MODE,DISPL,ION,IOP)
03230 DIMENSION X(200)
03231C
03232C  -  TO PLOT A LINEAR AXIS.
03233C
03240 XMAX=1.05*XMAX
03250 XMIN=0.95*XMIN
03260 ALGN=DISPL/4.0
03270 VINC=(XMAX-XMIN)/4.0
03280 CALL LINAX(1.7,0.8,MODE,ALGN,4,XMIN,VINC,5,ION,IOP,-1,1)
03290 RETURN
03300 END
```

```
03310 SUBROUTINE XTITLE
03311C
03312C  -  TO ENTER A TITLE AND PREPARE FRAME FOR MICROFILM.
03313C
03320 DIMENSION IX(2),IY(2),ITTL(3)
03330 DATA IX(1),IX(2)/10H  CHANNEL ,10H NO.       /
03340 DATA IY(1)/10H  COUNTS  /
03350 CALL PROMPT(11HENTER TITLE,11)
03360 READ(5,10)(ITTL(I),I=1,3)
03370 10 FORMAT(3A10)
03380 CALL PROMPT(20HENTER TITLE POSITION,20)
03390 READ(5,*)XP,YP
03400 CALL SYMBOL(8.0,0.0,0.2,IX,0.0,20)
03410 CALL SYMBOL(0.2,7.0,0.2,IY,90.0,10)
03420 CALL SYMBOL(XP,YP,0.2,ITTL,0.0,30)
03430 CALL PROMPT(14HHARD COPY, Y/N,14)
03440 READ(5,11)ANS
03450 IF(ANS.EQ.1HY)CALL HARDCPY
03460 11 FORMAT(1A1)
03470 RETURN
03480 END


03490 SUBROUTINE SMOTH(N,X,Y)
03501C
03502C  -  CONDUCTS A 5 POINT SMOOTHING OF THE DATA AND DISPLAYS.
03503C
03504 DIMENSION X(200), Y(200), YS(200)
03510 M=N-2
03520 DO 10 I=3,M
03530 I1=I-1
03540 I2=I-2
03550 J1=I+1
03560 J2=I+2
03570 YS(I)=((Y(I2)+Y(J2))*(-3.0)+(Y(I1)+Y(J1))*12.0+Y(I)*17.0)/35.0
03580 10 CONTINUE
03590 YS(1)=Y(1)
03600 YS(2)=Y(2)
03610 MM=N-2
03620 CALL POINTS(X,YS,MM)
03630 RETURN
03640 END


03650 SUBROUTINE ASSIST(ANS)
03651C
03652C  -  HELP SUBROUTINE FOR BEGINNERS
03653C
03660 CALL NEWPAGE
03670 CALL PROMPT(32HEXPLANATION OF CONTROL STATEMENT,32)
03680 CALL PROMPT(43HO - CLEARS SCREEN AND REPLOTS THE SAME PEAK,43)
03690 CALL PROMPT(37HN -   "       "    "  PLOTS NEXT PEAK,37)
03700 CALL PROMPT(17HL - STOPS PROGRAM,17)
03710 CALL PROMPT(23HS - SKIPS THE NEXT PEAK,23)
03720 CALL PROMPT(36HC - STARTS COVELL TYPE BG CORRECTION,36)
03730 CALL PROMPT(36HP -   "    POLYNOMIAL  BG      "    ,36)
03740 CALL PROMPT(40HH - INITIATES MICROFILM HARD COPY OPTION,40)
03750 CALL PROMPT(41HSM - EXECUTES A 5 POINT SMOOTHING ROUTINE,41)
03760 CALL PROMPT(27HTYPE GO TO CONTINUE PROGRAM,27)
03770 READ(5,1)A
03780 1 FORMAT (1A2)
03790 IF(A.EQ.2HGO)CALL NEWPAGE
03800 ANS=1HO
03810 RETURN
03820 END
```

```
03830 SUBROUTINE POLY(M,X,F,W,K1,N,S , ,L
03831C
03832C  -  POLYNOMIAL SUBROUTINE FROM THE NAG LIBRARY (E02ABF).
03833C
03840 INTEGER P01AAF,IFAIL,I,K2,K,ISWX,ICOMP,J,KTEMP,KK,J1,M,K1,N
03850 DOUBLE PRECISION SRNAME
03860 REAL ZERO,ONE,FOUR,TWO,P6,A,AL(51),B,BE(51),CLP(52),CP(51),
03870+CPSAVE(51),CTP(51),DELSQ,DU,F(M),OM,P(K1),S(51),S1(K1),SIMIN,TP(200)
03880+TW,W(M),X(M),XLP(200),XLW,XTEMP
03890 LOGICAL L
03900 DATA ZERO/0.0/,ONE/1.0/,FOUR/4.0/,TWO/2.0/,P6/0.6/
03910 IF(M.GT.200)IFAIL=P01AAF(0,1,SRNAME)
03920 IF(K1.GE.51.OR.K1.GE.M)IFAIL=P01AAF(0,2,SRNAME)
03930 DO 20 I=1,M
03940 IF(W(1).LE.ZERO)IFAIL=P01AAF(0,3,SRNAME)
03950 20 CONTINUE
03960 DO 40 I=2,M
03970 IF(X(I).LE.X(I-1))IFAIL=P01AAF(0,4,SRNAME)
03980 40 CONTINUE
03990 K2=K1+1
04000 K=K1-1
04010 N=K
04020 DO 60 I=1,K1
04030 CP(I)=ZERO
04040 60 CONTINUE
04050 BE(1)=ZERO
04060 CLP(2)=ZERO
04070 CLP(1)=ZERO
04080 DELSQ=ZERO
04090 OM=ZERO
04100 TW=ZERO
04110 SIMIN=ZERO
04120 ISWX=0
04130 CTP(1)=ONE
04140 ICOMP=1
04150 DO 80 I=1,M
04160 DELSQ=DELSQ+W(1)*F(1)**2
04170 TP(1)=ONE
04180 XLP(I)=ZERO
04190 OM=OM+W(I)*F(I)
04200 TW=TW+W(I)
04210 80 CONTINUE
04220 S(1)=OM/TW
04230 CP(1)=S(1)
04240 DELSQ=DELSQ-S(1)*OM
04250 XTEMP=M
04260 S1(1)=ABS(DELSQ/(XTEMP-ONE))
04270 A=FOUR/(X(M)-X(1))
04280 B=-TWO-A*X(1)
04290 DO 100 I=1,M
04300 X(1)=A*X(1)+B
04310 100 CONTINUE
04320 DO 260 I=1,K
04330 DU=ZERO
04340 DO 120 J=1,M
04350 DU =DU+W(J)*X(J)*TP(J)**2
04360 120 CONTINUE
04370 AL(I+1)=DU/TW
04380 XLW=TW
04390 TW=ZERO
04400 OM=ZERO
04410 DO 140 J=1,M
04420 DU=BE(1)*XLP(J)
04430 XLP(J)=TP(J)
04440 TP(J)=(X(J)-AL(I+1))*TP(J)-DU
04450 TW=TW+W(J)*TP(J)**2
04460 OM=OM+W(J)*F(J)*TP(J)
```

```
04470 140 CONTINUE
04480 BE(I+1)=TW/XLW
04490 S(I+1)=OM/TW
04500 DELSQ=DELSQ-S(I+1)*OM
04510 KTEMP=M-I-1
04520 XTEMP=KTEMP
04530 SI(I+1)=ABS(DELSQ/XTEMP)
04540 IF(L) GO TO 200
04550 IF(ISWX.EQ.1)GO TO 180
04560 IF(SI(I+1).LT.SI(I))GO TO 200
04570 M=I-1
04580 ICOMP=1
04590 ISWX=1
04600 SIMIN=SI(I)
04610 DO 160 J=1,K1
04620 CPSAVE(J)=CP(J)
04630 160 CONTINUE
04640 GO TO 200
04650 180 IF(SI(I+1).GE.(P6*SIMIN))GO TO 200
04660 ICOMP=0
04670 ISWX=0
04680 M=K
04690 200 DO 220 J=1,I
04700 DU=CLP(J+1)*BE(I)
04710 CLP(J+1)=CTP(J)
04720 CTP(J)=CLP(J)-AL(I+1)*CTP(J)-DU
04730 CP(J)=CP(J)+S(I+1)*CTP(J)
04740 220 CONTINUE
04750 CP(I+1)=S(I+1)
04760 CTP(I+1)=ONE
04770 CLP(I+2)=ZERO
04780 IF(ICOMP.EQ.ZERO.OR.ISWX.EQ.ZERO) GO TO 260
04790 IF(I.NE.K)GO TO 260
04800 DO 240 J=1,K1
04810 CP(J)=CPSAVE(J)
04820 240 CONTINUE
04830 260 CONTINUE
04840 CLP(1)=1
04850 CPSAVE(1)=1
04860 P(1)=CP(1)
04870 DO 280 I=2,K1
04880 CLP(I)=1
04890 CPSAVE(I)=B*CPSAVE(I-1)
04900 P(1)=P(1)+CP(I)*CPSAVE(I)
04910 280 CONTINUE
04920 DO 320 J=2,K1
04930 CLP(1)=CLP(1)*A
04940 P(J)=CP(J)*CLP(1)
04950 KK=2
04960 J1=J+1
04970 IF(J1.GT.K1)GO TO 340
04980 DO 300 I=J1,K1
04990 CLP(KK)=A*CLP(KK)+CLP(KK-1)
05000 P(J)=P(J)+CP(I)*CLP(KK)*CPSAVE(KK)
05010 KK=KK+1
05020 300 CONTINUE
05030 320 CONTINUE
05040 340 A=ONE/A
05050 DO 360 I=1,M
05060 X(I)=(X(I)-B)*A
05070 360 CONTINUE
05080 RETURN
05090 END
```

Appendix 3.1

Alnoite Analyses.

	PHN3541	PHN3543	PHN3544	PHN3545	PHN3552 Autolith	PHN3553	PHN3553 Mica	PHN3565
La	91.8	83.4	82.6	85.4	125.	76.1	1.78	101.
Ce	201.	184.	195.	199.	304.	174.	1.87	229.
Nd	82.6	80.5	65.4	71.9	102.	73.8	-	92.9
Sm	16.3	14.8	14.9	15.6	21.7	13.7	0.172	5.39
Eu	4.88	4.39	4.65	4.73	7.05	4.16	0.059	5.39
Tb	1.82	1.69	1.84	1.74	2.62	1.57	-	1.96
Ho	1.15	n.a.	n.a.	1.16	1.99	1.15	-	1.52
Yb	1.86	1.68	1.93	1.79	2.69	1.72	0.06	2.15
Lu	0.28	0.28	n.a.	0.21	0.32	0.23	-	0.30
Co	57.	53.	98.	53.	65.	48.	92.	71.
Cr	415.	377.	595.	639.	567.	386.	23.5	681.
Sc	14.9	13.5	15.6	15.0	17.9	12.4	2.75	15.0
U	3.8	4.2	2.6	2.5	4.4	2.5	0.3	3.4
Th	13.2	12.7	11.6	13.5	19.6	10.7	0.5	15.0
Cs	0.3	0.6	1.5	1.5	0.5	0.5	1.2	1.8
La/Co	1.61	1.57	0.84	1.61	1.92	1.59	0.02	1.42
La/Sc	6.16	6.18	5.29	5.69	6.98	6.14	0.65	6.73
Cr/Co	7.28	7.11	6.07	12.1	8.72	8.04	0.26	9.59

Lamprophyre Analyses.

	AR.1b	AR.2a	AR.3	Ar.5	AR.6 (1)	AR.6 (2)	AR.7	AR.8 (1)	AR.8 (2)
La	133.	197.	113.	108.	190.	181.	118.	204.	200.
Ce	266.	402.	249.	248.	391.	390.	250.	454.	455.
Nd	118.	180.	104.	110.	178.	173.	104.	203.	209.
Sm	19.3	30.6	18.8	19.4	30.1	29.3	17.8	32.6	33.7
Eu	4.55	6.67	4.68	4.67	6.64	6.73	4.19	7.78	8.30
Tb	1.61	2.17	1.56	1.55	2.15	1.96	1.49	2.49	2.65
Ho	1.35	1.60	1.10	1.35	1.51	1.53	1.04	1.92	1.59
Yb	1.62	1.77	1.62	1.36	2.06	1.86	1.41	1.95	1.98
Co*	32.	31.	44.	47.	26.		76.	47.	
Th*	44.	60.	25.	24.	55.		29.	57.	
Sc*	16.	14.	16.	17.	15.		14.	24.	

	AR.9	AR.11	AR12 (1)	AR.12 (2)	AR.13	AR.15 (1)	AR.15 (2)	AR.16 (1)	AR.16 (2)
La	228.	179.	156.	155.	155.	183.	171.	114.	117.
Ce	331.	388.	362.	355.	357.	394.	369.	253.	252.
Nd	141.	166.	148.	147.	146.	170.	155.	105.	106.
Sm	22.5	29.3	24.2	24.9	23.2	28.1	27.1	21.2	16.2
Eu	5.29	6.32	5.89	6.11	5.54	6.48	6.21	3.73	3.90
Tb	1.85	2.04	1.77	1.87	1.85	2.17	1.99	1.10	1.20
Ho	1.68	1.63	1.39	1.62	1.35	1.75	1.43	1.25	1.25
Yb	2.05	2.02	2.02	2.15	1.77	1.94	1.85	1.50	1.43
Co*	45.	33.	42.		42.	37.		47.	
Th*	66.	54.	63.		90.	57.		54.	
Sc*	17.	16.	20.		21.	15.		16.	

	AR.17		AR.18
	1	2	
La	128.	130.	152.
Ce	280.	289.	317.
Nd	119.	118.	137.
Sm	19.2	20.3	21.5
Eu	4.24	4.53	5.23
Tb	1.41	1.51	1.83
Ho	1.32	1.34	1.42
Yb	1.43	1.54	2.12
Co*	38.		42.
Th*	75.		46.
Sc*	14.		19.

* Data from S.W.Bachinski, (pers. comm.) Using techniques as described in chapter 2 of this work.

Nos. 1 & 2 above columns refer to duplicate analyses carried out during different irradiations.

Kimberlite Analyses.

	PHN1334	PHN1598	PHN1725	PHN2827	PHN2827 (dup)	PHN3008
La	98.5	47.9	51.5	91.8	88.6	70.9
Ce	196.	96.8	105.	179.	178.	147.
Nd	68.8	37.2	43.3	71.4	70.8	56.9
Sm	9.64	5.89	7.41	10.9	11.2	9.86
Eu	2.53	1.64	1.94	2.87	2.87	2.59
Tb	0.71	0.50	0.70	0.78	0.83	0.92
Ho	0.47	0.42	0.57	0.52	0.59	0.64
Yb	0.71	0.63	0.82	0.76	0.78	1.17
Lu	0.08	0.08	0.10	0.12	0.11	0.13
Co	81.	86.	70.	87.	89.	78.
Cr	1460.	1110.	1330.	1610.	1520.	1020.
Sc	13.0	14.7	14.0	12.9	13.1	15.5
U	2.71	1.54	1.57	2.57	2.73	2.34
Th	13.7	6.34	6.57	11.2	11.7	9.94
Cs	1.13	1.12	1.01	1.15	0.93	-

PHN1334 - Kolo.

PHN1598 - Thaba Putsoa.

PHN1725 - Ramatseliso.

PHN2827 - Liqhobong.

PHN3008 - Abbotsford. (E. Griqualand)

	PHN2811	PHN2201	PHN2384	PHN2731	PHN2732	PHN2779	PHN2796	PHN3249
La	23.4	169.	170.	88.7	98.8	151.	187.	189.
Ce	46.7	352.	333.	196.	204.	294.	352.	358.
Nd	18.4	122.	118.	75.	84.9	107.	109.	124.
Sm	2.87	14.0	17.0	11.0	13.5	13.6	11.8	17.6
Eu	0.70	3.06	4.04	3.06	3.37	3.77	2.37	4.35
Tb	0.26	0.75	1.18	1.03	1.10	1.05	0.53	1.28
Ho	0.21	0.52	0.80	0.60	0.74	0.53	0.42	0.80
Yb	0.48	0.73	0.94	1.07	1.11	0.63	0.51	0.91
Lu	0.10	0.10	0.14	0.09	0.13	0.07	0.08	0.06
Co	88.	94.	88.	67.	71.	79.	85.	79.
Cr	1150.	2380.	1960.	1390.	1250.	1490.	2090.	1810.
Sc	7.3	17.5	16.2	12.4	12.8	14.7	18.2	16.4
U	0.94	4.53	4.33	3.09	3.22	4.65	2.22	4.49
Th	4.2	28.2	20.5	12.0	13.2	17.7	29.5	22.7
Cs	1.80	2.38	1.47	11.3	9.0	1.74	10.9	1.94

PHN2811 - Jagersfontein.
PHN2201 - Star Mine.
PHN2384 - Frank Smith Mine.
PHN2731 - Wesselton
PHN2732 - "
PHN2779 - Frank Smith Mine.
PHN2796 - Bellsbank.
PHN3249 - Frank Smith Mine.

	PHN1867	PHN1870
La	147.	107.
Ce	255.	201.
Nd	111.	81.2
Sm	16.7	12.1
Eu	4.63	3.42
Tb	1.42	0.97
Ho	0.89	0.46
Yb	1.01	1.18
Lu	0.14	0.16
Co	93.	87.
Cr	1120.	850.
Sc	16.7	14.5
U	3.40	2.64
Th	18.9	13.8
Cs	0.91	1.00

PHN1867 & PHN1870 - Monastery Mine, Orange Free State.

Appendix 4.1 Major and trace element analyses of the ultrabasic xenoliths.

Analyses performed by XRF at the University of Leeds by Alan Gray. H_2O^+, H_2O^-, CO_2 and Ferrous iron determined by wet chemical methods; analyst D. T. Richardson, University of Leeds.

Composition of garnet lherzolite, and some garnet harzburgite nodules from kimberlites in Southern Africa. Pyrolite quoted from Ringwood (1966)

PHN	1569	2492	2759	2764	2766/6	2782	2814	2823	2848	2860	2862	2713	2771	2780	2819	2829	2838	2839	3040	pyrolite
wt%																				
SiO_2	6.55	42.46	45.75	44.03	45.14	42.30	40.55	45.04	45.00	40.73	45.20	45.03	40.04	37.37	42.71	43.45	43.19	41.31	41.93	45.16
TiO_2	0.02	0.24	0.01	0.02	0.04	0.19	0.04	0.02	0.01	0.06	0.07	0.09	1.27	0.18	0.10	0.14	0.26	0.16	0.15	0.71
Al_2O_3	1.07	1.23	1.80	1.13	0.97	1.41	0.92	0.96	0.64	0.71	0.50	1.91	2.08	2.85	2.78	2.64	3.83	0.96	2.31	3.54
Fe_2O_3	1.35	3.00	1.52	1.82	1.99	2.18	2.14	1.88	7.26*	2.40	1.94	1.81	2.04	3.73	8.20*	8.58*	11.16*	1.69	2.60	0.46
FeO	4.79	4.14	4.32	4.36	4.18	4.15	4.33	4.22		4.07	6.86	4.90	4.51	7.24				6.32	5.49	8.04
MnO	0.11	0.11	0.11	0.11	0.11	0.10	0.10	0.09	0.11	0.09	0.12	0.12	0.11	0.12	0.12	0.12	0.14	0.12	0.13	0.14
MgO	43.77	42.22	41.53	43.24	43.57	41.82	42.97	42.72	44.17	43.32	42.80	39.82	37.05	39.29	38.81	39.95	36.59	44.32	40.05	37.47
CaO	0.84	1.16	1.00	0.95	0.95	0.83	0.45.	0.54	0.54	0.29	0.46	1.58	5.68	0.94	2.31	2.80	2.71	0.88	2.26	3.08
Na_2O	0.06	0.02	0.09	0.10	0.19	0.10	0.03	0.02	0.10	0.02	0.05	0.14	0.52	0.15	0.18	0.32	0.30	0.11	0.29	0.57
K_2O	0.01	0.11	0.12	0.11	0.28	0.11	0.14	0.02	0.10	0.23	0.01	1.99	1.14	0.04	0.04	0.10	0.15	0.01	0.05	0.13
P_2O_5	0.03	0.05	0.05	0.05	0.07	0.06	0.03	0.01	0.03	0.15	0.08	0.04	0.14	0.07	0.01	0.03	0.02	0.01	0.29	
H_2O^-	0.06	0.14	0.14	0.12	0.08	0.16	0.20	0.20		0.24	0.01	0.14	0.22	0.22				0.09	0.22	
H_2O^+	1.49	4.58	3.03	3.73	2.99	5.33	6.44	3.36	1.19+	6.84	1.13	2.48	4.23	6.19	4.37+	1.09+	1.17+	2.16	4.96	
CO_2	n.d.	n.d.	n.d.	n.d.	n.d.	n.d.	n.d.	n.d.		n.d.	n.d.	n.d.	1.22	0.20				n.d.	n.d.	
	100.15	99.46	99.47	99.77	100.56	98.74	98.34	99.08	99.15	99.15	99.23	100.05	100.25	98.59	99.63	99.22	99.52	98.62	100.73	
ppm																				
Cr	2826	2495	3166	3090	2716	2392	1919	2535	2356	2075	2430	3364	5734	1952	2895	2817	2919	3433	2285	
Co	90	96	87	95	84	86	95	96	101	99	117	88	67	126	101	111	99	102	96	
Ni	2009	1926	1805	2076	2061	1914	2027	2111	2201	2121	2300	1885	1518	2096	1846	1936	1781	2150	2065	
Zn	16	27	23	23	51	24	24	22	27	22	70	29	24	61	31	35	57	36	34	
Rb	<3	5	5	4	7	5	5	2	5	8	<3	17	87	2	3	<3	9	<3	<3	
Sr	17	47	36	46	92	35	32	11	33	27	15	51	240	18	10	46	31	9	29	
Zr	7	18	18	13	15	13	<3	<3	9	4	<3	24	27	19	6	12	13	8	9	
Nb	3	11	5	5	9	6	7	4	6	5	4	5	16	3	2	4	2	1	<3	
Ba	<3	51	30	37	57	151	36	27	15	38	(Pb<3)	47	171	58	9	29	75	3	9	

Appendix 5.1 Whole rock trace element analyses of the granulite and pyroxenite xenoliths

Group 1 Granulites (High La/Yb)

	MAT12	L20	PHN 1646	PHN 1919	PHN 2533	PHN 1670	M1	PHN 2852	L6
La	17.8	16.1	14.9	-	5.25	4.53	4.11	3.07	0.77
Ce	44.6	38.3	35.2	13.8	7.19	12.4	10.9	7.74	1.33
Nd	25.2	18.9	20.0	8.1	2.33	4.88	5.50	4.25	-
Sm	5.46	4.78	4.95	2.30	0.63	0.97	1.32	1.39	0.15
Eu	1.93	1.57	1.52	1.20	0.718	0.956	0.64	0.966	0.31
Tb	0.88	0.75	0.77	0.40	0.16	0.18	0.24	0.22	-
Ho	1.00	0.90	0.88	-	0.46	-	0.32	0.25	-
Yb	2.87	2.62	2.49	1.30	1.32	0.56	0.90	0.77	0.06
Lu	0.41	0.36	0.37	0.20	0.22	0.06	0.13	0.13	-
Co	60.	74.	60.	53.	38.	63.	62.	37.	57.
Cr	197.	186.	189.	104.	125.	342.	216.	370.	217.
Sc	34.4	31.0	31.3	28.8	41.3	14.3	19.0	20.5	3.2

Group 2 Granulites (Low La/Yb)

	LQ4	PHN 2532*	L12b	L12a	OVK 10303	PHN 2588	LT2+
La	7.27	6.99	1.84	1.76	1.39	0.55	27.3
Ce	24.6	21.5	4.32	3.84	4.29	-	58.4
Nd	21.5	9.63	5.07	2.97	1.74	-	21.2
Sm	7.42	2.98	1.99	1.38	0.68	0.58	3.71
Eu	2.96	1.26	0.79	0.65	0.44	0.64	1.48
Tb	1.63	0.81	0.48	0.33	0.18	0.15	0.59
Ho	2.23	1.19	0.73	0.45	0.22	0.22	0.80
Yb	6.61	3.34	2.11	1.21	0.67	0.68	1.72
Lu	1.04	0.51	0.31	0.22	0.12	0.10	0.25
Co	72.	80.	83.	56.	51.	-	30.
Cr	27.	257.	771.	245.	310.	-	15.
Sc	39.4	40.7	41.9	28.8	22.9	-	16.5

*Eclogite

+Felsic granulite

Garnet Pyroxenites.

	PHN 2495	L9	L17	L16
La	20.0	5.73	4.33	4.07
Ce	60.6	15.9	10.9	8.62
Nd	34.3	7.70	6.97	7.49
Sm	8.32	2.56	2.22	2.38
Eu	2.19	0.87	0.82	0.70
Tb	1.16	0.54	0.49	0.42
Ho	1.27	0.67	0.50	0.55
Yb	3.33	1.81	1.30	1.40
Lu	0.48	0.29	0.24	0.22
Co	85.	82.	72.	64.
Cr	1380.	707.	452.	3220.
Sc	31.5	61.3	43.2	49.3

Appendix 5.2 Trace element analyses of separated minerals

Garnets:-	Granulites.								Pyroxenites.		
	PHN 1646	L20	PHN 1919	PHN 1919	L13	OVK 10303	PHN 2588	PHN 2533	L9	L17	L16
La	2.58	0.52	0.28	0.29	0.60	0.27	0.01	0.43	0.3	0.25	0.60
Ce	-	-	-	-	-	-	-	-	-	-	-
Nd	-	-	-	-	-	-	-	-	-	-	-
Sm	3.43	2.87	1.62	1.67	1.07	0.69	0.44	0.46	1.09	0.83	0.82
Eu	1.65	1.36	1.09	1.05	0.72	0.54	0.68	0.81	0.65	0.55	0.52
Tb	1.48	1.35	0.72	0.71	0.50	0.26	0.32	0.27	1.09	0.69	0.80
Ho	2.32	2.28	1.12	1.07	0.78	0.59	0.52	0.67	2.49	1.34	1.71
Yb	6.41	5.73	2.95	3.46	2.11	1.52	1.87	2.93	7.36	3.24	4.91
Lu	0.87	0.97	0.45	0.46	0.35	0.24	0.23	0.43	1.17	0.53	0.75
Co	67.	64.	70.	72.	67.	56.	63.	48.	65.	68.	69.
Cr	178.	196.	105.	96.	220.	241.	185.	72.	661.	533.	2750.
Sc	53.2	50.4	46.9	47.8	45.5	40.1	36.5	46.8	75.3	50.2	74.3

Duplicate PHN1919 garnet analyses are included to illustrate precision.

Clinopyroxenes:- Granulites. Pyroxenites.

	PHN 1646	L20	PHN 1919	L13	OVK 10303	PHN 2588	PHN 2533	L9	L17	L16
La	21.5	15.4	9.9	1.59	1.90	1.39	9.32	7.14	5.03	4.92
Ce	64.8	55.7	30.0	8.00	10.2	3.32	15.7	21.4	13.8	16.6
Nd	43.7	39.0	17.0	8.30	7.59	3.83	5.93	16.6	-	12.1
Sm	10.4	9.67	4.42	2.25	1.43	1.32	1.19	3.59	3.55	3.34
Eu	2.53	2.42	1.32	0.72	0.59	1.02	0.91	1.11	1.10	1.00
Tb	0.55	0.49	0.23	0.15	0.10	0.14	-	0.38	0.30	0.40
Ho	-	-	-	-	-	-	-	-	-	-
Yb	0.36	0.18	0.18	-	0.05	0.07	0.20	0.17	0.16	0.16
Lu	-	-	-	-	-	-	-	-	-	-
Co	49.	41.	41.	29.	23.	31.	36.	35.	37.	31.
Cr	166.	191.	105.	360.	340.	240.	119.	543.	515.	2560.
Sc	37.6	38.1	34.0	21.2	17.0	24.4	46.7	68.5	42.7	49.7

Plagioclases:- Orthopyroxenes:-

	PHN 1646	L20	PHN 1919	L13	OVK 10303	PHN 2588	PHN 2533	L9	L16
La	12.8	9.09	6.60	2.40	3.1	-	4.1	-	-
Ce	14.3	13.2	6.0	3.5	2.8	-	1.8	-	-
Sm	0.70	0.34	0.20	0.08	0.08	0.04	-	-	-
Eu	0.68	0.54	0.47	0.23	0.18	0.18	0.22	-	-
Co	-	-	-	-	-	-	-	111.	102.
Cr	-	-	-	-	-	-	-	99.	785.
Sc	3.8	0.4	2.2	0.22	1.6	1.2	1.6	4.78	5.23

REFERENCES

AKIMOTO, S.I. (1972) The system MgO - FeO - SiO_2 at high pressures and temperatures - phase equilibria and elastic properties. in - A.R. Risema ed. The Upper Mantle; Elsevier, New York. 161 - 187

ALLEGRE, C.J., PINEAU, F.,BERNAT, M.& JAVOY, M. (1971) Evidence for the occurrence of carbonatites on the Cape Verde and Canary Islands. Nature, 233 103 - 104.

ARTH, J.G., & HANSON, G.N. (1975) Geochemistry and origin of the early Precambrian crust of northern Minnesota. Geochim. Cosmochim. Acta 39 325 - 362.

BACHINSKI, S.W. & SCOTT, R.B. (1979) Rare earth and other trace element contents and the origin of minettes (mica lamprophyres). Geochim. Cosmochim. Acta 43 93 - 100.

BARRET, D.R. & BERG, G.W. (1975) Complementary petrographic and strontium isotope ratio studies of South African kimberlites. Phys. Chem. Earth 9 619 - 654.

BOETTCHER, A.L., MYSEN, B.O. & MODRESKI, P.J. (1975) Melting in the mantle: phase relationships in natural and synthetic peridotite - H_2O and peridotite - H_2O - CO_2 - C - H - O - S with application to kimberlite. Phys. Chem. Earth 9 855 - 869.

BOYD, F.R. (1973) A pyroxene geotherm. Geochim. Cosmochim. Acta. 37 2533 - 2546.

——— (1976) Inflected and non-inflected geotherms. Carnegie Inst. Washington Yb. 75 521 - 523.

——— & McCALLISTER, R.H. (1976) Densities of fertile and sterile garnet peridotites. Geophys. Res. Lett. 3 509 - 512.

——— & NIXON, P.H. (1975) Origins of the ultramafic nodules from some kimberlites of northern Lesotho and the Monastery Mine, South Africa. Phys. Chem. Earth 9 431 - 454.

——— & NIXON, P.H. (1978) Ultramafic nodules from the Kimberley pipes, South Africa. Geochim. Cosmochim. Acta. 42 1367 - 1382.

BRAVO, M.S. & O'HARA, M.J. (1975) Partial melting of phlogopite bearing synthetic spinel- and garnet-lherzolites. Phys. Chem. Earth. 9 845 - 854.

BRUNFELT, A.O., ROELANDTS, I. & STEINNES, E. (1974) Determination of rubidium, caesium, barium and eight rare earth elements in ultramafic rocks by neutron activation analysis. Analyst. 99 277 - 284.

BRUNFELT, A.O. & STEINNES, E. (1973) Determination of rare earths in silicate rocks by neutron activation and a simple group separation. J. Radioanal. Chem. 13 11 - 20.

BRUNE, D. & JIRLOW, K. (1964) Optimisation in activation analysis by means of epithermal neutrons. Determination of molybdenum in steel. Nukleonik. 6 242 - 244.

BULTITUDE, R.J. & GREEN, D.H. (1971) Experimental study of crystal - liquid relationships at high pressures of olivine nephelinite and basanite composition. J. Petrol. 12 121 - 147.

BURNS, R.G. (1970) "Mineralogical Applications of Crystal Field Theory" Cambridge, London

CARDER, W. & BRAY, C. (1974) Four computer programs for the evaluation of data from neutron activated geological material. U.L.R.C. Internal Rept.

CARMICHAEL, I.S.E., TURNER, F.J. & VERHOOGEN, J. (1974) "Igneous Petrology" McGraw-Hill, New York.

CLARK, S.P. & RINGWOOD, A.E. (1974) Density distribution and constitution of the mantle. Rev. Geophys. 2 35 - 88.

CLEMENT, C.R. (1979) The origin and infilling of kimberlite pipes. Abstracts. De Beers 2nd Kimberlite Symposium, Cambridge, July 1979.

COBB, J.C. (1967) Determination of lanthanide distributions by neutron activation and direct gamma counting. Anal. Chem. 39 127 - 131.

COVELL, D.F. (1959) Determination of gamma ray abundance directly from the total absorption peak. Anal. Chem. 31 1785 - 1790.

CULLERS, R.L. & MEDARIS, G. (1977) Rare earth elements in carbonatites and co-genetic alkaline rocks. Examples from Seabrook Lake and Callender Bay, Ontario. Contrib. Mineral. Petrol. 65 143 - 153.

DANCHIN, R.V., FERGUSON, J., McIVER, J.R. & NIXON, P.H. (1975) The composition of late stage kimberlite fluids as revealed by nucleated autoliths. Phys. Chem. Earth. 9 235 - 245.

DAVIS, B.T.C. & BOYD, F.R. (1966) The join $Mg_2Si_2O_6$ - $CaMgSi_2O_6$ at 30 kilobars pressure and its application to pyroxenes from kimberlites. J. Geophys. Res. 71 3567 - 3576.

——— & SCHAIRER, J.F. (1965) Melting relations in the join diopside - forsterite - pyrope at 40 kilobars and at one atmosphere. Carnegie Inst. Washington Yb. 64 123 - 126.

DAWSON, J.B. & HAWTHORNE, J.B. (1973) Magmatic sedimentation and carbonatitic differentiation in kimberlite sills at Benfontein, South Africa. J. Geol. Soc. Lond. 129 61 - 73.

——— & SMITH, J.V. (1977) The MARID (mica - amphibole - rutile - ilmenite - diopside) suite of xenoliths in kimberlite. Geochim. Cosmochim. Acta. 41 309 - 323.

DENECHAUD, E.B., HELMKE, P.A. & HASKIN, L.A. (1970) Analysis for the rare earth elements by neutron activation and Ge(Li) spectrometry. J. Radioanal. Chem. 6 97 - 113.

DOSTAL, J. & CAPEDRI, S. (1979) Rare earth elements in high grade metamorphic rocks from the western Alps. Lithos 12 41 - 49.

DRESSLER, B. (1975) Lamprophyres of the north central Labrador trough, Quebec, Canada. Neues. Jahrb. Min. Mh. 268 - 280.

EBY, G.N. (1975) Abundance and distribution of the rare earth elements and yttrium in the rocks and minerals of the Oka carbonatite complex, Quebec. Geochim. Cosmochim. Acta. 39 597 - 620.

EHRENBERG, S.N. (1977) Garnet peridotite xenoliths in minette from the Navajo volcanic field. Ext. Abstracts 2nd Int. Kimberlite Conf. Santa Fe.

ERLANK, A.J. & RICKARD, R.S. (1977) Potassic richterite bearing peridotites from kimberlite and the evidence they provide for mantle metasomatism. Ext. Abstracts 2nd Int. Kimberlite Conf. Santa Fe.

FESQ, H.W., KABLE, E.J.D. & GURNEY, J.J. (1975) Aspects of the geochemistry of kimberlites from the Premier Mine and other selected South African occurrences with particular reference to the rare earth elements. Phys. Chem. Earth. 9 687 - 709.

FINNERTY, A.A. & BOYD, F.R. (1979) Pressure dependent solubility of calcium in forsterite coexisting with diopside and enstatite. Carnegie Inst. Washington Yb. 78 713 - 717.

FLYNN, R.T. & BURNHAM, C.W. (1978) An experimental determination of rare earth partitioning coefficients between a chloride containing vapour phase and silicate melts. Geochim. Cosmochim. Acta. 42 685 - 701.

FREY, F.A. (1969) Rare earth abundances in a high temperature peridotite intrusion. Geochim. Cosmochim. Acta. 33 1429 - 1447.

——— & GREEN, D.H. (1974) The mineralogy, geochemistry and origin of lherzolite inclusions in Victorian basanites. Geochim. Cosmochim. Acta 38 1023 - 1059.

FREY, F.A., GREEN, D.H. & ROY, S.D. (1978) Integrated models of basalt petrogenesis: A study of quartz tholeiites to olivine melilitites from south eastern Australia utilising geochemical and experimental petrological data. J. Petrol. 19 463 - 513.

——— & PRINZ,M. (1977) Ultramafic inclusions from San Carlos, Arizona Earth Planet. Sci. Lett. 38 129 - 176.

FYFE, W.S. (1970) Some thoughts on granitic magmas. Geol. J. Spec. Issue 2 (Mechanisms of Igneous Intrusion. ed. N.Rast.) 201 - 216.

GAST, P.W. (1968) Trace element fractionation and the origin of tholeiitic and alkaline magma types. Geochim. Cosmochim. Acta. 32 1057 - 1086.

GOLDSCHMIDT, V.M. (1937) The principles of distibution of chemical elements in minerals and rocks. J. Chem. Soc. 655 - 672.

——— (1954) "Geochemistry" Clarendon, Oxford.

GORDON, G,E., RANDLE, K., GOLES, G.G., CORLISS, J.B., BEESON, M.H. & OXLEY, S.S. (1968) Instrumental activation analysis of standard rocks with high resolution gamma ray detectors. Geochim. Cosmochim. Acta. 32 369 - 396.

GREEN, H.W. & GUEGUEN, Y. (1974) Origin of kimberlite pipes by diapiric upwelling in the upper mantle. Nature (London) 249 617 - 620.

GRIFFIN, W.L., CARSWELL, D.A. & NIXON, P.H. (1979) Lower crustal granulites and eclogites from Lesotho. In "The Mantle Sample; inclusions from kimberlites and other volcanics" ed. F.R.Boyd and H.O.A.Meyer. A.G.U. 59 - 86.

HAMILTON, P.J., EVENSEN, N.M., O'NIONS, R.K., SMITH, H.S. & ERLANK, A.J. (1979) Sm - Nd dating of Onverwacht group volcanics, southern Africa. Nature (London) 279 298 - 300.

HARRIS, P.G. & MIDDLEMOST, E.A.K. (1969) The evolution of kimberlites. Lithos 3 77 - 88.

HASKIN, L.A., HASKIN, M.A., FREY, F.A. & WILDEMAN, T.R. (1968) Relative and absolute terrestrial abundances of the rare earths. in "Origin and distribution of the elements" ed. L.H.Ahrens. Pergamon, New York 889 - 912.

HENDERSON, P. (1975) Geochemical indicator of the efficiency of fractionation in the Skaergaard intrusion, East Greenland. Mineral. Mag. 40 285 - 292.

HERTOGEN, J. & GIJBELS, R. (1971) Instrumental neutron activation analysis of rocks with a low energy photon detector. Analyt. Chim. Acta. 56 61 - 82.

HOOKER, P.J., O'NIONS, R.K. & PANKHURST, R.J. (1975) Determination of rare earth elements in U.S.G.S. standard rocks by mixed solvent ion exchange and mass spectrometric isotope dilution. Chem. Geol. 16 189 - 196

IRVING, A.J. (1974) Geochemistry and high pressure experimental studies of garnet pyroxenite and pyroxene granulite xenoliths from the Delegate basalt breccia pipes, Australia. J.Petrol. 15 1 - 40.

JACKSON, E.D. & WRIGHT, T.L. (1970) Xenoliths from the Honolulu volcanic series, Hawaii. J. Petrol. 11 405 - 430.

JAKES, P. & TAYLOR, S.R. (1974) Excess europium content in Precambrian sedimentary rocks and continental evolution. Geochim. Cosmochim. Acta. 38 739 - 745.

JANARDHAN, A.S., NEWTON, R.C. & SMITH, J.V. (1979) Ancient crustal metamorphism at low p(H_2O): Charnockite formation at Kabbaldurga, S. India. Nature, London 278 511 - 513.

KABLE, E.J.D., FESQ, H.W. & GURNEY, J.J. (1975) The significance of inter- element relationships of some minor and trace elements in South African kimberlites. Phys. Chem. Earth 9 709 - 734.

KUSHIRO, I. (1973) Partial melting of garnet lherzolites in kimberlites at high pressure. in "Lesotho Kimberlites" ed. P.H.Nixon, Lesotho Nat. Dev. Corp. Maseru 294 - 299.

LEYRELOUP, A., DUPUY, C. & ANDIAMBOLOLONA, R. (1977) Catazonal xenoliths in French neogene volcanic rocks. Contrib. Mineral. Petrol. 62 283 - 300.

LIU, L. (1974) Silicate perovskite from phase transformations of pyrope garnet at high pressures and temperatures. Geophy. Res. Lett. 1 277 - 280.

LOUBET, M., BERNAT, M., JAVOY, M. & ALLEGRE, C. (1972) Rare earth contents in carbonatites. Earth Planet. Sci. Lett. 14 226 - 232.

McGETCHIN, T.R., NIKHANJ, Y.S. & CHODOS, A.A. (1973) Carbonatite - kimberlite relations at the Cane Valley diatreme, San Juan County, Utah. J. Geophys. Res. 78 1853 - 1869.

McGETCHIN, T.R. & ULLRICH, G.W. (1973) Xenoliths in maars and diatremes with inferences for the Moon, Mars and Venus. J. Geophys. Res. 78 1833 - 1853.

McMAHON, B.M., HAGGERTY, S.E. & BENCE, R. (1979) Oxide mineral chemistry and oxygen fugacities of the Benfontein Sills, South Africa. Abstracts, De Beers Kimberlite Symposium, Cambridge, July 1979.

MEHNERT, K.R. (1975) The Ivrea Zone: A model of the deep crust. Neues. Jahbr. Miner. Abh. 125 156 - 199.

MERCIER, J-C. & CARTER, N.L. (1975) Pyroxene geotherms. J. Geophys. Res. 80 3349 - 3362.

MEYER, H.O.A. (1977) Mineralogy of the upper mantle: a review of the minerals in mantle xenoliths from kimberlite. Earth Sci. Rev. 13 251 - 281.

MITCHELL, R.H. & BELL, K. (1976) Rare earth element geochemistry of potassic lavas from the Birunga and Toro-Ankole regions of Uganda, Africa. Contrib. Mineral. Petrol. 58 293 - 303.

——— & BRUNFELT, A.O. (1975) Rare earth element geochemistry of kimberlite. Phys. Chem. Earth 9 671 - 686.

MORTEN, L., BRUNFELT, A.O. & MOTTANA, A. (1979) Rare earth abundances in super ferrian eclogites from the Voltri Group (Pennidic Belt, Italy). Lithos 12 25 - 32.

MYSEN, B.O. (1979) Experimental determination of crystal-vapour partition coefficients for rare earth elements to 30kbar pressure. Carnegie Inst. Washington Yb. 77 689 - 695.

NIKISHOV, K.N., KOVAL'SKY, V.V. & MARSHINTSEV, V.K. (1972) Alkaline ultrabasic rocks (alnoites, kimberlites and carbonatites) of N.E. Siberian platform. Proc. 24th Intern. Geol. Congr. Montreal 14 51 - 55.

NIXON, P.H. (1973) (editor) "Lesotho Kimberlites" Lesotho Nat. Dev. Corp. Maseru.

——— & BOYD, F.R. (1973) Petrogenesis of the granular and sheared ultrabasic nodule suites in kimberlites. in "Lesotho Kimberlites" ed. P.H.Nixon. 48 - 56.

——— & BOYD, F.R. (1979) Garnet bearing lherzolites and discrete nodules from the Malaita alnoite, Solomon Islands, S.W. Pacific, and their bearing on an oceanic mantle and geotherm. in "The mantle sample: inclusions in kimberlites and other volcanics." eds. F.R.Boyd and H.O.A. Meyer. A.G.U.

——— & COLEMAN, P.J. (1978) Garnet bearing lherzolite and discrete nodule suites from the Malaita alnoite, Solomon Islands, and their bearing on the nature and origin of the Ontong-Java Plateau. Bull. Aust. Soc. Expl. Geophys. 9 103 - 106.

———, MITCHELL, R.H. & ROGERS, N.W. (in preparation) Petrogenesis of alnoitic rocks fromthe Solomon Islands, Melanesia.

OTTONELLO, G., PICCARDO, G.B., MAZZUCOTELLI, A. & CIMMINO, F (1978) Clinopyroxene-orthopyroxene major and rare earth element partitioning in spinel peridotite xenoliths from Assab (Ethiopia). Geochim. Cosmochim. Acta. 42 1817 - 1828.

PAUL, D.K. & POTTS, P.J. (1976) Rare earth abundances in kimberlites from Greenland and Zambia. Chem. Geol. 18 161 - 167.

PEARCE, J.S. & CANN, J.R. (1973) Tectonic setting of basic volcanic rocks determined using trace element analysis. Earth Planet. Sci. Lett. 19 140 - 153.

PHILPOTTS, J.A., SCHNETZLER, C.C & THOMAS, H.H. (1972) Petrogenetic implications of some new geochemical data on eclogitic and ultrabasic inclusions. Geochim. Cosmochim. Acta. 36 1131 - 1166.

QUITTNER, P. (1972) "Gamma ray spectroscopy" Adam Hilger Ltd. London.

RIDLEY, W.I. & DAWSON, J.B. (1975) Lithophile trace element data bearing on the origin of peridotite xenoliths, ankaramite and carbonatite from Lashaine volcano, N. Tanzania. Phys. Chem. Earth. 9 559 - 569.

RINGWOOD, A.E. (1955) The principles governing trace element distribution during magmatic crystallisation: part 1 - The influence of electro - negativity. Geochim. Cosmochim. Acta. 7 189 - 202.

——— (1966) Mineralogy of the Mantle in "Advances in Earth Sciences" ed. P.M.Hurley. M.I.T. Press Cambridge, Mass. 357 - 399.

RODEN, M.F. (1977) Field geology and petrology of the minette diatreme at Buell Park, Apache County, Arizona. Ext. Abstracts 2nd Intern. Kimberlite Conference, Santa Fe.

ROGERS, N.W. (1977) Granulite xenoliths from Lesotho kimberlites and the lower continental crust. Nature, London 270 681 - 684.

ROGERS, V.C. (1970) Detection limits for gamma ray spectral analysis. Anal. Chem. 42 807 - 808.

ROUTTI, J.T. & PRUSSIN, S.G. (1965) Photopeak method for the computer analysis of gamma ray spectra from semi-conductor detectors. Nucl. Instrum. Methods. 72 125 - 142.

SHAW, D.M. (1970) Trace element fractionation during anatexis. Geochim. Cosmochim. Acta. 34 237 - 243.

SHIMIZU, N. (1975) Rare earth elements in garnets and clinopyroxenes from garnet lherzolite nodules in kimberlites. Earth Planet. Sci. Lett. 25 26 - 32.

——— & ALLEGRE, C.J. (1978) Geochemistry of transition elements in garnet lherzolite nodules in kimberlites. Contrib. Mineral. Petrol. 67 41 - 50.

SMITH, M.R. (1979) Textural studies of large peridotite nodules. Abstracts De Beers Kimberlite Symposium, Cambridge, July 1979.

STEINNES, E. (1971) Some neutron activation methods for the determination of minor and trace elements in rocks. Institute for Atomic Energy, Kjeller, Norway.

STROGEN, P. (1974) The sub-Palaeozoic basement in central Ireland. Nature London, 250 5462 - 5463.

SUN, S.S. & HANSON, G.N. (1975) Origin of Ross Island basanitoids and limitations upon the heterogeneity of mantle sources for alkali basalts and nephelinites. Contrib. Mineral. Petrol. 52 77 - 106.

THORPE, R.S. (1978) The parental basaltic magma of granites from the Isle of Skye, N.W. Scotland. Mineral. Mag. 42 157 - 158.

UPTON, B.G.J., ASPEN, P., GRAHAM, A. & CHAPMAN, N.A. (1976) Pre-Palaeozoic basement of the Scottish Midland Valley. Nature, London. 260 517 - 518.

VON KNORRING, O. & Du BOIS, G.G.B. (1961) Carbonatite lava from Fort Portal area in western Uganda. Nature, London. 192 1064 - 1065.

WAGNER, P.A. (1928) The evidence of the kimberlite pipes on the constitution of the outer part of the Earth. S. Afr. J. Sci. 25 127 - 148.

WILLIAMS, H. (1936) Pliocene volcanics of the Navajo-Hopi country. Geol. Soc. Am. Bull. 47 111 - 172.

WILLSHIRE, H.G. & SHERVAIS, J.W. (1975) Al - augite and Cr - diopside ultramafic xenoliths in basaltic rocks from western United States. Phys. Chem. Earth 9 257 - 272.

WOOD, B.J. & BANNO, S. (1973) Garnet-orthopyroxene and orthopyroxene-clinopyroxene relationships in simple and complex systems. Contrib. Mineral. Petrol. 42 109 - 124.

WOOLSEY, T.S., McCALLUM, M.E. & SCHUMM, S.A. (1975) Modelling of diatreme emplacement by fluidisation. Phys. Chem. Earth 9 29 - 42.

YODER, H.S. (1975) Relationship of melilite bearing rocks to kimberlite: Apreliminary report on the system akermanite - CO_2. Phys. Chem. Earth 9 883 - 894.

——— (1976) "Generation of Basaltic Magmas." Nat. Academy of Sci., Washington.

Vol III - N° 1 April 1979

ISSN : 0150 – 5505

Reprinted from :

GEOSTANDARDS NEWSLETTER

Journal { consacré à l'étude et à la promotion des échantillons géochimiques de référence
devoted to the study and promotion of geochemical reference samples

INFORMATION FOR CONTRIBUTORS

SCOPE AND AIMS

GEOSTANDARDS NEWSLETTER serves as a *forum* for exchange of ideas and information on geochemical reference samples (GRS). It also serves as a *medium* for rapid dissemination of analytical data on GRS of minerals, ores, and rocks, Papers published in GEOSTANDARDS NEWSLETTER are therefore, mainly concerned with :

- Publication of reports of collaborative studies on GRS, including compilations of analytical data
- Critical evaluation of the methods of preparing GRS and of processing of their data
- Periodic updating of recommended values
- Catalogue of available GRS
- Promotion and study of available GRS
- Programmes for new GRS
- Diologues between geoanalysts, geochemists, and GRS producers.

MANUSCRIPT REQUIREMENTS

Language. The three official languages of the journal are English, French, and German. Occasionally, papers in other languages will be considered on the recommendation of appropriate regional editors.

Text. Scripts must be typed, with double spacing, on one side of the page only and submitted in triplicate. An informative abstract, in proportion to the main text but not exceeding 200 words, must accompany each article. Original typed tables and illustrations should be submitted; each one on a separate sheet and in a form suitable for photographic reproduction.

References. References to the literature in the text should be identified by numbers in parentheses and should be fully listed at the end of the main text with no abbreviations of the journal titles. Two examples are :

(1) F.Chayes (1970)
Another last look at GI-WI, Journal of the International Association for Mathematical Geology, 2 : 207-209.
(2) A.A.Smales and L.R.Wager (1960)
Methods in Geochemistry, 464 pp, Interscience.

Submission. Authors are invited to submit their papers either directly to the appropriate regional editor (recommended procedure) or to the Editor-in-Chief. In the case of papers with joint authors, the name of the author with whom editors should correspond should be indicated. Authors will be consulted on the final draft of their paper but no proofs will be forwarded to them for corrections. Reprint order forms must be completed and despatched along with the approved final draft.

SUBSCRIPTION SYSTEM

The GEOSTANDARDS NEWSLETTER is published by the International Working Group (IWG) of the Association Nationale de la Recherche Technique, Paris. The annual membership fee to the IWG is 250 FF. Each member will receive the journal free of charge (2 issues per year) and will be sent on request GRS prepared and distributed by the IWG. Members are encouraged to, but not obliged to, contribute analytical data on the GRS prepared by the IWG and, in general, promote the study of GRS. The journal can also be purchased at a price of 70 FF per issue.

The membership fee which includes subscription to GEOSTANDARDS NEWSLETTER is payable to :

GEOSTANDARDS, 15, rue Notre-Dame-des-Pauvres, Case Officielle N° 1, 54500 VANDOEUVRE-lès-NANCY (FRANCE).

Bank account : N° 75135 60 41 A. Sté Nancéienne de Crédit Industriel et Varin Bernier, 4, Place André Maginot, 54000 NANCY.

Comparison of Rare-Earth Element Data Obtained by Neutron Activation Analysis Using International Rock and Multi-Element Solution Standards

G.D. BORLEY

Departement of Geology, Imperial College of Science and Technology, London SW7, England

N.ROGERS

University of London Reactor Centre, Silwood Park, Sunninghill, Ascot, Berks SL5 7PY, England

The authors have used a high-purity multi-element solution, containing known quantities of individual rare earth elements, as a reference standard in neutron activation analysis of rare earths in several international standard rocks. The data obtained by the authors have been compared with those obtained using the international standard rock Basalt BCR-1 as a reference material. The authors' data compare favourably with those obtained by other workers, particularly for the more basic rock types, and encourages the authors to suggest that a multi-element solution standard can be used successfully for neutron activation analysis of rare earth elements. High values obtained for Ce in Basalt BCR-1, however, might indicate that the behaviour of Ce in solution needs further investigation.

It is common for analysis of silicate materials to be made using international rock standards as reference samples. This procedure is not always possible; firstly, because there is a shortage of reliable data for some standard rocks; secondly, many of the standard rocks are in short supply or are no longer obtainable. This study was made in order to determine to what extent a standard elemental solution of known composition could be used as a satisfactory substitute for international rock standards in Instrumental Neutron Activation Analysis of rare earth elements. Basalt BCR-1 and several other standard rocks were analysed against a multi-element standard solution, after which two standard rocks, Basalt JB-1 and Knippa Basalt, were analysed against BCR-1 and the standard solution (information about distributors of these rock standards are given at the end of the paper).

PREPARATION AND IRRADIATION OF SAMPLES

The standard rock powders were used as received from the distributing agencies. Preparation of the multi-element standard rare earth solution was by mixing, in the appropriate proportions, aliquots of high-purity standard solutions of the individual rare earth elements that had been prepared by Johnson Matthey Chemicals Ltd. (address at the end of the paper). The dilution was such that 100µl of the multi-element solution contained similar amounts of the rare earths as approximately 100mg of BCR-1. Certain elements, however, were added to the solution in slightly greater quantities in order to improve counting statistics, e.g. Ho, Lu and Tm.

In preparation for irradiation, approximately 100mg of each rock powder was weighed into a small polythene capsule and sealed. The rare earth standards were prepared by evaporating 100µl of the multi-element solution onto 1.3cm diameter filter papers; the filter papers were then sealed into small polythene capsules in the same manner as for the rock powders. Eight or nine rock powder samples and three standard samples were then sealed into polythene core tubes. The three standards were arranged at each end of the outer tube with one in the middle to allow for the later correction of any systematic variation in the observed count rates attributable to neutron flux gradients within the reactor. The capsules were irradiated for 30 hours in a thermal neutron flux of 1×10^{12} n $cm^{-2} s^{-1}$, in the University of London Reactor at Silwood Park, Ascot. Although analytical errors might possibly arise from the self-shielding of neutrons in rock powders as against evaporated

solutions, the authors consider that self-shielding is only likely to be a significant problem in rocks containing abundant elements of large neutron cross-section, e.g. boron.

COUNTING CONDITIONS

After four or five days decay, the samples were counted for up to 5 x 10^3 secs. on a 42cm³ Ge(Li) detector (resolution 1.81KeV FWHM at 1.33MeV) to determine La and Lu. They were also counted for a similar length of time on a 1cm³ intrinsic Ge LEPD (resolution 500eV at 122KeV) to detect the short-lived activities due to Sm and Ho. The samples were then allowed to decay for a further 1-3 weeks. This reduces the contribution to the continuum of ^{24}Na, reduces the dead-time and increases the peak to background ratio of the rare earth element activities. After this decay, the samples were again counted on the LEP detector for 3 x 10^3 to 2 x 10^4 secs. to determine Yb, Tm, Tb, Nd, Eu and Ce. Information on the nuclides and photopeak energies used is summarised in Table 1.

Table 1. Data on nuclides and photopeaks used

Element	Nuclide	$t_{\frac{1}{2}}$	Energy of photopeaks used (keV)	Optimum decay irradiation after (before counting)
La	^{140}La	40.3 hours	328.8, 487.1, 1596.5, 815.7	4 - 5 days
Ce	^{141}Ce	32.5 days	145.4	2 - 4 weeks
Nd	^{147}Nd	11.1 days	91.4	2 - 4 weeks
Sm	^{153}Sm	46.7 hours	103.2, 69.7	4 - 5 days
Eu	^{152}Eu	12.2 years	121.8	2 - 4 weeks
Gd	^{153}Gd	242 days	97.4, 103.2	2 - 3 months
Tb	^{160}Tb	72.3 days	86.8	2 - 4 weeks
Ho	^{166}Ho	26.8 hours	80.6	4 - 5 days
Tm	^{170}Tm	128 days	84.4	2 - 4 weeks
Yb	^{169}Yb	30.7 days	63.1	2 - 4 weeks
Lu	^{177}Lu	6.75 days	208.4	1 - 2 weeks

The peak area integrated counts were initially corrected for background and, for the rock powders especially, interfering nuclide peaks, e.g. the ^{170}Tm photopeak at 84.4KeV was corrected for a ^{182}Ta interference estimated (from standard spectra) to be equivalent to 17% of the 100.3KeV ^{182}Ta photopeak counts. Following these corrections the rare earth concentrations were calculated using a computer program that corrects for peak integral decay, and neutron flux variations along the length of the core tubes during irradiation (details of the computer programs are available from the authors).

RESULTS

Table 2 lists the average of 10 determinations of the rare earth elements in BCR-1 with their respective 1 σ values expressed as percentages (these percentages apply to other new data presented in the paper). It can be seen that, for most elements, the values agree well with those of Flanagan (1) and the compilation of Taylor and Gorton (2), although the standard deviation of Tm is large. It is considered that this is caused by having to use the 84.4KeV peak of ^{170}Tm which is not very intense, in terms of peak area counts, and for which a correction due to the large interference from ^{182}Ta has to be made. The high value obtained for Ce in BCR-1 using the multi-element solution as standard is the other obvious feature of the data in Table 2. It is not clear why the value is consistently high; a possible answer could be that Ce in the solution standard might become oxidised over a period of time and precipitate from solution to a slight extent, thereby enhancing the apparent Ce level in samples being analysed against it. However, it could be that the values of Ce in BCR-1 currently being used are too low. The behaviour of Ce in solution may need further investigation.

Table 2. REE data (ppm) for BCR-1 Basalt, using and elemental solution standard (ESS)

REE	Concentration in ESS (µg/100µl)	BCR-1 This work	Other data ref. 2	Other data ref. 1
La	3.0	25.1 ± 6%	24.2	26
Ce	6.0	56.2 ± 6%	53.7	53.9
Nd	5.0	27.0 ± 7%	28.5	29
Sm	0.60	6.77 ± 4%	6.70	6.6
Eu	0.200	1.95 ± 3%	1.95	1.94
Tb	1.0	1.11 ± 7%	1.08	1.0
Ho	1.0	1.27 ± 7%	1.33	1.2
Tm	1.0	0.60 ± 14%	0.51	0.6
Yb	0.50	3.46 ± 5%	3.48	3.36
Lu	1.0	0.53 ± 10%	0.55	0.55

Flanagan (1), Taylor and Gorton (2)

Table 3 gives data for other international standard rocks run against the multi-element solution standard. The average of five analyses of G-2 Granite shows that although the data do not agree particularly well with those of Flanagan (1) they are well within the range quoted for other NAA analyses reported by Govindaraju and Roelandts (3). Like the earlier Granite G-1 and the more recent Granite JG-1 samples, G-2 is coarser grained than the various standard basalts that are available, and it may be that the granites will be less satisfactory as a consequence for trace element analysis. Results

Table 3. REE data for international standard rocks using an elemental solution standard*

	G-2 data (ppm)			W-1 data (ppm)			AGV-1 data (ppm)		
REE	This work(a)	Others (1)	(Ref) (3)	This work(b)	Others (1)	(Ref) (4)	This work(b)	Others (1)	(Ref) (3)
La	84.4	96	75-102	10.6	9.8	11.1	36.8	35	37.3
Ce	179	150	110-180	24.5	23	25	73.2	63	68.2
Nd	51.7	60	46-69	14.8	15	<30	32	39	38.1
Sm	7.4	7.3	5.4-10	3.4	3.6	3.4	6.07	5.9	5.79
Eu	1.35	1.5	1.05-2.4	1.12	1.11	1.08	1.65	1.7	1.68
Tb	0.55	0.54	0.30-0.75	0.72	0.65	0.67	0.65	0.70	0.64
Ho	0.35	0.4		1.18	0.69	ND	0.76	ND	ND
Yb	0.84	0.88	0.56-1.3	2.1	2.1	1.9	2.2	1.7	1.6
Lu	0.21	0.11	0.05-0.32	0.31	0.35	0.36	0.24	0.28	0.26

(1) Flanagan; (2) Govindaraju & Roelandts; (4) Laul & Rancitelli

a - 5 analyses; b - 1 analysis

*Concentrations in elemental standard as given in Table 2

for Andesite AGV-1 and Diabase W-1 were obtained from single analyses only as lack of material did not permit replication. New data for AGV-1 are not wholly satisfactory on a comparative basis, but they compare well with many of the "usable" values quoted by Govindaraju and Roelandts (3), and they come well within the range obtained from other NAA determinations given by the latter authors. Apart from the data given by Flanagan (1) there are few rare earth element analyses available for W-1, an exception being a recent analysis by Laul and Rancitelli (4) using neutron activation. Their data are also given in Table 3, and, considering that the present authors' data were obtained from a single analysis only, the two sets of data are seen to be in good agreement.

Table 4 gives results obtained for Basalt JB-1 and Knippa Basalt using, firstly, BCR-1 and, secondly, the multi-element solution as standards. In the absence of compiled NAA rare earth element data for BCR-1 the values used for this rock were those obtained by Gast et al (5), who analysed it by an isotope dilution method at the same time as they analysed Knippa Basalt. As the latter rock has also been analysed by the present authors it seemed useful to use the BCR-1 data of Gast et al (5) for comparison as a standard. Two elements, Ho and Tb, were not determined by Gast et al (5) and the values used for BCR-1 for these elements were taken from Flanagan (1). The data obtained for JB-1 and Knippa Basalt using BCR-1 and the solution standard respectively, are considered to compare well, particularly in view of the problem of separating interfering peaks from the rare earth element peaks in the rock powder spectra, a problem that does not exist for the solution standard. Results for Tb, Ho and Lu are least satisfactory but counting statistics for these elements are poor on the rock powders, and impracticably long count times would probably be necessary to improve the data further. Other rare earth element data on these two rocks are sparse, especially so on the Knippa Basalt; the Flanagan (1) averages on JB-1 are given and, as well as the data obtained on Knippa Basalt by Gast et al (5), the average of eight NAA determinations of Knippa Basalt by Jacobs et al (6) are given in Table 4 for comparison. The data sets are considered to be in reasonable agreement but more data generally on these two rocks are clearly desirable. This is particularly important for Knippa Basalt as Jacobs et al (6) suggested that the rock may be heterogeneous.

Table 4. REE data for JB-1 Basalt and Knippa Basalt using BCR-1 Basalt and elemental solution standards (ESS)*

REE	BCR-1 values (ppm) used Ref. 5	JB-1 data (ppm) This work using BCR-1[a]	JB-1 data (ppm) This work using ESS[b]	JB-1 data (ppm) Others Ref. 1	Knippa Basalt data (ppm) This work using BCR-1[c]	Knippa Basalt data (ppm) This work using ESS[c]	Knippa Basalt data (ppm) Others (Ref) (5)	Knippa Basalt data (ppm) Others (Ref) (6)
La	26.2	38.6	37.6	36	52.7	53.1	54.7	53.1
Ce	54.9	69.1	67.1	67	119	116	111	111
Nd	28.8	27	28.3	25	53.7	53.5	54.3	ND
Sm	6.74	5.2	5.3	4.8	11.1	11.7	11.2	11.3
Eu	1.97	1.58	1.48	1.52	3.36	3.43	3.42	3.34
Tb	1.0 (Ref.1)	0.84	0.76	0.5	1.05	1.32	ND	1.31
Ho	1.2 (Ref.1)	0.81	0.93	ND	0.77	1.11	ND	ND
Yb	3.69	1.82	1.91	2.1	1.39	1.43	1.71	1.51
Lu	0.59	0.28	0.31	0.31	0.26	0.26	0.216	0.242

(1) Flanagan; (5) Gast et al; (6) Jacob et al.
a - 6 analyses; b - 7 analyses; c - 4 analyses.
* Concentrations in elemental standards are given in Table 2.

CONCLUSION

Use of a multi-element solution standard for rare earth element analysis by NAA has produced encouraging results. Data obtained on several international rock standards compare well with data obtained by other techniques and with other data obtained by NAA.

ACKNOWLEDGEMENTS

Mr. M. Kerridge, Reactor Centre Director, is thanked for providing analytical facilities at the Centre. The first author appreciates the general advice given by Mrs. S. Parry; the second author acknowledges receipt of a SRC postgraduate studentship.

RESUME

Les auteurs ont employé une solution multi-élémentaire de haute pureté (SME), contenant des quantités connues d'éléments de terres rares, en tant qu'échantillon de référence en analyse par activation neutronique de terres rares dans plusieurs standards géochimiques internationaux. Les données ainsi obtenues sont comparées avec celles obtenues en utilisant le Basalte BCR-1 comme échantillon de référence. Cette comparaison s'avère être favorable et encourage les auteurs de suggérer la SME pour l'analyse de terres rares. Toutefois, la valeur élevée enregistrée pour Ce dans Basalte BCR-1 semble indiquer qu'un examen plus approfondi est nécessaire pour comprendre le comportement de Ce en solution.

SUPPLIERS OF STANDARD MATERIALS

United States Geological Survey, Washington, D.C. 20242, U.S.A. supplied Granite G-1, Basalt W-1 (no longer available), Basalt BCR-1, Andesite AGV-1 and Granite G-2.

Geochemical Research Section, Geological Survey of Japan, 135 Hisamoto-cho, Takatsu, Kawasaki, Japan, supplied Basalt JB-1 and Granite JG-1.

Dr. V. Dietrich, Institut für Kristallographie und Petrographie, Eidgenossische Technische Hochschule, Zurich, Switzerland, supplied the sample of Knippa Basalt.

Johnson Matthey Chemicals Ltd., Orchard Road, Royston, Herts, SG8 5HE, England supplied the high-purity rare earth element solutions from which the multi-element solution standard was prepared.

REFERENCES

(1) F.J. Flanagan (1973)
1972 values for International Geochemical Reference Samples, Geochimica et Cosmochimica Acta, 37 : 1189-1200.

(2) S.R. Taylor and M.P. Gorton (1977)
Geochemical application of spark source mass spectrography - III : Element sensitivity, precision and accuracy, Geochimica et Cosmochimica Acta, 41 : 1375-1380.

(3) K. Govindaraju and I. Roelandts (1977)
Neutron Activation Analysis of two U.S.G.S. standard rocks (Granite G-2 and Andesite AGV-1) and discussion in the light of compiled data. Geostandards Newsletter, 1 : 163-179.

(4) J.C. Laul and L.A. Rancitelli (1977)
Multielement analysis by sequential instrumental and radiochemical neutron activation. Jouranl of Radioanalytical Chemistry, 38 : 461-475.

(5) P.W. Gast, N.J. Hubbard and H. Wiesmann (1970)
Chemical compositions and petrogenesis of basalts from Tranquillity Base. Proc. Apollo 11 Lunar Sci. Conf., Geochimica et Cosmochimica Acta, Suppl. 1, 2, 1143-1163.

(6) J.W. Jacobs, R.L. Korotev, D.P. Blanchard and L.A. Haskin (1977)
A well tested procedure for instrumental neutron activation analysis of silicate rocks and minerals. Journal of Radioanalytical Chemistry, 40 : 93-114.

RECOMMANDATIONS AUX AUTEURS

FINALITE ET OBJECTIFS

GEOSTANDARDS NEWSLETTER offre une *tribune* pour l'échange des idées et des informations sur des Echantillons Géochimiques de Référence (EGR). Il doit également permettre la dissémination rapide de données analytiques sur les EGR de minéraux, minerais et roches. Les articles publiés dans GEOSTANDARDS NEWSLETTER concernent donc principalement :

- Publication de rapports d'études coopératives sur les EGR, y compris des compilations de données analytiques
- Evaluation critique des méthodes de préparation des EGR et de l'interprétation des données les concernant
- Mises à jour périodiques des valeurs recommandées
- Inventaire des EGR disponibles
- Promotion et étude des EGR disponibles
- Programmes pour les nouveaux EGR
- Dialogues entre géoanalystes, géochimistes et producteurs des EGR.

SPECIFICATIONS RELATIVES AU MANUSCRIT

Langues. Les trois langues officielles du journal sont l'allemand, l'anglais et le français. Occasionnellement, des articles dans d'autres langues seront pris en considération sur la recommandation particulière d'un rédacteur régional compétent.

Texte. Les manuscrits doivent être dactylographiés recto, en double interligne, et soumis en triple exemplaire. Un résumé très explicite, en proportion du texte principal, mais ne dépassant pas 200 mots, doit être joint avec chaque manuscrit. Les Tableaux et les figures doivent être fournis sur des feuilles séparées et sous une forme se prêtant à la reproduction photographiques.

References. Les références bibliographiques doivent être repérées par des chiffres entre parenthèses et doivent être rassemblées entièrement à la fin du texte sans aucune abréviations du titre du journal. Exemples :

(1) F.Chayes (1970)
Another last look at G1-W1, Journal of the International Association for Mathematical Geology, 2 : 207-209.
(2) A.A.Smales and L.R.Wager (1960)
Methods in Geochemistry, 464 pp, Interscience.

Envoi des manuscrits. Les auteurs sont invités à soumettre leurs manuscrits directement au rédacteur régional approprié (procédure recommandée) ou au Rédacteur en Chef. Dans le cas d'articles présentés par plusieurs auteurs, le nom de l'auteur principal avec qui les éditeurs doivent se mettre en rapport, doit être précisé. Les auteurs seront consultés sur le dernier projet mais les épreuves finales ne leur seront pas adressées. Les bons de commande pour les tirés-à-part doivent être complétés et expédiés avec le projet final.

ABONNEMENT

GEOSTANDARDS NEWSLETTER est publié par le Groupe International de Travail (GIT) de l'Association Nationale de la Recherche Technique, Paris. La cotisation annuelle au GIT est de 250 F. Chaque membre reçoit le journal sans aucun frais (2 numéros par an), et également sur demande, un lot des EGR préparés et distribués par le GIT. Les membres sont invités, sans que ce soit une obligation, à contribuer aux données analytiques sur les EGR préparés par le GIT et, en général, à promouvoir l'étude des EGR. Le journal peut être acheté, hors abonnement, au prix de 70 F le numéro.

La cotisation qui comprend l'abonnement au journal GEOSTANDARDS NEWSLETTER est payable à l'adresse suivante :

GEOSTANDARDS, 15, rue Notre-Dame-des-Pauvres, Case Officielle N° 1, 54500 VANDOEUVRE-lès-NANCY (FRANCE).

Cpte bancaire: N° 75135 60 41 A. Sté Nancéienne de Crédit Industriel et Varin Bernier, 4, Place André Maginot, 54000 NANCY.

Volume III Numéro 1 Avril 1979

GEOSTANDARDS NEWSLETTER

Published by the Working Group "Analytical Standards of Minerals, Ores, and Rocks" of the Association Nationale de la Recherche Technique, with the assistance of the Centre Nationale de la Recherche Scientifique.

Address : C.R.P.G.
15, rue Notre Dame des Pauvres, Case Officielle n° 1,
54500 Vandoeuvre-lès-Nancy (France). Tél. 51.22.13.

Directeur de la publication : H. de la Roche.